

MULTILAYER MEMBRANES FOR INTERMEDIATE TEMPERATURE POLYMER ELECTROLYTE FUEL CELLS

by

CAROLINA MUSSE BRANCO

A thesis submitted to the University of Birmingham for the degree of DOCTOR
OF PHILOSOPHY

Centre for Hydrogen and Fuel Cell Research
School of Chemical Engineering
University of Birmingham
May 2017

UNIVERSITY OF
BIRMINGHAM

University of Birmingham Research Archive

e-theses repository

This unpublished thesis/dissertation is copyright of the author and/or third parties. The intellectual property rights of the author or third parties in respect of this work are as defined by The Copyright Designs and Patents Act 1988 or as modified by any successor legislation.

Any use made of information contained in this thesis/dissertation must be in accordance with that legislation and must be properly acknowledged. Further distribution or reproduction in any format is prohibited without the permission of the copyright holder.

ABSTRACT

IT-PEFC operating at 120 °C and not the usual 80 °C has many advantages, such as faster chemical reactions. If the gas humidification is reduced, simpler and lighter humidifiers can be used, leading to a reduction in the fuel cell total cost. However, at this condition the current commercial membrane Nafion is not able to hold water and perform satisfactorily. Therefore, in this study the application of multilayer membranes for IT-PEFC was investigated. These membranes were divided into two groups, a first with external layers of Nafion and an inner layer of sulphonated polyindene, and a second with external layers of Nafion and an inner layer of graphene oxide. The membrane preparation method was also investigated. The multilayer membranes were prepared by hot pressing and solution casting. As a result, cast multilayer membranes showed better performance and proton conductivity than hot pressed. Delamination and low interface interaction were the main drawbacks for hot pressed membranes. Cast multilayer sulphonated polyindene membranes showed higher performance than Nafion at 120 °C and 20% of relative humidity. In the meantime, cast graphene oxide multilayer membranes showed higher water uptake and open circuit voltage than Nafion.

ACKNOWLEDGMENT

I would like to thank my supervisors Prof. Dr. Robert Steinberger-Wilckens and Dr. Surbhi Sharma for their guidance and advice.

The support of Science without Borders, Coordenação de Aperfeiçoamento de Pessoal de Nível Superior, CAPES, Brazil in the form of PhD studentship is gratefully acknowledged.

I would like to thank Prof. Dr. Maria Madalena de Camargo Forte for her advice and friendship.

Thanks for all master and undergraduate students that help me during the experimental development.

A final thanks for all colleagues from the Centre for Hydrogen and Fuel Cell Research.

TABLE OF CONTENTS

List of Illustrations	vii
List of Tables	xiv
Glossary of Terms and Abbreviations	xvi
Chapter I – Introduction	1
1.1. Objectives	8
1.2. Thesis Structure	9
Chapter II – A Review of IT-PEFC Membranes	11
2.1. Composite membranes	16
2.1.1. Organic fillers	18
2.1.2.1. Metal Oxides	23
2.1.2.2. Carbon nanomaterials	30
2.2. Multilayer Membranes	44
2.2.1. Hot Pressing	47
2.2.2. Solution casting	51
2.2.3. Dip coating	58
2.3. Conclusions	64
Chapter III – Synthesis of Materials	67
3.1. Synthesis of polyindene	67
3.2. Sulphonation of polyindene	68
3.3. Synthesis of graphene oxide	69
3.4. Chemical characterization	70
3.4.1. FT-IR	70
3.4.2. XRD	72
3.4.3. XPS	74
3.5. Thermal behaviour	75
3.5.1. TGA	75
3.5.2. DSC	78
3.6. Conclusions	79
Chapter IV – Membranes Preparation	80
4.1. Single layer membranes	83
4.1.1. Nafion single layers	83

4.1.2. SPInd single layers	85
4.1.3. GO single layers	87
4.2. Hot pressed membranes	91
4.3. Cast membranes	101
4.3.1. Nafion/sulphonated polyindene/Nafion multilayer membranes	103
4.3.2. Nafion/graphene oxide/Nafion multilayer membranes	109
4.4. Membrane activation	114
4.5. Conclusions	114
Chapter V – The Influence of SPInd on the Membrane Performance	116
5.1. Hot-pressed membranes	116
5.1.1. Microstructure	117
5.1.2. Water uptake and ion exchange capacity	119
5.1.3. Proton conductivity	125
5.2. Cast Membranes	130
5.2.1. Multilayer membrane microstructure	130
5.2.2. Water uptake and ion exchange capacity	132
5.2.3. Conductivity	136
5.2.4. Single cell test	141
5.3. Conclusions	155
Chapter VI – The Influence of GO on the membrane performance	158
6.1 Hot pressed membranes	159
6.1.1. Structural analysis	160
6.1.2. Water uptake and ion exchange capacity	161
6.1.3. Proton conductivity	165
6.1.4. Single cell test	167
6.2. Cast membranes	173
6.2.1 Structural analysis	173
6.2.2. Water uptake and ion exchange capacity	174
6.2.3. Proton conductivity	178
6.2.4. Single cell performance	186
6.2.5. Interface Analysis	203
6.2.4. Post-test of membranes	204
6.3. Conclusions	206
Chapter VII – Summary and Perspectives	208
7.1. Conclusions	208
7.2. Suggested future work	211
Appendix	212
A. Detailed experimental procedures	212

<i>A.1. Materials characterization</i>	212
<i>A.2. Tests on the Membranes</i>	214
List of Publications	219
References	220

LIST OF ILLUSTRATIONS

Figure 1.1: Schematic view of a general fuel cell.....	2
Figure 1.2: Fuel cell stack exploded view.....	4
Figure 1.3: Schematic of the membrane groups developed in this study.....	8
Figure 1.4: Two multilayer membrane structures aimed at this work. On the left Nafion/GO/Nafion and on the right N/SPInd/N. In the insets the proposed mechanisms of proton transport, both through water bridges and functional groups, are shown.....	8
Figure 2.1: Nafion chemical structure.....	11
Figure 2.2: Schematic of Grotthuss mechanism scheme showing the proton movement between sulphonic acid groups in the hydronium form.....	12
Figure 2.3: Zundel-ion and Eigen-ion structures showing the formation and cleavage of hydrogen bonds for the protons transport in a hydrated membrane.....	14
Figure 2.4: SEM micrographs of the PES/PVP membranes (a) without, with (b) 3%, (c) 5% and (d) 7% of PTFE.....	19
Figure 2.5: Schematic representing the fuel path (dashed line) in (a) the membrane with no filler and (b) the composite membrane with the filler particles (small red circles).....	26
Figure 2.6: (a) Polarization curves obtained in a PEFC at 140 °C feed with H ₂ and O ₂ using a well-ordered (PBI Iso) and 1 wt.% CNT filled PBI membrane, undoped (PBNT 1%) and doped (PBpNT 1%) with phosphoric acid. (b) Schematic illustration of the PBpNT membrane showing the PBI structure and phosphoric and phosphonic groups....	32
Figure 2.7: (a) Proton conductivity of the composite and the recast Nafion membranes at different temperature; besides the two Nafion membranes, the other membranes are the composite membranes of Nafion and carbon nanotubes with and without imidazole (Im). (b) Schematic illustration of the Nafion/CNT doped with Imidazole membrane, in which is possible to note the new path for the proton transport via Grotthuss mechanism.....	33

Figure 2.8: (a) Water uptake and (b) i-V curve for the membrane with 3 wt.% of GO and (c) i-V curve for the membrane with 3 wt.% of Pt-G, changing the humidity from 100 to 40% (d) The performance of a DMFC with Nafion/2 wt.% GO.....	41
Figure 2.9: Water concentration profile ($S_{v(OH)}$) in the membranes with Raman Analysis: (a) Aquivion/Nafion and (b) Nafion/Aquivion.....	50
Figure 2.10: (a) Schematic of multilayer membrane structure as shown by Wu <i>et al.</i> (b) DMFC single test with the multilayer membranes.....	51
Figure 2.11: (a) Single PEFC cell test; (b) PEFC durability test at room temperature	55
Figure 2.12: Schematic of the multilayer membrane with SPPSU external layers and inner layer of SiO ₂ + PEI.....	56
Figure 2.13: (a) Schematic of the Nafion, PDDA, GO multilayer membrane; (b) methanol crossover test for a) Nafion and b) 2 bilayer membrane; (c) DMFC single test studies for various bilayers.....	61
Figure 3.1: Reaction of polyindene sulphonation.....	68
Figure 3.2: Set up for GO synthesis reaction.....	69
Figure 3.3: FT-IR spectra for PInd and SPInd.....	71
Figure 3.4: FT-IR spectra for GO.....	72
Figure 3.5: XRD scan of GO.....	73
Figure 3.6: XPS fitting curve of synthesized GO.....	74
Figure 3.7: PInd and SPInd thermograms curves by TGA.....	76
Figure 3.8: TGA curves of GO.....	77
Figure 3.9: DSC curves for PInd and SPInd.....	78
Figure 4.1: (a) Thin SPInd membrane cast over Nafion layer to use as inner layer in [N _C /SPInd _C /N _C] _{HP} . (b) Micrograph image of the cross-section of the SPInd _C membrane, 3500x magnification, 20 μm scale.....	87

Figure 4.2: (a) Vacuum assisted filtration to produce GO film. Inset: thin filtrated GO film. (b) Semi-ordered mechanism to form the GO film by filtration, where ρ_d is the density of the dispersion and ρ_p is the density of the paper.....	88
Figure 4.3: GO filtered films (a) cross section, 3500x magnification, 20 μm scale and (b) surface 1000x magnification, 50 μm scale.....	89
Figure 4.4: (a) EDS spectrum for the GO_F film, (b) EDS spectrum for the GO-30N_F film and (c) elemental mapping for the GO-30N_F film for the elements fluor, carbon, oxygen, and sulphur (top to bottom).....	91
Figure 4.5: GO multilayer membrane after HP with each external layer of Nafion stuck on the aluminium foil.....	97
Figure 4.6: Schematic illustration of the hot pressing procedure to obtain the multilayer membranes (a) $[\text{N}_C/\text{SPInd}_C/\text{N}_C]_{\text{HP}}$, (b) $[\text{N}_C/\text{GO}_F/\text{N}_C]_{\text{HP}}$ and (c) $[\text{N}/\text{N}]_{\text{HP}}$	99
Figure 4.7: Lateral view of (a) $[\text{N}_C/\text{SPInd}_C/\text{N}_C]_{\text{HP}}$ and (b) $[\text{N}_C/\text{GO}_F/\text{N}_C]_{\text{HP}}$ membranes. Front view (c) $[\text{N}_C/\text{SPInd}_C/\text{N}_C]_{\text{HP}}$ and (d) $[\text{N}_C/\text{GO}_F/\text{N}_C]_{\text{HP}}$ membranes.....	101
Figure 4.8: Schematic illustration of the casting process to produce $[\text{N}_C/\text{GO}_C/\text{N}_C]_C$ and $[\text{N}_C/\text{SPInd}_C/\text{SPInd}_C]_C$	102
Figure 4.9: $[\text{N}_C/\text{SPInd}_C/\text{N}_C]_C$ membranes by cast parameters attempt: (a) attempt A, same conditions as Nafion bilayer; (b) attempt C, lower temperature casting SPInd; (c) attempt D, annealing before the addition of the third layer.....	105
Figure 4.10: $[\text{N}_C/\text{SPInd}_C/\text{N}_C]_C$ with (a) 5 wt.%, (b) 10 wt.% and (c) 20 wt.% of Nafion in the inner layer.....	106
Figure 4.11: $[\text{N}_C/x\text{GO}_C/\text{N}_C]_C$ membranes with x equal to (a) 0.5wt.%, (b) 2.5wt.%, (c) 4.5wt.% and (d) 6.5wt.%.....	112
Figure 4.12: Two views of $[\text{N}_C/6.5\text{GO}_C/\text{N}_C]_C$ membrane delaminated after cutting.....	113
Figure 5.1: Micrographic images from $[\text{N}_C/\text{SPInd}_C/\text{N}_C]_{\text{HP}}$ membranes with zoom of (a) 500x, (b) 2000x, (c) 3500x and (d) 6500x.....	118
Figure 5.2: Water uptake and ion exchange capacity of the membranes, at room temperature.....	121
Figure 5.3: Bubbles in the $[\text{N}_C/\text{SPInd}_C/\text{N}_C]_{\text{HP}}$ membrane when soaked in water.....	121

Figure 5.4: Proton conductivity test in the Scribner 850e Fuel Cell system.....	125
Figure 5.5: Proton conductivity at (a) 80 °C, (b) 100 °C and (c) 120 °C. (d) Proton conductivity of multilayer membrane Nc/SPIIndc/Nc at different temperatures; O.T.: Operating temperature.....	126
Figure 5.6: Cross-section SEM images of (a) 1:1:1.5 [Nc/SPIIndc/Nc]c membrane and (b) Nc membrane.....	131
Figure 5.7: Water uptake of multilayer membranes by composition of each layer.....	133
Figure 5.8: Ion exchange capacity and hydration number of the cast SPIInd multilayer membranes.....	134
Figure 5.9: Comparison between hot pressed and cast SPIInd multilayer membranes.....	136
Figure 5.10: Cast MM proton conductivity curves at (a) 80 °C, (b) 100 °C and (c) 120 °C.....	137
Figure 5.11: Arrhenius plot with RH of (a) 20%, (b) 40%, (c) 60% and (d) 80%.....	139
Figure 5.12: Arrhenius plot with 100 % of RH.....	140
Figure 5.13: Polarization and power curves with (a) 20% of relative humidity and 80 °C of operation temperature, (b) 40% of relative humidity and 80 °C of operation temperature. Back pressure 0.18 MPa, H ₂ /Air at rate of 1 and 2.5 L/min, respectively....	144
Figure 5.14: Polarization and power curves with (a) 60% of relative humidity and 80 °C of operation temperature, (b) 80% of relative humidity and 80 °C of operation temperature. Back pressure 0.18 MPa, H ₂ /Air at rate of 1 and 2.5 L/min, respectively....	145
Figure 5.15: Polarization and power curves with (a) 100% of relative humidity and 80 °C of operation temperature, (b) 20% of relative humidity and 100 °C of operation temperature. Back pressure 0.18 MPa, H ₂ /Air at rate of 1 and 2.5 L/min, respectively....	146
Figure 5.16: Polarization and power curves with (a) 40% of relative humidity and 100 °C of operation temperature, (b) 60% of relative humidity and 100 °C of operation temperature. Back pressure 0.18 MPa, H ₂ /Air at rate of 1 and 2.5 L/min, respectively....	147
Figure 5.17: Polarization and power curves with (a) 80% of relative humidity and 100 °C of operation temperature, (b) 100% of relative humidity and 100 °C of operation temperature. Back pressure 0.18 MPa, H ₂ /Air at rate of 1 and 2.5 L/min, respectively....	148

Figure 5.18: Polarization and power curves with (a) 20% of relative humidity and 120 °C of operation temperature, (b) 40% of relative humidity and 120 °C of operation temperature. Back pressure 0.18 MPa, H ₂ /Air at rate of 1 and 2.5 L/min, respectively....	149
Figure 5.19: Polarization and power curves with (a) 60% of relative humidity and 120 °C of operation temperature, (b) 80% of relative humidity and 120 °C of operation temperature. Back pressure 0.18 MPa, H ₂ /Air at rate of 1 and 2.5 L/min, respectively....	150
Figure 5.20: Polarization and power curves with 100% of relative humidity and 120 °C of operation temperature. Back pressure 0.18 MPa, H ₂ /Air at rate of 1 and 2.5 L/min, respectively.....	151
Figure 5.21: [N _C /SPInd _C /N _C] _C 1:1:1.5 membrane (a) before and (b) after PEFC single cell test.....	154
Figure 6.1: SEM images of the cross-section of (a) [N _C /GO-20N _F /N _C] _{HP} and (b) [N _C /GO _F /N _C] _{HP} membranes.....	161
Figure 6.2: Multilayer membranes water uptake (left bar) and IEC (right bar) plots.....	162
Figure 6.3: [N _C /GO _F /N _C] _{HP} soaked in water to emphasize the formation of bubbles and swelling.....	163
Figure 6.4: [N _C /GO-20N _F /N _C] _{HP} membrane (a) before and (b) after the activation.....	165
Figure 6.5: Membranes proton conductivity, where the number over the brackets represents temperature.....	167
Figure 6.6: Polarization curves at 80 °C with (a) low humidity and (b) high humidity. Back pressure 0.18 MPa, H ₂ /Air at rate of 1 and 2.5 L/min, respectively.....	169
Figure 6.7: Polarization curves at 100 °C with (a) low humidity and (b) high humidity. Back pressure 0.18 MPa, H ₂ /Air at rate of 1 and 2.5 L/min, respectively.....	170
Figure 6.8: Polarization curves at 120 °C with (a) low humidity and (b) high humidity. Back pressure 0.18 MPa, H ₂ /Air at rate of 1 and 2.5 L/min, respectively.....	171
Figure 6.9: Freeze-cracked [N _C /GO-20N _F /N _C] _{HP} cross-section (a) before and (b-d) after soaked in water. Arrows highlight voids and delamination due to water effect.....	172
Figure 6.10: SEM image of (a) [N _C /0.5GO _C /GO _C] _C and (b) [N _C /2.5GO _C /GO _C] _C membranes.....	174

Fig 6.11: WU (blue line) and IEC (red line) with respect to GO content in the MM without Nafion in the inner GO layer. (b) WU and (c) IEC of the multilayers with respect to Nafion content in the inner GO layer.....	175
Figure 6.12: Proton conductivity curves of $[N/xGO/N]_c$ membranes varying the RH, at (a) 80 °C, (b) 100 °C and (c) 120 °C where the $x=0$ represents single layer cast Nafion membrane.....	179
Figure 6.13: Proton conductivity of $[N_c/0.5GO-yN_c/N_c]_c$ at (a) 80 and 100 °C and (b) 120 °C.....	183
Figure 6.14: Proton conductivity of $[N_c/2.5GO-yN_c/N_c]_c$ at (a) 80 and 100 °C and (b) 120 °C. (c) Proton conductivity of $[N_c/4.5GO-yN_c/N_c]_c$ at 80 and 100 °C.....	184
Figure 6.15: Proton conductivity of $[N_c/4.5GO-yN_c/N_c]_c$ at (a) 120 °C. Proton conductivity of $[N_c/4.5GO-yN_c/N_c]_c$ at (b) 80 and 120 °C and (c) 120 °C.....	185
Figure 6.16: NFIL membranes polarization curves with 20% of RH at (a) 80 and 100 °C and (b) 120 °C. Back pressure 0.18 MPa, H_2 /Air at rate of 1 and 2.5 L/min, respectively..	188
Figure 6.17: NFIL membranes polarization curves with 40% of RH at (a) 80 and 100 °C and (b) 120 °C. Back pressure 0.18 MPa, H_2 /Air at rate of 1 and 2.5 L/min, respectively..	189
Figure 6.18: NFIL membranes polarization curves with 60% of RH at (a) 80 and 100 °C and (b) 120 °C. Back pressure 0.18 MPa, H_2 /Air at rate of 1 and 2.5 L/min, respectively..	190
Figure 6.19: NFIL membranes polarization curves with 80% of RH at (a) 80 and 100 °C and (b) 120 °C. Back pressure 0.18 MPa, H_2 /Air at rate of 1 and 2.5 L/min, respectively..	191
Figure 6.20: NFIL membranes polarization curves with 100% of RH at (a) 80 and 100 °C and (b) 120 °C. Back pressure 0.18 MPa, H_2 /Air at rate of 1 and 2.5 L/min, respectively..	192
Figure 6.21: NFIL membranes power curves at (a) 80 and 100 °C, RH =20%; (b) 120 °C, RH =20%; (c) 80 and 100 °C, RH =40%; (d) 120 °C, RH =40%; (e) 80 and 100 °C, RH =60% and (f) 120 °C, RH =60%. Back pressure 0.18 MPa, H_2 /Air at rate of 1 and 2.5 L/min, respectively.....	193
Figure 6.22: NFIL membranes power curves at (a) 80 and 100 °C, RH =80%; (b) 120 °C, RH =80%; (c) 80 and 100 °C, RH =100% and (d) 120 °C, RH =100%. Back pressure 0.18 MPa, H_2 /Air at rate of 1 and 2.5 L/min, respectively.....	194

Figure 6.23: $[\text{N}_c/4.5\text{GO-yN}_c/\text{N}_c]_c$ membrane polarization curves with RH of 20% at (a) 80 and 100 °C and (b) 120 °C. Back pressure 0.18 MPa, H_2/Air at rate of 1 and 2.5 L/min, respectively.....	196
Figure 6.24: $[\text{N}_c/4.5\text{GO-yN}_c/\text{N}_c]_c$ membrane polarization curves with RH of 40% at (a) 80 and 100 °C and (b) 120 °C. Back pressure 0.18 MPa, H_2/Air at rate of 1 and 2.5 L/min, respectively	197
Figure 6.25: $[\text{N}_c/4.5\text{GO-yN}_c/\text{N}_c]_c$ membrane polarization curves with RH of 60% at (a) 80 and 100 °C and (b) 120 °C. Back pressure 0.18 MPa, H_2/Air at rate of 1 and 2.5 L/min, respectively	198
Figure 6.26: $[\text{N}_c/4.5\text{GO-yN}_c/\text{N}_c]_c$ membrane polarization curves with RH of 80% at (a) 80 and 100 °C and (b) 120 °C. Back pressure 0.18 MPa, H_2/Air at rate of 1 and 2.5 L/min, respectively	199
Figure 6.27: $[\text{N}_c/4.5\text{GO-yN}_c/\text{N}_c]_c$ membrane polarization curves with RH of 100% at (a) 80 and 100 °C and (b) 120 °C. Back pressure 0.18 MPa, H_2/Air at rate of 1 and 2.5 L/min, respectively	200
Figure 6.28: $[\text{N}_c/4.5\text{GO-yN}_c/\text{N}_c]_c$ membrane power curves at (a) 80 and 100 °C, RH = 20%; (b) 120 °C, RH = 20%; (c) 80 and 100 °C, RH = 40%; (d) 120 °C, RH = 40%; (e) 80 and 100 °C, RH = 60% and (f) 120 °C, RH = 60%. Back pressure 0.18 MPa, H_2/Air at rate of 1 and 2.5 L/min, respectively.....	201
Figure 6.29: $[\text{N}_c/4.5\text{GO-yN}_c/\text{N}_c]_c$ membrane power curves at (a) 80 and 100 °C, RH = 80%; (b) 120 °C, RH = 80%; (c) 80 and 100 °C, RH = 100% and (d) 120 °C, RH = 100%. Back pressure 0.18 MPa, H_2/Air at rate of 1 and 2.5 L/min, respectively.....	202
Figure 6.30: Proton conductivity of $[\text{N}_c/4.5\text{GO-yN}_c/\text{N}_c]_c$ membranes at 120 °C and RH 60% before and after delamination test. Inset: $[\text{N}_c/4.5\text{GO-20N}_c/\text{N}_c]_c$ membrane after delamination cycles, the arrows highlight the three membranes layers.....	204
Figure 6.31: Cross-section of $[\text{N}_c/4.5\text{GO-5N}_c/\text{N}_c]_c$ membrane (a) before and (b) after single cell test. Cross-section of $[\text{N}_c/6.5\text{GO}_c/\text{N}_c]_c$ membrane (c) before and (d) after single cell test.....	205

LIST OF TABLES

Table 1.1: Summary of FCs types with selected properties.....	3
Table 2.1: MeOH permeability data of Nafion 117, 212, cast Nafion and Nafion/PVA membranes.....	21
Table 2.2: Characteristics of composite membranes for PEFC/DMFC compared with Nafion membranes. Where selectivity is defined as proton conductivity divided by methanol permeability.....	42
Table 2.3: Comparison of composite and multilayer approach for membrane preparation and new trends in these.....	46
Table 2.4: Proton conductivity at 100% RH as a function of the temperature and at 10% RH as a function of time.....	57
Table 2.5: Properties of hot pressed and solution cast membranes.....	58
Table 2.6: Properties of reported multilayers prepared by dip coating.....	62
Table 2.7: Routes to obtain a multilayer membrane.....	64
Table 4.1: Layer structure of the membranes prepared.....	81
Table 4.2: Volume of Nafion solution required to achieve the target thickness.....	83
Table 4.3: Approaches to cast single layer of SPInd with 50 μm of thickness.....	86
Table 4.4: Hot pressing parameters for $[\text{N}_\text{C}/\text{N}_\text{C}]_{\text{HP}}$ membrane sandwiched between aluminium foil.....	93
Table 4.5: Hot pressing parameters detailed for the multilayer membranes $[\text{N}_\text{C}/\text{SPInd}_\text{C}/\text{N}_\text{C}]_{\text{HP}}$ sandwiched between aluminium foils.....	94
Table 4.6: Hot pressing parameters for the membranes $[\text{N}_\text{C}/\text{GO}_\text{F}/\text{N}_\text{C}]_{\text{HP}}$	96
Table 4.7: Hot pressing parameters for the multilayer membranes with PTFE sheets cover.....	100
Table 4.8: Parameters to dry each layer of the membrane $[\text{N}_\text{C}/\text{SPInd}_\text{C}/\text{N}_\text{C}]_\text{C}$	104

Table 4.9: Properties of $[N_c/SPInd_c/N_c]_c$ varying the content of Nafion in the inner layer of SPInd.....	107
Table 4.10: Detailed layers composition of $[N_c/SPInd_c/N_c]_c$ membranes.....	109
Table 4.11: Summary of the membranes preparation methods.....	115
Table 5.1: Detailed physical properties of the membranes.....	123
Table 5.2: Comparison between the membranes proton conductivity with low humidity at 80, 100 and 120 °C.....	129
Table 5.3: Detailed properties of single and multilayer membranes.....	135
Table 5.4: Membranes activation energy at the temperature range of 80-120 °C and with 100% of relative humidity.....	140
Table 5.5: Membranes detailed voltages and power.....	152
Table 6.1: Detailed values of water uptake and ion exchange capacity.....	178

GLOSSARY OF TERMS AND ABBREVIATIONS

AFC	Alkaline Fuel Cell
C	Casting
CNT	Carbon Nanotube
DAFC	Direct Alcohol Fuel Cell
DEFC	Direct Ethanol Fuel Cell
DI	Deionized
DMF	Dimethylformamide
DMFC	Direct Methanol Fuel Cell
DMSO	Dimethyl sulphoxide
DOE	US Department of Energy
DSC	Differential scanning calorimetry
EDS	Energy Dispersive X-ray Spectroscopy
ESEM	Environmental scanning electron microscope
F	Filtration
FC	Fuel Cell
FT-IR	Fourier infrared spectroscopy
GDE	Gas diffusion electrode
GO	Graphene Oxide
HP	Hot pressing
HT-PEFC	High Temperature Polymer Electrolyte Fuel Cell
IEC	Ion Exchange Capacity
IT-PEFC	Intermediate Temperature Polymer Electrolyte Fuel Cell
MCFC	Molten Carbonate Fuel Cell
MEA	Membrane Electrode Assembly
MM	Multilayer membranes
N	Nafion

NFIL	Nafion free-inner layer
OT	Operation temperature
PAFC	Phosphoric Acid Fuel Cell
PBI	Polybenzimidazole
PDDA	Poly(diallyldimethylammonium chloride)
PEFC	Polymer Electrolyte Fuel Cell
PEM	Proton Exchange Membrane
PFSA	Perfluorinated sulphonic acid
PInd	Polyindene
PTFE	Polytetrafluoroethylene
PVA	Polyvinyl Alcohol
PVA	Poly(vinyl alcohol)
RH	Relative humidity
SEM	Scanning electron microscope
SOFC	Solid Oxide Fuel Cell
SPInd	Sulphonated polyindene
T _g	Glass Transition Temperature
TGA	Thermogravimetric analysis
W _d	Dry weight
WU	Water Uptake
W _w	Wet weight
XPS	X-ray photoelectron spectroscopy
XRD	X-ray diffraction
λ	Hydration number
σ	Proton conductivity

CHAPTER I – INTRODUCTION

In recent years, the general concern about environmental issues has led to extensive research and discussions about sustainability and cleaner technologies in all spheres. In the energy field, renewable green energy sources such as wind, solar and others have been highlighted. Fuel Cells (FCs) are one of these greener alternatives. They are simple devices, which transform chemical energy, for instance of hydrogen, directly to electrical energy with only heat and water as by-products. Thus, there are no SO_x, NO_x, CO₂ and CO emissions (mainly responsible for the greenhouse effect) unlike in combustion engines running on fossil fuels. Besides this, FCs have the unique quality of using a variety of fuels and are not limited to resources such as fossil fuels.

Since the discovery of the fuel cell principle by Grove and Schönbein in the 19th century [1], FCs have evolved considerably; however, the general concept remains the same and is presented in Figure 1.1. In the cell, there is one anode and one cathode separated by an electrolyte. The anode is fed with hydrogen (fuel). The hydrogen molecule is broken in two electrons and two protons. The protons are transported through the electrolyte, while the electrons are transported through an external electrical circuit to reach the cathode. In the cathode, which is fed with air, an oxygen atom combines with two protons and two electrons generating water and heat. FCs are not only a promising technology. They are already being applied commercially with success in the automotive industry, portable devices, off grid buildings, small boats, and other applications.

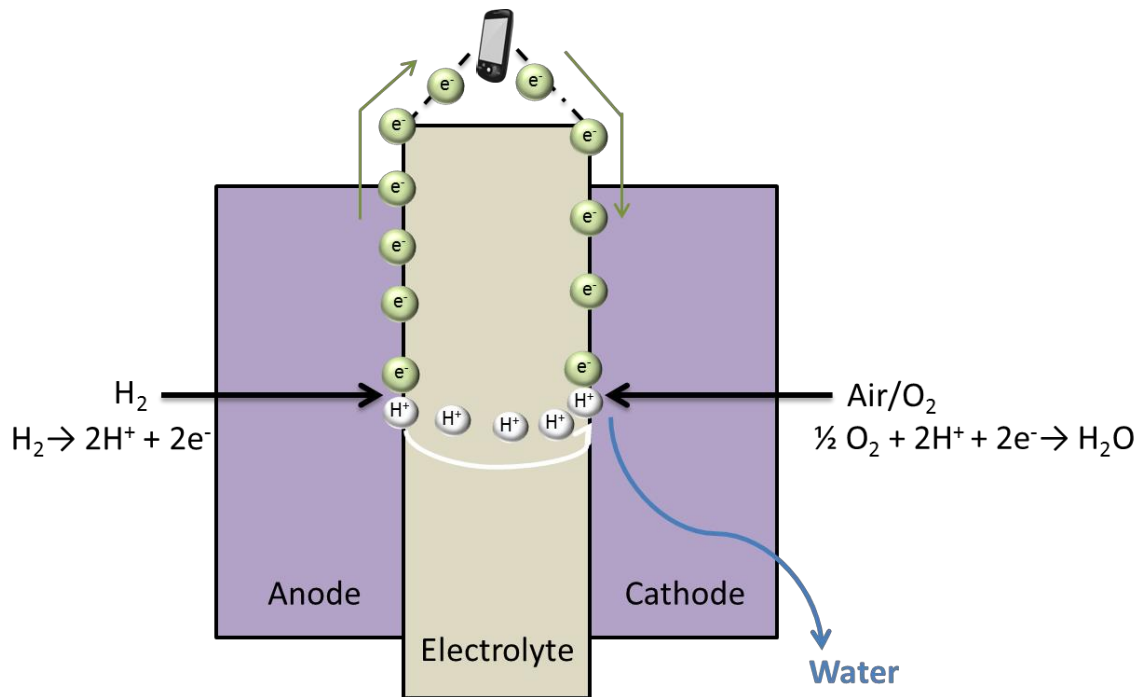


Figure 1.1: Schematic view of a general fuel cell.

Although the fuel cell concept is very simple, there are many types of FC, which can be classified into different categories. In this study, FCs will be classified according to the nature of their electrolyte. These groups, along with some of their properties, are summarised in Table 1.1. The first group is Alkaline Fuel Cell (AFC) in which the electrolyte is a strong alkaline base such as KOH. AFCs were one of the first successful FCs, and were part of the energy supply of the NASA spaceships from as early as 1959 onwards [1]. AFCs present low power and operate at low temperatures. Unlike all others FCs, hydroxide ions and not protons diffuse through the electrolyte, with reverse ion movement than presented in Fig.1.1 [2]. The next group is the Polymer Electrolyte Fuel Cell (PEFC), in which the electrolyte is a proton exchange membrane (PEM) as shown in Fig 1.1. The PEFC is one of the most studied FC and it is especially suited for mobile applications such as cars due to the low temperature operation, high power density and low weight compared with other FC groups.

Companies such as Toyota and Hyundai have commercialised the firsts PEFC passenger cars in the past two years, while Honda started to sell their model in 2016 [3, 4]. In PEFCs, there is a sub-group denominated Direct Alcohol Fuel Cell (DAFC) which has the same components than a regular PEFC but is supplied with an alcohol and not hydrogen in the anode. The main DAFCs are the Direct Methanol Fuel Cell (DMFC) and the Direct Ethanol Fuel Cell (DEFC) supplied with methanol and ethanol, respectively. The third group is the Phosphoric Acid Fuel Cell (PAFC). Although there are many studies in doped PEM with phosphoric acid for PEFC [5-7], the PAFC differentiates from PEFC because the acid electrolyte is trapped in the liquid form in a silicon carbide [8] and not in a polymer. The following group is the Molten Carbonate Fuel Cell (MCFC) and together with the next group is classified as high temperature FC, operating above 650 °C [8]. The last group has been intensely studied too, and is called Solid Oxide Fuel Cell (SOFC) in which the electrolyte is a solid ceramic. It has high electrical efficiency (>60%) [9] and is dedicated, together with MCFC, specially for stationary applications operating on natural gas.

Table1.1: Summary of FC types with selected properties (Adapted from [8, 10, 11]).

Type of FC	Electrolyte	Ion transported	Temperature (°C)	Power
AFC	Strong base	H ⁺	50 – 200	W/kW
PEFC	Polymer membrane	OH ⁻	60 – 200	W/kW
PAFC	Phosphoric acid in silicon carbide	H ⁺	220	kW
MCFC	Molten carbonate in aluminium oxide	CO ₃ ⁻	>650	kW/MW
SOFC	Zirconia	O ⁻	500 – 1000	kW/MW

The main components of a PEFC are the two bipolar plates, two electrodes (anode and cathode), gas diffusion layers and a polymeric electrolyte. The bipolar plates are

manufactured with a conductive material. Graphite is widely used in academic research, however due to difficulties in machining graphite, it has been avoided commercially [12]. Metallic plates are more used due to the easy machining and high elasticity, such as with stainless steel [12, 13]. The plates represent a considerable part of PEFC costs and weight [14]. The flow channels, in which hydrogen and air/oxygen are transported for the electrodes, are stamped into the bipolar plates. Figure 1.2 presents the exploded view of the fuel cell stack.

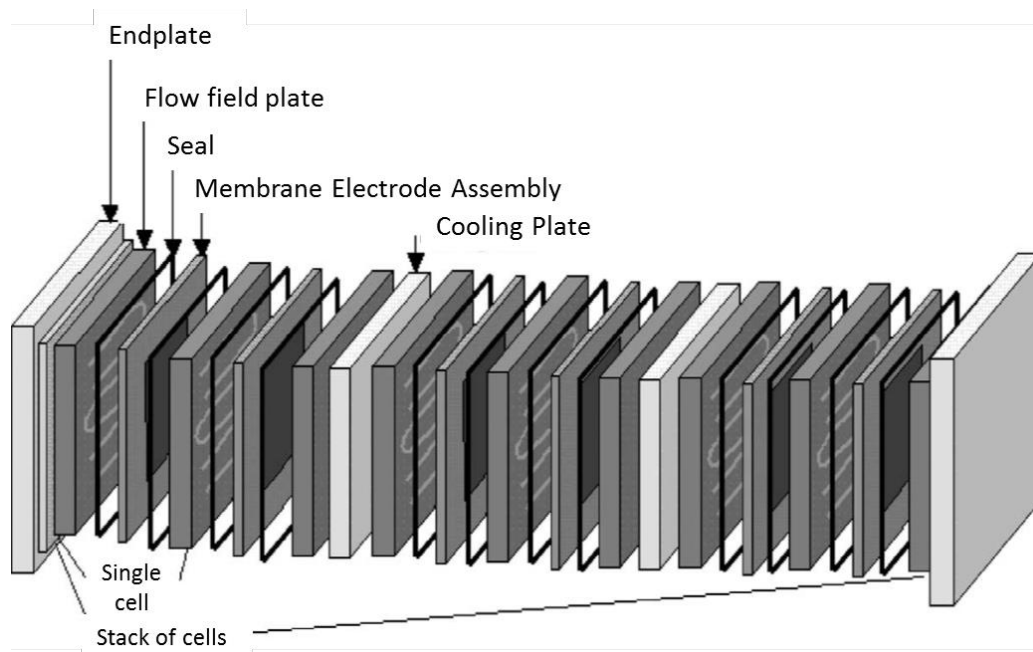


Figure 1.2: Fuel cell stack exploded view [15].

The electrodes are composed with a catalyst, a support material and polymer binders. The catalyst mostly used is platinum; however, it is subject to contamination with carbon monoxide impurities from the fuel gas. Therefore, the fuel must be pure, increasing the PEFC general cost. The most common support material usually is carbon black. The electrodes are applied on the surface of a gas diffusion layer, usually carbon paper or fabric. One of the biggest challenges in PEFC is to reduce the amount of Pt used [16]. Pt is a rare metal of high

cost; therefore, the reduction in Pt content decreases the PEFC cost considerably. The United States Department of Energy (DOE) determined in a report in 2015 [17] that the cost of an automotive PEFC with 80 kW project to 2016 is \$53/kW with a volume of 500000 units produced per year. The reduction in the cost is based on the use of a low Pt content catalyst (PtNi). DOE targets the cost for 2020 to be \$40/kW with the same amount of units.

Gaskets are another component, commonly made with PTFE, and are used to seal the membrane, electrodes, gas diffusion layer and bipolar plates. A polymeric membrane forms the inner layer (as the proton conducting electrolyte) of a PEFC single cell. Together with the electrodes, it forms the Membrane-Electrode-Assembly (MEA). The main function of the membrane is to transport protons. Therefore, the membrane should have three essential properties: i) proton conductivity; ii) electronic insulation; iii) gas impermeability. Besides the obvious proton conductivity to allow proton transport, the electron insulating property is essential to guarantee that all electrons are transported through the external circuit to enable a current. If the membrane is gas permeable, the oxygen and the hydrogen will react inside the membrane generating hot spots and further degradation. Although these properties are well established, in the actual commercial membranes issues still persist. Many solutions have been tested in membrane studies and this is discussed in detail in the next chapter.

The most common membranes are the perfluorinated sulphonic acid (PFSA) with two phases: hydrophobic and hydrophilic [18]. Among the commercial PEMs, the most successful is Nafion® from Du Pont Co. It is a polymeric membrane first developed in the 1960's [19] for electrochemical filtration and separation of specific ions [20]. However, due to the presence

of sulphonic acid groups, Nafion's transition for PEFC applications was natural. These acid groups are responsible for water retention in Nafion. This is essential for proton transport through vehicular and hopping mechanisms, which will be discussed in the next chapter. However it is important to highlight that there are three types of water in the membrane structure: free ones, lightly bound ones, and strongly bound ones. Free water is easily eliminated when the fuel cell is heated. The strongly bound water is stable with the bonds with the polymer structure, and is not available to bond with the proton coming from the anode. Thus, these types of water do not participate in the proton transport. The lightly bound one is the water responsible for the proton transport. This kind of water is the challenge to increase in the membrane.

The usual PEFC operation temperature is between 80 – 100 °C. However, when the operating temperature is increased to values between 100 – 120 °C, the fuel cell is called Intermediate Temperature PEFC (IT-PEFC). At these (IT-PEFC) conditions, there are some notable advantages in the fuel cell operation. These include: a) chemical reactions of hydrogen oxidation and oxygen reduction are accelerated, increasing the fuel cell efficiency [21]; b) easier heat management: as the operating temperature is increased, the temperature difference between external environment and the fuel cell also increases and heat rejection and removal by heat exchangers is facilitated, this will allow the IT-PEFCs cooling system to be simplified, reducing weight and costs of the system [21, 22]; c) easier water management: at low temperature, two phases of water (liquid and gas) are present, which makes it difficult to define the water behaviour inside the PEFC. Moreover, water transported with the gas flow for humidification can condensate in the flow channels inducing flooding and consequently reducing the gas flow. Optimising the value of

backpressure, water will only exist in vapour phase inside the IT-PEFC, making the humidity balance easier to manage [21-23].

Despite all these major advantages that improve the general performance of a PEFC, there are some drawbacks in the applicability of an IT-PEFC. The main issue is membrane functionality. At low gas humidification at intermediate temperatures, Nafion and regular PFSA membranes cannot hold water [24, 25]. Therefore, the insufficiently humidified membrane is not able to transport enough protons to sustain the FC performance. Thus, in IT-PEFC with Nafion, the gas humidification system is complex, increasing the general cost of the fuel cell. Accordingly, alternative membranes for IT-PEFC systems are necessary.

In this work two sets of multilayer membranes were designed for operating in IT-PEFC at low humidification. Set A was composed of Nafion external layers and sulphonated polyindene (SPInd) in an inner layer. Set B was composed of Nafion external layers and graphene oxide (GO) in an inner layer. SPInd is a hydrophilic polymer with outstanding proton conductivity. GO is also highly hydrophilic and extremely thermal resistant. Because of this, both can be suggested for IT-PEFC use. Further discussion about the reason for the selection of both materials is presented in the following chapters. To compare the different behaviours due to the nature of the materials in the multilayer membrane and the interfacial interaction, a control group with Nafion and its bilayers was prepared. Besides the influence of the materials, the routes to make the membranes were studied. The chosen mechanisms were hot pressing (HP) and casting. The summary of the work developed within this thesis is shown in the schematic illustration in Figure 1.3.

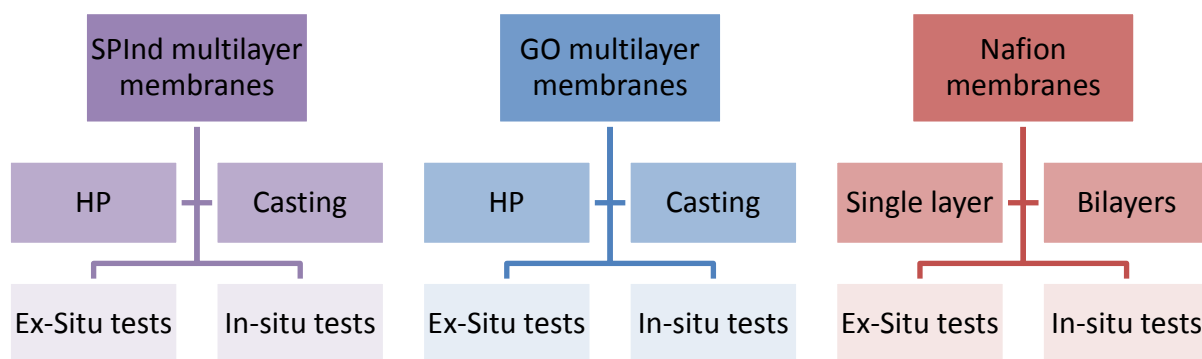


Figure 1.3: Schematic of the membrane groups developed in this study.

1.1. Objectives

The aim of this work is to develop a multilayer membrane to be used as a PEM in IT-PEFC. The membrane consists of two external layer of Nafion and an inner layer of a different material, which can be inorganic graphene oxide (GO) or the organic polymer SPInd as seen in Figure 1.4. Each one of the materials will provide specific characteristics such as the high hydrophilicity from GO and proton conductivity from SPInd.

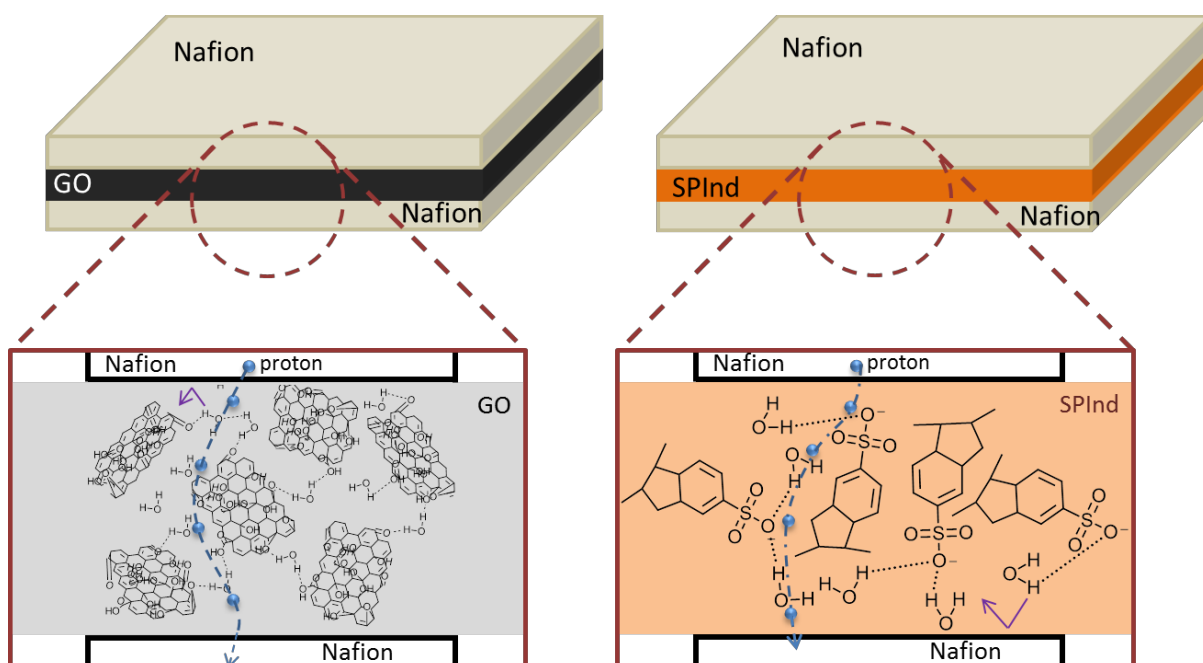


Figure 1.4: Two multilayer membrane structures aimed at this work. On the left Nafion/GO/Nafion and on the right N/SPInd/N. In the insets the proposed mechanisms of proton transport, both through water bridges and functional groups, are shown.

The objective is to evaluate the influence of membrane preparation methods on the fuel cell performance and properties such as proton conductivity and water retention. The two methods analysed were hot pressing and casting. Furthermore, the objective is to investigate the interface behaviour due to the choice of inner layer material or preparation method. For those results to be achieved the following items need to be addressed:

- Influence of the material inner layer and preparation method on the membrane water retention.
- Influence of the material inner layer and preparation method on the membrane proton conductivity.
- Relation between fabrication method/membranes material on delamination.
- Optimum composition in each group of membranes.

1.2. Thesis Structure

The thesis is divided into seven chapters. Here is a short summary of what each chapter presents:

Chapter I: Introduction

Chapter II: A Review of IT-PEFC Membranes – This chapter focuses on the membranes reported in the literature for PEFC, especially IT-PEFC. It discusses properties of the membranes such as transport of protons. The composite and multilayer membranes developed for fuel cells are presented and based on this discussion the membranes studied in this thesis are chosen.

Chapter III: Synthesis of Materials – Covers the synthesis and preparation of the base materials for the multilayer membranes, GO and SPInd, and the reason why these two materials were selected. It also discusses the materials characterization.

Chapter IV: Membranes Preparation – This chapter summarizes all the membranes prepared in this work and the optimization of the fabrication methods. The membranes are divided in three main groups, membranes with SPInd, membranes with GO, and Nafion membranes. The preparation methods used are casting and hot pressing.

Chapter V: Influence of SPInd on the Membrane Performance – Contains the main results for the SPInd inner layer membranes prepared by casting and hot pressing. It discusses the influence of SPInd sulphonic groups on the water retention and whether this leads to a better performance; both preparation methods are compared.

Chapter VI: Influence of GO on the Membrane Performance – Analyses the membranes with an inner layer of GO and its high hydrophilicity as an influence on the PEFC operation temperature; also compares the preparation methods.

Chapter VII: Summary and Perspectives – This last chapter presents the main conclusions of this study and suggests future studies based on the present one.

CHAPTER II – A REVIEW OF IT-PEFC MEMBRANES¹

Proton exchange membranes are a sub-category of ion exchange membranes, which have been used quite successfully in diverse industries and applications (such as dialysis, electrolyzers, and desalination of water, amongst others) [26-28] before the advent of the PEFC. PFSA polymers, usually fluorinated copolymers of tetrafluoroethylene-co-sulphonic acid monomers with high thermal and chemical stability, are the most successfully used commercial membranes for PEFC and alcohol fuel cells. The PFSA membranes have two phases: a hydrophobic phase consisting of tetrafluoroethylene (PTFE) forming the backbone (Figure 2.1, block m) which provides mechanical strength, and a hydrophilic phase consisting of side chains having a sulphonic acid group (Fig. 2.1, block n) which is responsible for the proton transport [24, 29].

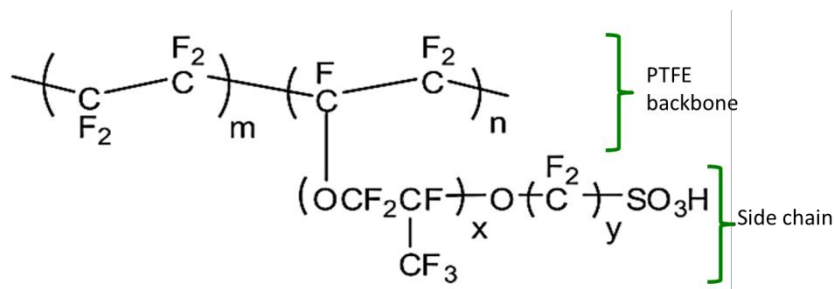


Figure 2.1: Nafion chemical structure (adapted from [30]).

In these PFSA membranes proton conductivity is due to the side chains separated from the main carbon chain, thus forming polar and non-polar regions. Proton transport through the electrolyte membrane can occur by the Grotthuss (also called hopping mechanism) and

¹ Part of this chapter is based on the published paper *New approaches towards novel composite and multilayer membranes for intermediate temperature-polymer electrolyte fuel cell*, 2016. See page 210.

vehicular (diffusion) mechanisms [29, 31]. According to the Grotthuss mechanism, protons that are linked to the sulphonic groups combine with water molecules in the hydronium (H_3O^+) form. A proton of the hydronium is then transferred to another water molecule bonded to a nearby sulphonic acid group (Figure 2.2), and these water molecules form the 'Water Bridge'. Thus, the proton hopping occurs through the network of hydrogen bonds. The higher the water molecule content attached to sulphonic acid groups (hydration number - λ), and the closer the water molecules are to each other, the faster proton the transport (facilitated between the SO_3^- groups) through the membrane. λ is defined as the number of water molecules per sulphonic acid group. On the other hand, according to the vehicular mechanism, the proton in the hydronium H_3O^+ ion, due to electrochemical differences, diffuses through the membrane with water molecules [32]. Although it is possible that both mechanisms are active simultaneously, the Grotthuss mechanism is considered to be the preferred and faster mechanism [33, 34].

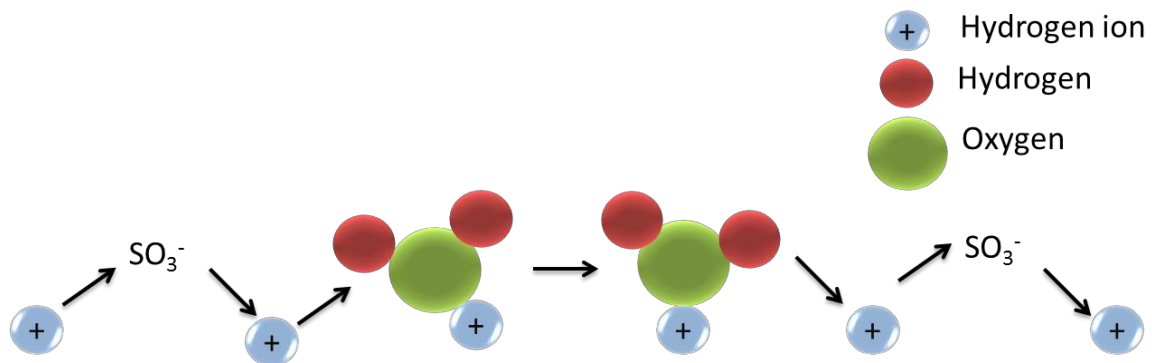


Figure 2.2: Schematic of Grotthuss mechanism scheme showing the proton movement between sulphonic acid groups in the hydronium form.

The most successful commercial PFSA membrane is Nafion[®], developed in the early 1970s by DuPont. The chemical structure of Nafion[®] consists of PTFE sequences with and without side

chains of perfluoroether, that end in sulfonic acid groups ($-\text{SO}_2\text{OH}$) (such as the fluoro 3,6-dioxo 4,6-octane sulphonic acid shown in Fig. 2.1). Other companies also made their own Nafion-like membranes, such as Flemion[®] from Asahi Glass Company Ltd, and the Dow membrane, developed by Dow Company [32]. Nonetheless, in spite of the extensive studies on polymer membranes to substitute Nafion, no reported membrane has so far achieved a performance comparable to that of Nafion in PEFC. There are many types of Nafion, but the most used for PEFC and DMFC are Nafion 117 and Nafion 212. Both membranes have an equivalent weight of 1100 g/eq, but the thicknesses are 180 and 50 μm , respectively.

Although some other membranes may exhibit certain properties that are better than Nafion, so far none seem to have the optimum balance between all the properties that demonstrated by Nafion. However, Nafion still suffers from various drawbacks like degradation due to dry conditions during start stop cycles, and due to fuel crossover, especially in DMFC systems, leading to a loss of cell performance as revealed by various long-term studies [35-38]. Moreover, recent studies [39-41] investigating the performance of membranes in IT-PEFC, suggest the need to develop new membranes which can solve specific problems faced by PEMs in this kind of environment. Operating at higher temperatures not only enables faster reaction kinetics for hydrogen oxidation and oxygen reduction but also a) enables better catalytic activity due to reduced poisoning from CO and other gases, and b) facilitates water management and removal [42]. However, the operation of IT-PEFC at temperatures between 100-120 $^{\circ}\text{C}$ means the PEM needs to be more robust, especially towards low humidity conditions, in order to maintain proton transport properties and prevent membrane degradation [38, 43].

While proton transport in hydrated membranes is commonly explained by the formation and cleavage of hydronium bonds, thermodynamically this route is not the most favourable. There are two widely accepted structures involving hydronium: the Zundel (H_5O_2^+) cation and Eigen (H_9O_4^+) cation complex (Figure 2.3). In the Zundel H_5O_2^+ complex, two water molecules in symmetric hydrogen bond share the proton equally. In the Eigen solvated structure, the hydronium ion is at the centre of the H_9O_4^+ complex and is strongly bonded to three neighbouring water molecules via hydrogen bonds [44]. Both complexes represent the ideal structures in a more general hydrogen bond network and define the diffusion of the hydrogen-bond structure in which the excess proton is transported/tunnelled back and forth. It is thought that both the complexes transform into each other and act as donors of protons by the formation and cleavage of hydrogen bonds. These bonds are not as strong as those in simple hydronium structures and therefore enable a faster proton transfer [44].

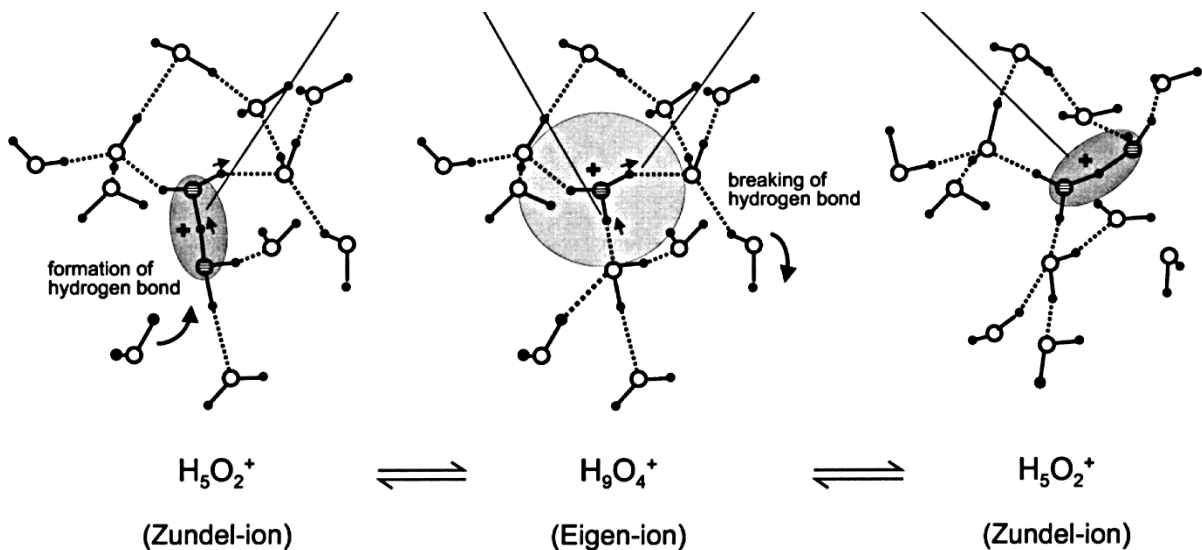


Figure 2.3: Zundel-ion and Eigen-ion structures showing the formation and cleavage of hydrogen bonds for the protons transport in a hydrated membrane. [44]

Proton diffusion, independent of transport mechanism, increases as temperature and membrane hydration level increase. Feng and Voth [45] in a modelling study investigating transport of protons have revealed that for λ values between 6 and 15 and for temperatures between 25 °C to 67 °C, the Grotthuss mechanism has a higher diffusion ratio than that of the vehicular mechanism. As the temperature and value of λ increase, the Grotthuss mechanism becomes more dominant. The activation energy available for proton transport drops for λ values less than 10 due to the different solvation structure at this level of hydration. Beyond this exception, the activation energy increases with λ being almost the same as in pure water when λ is 15. The indispensability of water to proton transport, as established by the various proton transport and diffusion mechanisms, underlines the importance of incorporation of hydrophilic groups in Nafion or any other PEMs to enable higher proton conductivity especially at elevated temperatures. Therefore, if a hydrophilic group is added, the water retention would improve resulting in better proton conductivity. This is the concept behind all composite membranes. Another new concept under investigation to achieve better PEMs, is the use of multilayer membranes. A multilayer design can bring together layers of different polymers each adding its unique characteristic property (mechanical strength, non-permeability, better water retention, etc.) to the multilayer membrane, eliminating the need for compromising one property for another when choosing a PEM material.

This chapter focuses on the new developments in composite and multilayer membranes for IT-PEFC and DMFC, highlighting the various unique and novel approaches towards multilayer membrane development. The composite membranes section covers both organic and inorganic filler membranes. This is followed by extensive analysis of recent reports on

multilayer membranes for use in IT-PEFC and DMFC, which led to the proposed membranes used in this study.

2.1. Composite membranes

Polymeric composites are materials with a polymeric matrix and a filler or reinforcement, which can be another polymer, ceramic or metal. The fillers used in PEM usually are ceramic or polymeric. The two components must have separate phases. The filler is used to improve one or more polymer properties or reduce the material costs. The routes to produce composite polymer membranes are similar to any other composite polymer. However, composite membranes can be considered as one of the first attempts to develop something better and challenge the existing industry standards.

The advantage of the use of composite membranes over blended membranes is that the properties of the filler and matrix are preserved and can give other characteristics that are not possible with blended membranes. Sulphonic acid groups are highly hydrophilic and for this reason many polymers are commonly sulphonated. Numerous studies have been reported on Nafion and other sulphonated polymers with the aim of improving the PEM properties such as mechanical resistance, proton conductivity, chemical and thermal stability, water uptake etc. [32, 33, 46-51]. Some of the aspects analysed have been inorganic fillers, cross-linked polymers, use of alternative solvents during membrane casting etc. A selection of these approaches is briefly discussed here. Donnadio *et al.* [52] developed a sulphonated poly(ether sulphone) (SPES) membrane with 34% degree of sulphonation (DS), and zirconium phosphate as filler. Their results revealed a maximum membrane conductivity of $4.5 \times 10^{-2} \text{ S.cm}^{-1}$ at 100 °C and 90% relative humidity (RH). The authors found

the conductivity of the membrane to be very stable up to 120 °C at 75% RH. The conductivity values for the SPES membrane, however, were found to be lower than those of Nafion 117. Park *et al.* [53] prepared a cross-linked sulphonated poly (arylene ether sulphone) (SPAES) membrane for DMFC application. Their crosslinked SPAES membranes revealed less water uptake, lower methanol permeability, and good mechanical and thermal strength compared to non-crosslinked membranes. Single cell DMFC testing of the membranes showed a performance similar to that of Nafion 115. Jun *et al.* [54] prepared a sulphonated poly(ether ether ketone) (SPEEK) membrane and analysed the effect of different polymer solvents on the resultant cast membrane for use in PEFCs. For the solvents, the authors used N-methyl-2-pyrrolidone (NMP), dimethylacetamide (DMAc), and dimethylformamide (DMF), and observed that the cast membrane prepared with NMP as the solvent showed a performance similar to that of Nafion 117. With this study, the authors brought to light the importance of the choice of casting solvent as well as the membrane activation treatment in determining the performance of a cast membrane. Silva *et al.* [55] used a sulphonated poly (styrene-co-acrylonitrile) membrane as PEM. Although the studies mentioned above contributed towards understanding the behaviour of proton transport through a sulphonated polymer, the sulphonated polymers or their blends usually did not achieve all the Nafion characteristics. This has led to the investigation of composite membranes that could be loaded with fillers in order to upgrade a given property such as mechanical resistance, proton conductivity, water uptake, gas barrier, or reduced fuel crossover and stability. In the case of the IT-PEFC, the use of composite membranes could help avoid Nafion degradation during operation at elevated temperatures.

Composite membranes can be loaded with organic or inorganic fillers. Some of the organic fillers are reinforcement polymer fibres or particles such as PTFE. Inorganic fillers are metal oxides and carbon based materials. Both inorganic and organic fillers have been used predominantly to increase proton conductivity and to act as a barrier to gas permeation. The following sub-sections concisely discuss the latest developments in the organic and inorganic filler based membranes.

2.1.1. Organic fillers

Organic materials are commonly used fillers in the polymeric composite membranes for FCs. They supply reinforcement and allow higher stability of the matrix polymer while making it more cost effective. The most commonly applied organic filler is PTFE fibre reinforcement. For example, Wang *et al.* [56] reported the membrane preparation of a sulphonated polyimide matrix. However, recent investigations show more inclination towards using inorganic or mixed organic/inorganic fillers in polymeric composite membranes which have been discussed extensively in previous reviews by Li *et al.* [57], Ahmed *et al.* [58], and Li *et al.* [59]. The development of organic composite membranes using a porous sheet with the conductive polymer solution has also been reported in the literature [60, 61]. Wu *et al.* [60] studied the accelerated stress degradation of the MEA in a PEFC where the PEM was a porous PTFE support impregnated with Nafion solution.

In a similar way Lu *et al.* [61] prepared a membrane with porous PTFE support impregnated with a solution of poly(ethersulphone)-poly(vinylpyrrolidone) (PES/PVP) and doped further with phosphoric acid. Figure 2.4 shows the cross sections of the membranes with different amounts of PTFE as prepared by the authors. In this case, the (PES/PVP) formed the

hydrophilic phase, which provides the proton conductivity, while the (PTFE) formed hydrophobic phase providing mechanical support and structure to the membrane. The authors found that the PEFC performance at 150 °C was considerably superior for the PTFE reinforced membrane and the best result was obtained at 180 °C with a 3% PTFE membrane without any humidification. A particular problem in this kind of membrane preparation is the low compatibility of the PTFE and PES/PVP due to the hydrophobicity of the fluorinated polymer. However, doping the membrane with phosphoric acid is reported to improve the interaction between the polymers. Although this membrane is not labelled as a multilayer membrane, this work can be seen as a transitional study between composite and multilayer membranes.

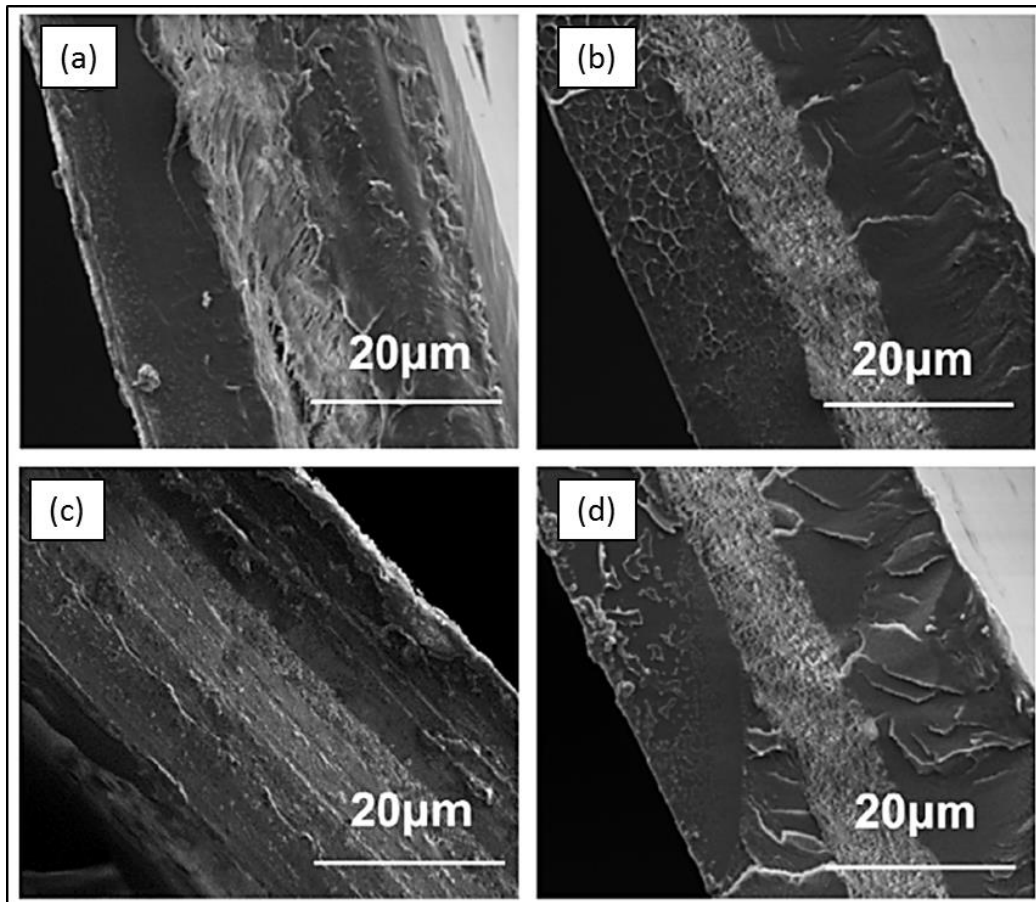


Figure 2.4: SEM micrographs of the PES/PVP membranes (a) without, with (b) 3%, (c) 5% and (d) 7% of PTFE. [61]

Organic composite membranes have also been used in DMFCs. In a recent study, Alvarez *et al.* [62] used polyamidoamine dendrimers as fillers in a Nafion matrix with the aim to avoid methanol crossover. Methanol crossover is one of the major issues affecting long-term performance of the DMFC system, as it leads to cathode catalyst poisoning and consequent a drop in OCV values. The investigations by Alvarez *et al.* [62] revealed that the methanol crossover was lower in the composite membrane when compared to recast Nafion in a DMFC single cell system operating at 100 °C with 2 M methanol. In another study, Lin *et al.* [63] evaluated porous PTFE impregnated Nafion membranes for use in DMFC. The single cell test was carried out at 70 °C with 2 M methanol for Nafion 117, Nafion 112, and PTFE/Nafion membranes. The data revealed that the power density as well as the current density were considerably higher (5 mW cm^{-2} , 350 mA cm^{-2}) for the polarisation studies carried out using composites membranes than those with Nafion membranes. The authors emphasised that even with lower proton conductivity than Nafion, the performance of the PTFE impregnated membranes was superior to that of Nafion because of the PTFE's ability to reduce the methanol crossover and minimise further degradation of the membrane.

Lin *et al.* [64] prepared a composite membrane for DMFC which was composed of a porous thin film of crosslinked poly(vinyl alcohol) (PVA) nanofiber impregnated with Nafion. The conductivity of the composite membrane was found to be lower than that of Nafion membranes, because, similar to PTFE, PVA is a non-conductive material. Furthermore, similar to the results for PTFE impregnated Nafion membranes, the voltage data obtained in a DMFC single cell operating with 2 M methanol with Nafion PVA impregnated membranes were superior to that of Nafion 117, 212, and cast Nafion membranes. Here again, it is the reduced methanol crossover (Table 2.1), which enables better membrane performance in

the DMFC environment. Due to the unique membrane microstructure of PVA nanofibers, it offers increased tortuosity making it difficult for the methanol molecules to cross over.

Table 2.1: MeOH permeability data of Nafion 117, 212, cast Nafion and Nafion/PVA membranes [64].

Membrane	P ($10^{-6} \text{ cm}^2 \text{ s}^{-1}$)	p = P/L ($10^{-4} \text{ cm s}^{-1}$)
$C_a = 2\text{M}$ (6.41 wt%)		
Nafion – 117	4.20 ± 0.09	2.4 ± 0.05
Nafion 212	4.73 ± 0.06	9.4 ± 0.1
Nafion – cast	5.09 ± 0.07	9.84 ± 0.02
N/VA-f-9.5-0.5	3.47 ± 0.07	6.6 ± 0.1
N/VA-9-1	2.83 ± 0.05	5.7 ± 0.1
N/VA-f-8-2	2.74 ± 0.09	5.3 ± 0.2
N/VA-b-9.5-0.5	4.11 ± 0.09	8.4 ± 0.2
N/VA-b-9-1	3.22 ± 0.05	6.2 ± 0.1

*P is the methanol permeability, L is the membrane thickness, and p is the rate of methanol permeability per unit of membrane thickness. C_a = MeOH concentration.

Organic composite membranes have been reported in the literature since the earliest papers about PEM [57, 65]. These early studies have already suggested that inorganic-organic composite membranes should be the approach of the future. Especially, since most investigations on organic composites use PTFE as filler or matrix. As seen in the papers discussed above, PTFE is a hydrophobic, ionic insulator. As such, it is expected neither to improve the proton conductivity nor to enable better water retention at high temperatures. It only acts as a barrier to reduce the fuel crossover enabling improved PEM efficiency in DMFC, DEFC which is subject to standard PEFC conditions only. However, some inorganic filler are capable of providing a barrier as well as increase the proton conductivity. Consequently, this has generated more interest in inorganic fillers and this shift in trend can be seen from the large number of studies published focussing on this subject over the last few years.

2.1.2. Inorganic fillers

Inorganic nanoparticles provide many advantages when added to a polymeric matrix due to their different nature providing new properties to the composite, especially improving mechanical strength. The variety of fillers can be divided into categories based on the properties offered or according to the type of materials. Zhang *et al.* [33], in a detailed review on polymer electrolyte membranes, classified the inorganic fillers used in composite membranes into three categories: i) inert hygroscopic, ii) proton conductivity, iii) hydrophilic and proton conductivity. The inert fillers in the first category are used specifically to decrease the fuel crossover and hold water. As they are hygroscopic, the water molecules are adsorbed onto them even under high temperature and low humidity conditions. These kinds of fillers may not always enable higher conductivity. The second category includes the fillers with high elastic modulus because of which they assure stability in the proton conductivity at higher temperatures. In the third category, fillers are both proton conductors and hygroscopic, and usually are sulphonated hygroscopic materials from the first group. Most of the literature reports are particularly focussed on the groups i and iii.

The present study categorises the fillers based on the material used, and are classified into two categories, namely i) metal oxides, and ii) carbon nanostructures. The metal oxides are inert hygroscopic materials, as in the first category of Zhang *et al.* [33], and are the most extensively used materials as fillers in fuel cell membranes. The second category of fillers can be further sub-divided into two groups based on the nanostructure of the carbon material: a) carbon nanotubes, and b) graphene oxide. These two carbon nanostructures have been

actively investigated in their native as well as various chemically modified forms due to their unique structural and chemical properties.

2.1.2.1. Metal Oxides

Certain hydrophilic metal oxides are known to increase the water up-take of PEM significantly, which facilitates the proton transport via the Grotthuss mechanism. Among the metal oxides, one of the most widely researched materials is silicon oxide. Other common metal oxides used for this purpose include TiO_2 [66, 67], ZrO_2 [68], and Fe_3O_4 [69].

Adjemian *et al.* [70] introduced hydrated SiO_2 (via sol-gel method) in the Nafion hydrophilic channels to improve the water retention for use in a PEFC above 100 °C. The authors reported that under high humidity conditions, the power density and voltage of the Nafion based system was higher than when a composite membrane was used. However, under low humidity condition better performance was achieved with the SiO_2 /Nafion membrane (with 6 wt.% of SiO_2), which was attributed to the higher water uptake of the membrane due to the presence of SiO_2 . However, the SiO_2 /Nafion membrane did not display the same stability as the Nafion membrane and when the long-term performance was compared, the composite showed poor performance under all tested conditions. In another study, Ke *et al.* [71] prepared Nafion/ SiO_2 composite membranes using an in-situ sol-gel method to achieve better size control over the SiO_2 nanoparticles. They performed studies with SiO_2 nanoparticles of 4 different sizes between 5-15 nm diameter particles, and reported that 10 nm SiO_2 particles resulted in the best performance in comparison to unmodified Nafion at high temperature (110 °C) and low humidity (59% RH). This study however, did not look into the long-term durability of the composite membrane. Kim *et al.* [72] used silica with other

polymers (sulphonated urethane acrylate-*co*-styrene and sulphonated polyimide) to obtain membrane for PEFC studies using a new preparation method, i.e. an *in-situ* surface grafting reaction of reactive dispersion of silica nanoparticles to obtain better nanoparticle dispersion even in higher concentrations. In another study, Thiam *et al.* [73] used Pd-SiO₂ nanofibers as filler in order to decrease methanol permeability of Nafion membranes for DMFC use. As SiO₂ is a hygroscopic material, when added in a polymer matrix, it holds water especially in low humidity conditions, and consequently these membranes show superior performance under extreme conditions. Pd being an electrochemical catalyst would enable the oxidation reaction in the presence of diffused methanol in the PEM, generating water that would then be adsorbed by the silica fibers, thus facilitating self-humidification. Here the size of the silica supported Pd nanofibers ranged from 100-200 nm and the authors reported that a filler loading of 3 wt.% Pd-SiO₂ was the optimum value to achieve improved proton conductivity and reduced methanol permeability. Various other studies [74, 75] have also reported the inclusion of metal catalyst nanoparticles in the membrane for the purpose of self-humidification. While the concept is interesting, without long term tests it is difficult to establish that the oxidation reaction inside the membrane does not lead to any peroxide (H₂O₂) formation which is known to cause membrane degradation in the presence of catalyst nanoparticles. [35, 76].

Devrim *et al.* [77] developed a composite membrane of Nafion/TiO₂ (with up to 10 wt.% of TiO₂ filler) and deposited the catalyst ink by ultrasonic solvent coating to test the MEA *in-situ*. Interestingly, the authors found that the water uptake, unlike some other fillers, was reduced in case of this composite membrane. The authors attributed this behaviour to the interaction between the hygroscopic TiO₂ and the hydrophilic fraction of Nafion because of

which the sulphonic groups could be hidden and would therefore be unable to adsorb a sufficient amount of water. This was further confirmed by the authors' experiments where at 25 °C Nafion membranes presented high conductivity but the conductivity decreased as the amount of TiO₂ was increased. While, at higher temperatures (50 to 90 °C) the study revealed lower proton conductivity for the Nafion membrane than with the composites membranes, it was found to decrease as the TiO₂ content increased from 2.5 to 10 wt.%. The authors hypothesised that even though the water uptake for the composite membranes was lower due to the TiO₂ – Nafion interaction, the TiO₂ was still able to hold water at higher temperatures. However, as the filler loading increased, an excess of TiO₂ would mask the SO₃H groups completely. The composite membranes were further tested in a single cell PEFC and compared with solution cast Nafion. The authors evaluated the cell performance at 80 °C, looking at various ratios of the inorganic filler. They also studied in detail the 2.5 wt.% TiO₂ system at various operating temperatures and the effect of the amount of TiO₂ on cell performance at low humidity (80 °C, 50% RH). The best cell performance was found for the 2.5 wt.% of TiO₂ at 80 °C, and the worst performance for 110 °C. The I-V curves from the study revealed that the loss of water led to the performance being compromised even if the proton conductivity was higher at higher temperatures. Possible agglomeration of TiO₂ at higher loadings was also suggested to adversely affect the cell performance.

In case of membranes used in DMFC systems, the addition of silicate nanocompounds have been commonly used [78-80] to considerably reduce the amount of methanol crossover, since it is one of the major issues affecting long-term performance. The addition of silicates increases the tortuosity of the membrane, decreasing methanol permeability, following the Nelson Law (Equation 2.1).

$$\tau = 1 + \left(\frac{L}{2D}\right) \phi \quad (\text{Equation 2.1})$$

where τ is the tortuosity factor, L is the length and D is the width of the silicate layer and ϕ is the volume of silicate in the polymer matrix [51]. However, the silicates act as physical barriers to water molecules, too. The path that the fuel must follow through the membrane is considered to be longer in the presence of these particles (Figure 2.5). The longer, zig-zag path which the methanol must follow in the composite membrane slows down the rate of crossover, increasing the durability of the membrane and the DMFC. Methanol crossover causes more serious problems than hydrogen crossover. Therefore, standard commercial membranes used in DMFC are thicker than those in PEFC in order to reduce the crossover. This use of thicker membranes also makes it easier to use silica fillers for the composite membranes used for DMFC. However, the concept of increasing tortuosity by adding filler nanoparticles can still be applied to PEFC using other filler materials. Although it is important to note that H_2 crossover will not be affected as significantly as methanol crossover, since the hydrogen molecule is much smaller.

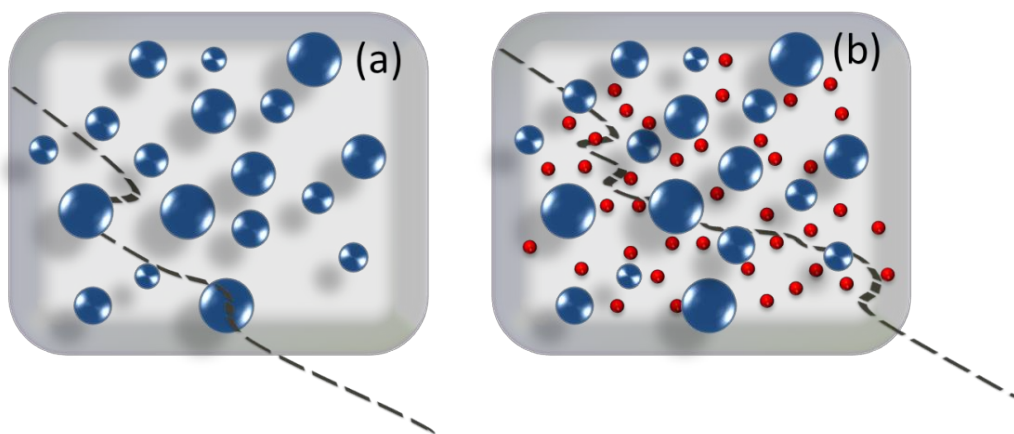


Figure 2.5: Schematic representing the fuel path (dashed line) in (a) the membrane with no filler and (b) the composite membrane with the filler particles (small red circles).

Since inorganic/polymer composite membranes are able to operate at higher temperatures as compared to polymer membranes, other metal oxide particles have also been keenly investigated. Devrim *et al.* [81] developed a nanocomposite membrane with 10 wt.% titanium silicon oxide (TiSiO_4) and Nafion for use in PEFC. The authors pointed out that the distribution of TiSiO_4 and its interaction with Nafion were very positive. The authors suggested that the chemical and electrostatic interactions between Nafion sulphonic groups and the nanoparticles enabled the orientation of the polymeric molecules around the inorganic nanoparticles facilitating homogeneous distribution of the nanoparticles in the membrane. TiSiO_4 /Nafion was found to show higher proton conductivity at temperatures above 55 °C and higher water uptake above 30 °C compared to the solution recast Nafion. The increase in proton conductivity was attributed to the significant increase in water uptake at higher temperatures (below 100 °C). The performance in a PEFC prototype at 85 °C was reported to be better with the composite membrane than with Nafion. The peak power density was reported to be higher, i.e. for 0.8 $\text{A}\cdot\text{cm}^{-2}$; the power density for 2.5 wt. % of TiSiO_4 was reported as 0.4 $\text{W}\cdot\text{cm}^{-2}$ while for Nafion it was reported as 0.25 $\text{W}\cdot\text{cm}^{-2}$. The authors claimed that the higher performance and slower degradation was achieved due to the addition of the oxides.

Mishra *et al.* [67] synthesised TiO_2 nanoparticles via a sol-gel method to use as filler in sulphonated PVA membranes for PEFC and DMFC. In this study, the effect of process variables within the sol-gel preparation method on the nanoparticle size and aggregation was investigated. Titanium dioxide, as for most inorganic oxides, is used as filler for the same reason as SiO_2 . The differences are in the specific characteristics, such as the conductivity, size or dispersion ratio of each type of filler, which influence the amount of inorganic

material that must be loaded. Factors like nanoparticle size distribution and aggregation behaviour are extremely important and play a strong role in determining the performance of the final composite membrane. Whilst the nanoparticle size and distribution would be strongly affected by the parameters used as well as the synthesis method employed, the aggregation behaviour will be affected by the nanoparticle-polymer interaction and hence even for the same filler, nanoparticles would vary from one polymer to another. However, very few studies have actually investigated these essential aspects in composite membrane behaviour.

Sangeetha Rani *et al.* [82] prepared a composite membrane with zirconium titanium phosphate (ZTP) loaded in a SPEEK matrix for DMFC. The authors investigated the effect of ZTP loading (5, 10 and 15 wt.% of ZTP loading) and noticed that the ion exchange capacity (IEC) increased with increase in loading up to 5 wt.% of ZTP. Beyond this loading, the IEC was reported to decrease and the loss in IEC was attributed to the strong interactions between the sulphonic acid groups of the polymer and ZTP. While IEC is a commonly used *ex-situ* characterisation technique for fuel cell membranes, the huge difference in the *in-situ* single cell and *ex-situ* test conditions means that the test does not always provide the most accurate results when compared to *in-situ* i-V or even proton conductivity. The test, however, can help provide insight into various possible mechanisms which could be responsible for PEM behaviour under given conditions. The authors also reported that the water uptake decreased as the loading of ZTP increased, and it was found to be even lower than that of SPEEK without any filler. This low water uptake was also attributed to the strong interactions between the matrix and the filler. This case is different from the oxides

discussed above, as ZTP is not a hygroscopic compound but offers higher proton conductivity.

As the oxides do not necessarily achieve satisfactory proton conductivity, one commonly used solution to overcome this is to functionalize these materials with specific groups that may increase the conductivity. The most commonly reported method for filler functionalization is to incorporate sulphonic groups because these are extremely hydrophilic. These groups enable water retention especially under high temperature and low humidity conditions. Zhai *et al.* [83] prepared sulphonated zirconia (S-ZrO₂) and used it as a filler in Nafion membranes for PEFC application. The amount of S-ZrO₂ filler used was varied from 0 to 20 wt. %. The authors found that the IEC values increased with the increasing amount of S-ZrO₂ due to addition of acid points via sulphonic groups. The water uptake was reported to be the highest for 10 wt.% of S-ZrO₂. Tests in a PEFC prototype at 80 °C and 120 °C revealed that performance of the 15 wt.% S-ZrO₂/Nafion (reported as the optimum ratio) membrane was slightly better than that of a commercial Nafion membrane, and at 120 °C the difference in the performance of the optimised composite and commercial membranes was quite significant due to the increased retention of water in the presence of S-ZrO₂. The authors found that above this loading (15 wt.%), the performance was always lower than that of the commercial membrane. Wu *et al.* [66] went one step further with TiO₂ fillers and sulphonated titanate nanotubes (TiO₂-NT) to achieve higher water uptake and proton conductivity. The single cell PEFC testing revealed an impressive power density, which was four times higher than when using Nafion. Sulphonation of oxide fillers has revealed itself to be a simple and fast solution to improve proton conductivity for PEM. For most oxides, the process of sulphonation is well known making it a convenient and

promising approach to use for preparation of composite membranes in PEFC and DMFC at high temperatures and low humidity.

Although the use of metal oxides as filler has enabled much improvement of the PEM, they too have some problems associated with them. The metal nanoparticles are often very difficult to disperse homogeneously in the polymer membrane, which is dependent upon their interaction with the polymer. Variable dispersion of the metal nanoparticles in the membrane matrix would mean that the performance of the composite will not be uniform throughout the bulk of the membrane. Also, the metal oxides inside the PEM have the potential to accelerate the oxidation and rate of membrane degradation over time and more long-term, durability type studies are required in this direction to understand the actual benefits and drawbacks of these fillers.

2.1.2.2. Carbon nanomaterials

Consequently, carbon nanomaterials have gained attention as they present high surface area, are inert and can be functionalized in different ways. Besides the metal oxides, carbon nanostructures have thus attracted a lot of interest as filler materials for composite PEMs over the past decade as these structures impart excellent properties to the membranes like i) increasing the chemical resistance, ii) reducing fuel crossover, iii) increasing the thermal and mechanical resistance, and iv) potentially increasing the proton conductivity depending on the structure. Moreover, unlike metal oxides, the loading of carbon nanomaterials required for achieving the desired membrane performance is much lower when compared to the metal nanoparticle loadings used. In principle, the lower weight of the filler nanomaterial would also allow easier more dispersion.

a) Carbon Nanotubes

Carbon nanotubes (CNT), are sheets of graphite wrapped as tubes. They have been used very successfully in polymeric composites over the last 10-15 years [84-86]. CNTs boast of excellent mechanical proprieties due to the tube chirality [87]. The use of CNTs as fillers in PEMs has gained a lot of momentum in the past decade.

Kannan *et al.* [88] modified CNTs with phosphonic groups for use in PEFC. The CNTs were used as filler for a matrix of phosphoric acid doped poly(benzimidazole) (PBpNT) and was phosphonated in two steps. The authors claim that the stronger hydrogen bond between the phosphonic groups and water molecule leads to higher proton conductivity. The mechanical resistance was reported to have increased due to the higher mechanical strength of CNTs compared to the polymer matrix.

On testing the membrane *in-situ*, (Figure 2.6 (a)) the authors affirmed that an improvement of 40% in the cell performance was observed when using the composite membrane due to the improved interface between the electrolyte and the catalyst. The PBpNT structure can be seen in the Figure 2.6(b). The dark lines represent the Nafion membrane, the blue circles are the phosphonic groups bonded to CNT, and the green circles are the phosphoric acid used to dope the membrane.

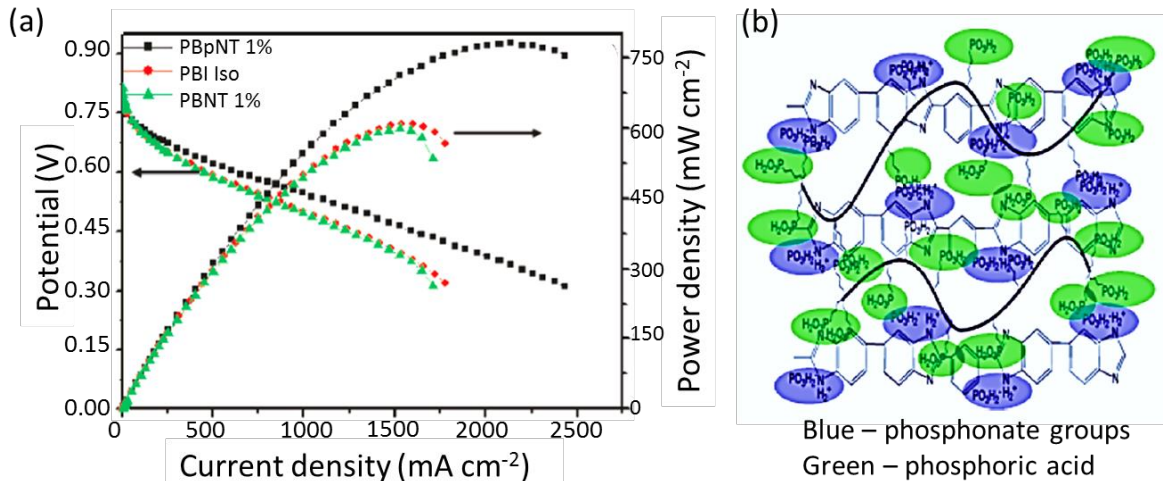


Figure 2.6: (a) Polarization curves obtained in a PEFC at 140 °C feed with H_2 and O_2 using a well-ordered (PBI Iso) and 1 wt.% CNT filled PBI membrane, undoped (PBNT 1%) and doped (PBpNT 1%) with phosphoric acid. (b) Schematic illustration of the PBpNT membrane showing the PBI structure and phosphoric and phosphonic groups [88]

CNTs have also been commonly used in DMFC membranes. In one study, Asgari *et al.* [89] developed a composite membrane for DMFC where they produced a Nafion matrix loaded with histidine doped multi walled carbon nanotubes (MWCNTs). Histidine is an imidazole amino acid. In this work, the authors found that the water uptake for the composite membrane was lower than that in Nafion, but the IEC value and the proton conductivity (Figure 2.7(a)) was higher in the composite membranes. The authors claimed that this happened due to the nitrogen in the histidine which attracts and attaches to the water present in the membrane via a hydrogen bond, facilitating the proton transport via the Grotthuss mechanism (Figure 2.7(b)).

The membrane proton conductivity displayed an expected drop around 100 °C because the free water escaped easily and only the hydrogen bonded water remained. According to the authors, this is exactly why the regular Nafion displayed higher water uptake (absorbs more free water) but lower proton conductivity (less bonded water).

Methanol permeability for the composite membrane was considerably lower. The low permeability and the high proton conductivity also showed a superior selectivity of the composite membrane under *in-situ* conditions. This study brought together two different lines of work, a CNT based filler and imidazole/ionic liquids (IL) for application at high temperature membranes. Some more studies on IL based fillers will be briefly discussed, later in this section.

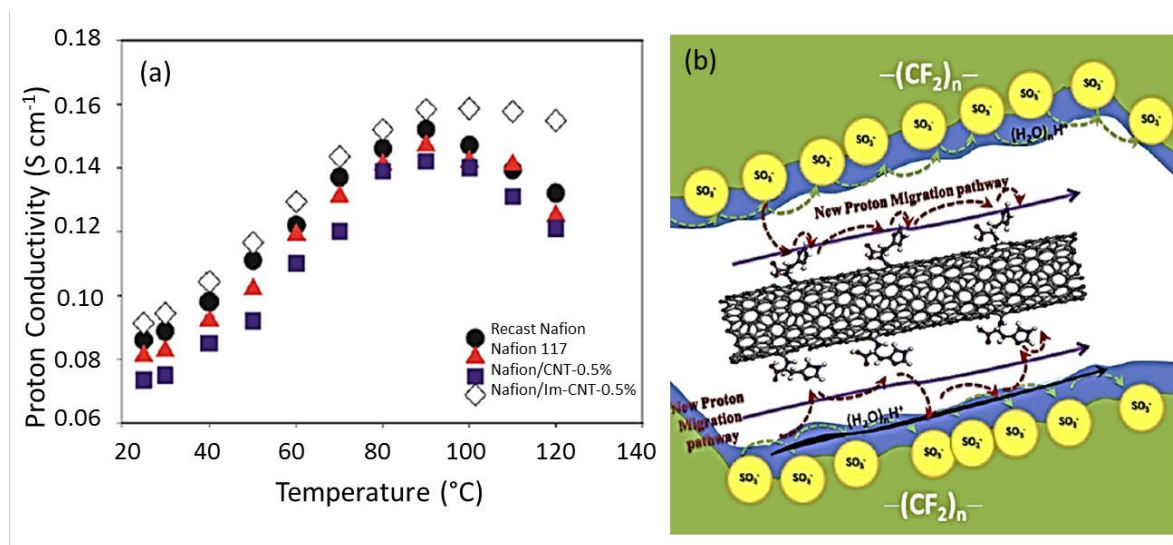


Figure 2.7: (a) Proton conductivity of the composite and the recast Nafion membranes at different temperature; besides the two Nafion membranes, the other membranes are the composite membranes of Nafion and carbon nanotubes with and without imidazole (Im). (b) Schematic illustration of the Nafion/CNT doped with Imidazole membrane, in which is possible to note the new path for the proton transport via Grotthuss mechanism. [89]

b) Graphene oxide

As a newly discovered material, graphene has attracted a lot of interest in the last few years and many initial studies looked into polymer-graphene composites for a wide variety of applications. Graphene has also been added and investigated for use in membranes for gas separation. [90] Not surprisingly, graphene used in some initial studies [91, 92] for membranes for fuel cells did not show any promising results. This is because it has high

electrical conductivity that would facilitate the electron transport across the membrane decreasing the fuel cell voltage. However, it does offer many other advantages like high mechanical strength, gas impermeability and large surface area. Further investigations diverted the interest of membrane scientists towards the use of graphene oxide (GO). GO is highly oxidized graphene sheet with a carbon to oxygen ratio of approximately 2:1 [93, 94], but unlike graphene, GO is an electronic insulator and a potential filler. The oxidation breaks the π - π bonds, separating the graphene sheets from the graphite stack, and leads to the formation of sp^2 graphitic domains surrounded by disordered sp^3 oxidized domains with oxygen groups [93, 95]. The presence of various oxygen groups (hydroxides, epoxides, carboxyls and carbonyls) turns GO into a very hydrophilic as well as insulating material [96, 97] while still retaining the high mechanical strength and gas impermeability as offered by graphene. GO due to its high surface area, could potentially allow easier proton transport and higher water uptake [91]. Its properties like these (hydrophilicity, electrical insulation and gas impermeability) that have generated a lot of interest in the use of GO as a filler in composite membranes for PEFC and DMFC in recent years.

In an attempt to address the important problem of methanol permeability in DMFC, Choi *et al.* [98] developed a composite GO/Nafion membrane with the rationale that GO would act as a barrier to fuel because of the higher tortuosity. GO is considered to enhance both backbone and side chains of Nafion when it is incorporated to the ionic cluster, thus improving both mechanical and thermal properties. The authors claim that the compatibility between both components is guaranteed due to their strong interfacial attraction. This is because just as Nafion presents hydrophobic fluoride backbone and hydrophilic $-\text{SO}_3^-$ groups; GO also presents both elements, with hydrophobic planes and hydrophilic edges.

They prepared membranes with GO loading ranging between 0.1 wt.% and 2 wt.%. The authors reported that below 0.1 wt.% the barrier effect of GO to methanol was not observed and above 2 wt.% a homogeneous distribution of GO in the Nafion matrix could not be achieved. Their studies revealed that the permeability for methanol with just 0.5 wt.% of GO was reduced to 60.2% of Nafion 112 at 25 °C. However, the proton conductivity studies revealed an opposite trend showing a decrease with increase in the GO filler content and was reported to be reduced to 55.3% of the pristine Nafion value with 2 wt.% GO loading. This was not completely unexpected as GO alone is not known to be an excellent proton conductor. Consequently, GO membranes were not reported to show high proton conductivity in the initial reports.

Later, Chien *et al.* [99] prepared a composite membrane with sulphonated graphene oxide (SGO)/Nafion for DMFC. The aim of using GO was to reduce the methanol crossover similar to the work reported by Choi *et al.* [98]. However, the addition of polar –SO₃⁻ molecules bonded in GO was also expected to allow higher proton transport. The authors investigated different amounts of loadings (0.05 to 5 wt.%) of SGO but the ideal ratio was reported to be between 0.05 and 0.5 wt.%. Above this value, it was reported that SGO tends to aggregate. The lowest methanol permeability was reported for membranes with loadings below 0.5 wt.% of SGO, which could achieve 20% lower permeability than commercial Nafion membrane 117 and 115. Moreover, the mechanical resistance (tensile strength) was also reported to be 100% higher than commercial Nafion. Zarrin *et al.* [100] functionalized graphene oxide with –SO₃⁻ groups and prepared a Nafion membrane with sulphonated GO as filler for PEFC. The acids groups were expected to compensate the loss in proton conductivity due to addition of GO, which would reduce fuel permeability. In this study, the

authors noticed that the water uptake and IEC for the composite membranes were similar to that of recast Nafion and the composite membrane had a better performance in a real PEFC environment than the recast Nafion. The peak power density for the composite membrane was reported to be more than 3.5 times higher than that recorded with Nafion, and the cell voltage, too, was higher at all measured currents. Hence, most recent studies show that despite the fantastic characteristics of GO, it is necessary to functionalise it with polar groups that can trap water in any situation. Pristine GO which is known to be hydrophilic and has a tendency to trap water molecules in between the graphene oxide sheets via H-bonding. However, as discussed before, such kind of water molecules are not able to contribute significantly towards proton conductivity and hence the need to have more sulphonated acid bonded water molecules.

However, while the proton conductivity increases with the degree of sulphonation (DS) in a PEM, its mechanical properties decay, and methanol/water permeability increases leading to accelerated membrane deterioration. The introduction of an inorganic group, such as SGO, should help minimise the negative effects of sulphonation of polymers, such as loss of mechanical strength, since these carbon nanostructures provide increased mechanical strength and also decrease methanol permeability by making the path more tortuous for the liquid fuel.

Many studies on functionalised graphene oxide used as filler in different polymer membranes have been reported in the last few years. Cao *et al.* [101] developed a composite membrane of GO/poly (ethylene oxide) for use in PEFC. In this work, GO was modified to have more carboxyl ($-\text{COOH}$) groups in order to increase the proton

conductivity. On testing an 80 μm thick membrane with 0.5 wt.% carboxylated GO, the authors found that the membranes displayed excellent mechanical properties such as tensile strength of 52.22 MPa, Young's modulus of 3.21 GPa, and a fracture elongation of about 5%. The GO/poly (ethylene oxide) membrane also showed increased ionic conductivity at 100% humidity as the operating temperature was increased from 25 to 60 °C. This study, however, did not investigate the effect of low RH and performance at temperatures 80 °C or above. Heo *et al.* [102] reported a composite membrane of sulphonated graphene oxide and sulphonated poly (ether-ether-ketone) SGO-SPEEK for DMFC application with the idea that the sulphonation of GO and SPEEK would increase the number of sulphonic groups and hence provide increased proton conductivity. The authors reported that the sulphonation not only increased the proton conductivity by allowing higher water retention but also improved the mechanical strength and reduced the methanol permeability. Jiang *et al.* [103] prepared a membrane of sodium dodecyl benzene sulphonate (SDBS) with GO adsorbed on the SPEEK filler to use in DMFCs. SDBS was expected to provide higher ionic conductivity compared to SPEEK, while GO would act as a barrier to methanol along providing mechanical strength and thermal stability. Their work revealed that the methanol permeability of the membrane SPEEK-SGO/SDBS was decreased by around 50% with 5 wt.% of SDBS when compared to pure PEEK.

Considering the positive effect of GO on the selectivity (ratio of proton conductivity and fuel crossover) of the membrane, Lin *et al.* [104] investigated the effect of preparation method on the GO/Nafion membranes on their properties and also investigated the performance in a DMFC in the presence of a high concentration of methanol. The aim of their work was to compare a dual-layer laminated GO/Nafion membrane, which used a 2D GO paper with a

traditional GO-dispersion based GO/Nafion membrane. This work can be considered as a transitional study, bridging the gap between composites and multilayer membranes. Although the authors did not refer to the membrane as a multilayer, they do call it a dual-layer laminate membrane. The authors first analysed the influence of GO by comparing the performance of a GO/poly (vinyl alcohol) (PVA) membrane and pure PVA membranes. The performance of the composite membrane (1.5 wt.% GO) was reported to be better than the pristine PVA membrane because of the reduction of methanol crossover due to the increased tortuosity provided by addition of GO. This was followed by the tests on laminate GO/Nafion and dispersion GO/Nafion membrane. The laminate membrane was prepared using a GO paper hot-pressed on to the Nafion surface, which was expected to improve the interfacial bond between the two layers. Interestingly, the laminate GO/Nafion showed significantly lower water uptake (WU) compared to Nafion 115 (28.8% for Nafion and 10.3% for the laminated GO/Nafion). However, the authors found the laminated GO/Nafion membranes shared this trend with the dispersion GO membranes (GO/Nafion and GO/PVA). The improved performance has been previously [105] attributed to the presence of the carboxyl and carbonyl groups in the GO which enable increased ionic conductivity due to the release of protons. In the evaluation of the ion exchange capacity (IEC) values of their membranes, the laminated GO/Nafion membrane showed a slightly greater IEC value. This trend was in agreement with the values observed for dispersion GO/Nafion membranes. The GO/PVA membrane, however, showed a reverse trend and this behaviour remains unexplained. The authors also reported that methanol permeability in the laminated GO/Nafion membranes was significantly lower than that reported in the studies performed by Kumar *et al.* [105] on GO dispersion based membrane. The decreased methanol crossover

was attributed to the orientation of the 2D GO sheets which was previously discussed in the study of Paredes *et al.* [106] who proposed that unlike the water molecules, the larger methanol molecules find it difficult to penetrate the GO interlayer spaces. The authors reported that the selectivity in laminated GO/Nafion membranes was 40% higher than that in Nafion 115. Finally, DMFC testing with various high concentrations of methanol revealed that the laminated GO/Nafion membranes demonstrated much higher stability and higher currents even as the methanol concentration increased from 2 M to 6 M. However, beyond this the performance was reported to have deteriorated. On the contrary, Nafion 115 showed a deteriorating performance with increasing methanol concentration as it increased from 2 M to 8 M.

More recently, Lee *et al.* [107] developed Nafion membranes with graphene oxide (Nafion/GO) and with reduced graphene-platinum (Nafion/Pt-G) as fillers to test in PEFC. The Pt loading in Pt-G (1.8 nm in average size) was reported to be 38 wt.% and the authors prepared composite membrane loadings with a variable filler content where GO and Pt-G percentage was varied from 0.5 wt.% to 4.5 wt.%. The authors compared the performance of the composite membranes with that of a recast Nafion membrane. The authors reported that all composite membranes revealed significantly higher tensile strength compared to recast Nafion. However, the water uptake studies revealed that while all GO filler composite membranes showed higher water uptake compared to recast Nafion, all the Pt-G filler composites showed relatively lower water uptake (WU) (Figure 2.8(a)). The authors attributed the lower WU for Pt-G based composites to the transformation of hydrophilic GO into hydrophobic reduced graphene upon Pt loading and electron loss in the GO due to formation of an electrical network resulting from the addition of excess of platinum.

Nevertheless, the proton conductivity for Pt-G composite membranes was reported to be higher than Nafion with all the filler content values. The authors claimed that Pt-G being an electronic conductor resulted in higher net ionic conductivity values for the Nafion/Pt-G systems. Interestingly, for the GO filler samples, only a loading of 4.5 wt% GO enabled higher proton conductivity than recast Nafion. The improved performance was attributed to the presence of a sufficiently high amount of oxygen functional groups in the GO, allowing proton pathways overriding the blocking effect for ionic clusters formed in Nafion by the GO. In the PEFC single cell test the 3.0 wt.% Nafion/GO was found to present the best results (Figure 2.8(b)) among all samples, including recast Nafion, and was followed by 0.5 wt.% Nafion/GO and 3 wt.% Nafion/Pt-G (Figure 2.8(c)). The superior performance of GO compared to that of Pt-G was considered to be due to its higher water content and consequently higher proton conductivity [74]. While the paper was a good attempt to simultaneously investigate the effect of adding GO and Pt-G filler to study the effect on membrane hydration, it did not investigate the effect of variable Pt loading in the Pt-G filler on the membrane performance. As the authors attributed the reduced WU of Pt-G systems to excess Pt loading, future studies looking into the performance of such filler with lower Pt content could be useful in improving the performance of such composites and the concept of using metal-rGO systems for self-humidification in membranes.

Table 2.2 summarises the methanol permeability, proton conductivity and selectivity information from some composite membranes and their performance in a FC in comparison with commercial Nafion. Most of them have a better *in-situ* performance, even if one or other propriety is not as good as that of Nafion.

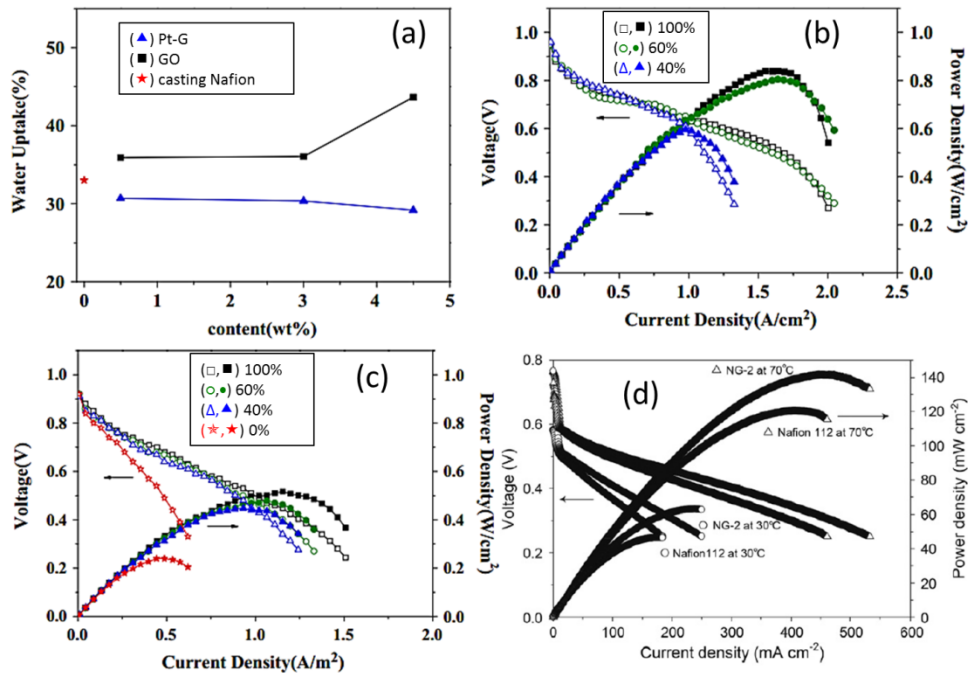


Figure 2.8: (a) Water uptake and (b) i-V curve for the membrane with 3 wt.% of GO and (c) i-V curve for the membrane with 3 wt.% of Pt-G, changing the humidity from 100 to 40% [107]; (d) The performance of a DMFC with Nafion/2 wt.% GO. [108]

In general, the complexity of composite membranes has increased in the recent past. There are a number of studies reporting on composite inorganic and organic materials, especially where organic fillers are modified with inorganic particles such as PTFE-SiO₂ [109, 110]. The advantage in using this kind of system is that the good interaction between the organic filler and the polymeric matrix is still present. Such complex structures, however, require that the composite materials and fillers be properly characterised before being tested in a membrane structure. Many of the studies on GO fillers often do not provide detailed material characterisation information on the GO used. GO is a highly heterogeneous material, factors like degree of oxidation and C:O ratio in the GO or SGO are often not investigated or reported which makes comparison of various studies using variable types of GO, therefore, very difficult. Often the mode of oxidation for GO preparation or reduction for reduced graphene when using Pt-G fillers have a significant impact on the ratio of residual oxygen

species which would have a variable effect on the behaviour of the GO/G-Pt filler. These could be some of the factors responsible for inconsistent and contradictory reports on the effect of GO filler in composite membranes. There remains the need for more systematic and thorough experimental studies in order to clearly identify the role and behaviour of GO and GO based fillers, especially where proton conductivity is concerned.

Table 2.2: Characteristics of composite membranes for PEFC/DMFC compared with Nafion membranes. Where selectivity is defined as proton conductivity divided by methanol permeability.

Study	Membrane	FC Type	Permeability to methanol ($\text{cm}^2 \text{s}^{-1}$)	Proton conductivity (S cm^{-1})	Selectivity (s cm^{-3})	Performance in a single FC
[108]	GO (2 wt.%) /Nafion	DMFC	\uparrow ($\sim 4 \times 10^{-7}$)	\approx (~ 0.02)	\uparrow (5.05×10^{-4})	\uparrow
[82]	ZTP(10 wt.%) /SPEEK	DMFC	\downarrow ($\sim 1 \times 10^{-6}$)	\approx (~ 0.06)	\uparrow (65×10^{-3})	NA
[111]	SGO/Nafion	DMFC	35% \downarrow	\uparrow	NA	\uparrow at 60 °C
[100]	SGO (10 wt.%) /Nafion	PEFC	NA	\approx ($\sim 10^{-1}$)	NA	\uparrow
[70]	SiO_2 /Nafion	PEFC	NA		NA	\uparrow in low RH
[81]	TiO_2 /Nafion	PEFC	NA	\uparrow (~ 0.3)	NA	\uparrow
[83]	SZrO_2 /Nafion	PEFC	NA	NA	NA	\approx
[112]	Pt-G/ SiO_2 /Nafion	PEFC	NA	\uparrow (~ 0.093 - 3 wt.% Pt-G/3 wt.% SiO_2)	NA	Best with 1.5 wt% Pt-G and 3 wt.% SiO_2
[113]	ZrNT (nanotubes) /Nafion	PEFC	NA	\uparrow (0.140 at 80 °C)	NA	\uparrow in low RH and at 80 °C
[114]	f-MWNT /Lotek 4200	DMFC	\downarrow less than 0.5×10^{-6}	\uparrow (~ 0.025)	NA	NA

* \uparrow higher with respect to Nafion; \downarrow lower with respect to Nafion; \approx approximate the same; NA = Not applicable

c) Other composites

Besides the studies on carbon nanostructures and metal oxides as loading/filler in composite membranes, there are new and different approaches using ionic liquids and composite membranes as mentioned before [89]. Padilha *et al.* [115] claim that with ionic liquid added to the electrolyte, the efficiency of the PEFC can be increased over the usual 40% to 61%. Xu *et al.* [116] functionalised the graphite oxide with 3-aminopropyltriethoxysilane ionic liquid to use as a filler in the membrane with a polybenzimidazole (PBI) matrix to use in IT and HT-PEFC. Ionic liquids are liquids with ions (salts), which would bond with the GO and could facilitate the hopping mechanism. The proton conduction in ionic liquids therefore is not water dependent. In this particular work, the authors used phosphoric acid with the PBI membrane, because it provides higher conductivity. While phosphoric acid can damage the membrane if used in excess, by using ionic liquid fillers, the membrane did not need high amounts of phosphoric acid to obtain high proton conductivity. Lee *et al.* [117] also developed a composite membrane with ionic liquid to use in PEFC with no humidification. The matrix was sulphonated poly(imide) and the ionic liquid was diethylmethylammonium trifluoromethanesulfonate ([dema][TfO]). In this work, the authors proved that the proton conductivity of the composite membrane is higher (approximately 10^3 times at 160 °C) than that of sulphonated poly(imide) alone. However, the single cell test was only conducted at ~80 °C. A similar idea of composite membrane was developed by Malik *et al.* [118]. Their matrix consisted of cross-linked SPEEK and the ionic liquid 1-butyl-3-methyl-imidazolium trifluoromethanesulfonate ([bmim][TfO]). They found that the SPEEK had little influence on the proton conductivity. As the amount of [bmim][TfO] was increased, the ionic conductivity also increased and seemed independent of temperature. The authors concluded that the

ionic liquid provides ionic mobility and flexibility to the membrane. Similar to Lee *et al.* [117], Liu *et al.* [119] made a composite membrane with PBI/[dema][TfO], but it was used in a H₂/Cl₂ fuel cell and not with H₂/O₂. To use this FC the membrane has to work in low or zero water environment, as otherwise the hydrogen chloride (reaction product) will consume all the water. In this case, the membrane showed good results for the fuel cell. The conductivity was reported to increase with the increase in the amount of ionic liquid.

All these reports used ionic liquid based membranes for the fuel cell to operate in low humidity conditions. Ionic liquids seem to be a good alternative to traditional filler materials in composite membranes. The considerably larger number of free ions allow easier pathway for protons as the distance between the neighboring active sites is shorter and the protons can move freely. Another possible line for future studies is to incorporate the use of ionic liquids in multilayer membranes (multilayer membranes are discussed in the next section). This is because phosphoric acid is widely used in multilayer membranes and the use of ionic liquid would help decrease the amount of acid used in the membrane, minimising the damage to the fuel cell due to the aggressive conditions generated in the presence of the acid.

2.2. Multilayer Membranes

Composite membranes and alternatively sulphonated polymers have been widely studied to substitute Nafion membranes. Nevertheless, there is a strong concern regarding the solubility of sulphonated polymers in water, and a consequent drop in the water dependent proton conductivity. An approach adopted recently to minimise these effects is the use of multilayer membranes. This approach is expected to help keep the best proprieties of each

layer/component intact while overcoming the drawbacks of each by using and combining layers of different membranes/polymer materials.

The concept of multilayer membranes, although new to fuel cells, is not new to membranes in general. In the past, multilayered polyelectrolyte membranes have been developed extensively for applications other than fuel cells such as filtration systems (air and gas purification), dialysis, ionic filtration membranes, etc. which require ion permeability through the electrolyte. Among these applications, multilayer polymer electrolyte membranes are probably most extensively researched in the field of dialysis. For example, Shan *et al.* [120] used multilayered systems for nano-filtration applications where they observed the selectivity for MgSO_4 ions. Hong *et al.* [121] worked with a system of sulphonated polystyrene and poly(diallyldimethylammonium chloride) for ionic separation using nanofiltration. Sheng *et al.* [122] used a layer-by-layer (LbL) method for developing a poly[(N,N'-dicarboxymethyl) allylamine] and protonated poly(allylamine) multilayer membrane to use as ion separator, providing higher Cu^{2+} ion permeability compared to Mg^{2+} ions. Some other studies [123-126] worked on multilayer polyelectrolytes for ion selectivity, investigating the effect of a) changing the layers and, b) the method of multilayer formation or even the ion transport. Although these systems differ in many aspects from PEFC membranes, the main idea of ion permeability through a multilayer membrane is common to all. Table 2.3 below summarises the advantages and disadvantages of composite and multilayer approaches.

Table 2.3 Comparison of composite and multilayer approach for membrane preparation and new trends in these.

Approach/Method	Composite Membranes	Multilayer Membranes
Advantages	Fast manufacture Known physical and chemical properties calculations	Countless combinations of materials and layers Retain the characteristics of each layer intact
Disadvantages	Difficult homogeneity Polymer matrix must be resistant to water	Extra interface problematic Longer time for manufacture
New trend	Use of carbon nanostructures and ionic liquids	Inner layer not just as a polymer, but with complex formulation

In the last 4 to 5 years, interest has slowly developed in the use of multilayer membranes for PEFC/IT-PEFC and DMFC applications. The most important function for PEFC membranes is the transportation of H^+ ions. While H^+ is a small ion, it still has the same characteristics and behaves as any other cation. As such, the rules of transport in multilayer membranes for nanofiltration can be carefully applied in these low temperature fuel cells. Hence, the experience and literature available on membrane development is, therefore, expected to enable not only a more professional approach towards the IT-PEFC and DMFC multilayer membrane development but also minimise the glitches and errors in the various preparation and layering procedures adopted for achieving the desired end. Unlike the composite membranes where the division was made on the basis of the nature of the materials, the multilayer membranes in this section are divided according to routes of preparation. This is because multilayer systems are more complex and may often involve many different types of materials constituting the various layers of the same membrane. As such, here we will

classify multilayer membranes on the basis of preparation methods. There are 3 main categories that the multilayer membranes can be divided into, based on preparation methods: i) hot pressed, ii) solution cast, and iii) dip coated. There are some novel approaches which do not fit into any of the three categories and these are briefly discussed towards at end of this section.

2.2.1. Hot Pressing

Hot Pressing is the simplest route to produce a multilayer membrane. Simply put, the process just involves pressing of two or more independent membrane layers (that are already cast) at high temperature. The membranes used for hot pressing can be commercial extruded membranes or those solution cast in the lab. When the layers are heated (usually close to or slightly below the polymer's glass transition temperature (T_g), under high pressure, they stick together via a mechanical bond between them to form a multilayer membrane. Yang *et al.* [127] fabricated a multilayer membrane with two external layers of Nafion membrane and one internal layer of SPEEK membrane by hot pressing to use in a DMFC. For control studies, this was compared with a single recast Nafion membrane of thickness similar to that of the multilayer membrane and another membrane consisting of three layers of Nafion combined by hot pressing. This was one of the first studies with multilayer membranes for fuel cells. It was an important study, not only because it was a first from the fuel cell point of view but also because it was carefully planned a) to compare performance with a single membrane which had the same thickness as the multilayer, and b) to take into account the possible effect of inter-layer interaction on the membrane

performance by using the three layers of Nafion membrane hot-pressed as one for the control study.

Many studies have since then been reported on hot pressed multilayer membranes for fuel cell applications. Based on the understanding that the strongly sulphonated polymers which are targeted to achieve higher proton conductivity invariably suffer from the drawback of increased water solubility, Chen *et al.* [128] prepared a layered Nafion membrane with an inner layer of sulphonated polysulfone (SPSU) with a 87% degree of sulphonation (DS). As SPSU can be dissolved in water, SPSU was placed between two layers of Nafion (with the electrode) and the three layers were hot pressed together to block the excess amount of water that could wash out SPSU. With 87% degree of sulphonation (DS), SPSU alone was reported to have three times higher water uptake than Nafion, and more than 50 times higher water uptake at 127 °C than at 20 °C. The only drawback, as discussed, is that such an SPSU membrane dissolves in water at 80 °C due to the higher $-\text{SO}_3^-$ content per repetitive unit of polysulphone since these polar groups have strong affinity to water. However, as expected, when the layered membrane Nafion/SPSU/Nafion was used in a PEFC system, SPSU was not washed out or dissolved and demonstrated a stable performance during the FC operation at 120 °C.

In another fascinating study, Peng *et al.* [129] developed a study looking into the water management in a multilayer membrane. The membrane was made by hot pressing of two commercial membranes: Nafion NRE212 and Aquivion™ E79-05s, each having a thickness of 50 µm. The hot-pressing in this case was performed in two steps: i) pressure of 0.05 MPa, at 170 °C was applied for 150 s; ii) pressure of 3.5 MPa at 170 °C was applied for 210 s. The

authors claimed that at this temperature the layers do not delaminate. The adhesion test of the membranes was carried out via a series of successive hydration and dehydration cycles performed at 80 °C. The water content and distribution were evaluated by in-situ Raman micro-spectroscopy, during fuel cell operation. These are novel methods of testing layer adhesion and water content compared to methods used in most reported works which use tensile testing and water uptake measurements for analysing these two parameters, respectively. According to the authors, the use of in-situ Raman micro-spectroscopy enabled the measurement of the actual hydration in the membrane in the region swept by the hydrated feed gas and allowed real-time monitoring of the water concentration evaluation under the changing working conditions inside the cell. Figures 2.9(a) and (b) show the water concentration profile in the MEA at a current of 222 mA cm^{-2} . The graphs further show that in both the cases water content was not lost at the interface, suggesting that the method developed to press the two membranes was efficient and formed a continuous interface. This work may lead to more comprehensive studies on water management in multilayer membranes. The concept of interface is a new parameter to be studied in the FC membrane development and many properties, such as water behaviour and proton transfer are still not understood for multilayer membrane systems. A wide range of studies would be required on both commercial as well as lab-scale membranes which are prepared using a variety of materials in order to develop a proper understanding of how the different layers behave and interact with each other at the interface before the characteristics and properties of the multilayer membranes interfaces can be fully appreciated.

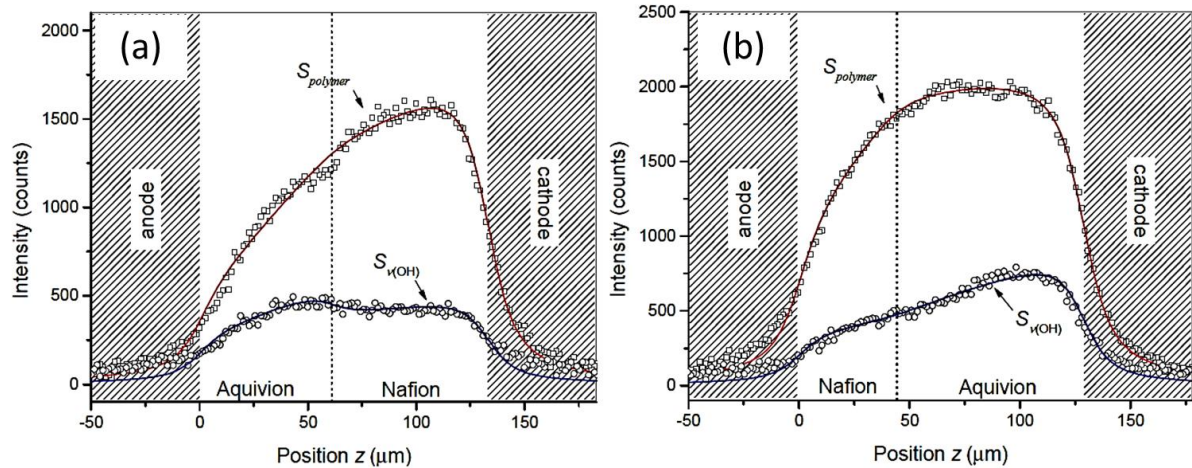


Figure 2.9: Water concentration profile ($S_{\text{H}_2\text{O}}$) in the membranes with Raman analysis: (a) Aquivion/Nafion and (b) Nafion/Aquivion [129].

Just as composite membranes, multilayer membrane structures in a fuel cell can also be prepared by combining materials other than polymers. Wu *et al.* [130] developed a very interesting membrane for the DMFC system. This multilayer structure contained three layers that were hot pressed together, where the two external layers were of Nafion 211 and the inner was a “reaction” layer as shown in Figure 2.10(a). This reaction layer was made of PtRu and SiO_2 nanoparticles dispersed in Nafion. The main idea behind such an arrangement was that any methanol and oxygen that would manage to permeate the outer membrane would react with the inner reaction layer. The water generated in the middle of the structure in this way would help maintain the membrane humidification while reducing the membrane’s internal resistance and improving the proton transport. When the membrane was tested in a single cell DMFC and its performance compared with that of a single layer of Nafion 212 (both 50 μm of thick), the multilayer membrane showed better performance (Figure 2.10(b)). The authors claimed that the reason for the improved performance was the improved water management within the membrane due to the presence of the PtRu and SiO_2 in the reaction layer.

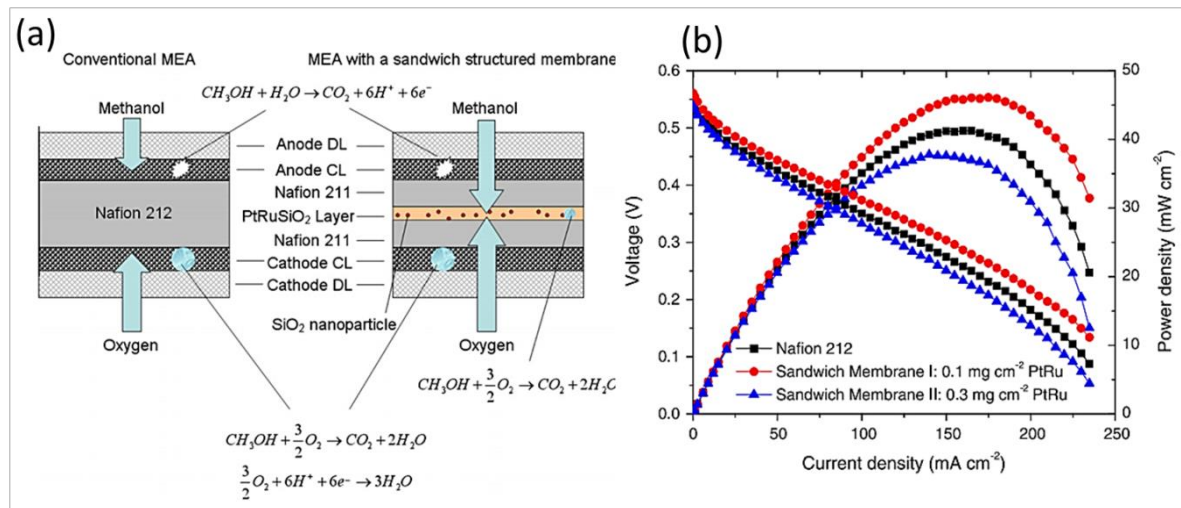


Figure 2.10: (a) Schematic of multilayer membrane structure as shown by Wu *et al.* (b) DMFC single test with the multilayer membranes. [130]

GO based multilayer membranes, due to the material's interesting characteristics, have also been evaluated in various studies for use in fuel cells. Gao *et al.* [131] prepared films of GO and ozonated GO by commonly used filtration method. These films were then hot pressed between Nafion layers. The authors claimed that after some tests the ozonated GO showed better results in a PEFC. However, those tests were evaluated only at low temperature (35 °C) and so the study did not report on the absorption of water and performance under more severe conditions.

2.2.2. Solution casting

Casting is the first and the oldest method used for the preparation of polymer membranes and films. Together with hot-pressing, casting is also a widely popular method for multilayer membrane preparation. In fact the two processes are commonly combined for multilayer membrane preparation as hot pressing cannot be carried out unless cast membranes are available for the same. The process of solution casting includes the preparation of a polymer

solution in a suitable solvent, which is then poured into a flat surface style vessel. The vessel is then usually placed in an oven to evaporate the solvents and the membrane is formed at the bottom of the vessel. After the first layer is ready, the second polymer solution is poured over the first layer and is dried in a similar way. In this process, a chemical bond is formed between the layers. The process can be used to prepare as many layers as required with virtually any combination of polymers.

Although the concept of a layered membrane with a sulphonated polymer has not been exploited much in the field of PEFCs, their use in DMFC have achieved some success [132-135]. Luo *et al.* [136] developed a layered PEM of Nafion/SPEEK to use in a vanadium redox flow battery. The presence of an inner layer of a non-fluorinated polymer (SPEEK) reduces cost and increases proton conductivity. As discussed earlier, usually these polymers do not possess a high chemical stability, so Nafion or another PFSA membrane would help provide chemical stability and minimise the degradation rate for the overall structure. Unlike the work reported by Chen *et al.* [128] in which the membrane was made by hot pressing the layers together, Luo *et al.* [136] and co-workers prepared this membrane by casting. The authors claimed that in this way the possibility of delamination of membrane layers, which decreases the battery performance, is minimised since the layers are bonded chemically and not just mechanically. The authors cast SPEEK in a flat glass, which was then dried and Nafion were cast over the SPEEK membrane, leading to a gradual interface between the layers. This study by Zhang *et al.* revealed that in the case of a vanadium battery the transport of ion (VO^{+2}) was lower in the Nafion/SPEEK membrane than in recast Nafion. The authors attributed this to the structure of SPEEK. However, the IEC values for Nafion/SPEEK membrane were considerably higher. Marrony *et al.* [137] also developed a bilayer

membrane with SPEEK/Nafion by the recast method investigating the different degrees of sulphonation of SPEEK for application in PEFC. The authors reported that no evidence of any tendency towards delamination was observed even under prolonged fuel cell operation of over 900 hours at 110 °C. Another interesting observation reported in their study was that different polymer multilayer systems even with sulphonated polymer of similar chemical composition can show different water uptake characteristics which can influence the direction of water production at the anode or cathode in an operating fuel cell.

In another study, Yang *et al.* [135] took a slightly different approach and prepared a cast multilayer membrane which was prepared with five thin layers of sulphonated poly(ether ether ketone) (SPEEK) and poly(vinyl alcohol) (PVA) placed alternately. The authors observed that the tendency of PVA to swell was restrained by the presence of alternately arranged SPEEK layers. Although the WU was low, the multilayer membrane achieved a good performance in DMFC because of its high selectivity, which meant that the methanol crossover was almost stopped. Li *et al.* [138] developed a three layer membrane, where the two external layers were made of sulphonated poly(imide) (SPI) and the inner layer was a SPEEK-SPI blend with 10 to 40 wt.% of SPI. The authors compared the multilayer membrane with a single membrane of SPEEK-SPI blend (10 to 40 wt.% SPEEK). The SPI membrane was solution cast, then the SPEEK membrane was cast over it, which was followed by another SPI layer. The SEM analysis revealed that the two external structures are similar while the inner layer was thinner and different. The authors suggested that the inner layer was thinner because the SPEEK migrated to the external layers. The small difference in the external layer thickness may also be caused by the migration of SPEEK. The authors found that SPEEK alone had higher water uptake than all other membrane compounds and the blend membranes

displayed higher WU than the equivalent multilayer. The authors reported that the proton conductivity of some of the triple-layer membranes was found to be higher than that of the corresponding blended membranes. This work put forth a balanced view of multilayer and composite/blend membranes suggesting that not all multilayer membranes work better than composites. The study revealed that the choice of the polymer and the method of preparation play a significant role in determining the performance of the membrane. In this case, the composite membrane was a better choice and also simpler to produce.

In the past 2-3 years, a wide variety of structures including variable number of layers, combination of organic and inorganic membrane layers have been investigated and reported for multilayer membranes using casting [139, 140]. Padmavathi *et al.* [141] developed a multilayer membrane by casting, where the inner layer consisted of SiO₂ mixed with 5wt.% aminated poly(sulphone) (APSu) sandwiched between two external layers made of sulphonate poly(sulphone) (SPSu). The APSu was used in order to retain water in the matrix and it was also expected to lower methanol crossover. The authors tested the membranes in both DMFC and PEFC systems. The authors studied five different multilayer structures where the amount of SiO₂ was varied between 2 and 10 wt.% and the total thickness was maintained around 120 μm. The authors found that in the PEFC the single SPSu displayed higher power and voltage (Figure 2.11(a) and (b)), while in DMFC the performance of the multilayer with 2 wt.% SiO₂ was found to be the best and attributed this to the higher selectivity of the multilayer. The superior performance and durability in DMFC is due to the very low methanol permeability. This is because the layer of SiO₂ and APSu offers more tortuosity to the path available for methanol molecules to permeate through the membrane compared to the conventional composite membrane. This study highlighted the viability of

multilayer membranes when comparing the DMFC and PEFC systems. While some multilayers maybe suitable for DMFC they may not be as suitable for PEFC. There is still a high demand for more robust and highly selective membranes for DMFC environments but the same membrane may not necessarily bring a significant benefit to a PEFC system. It would, however, be interesting to see how such a membrane would behave in an IT-PEFC environment where water retention is a very critical parameter.

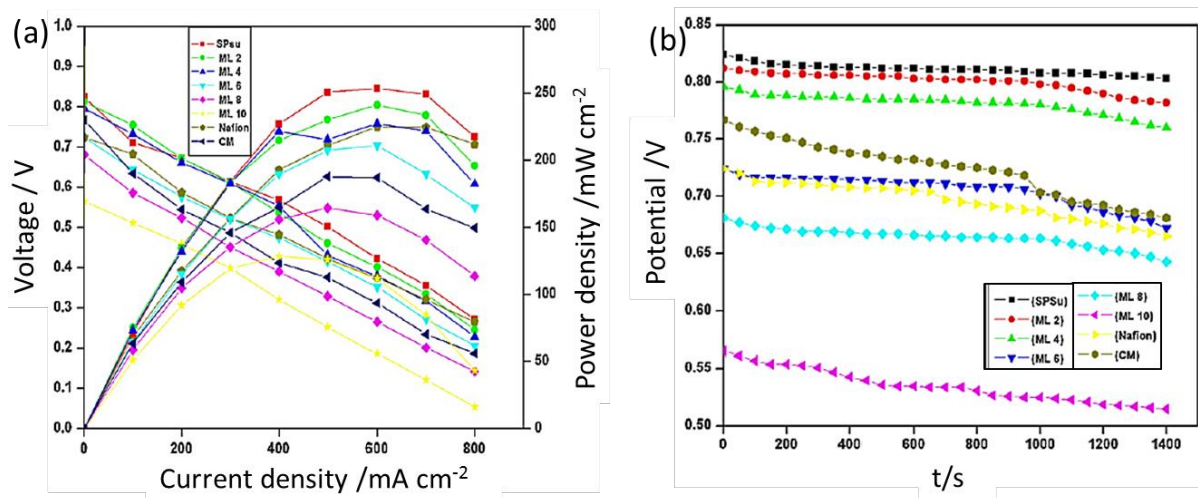


Figure 2.11: (a) Single PEFC cell test; (b) PEFC durability test at room temperature [141].

The main idea in PEMs is to find an optimum behaviour between excellent proton transport and maximum resistance to fuel crossover. If the path is too tortuous, then neither the proton nor the fuel would pass through the membrane. If the path is completely non-tortuous both proton and fuel would cross over to the cathode side. Consequently, studies have been looking into identifying the best possible middle-path. The inferior results for multilayer and composite membranes with inorganic filler materials at high RH just show that in these conditions there is no need of inorganic fillers to transport the protons. But when used under low RH conditions the hygroscopic silica helps retain the water. Lee *et al.*

[139] prepared a multilayer membrane with an inner layer of SiO_2 via solution casting. This was aptly termed as a ‘multilayer-structured composite membrane’ by the authors. The two external layers in this multilayer were cast of sulphonated poly(phenyl sulphone) (SPPSU). The inner layer, however, was a composite of SiO_2 and amorphous thermoplastic polyetherimide (PEI) binder (Figure 2.12). The authors claimed that such an arrangement of SiO_2 would provide an independent ceramic layer comprising closely-packed SiO_2 nanoparticles in contrast to a bulk composite membrane which would consist of randomly dispersed SiO_2 nanoparticles. Further testing and characterisation of the membranes by the authors under low (RH of 10%) and high (RH at 100%) humidity conditions (Table 2.4) revealed that this arrangement of SiO_2 was not only effective in suppressing dimensional change in SPPSU but also in enhancing proton conductivity of the multilayer composite membrane. The authors also reported that the decrease of proton conductivity in low humidity conditions, which is commonly encountered in conventional water-swollen membranes, was minimised in these multilayer composite membranes.

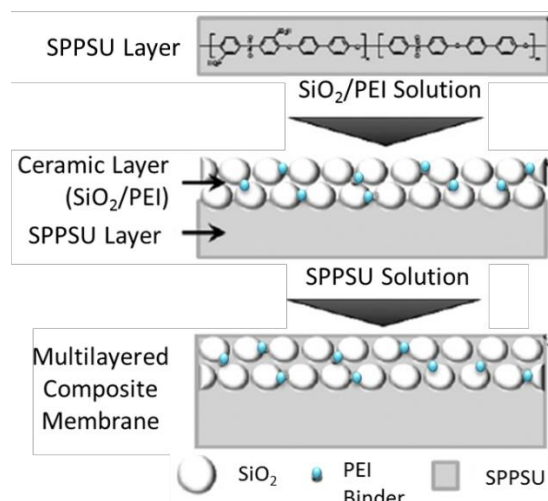


Figure 2.12: Schematic of the multilayer membrane with SPPSU external layers and inner layer of $\text{SiO}_2 + \text{PEI}$ [139].

Table 2.4: Proton conductivity at 100% RH as a function of the temperature and at 10% RH as a function of time [141].

	Temperature (°C)	Proton conductivity (S cm ⁻¹) (100% RH)	Time (min)	Proton conductivity (S cm ⁻¹) (10% RH)
Pristine SPPSU	30	~ 0.115	0	~ 0.090
	40	~ 0.123	30	~ 0.067
	50	~ 0.135	60	~ 0.015
	60	~ 0.156	90	~ 0.01
	70	~ 0.172	120	~ 0.00
	80	~ 0.217	150	~ 0.00
Bulk Composite	30	0.065	0	~ 0.053
	40	~ 0.078	30	~ 0.051
	50	~ 0.086	60	~ 0.041
	60	~ 0.094	90	~ 0.025
	70	~ 0.106	120	~ 0.023
	80	0.118	150	~ 0.000
Multilayered Composite	30	0.075	0	~ 0.056
	40	~ 0.086	30	~ 0.055
	50	~ 0.100	60	~ 0.048
	60	~ 0.108	90	~ 0.037
	70	~ 0.124	120	~ 0.027
	80	0.137	150	~ 0.008

Table 2.5 displays a compilation of the proton conductivity and water uptake values reported for various multilayer membranes prepared via hot-pressing and solution casting. There are more studies reported for use of multilayer membranes in DMFC than for PEFC. Although some of the reported works investigated membranes with thickness lower than 100 μm , most of it used sulphonated polymers in one or all layers combined with mechanically strong polymers such as SPEEK.

Table 2.5: Proprieties of hot pressed and solution cast membranes.

Study	FC	Layers	Route	Thickness (μm)	σ (S cm^{-1})	WU (%)
[142]	DMFC	Chitosan/N/Chitosan	C	100	0.1635 – at 90 °C	NA
[135]	DMFC	1 or 5 bilayers: SPEEK + PVA	C	NA	for 1 bilayer: 0.017; for 5 bilayers: 0.055 at 80 °C	1 bil - 76.2; 5 bil - 30.5
[132]	DMFC	SPEEK/SPDS-diph/SPEEK	C	5--30	0.031 at 80 °C	18.2
[127]	DMFC	N/SPEEK/N	HP	115-135	NA	NA
[138]	DMFC	SPI/SPEEK/SPI	C	NA	0.149 at 100 °C	31.48
[139]	PEFC	SPPS/SiO ₂ + PEI/ SPPS	C	120	0.137 at 80 °C	NA
[143]	PEFC	SPSU/PTFE	HP	40	0.00256	NA

*C = cast; HP = hot pressing; N = Nafion; SPEEK = sulphonated poly(ether ether ketone); PVA = poly(alcohol vinyl); SPDS-diph = sulphonated poly(diphenylsulfone - diphenol); SPPS = Sulphonated poly(phenyl sulphone); PEI = polyeheterimide; SPSU = sulphonated poly(sulphone); SPI = sulphonated poly(imide); NA = not applicable

2.2.3. Dip coating

Another common route for producing membranes is dip coating. This method is capable of producing the thinnest membranes, but it is also the one with more limitations associated with it. The method involves producing an initial membrane (or using a commercial membrane) using any of the two methods listed above. Then, a solution of the polymer that will form the external/next membrane layer is made in an appropriate solvent. The initial membrane is then dipped in the polymer solution and the polymer solution gets attached in both sides of the initial membrane. The resultant three-layer membrane is then allowed to dry. Once the membrane is dry, this process of dipping can be repeated as many times using another (or same) polymer solution depending on the polymer needed and the number of layers required. One of the major advantages of this method is that this process allows the formation of multilayer membranes with large number of thin layers such that the final thickness can still be 15-20 μm even when using 10-20 layers. Wang *et al.* [144] developed a

multilayer membrane using this process where the inner membrane was a sulphonated polyimide (SPImd) which was then dipped in a Nafion solution. The authors suggested that the Nafion would adhere to both sides of polyimide providing a higher durability to the central layer. With this method, the authors achieved an extremely thin composite membrane of 15 μm , with each Nafion side layer of 2 μm thickness. Lin *et al.* [145] also prepared a multilayer membrane with Nafion-SPImd-Nafion. Here, sulphonated poly(amic acid) (SPAA) was used as a precursor. After the coating, the membrane was dried and SPAA imidized to SPImd. The authors carried out the imidization as the last step during solvent evaporation. According to the authors, this helped improve the interaction between the Nafion and SPImd layers. The in-situ PEFC performance of the multilayer membrane was compared to that of a pure SPImd membrane and the multilayer showed a better performance. The authors attributed the enhanced stability to the use of Nafion layers and found that the performance of the multilayer was similar to that of commercial Nafion 212 at 70 °C. Zhong *et al.* [146] achieved lower methanol crossover and better selectivity (in DMFC) with a multilayer membrane made with the Layer-by-Layer (LbL) method which is similar to dip coating. The authors prepared the base layer of silicon containing sulphonated polystyrene/acrylate (SisPS/A) which was dipped alternately in solutions of chitosan and SisPS/A making the total number of these bilayers between 5, 10 and 15. The membrane was then heated to achieve a crosslinked structure in order to enhance the mechanical strength and durability. The authors found that the durability of the polymer coated by cross-linked structure helped reduce the methanol permeability by facilitating higher selectivity (relation between fuel crossover and proton conductivity). However, the authors also reported that the crosslinking resulted in suppression of some hydrophilic sites. As a

result, the water uptake of the multilayer membranes was reported to decrease with the increasing number of cross-linked LbL self-assembled bilayers. The authors reported that the water uptake of SisPS/A membrane was reduced from approximately 50.1% at 25 °C, to 47.2%, 46.6% and 45.7%, for the c-SisPS/A-CS membranes sandwiched between 5, 10 and 15 bilayers, respectively. Consequently, the water uptake of the multilayer membranes was reduced and the resultant proton conductivity of these multilayer membranes was found to be lower than that of Nafion. However, in the absence of any in-situ testing in this study, the overall effect of increased selectivity and reduced proton conductivity remains debatable especially since some other studies on DMFC systems, as mentioned earlier, seem to show improved/ enhanced performance simply due to reduced methanol crossover.

Yuan *et al.* [147] also attempted to reduce the methanol permeability in DMFC by developing a multilayer membrane via dip coating method. In this study, the authors immersed Nafion in poly(diallyldimethylammonium chloride) (PDDA) and graphene oxide solution in succession. The Nafion membrane (due to the sulphonic groups on the surface) and the GO (due to the carboxyl and the phenolic hydroxyl groups) are both negatively charged while PDDA has a positive surface charge. Thus, just due to the difference of charges all layers were held together (Figure 2.13(a)). To evaluate the methanol crossover, the authors compared the prepared multilayer membrane with Nafion membrane (Figure 2.13(b) and concluded that the multilayer presented a lower methanol oxidation current at the same voltages, confirming that the methanol was being blocked better in the multilayer system. All the multilayer membranes show superior performance compared to Nafion (Figure 2.13(c)), but the performance decreased as the number of bilayers increased. The authors discussed that the better performance compared to Nafion was achieved because

the bilayers blocked the methanol. However, as the number of bilayers increases, it may also make the proton transport difficult. Hence, in order to achieve the optimum performance, the number of layers and thickness of each needs to be carefully examined for each polymer/multilayer system.

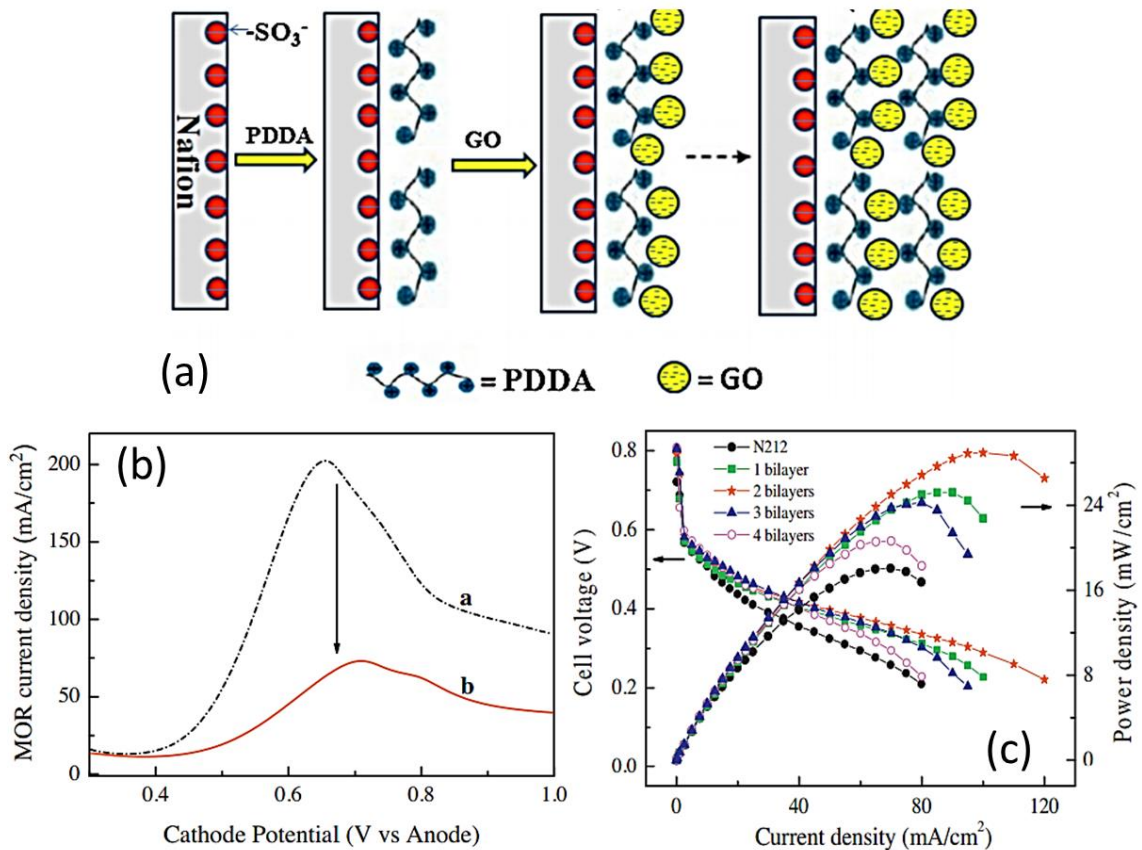


Figure 2.13: (a) Schematic of the Nafion, PDDA, GO multilayer membrane; (b) methanol crossover test for a) Nafion and b) 2 bilayer membrane; (c) DMFC single test studies for various bilayers. [147]

Table 2.6 shows the water uptake and proton conductivity values reported for multilayer membranes prepared by dip coating. In this methods the number of layers usually is much higher than with the membranes those prepared using solution casting and hot pressing (3-5 layers) methods. The proton conductivity changes considerably due to the number of layers, the layer thickness, and also the material of the polymers or composite materials used. Some of them show higher values than those of Nafion under the same conditions.

The dependence on the material is evident; even when the method is suitable for the application, if the material is not fit for FC, the results will not be satisfactory. The same trend can be seen for water uptake, although the water uptake values for the multilayer with a highly sulphonated polymer inner layer are usually reported to be lower when compared to the equivalent monolayer of the sulphonated polymer alone. More important than water uptake, are the dimensional variations in polymer layers. In multilayer structures the external layers block these variations, especially in dip coating due to the great number of layers.

Table 2.6: Properties of reported multilayers prepared by dip coating

Study	FC	Layers	No. of layers	σ (S cm ⁻¹)	WU (%)
[144]	PEFC	N/SPI/N	3	0.07 (80 °C)	NA
[148]	PEFC	SPFEK + PDDA/PSS	NA	0.061 (80 °C, 100% RH)	47 (30 °C)
[149]	DMFC	N + ScPAESu/GLU	1 (initial) + 1 to 50x 2 (dip both sides)	0.067 (Layers: 25 x2, at 30°C)	21.3
[150]	DMFC	SPA EK + PAni	1 + 5 x2	0.24 (80 °C)	93.8
[151]	DMFC	N + PAH/PSS +salt	1 + 5 up to 20 x2	0.08791 (Layers: 5 x2, in 0.1M NaCl, 22°C)	NA
[152]	DMFC	N + HPT/PDDA	1 + 1 up to 5 x2	0.03 (Layers: 5 x2)	NA
[153]	DMFC	PE/PSS + PVI/PAAmHS	1+ 1 x2	0.122	NA
[154]	DMFC	SPA EK + PWA/PPy	1+ 1 to 5 x2	0.0299 (Layers: 10x 2, 80°C)	49.85
[155]	DMFC	N + SPA EK- c/Chitosan	NA	0.131 (80°C)	23.5
[133]	DMFC	N + PDDA-PAA	NA	0.086	NA
[133]	DMFC	PAH-PAA	NA	0.068	NA
[156]	DMFC	PPy/N/PPy	3	NA	NA

*SPS = sulphonated polystyrene; N = Nafion; ScPAESu = sulphonated cardo poly(arylene ether sulphone); GLU = glutaraldehyde; SPA EK = sulphonated poly(arylene ether ketone); PAni= polyaniline; PAH = poly(allylamine hydrochloride); PWA = phosphotungstic acid; PDDA = poly(diallyl dimethyl ammonium chloride); SPI = sulphonated polyimide; PE = poly(ethylene); PSS = poly(styrene sulfonic acid); PVI = poly(vinylimidazole); PAAmHS = poly(acrylamide methyl propane sulfonic acid); PPy= polypyrrol; SPA EK-c = sulfonated poly(arylene ether ketone) bearing carboxyl groups; PAA = poly(acrylic acid); WU = water uptake; SPFEK = sulfonated poly(fluorenyl ether ketone), PAN = poly(acrylonitrile). All the WU are at room temperature if not informed.

Apart from the preparation methods discussed above, many other novel routes have been developed to obtain the multilayer membranes. But the three more widely used in the FC area continue to be hot pressing, casting, and dip coating. Hot pressing is the simplest route, which allows the possibility of using commercial extruded membranes that usually have higher proton conductivity. Although, in this method the only bond that is formed between the layers is mechanical, so under severe environmental conditions (e.g. inside the fuel cell systems where they would face continuous expansion and compression) there is a possibility of delamination of the layers. On the other hand, during casting the interaction between the layers is mechanical as well as chemical, which makes the bond stronger, thus, reducing the chances of delamination. However, the choice of solvent is very crucial in this process. Care needs to be taken such that the solvent of one layer does not damage/dissolve the underlying layer. Moreover, unlike hot pressing, casting excludes the possibility of using extruded membranes, which is a clear disadvantage since extruded membranes usually have better mechanical properties. Alternatively, dip coating brings in the prospect of achieving extremely thin layers and generating a final membrane with a large number of bi-layers, even 20 or 50. Having a large number of layers on the side will help block and minimise the dissolution of the highly sulphonated and hydrophilic polymers that would otherwise dissolve in water. Another advantage of this process is that any change in the dimensions of the inner layers will be minimised dramatically, thus decreasing the wash-out rate. The only major requirement of this procedure is that the base membrane must have high mechanical strength in order to endure repeated dipping. Table 2.7 summarises advantages and disadvantages of these three methods.

Table 2.7: Routes to obtain a multilayer membrane.

<i>Method</i>	<i>Advantages</i>	<i>Disadvantages</i>
Hot Pressing	<ul style="list-style-type: none"> ✓ Physical interaction between layers ✓ Fast method ✓ Solvent free ✓ Can use extruded membrane 	<ul style="list-style-type: none"> ✓ Delamination
Solvent Casting	<ul style="list-style-type: none"> ✓ Chemical interaction between layers. ✓ No delamination ✓ Can use polymers with low mechanical strength. 	<ul style="list-style-type: none"> ✓ Use of solvents ✓ No extruded membranes
Dip Coating	<ul style="list-style-type: none"> ✓ Chemical interaction between layers ✓ No delamination ✓ Thinner layers ✓ Allows large no. of bi-layers. 	<ul style="list-style-type: none"> ✓ Only base membrane can be extruded ✓ High strength base membrane needed.

2.3. Conclusions

Various different composites based on organic as well as inorganic fillers have been reported extensively for use in IT-PEFC to overcome the problems faced by Nafion under high temperature and low humidity conditions. Composite membranes are certainly the next step forward to use Nafion-like membranes in an IT-PEFC/DMFC environment. The use of hydrophilic fillers increases the water uptake leading to higher proton conductivity of the membrane. It also helps in the stability of the membrane and provides a tortuous path to prevent the fuel crossover. While SiO₂ and TiO₂ based fillers have been researched heavily in the last decade with some very interesting results, the search for other fillers and fresh combinations of filler and polymer materials continues in the bid to make the PEM more durable and efficient. The methods used to develop composite membranes are very well known since they are a polymer matrix with loadings. Studies reported on the use of graphene oxide and carbon nanotubes as fillers and as Nafion free membranes show these

to be promising materials for PEM applications especially because they provide increased mechanical strength. Chemical modifications of GO such as carboxylation and sulphonation have been carried out enabling further improvement of the desired properties such as increased proton conductivity along with its inherent property as an electronic insulator. However, despite the volume of work reported with this material there are still quite a few parameters like water content in GO, carbon to oxygen ratio, and degree of sulphonation as well as the percentage of GO as a filler which need to be inspected and investigated extensively in order to understand its behaviour as a filler. It would also be interesting to see if more than one filler could be effectively used in composite membranes to generate membranes with multiple attributes, which may be suitable and effective under variable conditions. This would, however, require detailed studies on the role of various functional groups that such fillers (like GO and ionic liquid) possess. Functional groups like sulphonic acids and phosphoric acid have long been known to play an important role in water retention and enhancing proton conductivity. Developing an understanding of the roles and interactions of functional groups (like carboxyl, hydroxyl), present in fillers like GO, with the functional groups present in the polymers would be vital for all future membranes.

On the other hand, recent studies on multilayer membranes have been mainly focussed on DMFC. However, some successful studies have also been reported for use in PEFC. This trend is likely to generate more research interest for DMFC and IT-PEFC as the concept has been quite successful in its previous applications. The multilayer concept is of particular importance for application in IT-PEFC where there is an acute requirement for membranes, which are more tolerant towards higher temperature and low humidity conditions compared to the existing industry standard materials like Nafion. The hybrid multilayer concepts like

the use of two external Nafion or other sturdy polymer layers on a sulphonated inner membrane would help strengthen its structure allowing the use of the best properties of each material. The external layers prevent the inner layer from being washed out or losing its mechanical resistance if it swells too much and help maintain its proton conductivity under more demanding conditions. The use of novel polymer and filler combinations along with innovative layering techniques could prove to be a paradigm shift in the field of low temperature fuel cell membrane development. The next step for multilayer membrane development could be to combine both composite and multilayer concepts, which can offer the advantages of both (such as reduced fuel crossover due to use of a composite filler membrane layer, and increased proton conductivity from the sulphonated polymer) while minimising the disadvantages associated with highly sulphonated membranes.

Therefore, this study proposes two concepts of multilayer membranes. The first concept uses Nafion in the external layers and sulphonated polyindene in the inner layer to enhance proton conductivity due to the highly sulphonated polymer. The second concept uses Nafion in the external layers and GO in the inner layer to increase the water retention due to oxygen groups.

CHAPTER III – SYNTHESIS OF MATERIALS

The first step to prepare the membranes was to select and synthesize the base material. These were Nafion solution, graphene oxide (GO), and sulphonated poly(indene) (SPInd). The Nafion solution was a commercial solution and was used as received. SPInd was prepared from the indene monomer while GO was prepared from graphite powder.

Nafion was chosen as the external layer to provide mechanical strength to the membrane. SPInd was chosen due to the numerous sulphonic groups available to bond with water and, then, accelerate the proton transport. GO was chosen due to the presence of oxygen groups which result in its highly hydrophilic properties, allowing strong hydrogen bonds with water.

This chapter explains how the materials, SPInd and GO, were synthesized and summarizes the results of the characterizations carried out to evaluate these materials.

3.1. Synthesis of polyindene

The synthesis of polyindene (PInd) was accomplished by cationic polymerization of indene initiated with aluminium trichloride as catalyst as previously reported by Brum *et al.* [157]. Specifically, in a reactor under inert atmosphere, 0.58 g of AlCl_3 and 90 mL of dichloroethane at $-20\text{ }^\circ\text{C}$ were added and stirred for 15 minutes at 550 rpm. This was followed by the addition of 46.9 g of indene monomer. This solution was stirred for another 3.5 h. Finally, 20 wt.% of sodium hydroxide was added to react with any residual free radicals and end the reaction. The excess solvent was evaporated and the slurry, thus obtained, was washed

three times with ethanol. The product was recovered by precipitating in ethanol, filtered, and purified by re-solubilisation in dichloroethane. Finally, it was dried under vacuum at 100 °C for 2 h and presented a light yellow colour.

3.2. Sulphonation of polyindene

The sulphonation of polyindene (Figure 3.1) was carried out using the previously reported process by Brum *et al.* [158]. Typically, 10 g of polyindene was dissolved with 40 mL of dichloroethane using magnetic stirring. This solution was transferred to a cylindrical vessel at -2.5 °C under N₂. To this, a 3 mL solution of chlorosulphonic acid with 10 mL of dichloroethane was added and stirred for 1 hour at 300 rpm. Following this, the excess of solvent was removed from the slurry and the slurry washed 3 to 4 times with hexane. Finally, the filtered product was dried in the oven at 60 °C and presented a dark yellow colour. The SPInd degree of sulphonation (30% sulphonated) was determined according to reference [158] by acid-base titration.

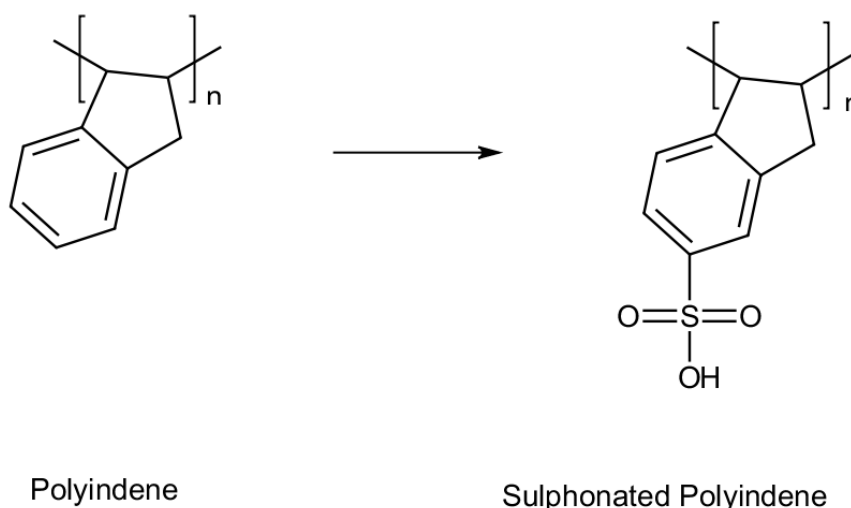


Figure 3.1: Reaction of polyindene sulphonation.

3.3. Synthesis of graphene oxide

Graphene oxide was produced by a modified Hummer's method [159]. The set for the reaction is shown in Figure 3.2. In a round flask, 3 g of graphite powder (Sigma-Aldrich), 101.4 mL of H_2SO_4 and 2.28 g of NaNO_3 were added. The solution was stirred until homogenised. Then, 13.5g of KMnO_4 were added to the solution drop by drop to oxidize the graphite. The flask was maintained in an ice bath as the reaction is highly exothermic. When the permanganate addition was finished, the solution was stirred further five days. After this, the excess of permanganate and solvents were removed. The slurry was washed with acid solution to remove any remaining KMnO_4 . The GO was washed with 500 mL of 5 wt.% H_2SO_4 (stirred for 2 h) and with 50 mL of 30 wt.% H_2O_2 , followed by further washing with 300 mL of 3 wt.% H_2SO_4 (stirred for 2 h) and with 20 mL of 5 wt.% H_2O_2 for a total of nine times. Between each washing, the slurry was separated from the solvent by filtration. Finally, the GO was washed ten times with 300 mL of water and stirred two hours each time. The GO was dried in an oven at 80 °C overnight.

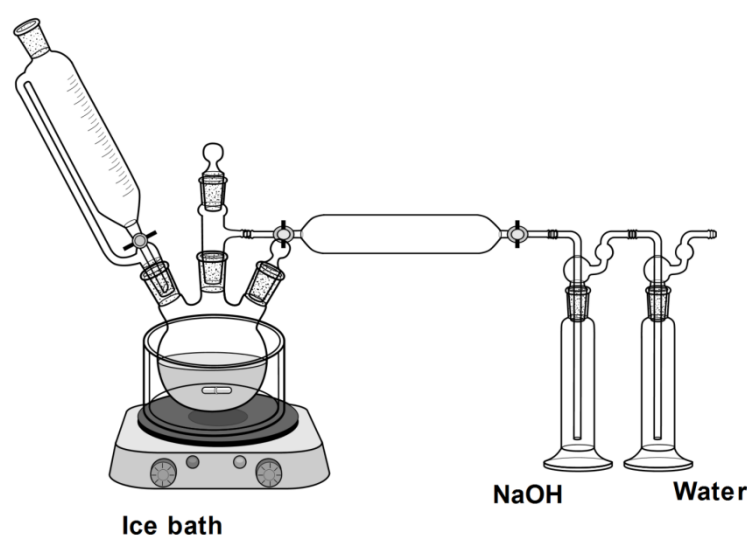


Figure 3.2: Set up for GO synthesis reaction.

This reaction is extremely explosive due to the strong oxidation agents. Thus, it is important to take some precautions besides keep the reaction in the ice bath. The reaction must be carried out in a fume hood with the sash always down protecting the scientist, especially at the beginning of KMnO_4 addition. This chemical must be added drop by drop to avoid explosions. Small batches of GO are recommended to synthesize, avoiding any increase in the explosive risk of the reaction. Finally, the gases generated in the reaction must be neutralized with a base and water [160], in this work NaOH as shown in Figure 3.2.

3.4. Chemical characterization

Both materials were characterized by Fourier infrared spectrometry (FT-IR). GO only was characterized by X-ray diffraction (XRD) and X-ray photoelectron spectroscopy (XPS). The results are described in the following sections. Three samples of each material were analysed. Details of the experimental protocols are in the Appendix.

3.4.1. FT-IR

The as-prepared PInd and GO were characterised by FT-IR, carried out using a PerkinElmer FT-IR Spectrum 100. The spectra were recorded between 4000 to 400 cm^{-1} .

PInd and 30% sulphonated PInd (SPInd) were synthesized successfully. A higher degree of sulphonation for SPInd was not chosen in order to avoid SPInd from being solubilized and lixiviated in water during fuel cell operation. The comparison between FT-IR curves for PInd and SPInd (Figure 3.3) revealed the characteristic peaks confirming the polymerization and sulphonation attributed to the H-C-H bonds. The absorbance peaks between 1605 and 1470 cm^{-1} correspond to C=C aromatic bonds. The absorbance peaks from 1460 to 1430 cm^{-1} were

ascribed to the sp^3 C-H bond and the peaks below 1000 cm^{-1} were accredited to C-H. All these peaks were observed in both PInd and SPlnd spectra. The absorbance peaks between 1150 and 1000 cm^{-1} attributed to the stretching of SO_3 groups linked to phenylene rings were only observed for SPlnd, demonstrating that the sulphonation was successful [157, 158]. Another absorbance peak unique to the SPlnd sample was observed at 1692 cm^{-1} . This was attributed to the C=O bond which suggests that some oxidation reaction involving the PInd molecules occurred. The indene polymerisation reaction is stopped by the addition of sodium hydroxide, which reacts with the propagating chain. During this time, the carbonyl group can be produced by partial oxidation of end-chain hydroxyl groups in the PInd molecules. The absorbance peak at $\sim 3300\text{ cm}^{-1}$ is the O-H band related to water and is only observed in SPlnd. The sulphonic groups present on SPlnd hold the water by hydrogen bonds, while in PInd there are no groups to attract the water.

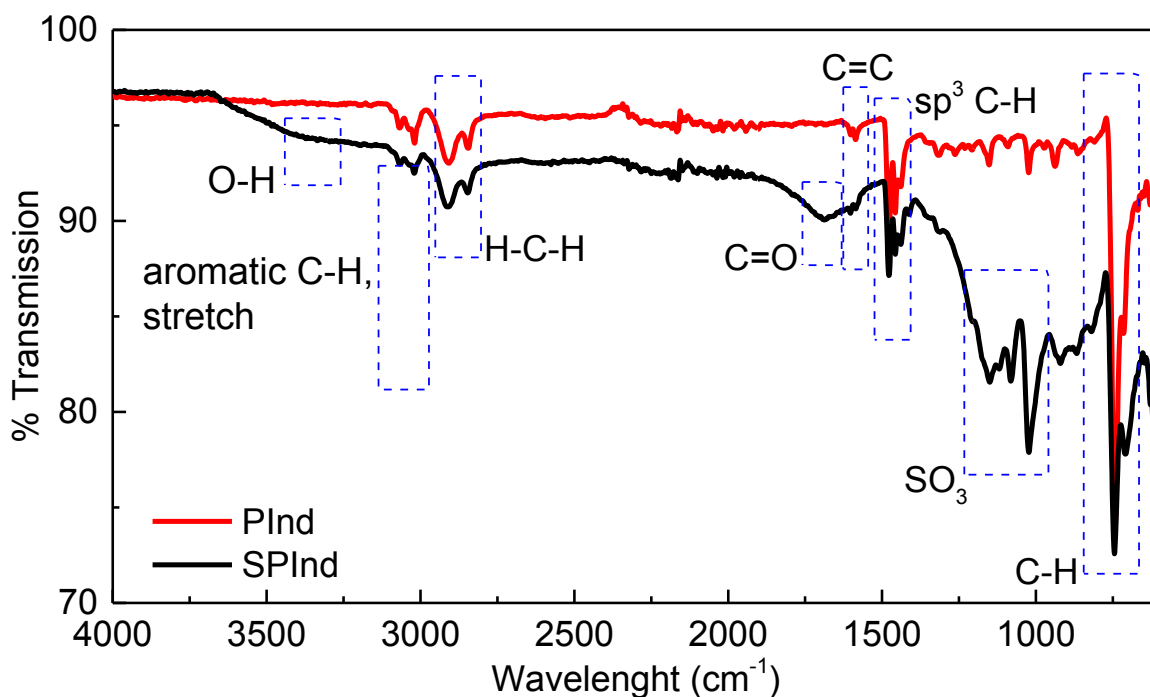


Figure 3.3: FT-IR spectra for PInd and SPlnd.

The reaction of graphite oxidation to GO was successful as can be confirmed by the FT-IR in Figure 3.4. The scan shows the peak in the wave number 3143 cm^{-1} related to the O-H stretch presented in GO [112, 161]. The wave number equal to 1713 cm^{-1} is due to the C=O stretch bonds also only present in GO [112, 162]. The C=C bond is responsible for the transmission peaks 1618 and 1578 cm^{-1} [161, 162]. The 1145 cm^{-1} transmission peak represents the C-H bond. Although some of the bonds are similar to graphite such as C=C and C-H, the high level presence of bonds with oxygen suggests that graphite was oxidised to graphene oxide.

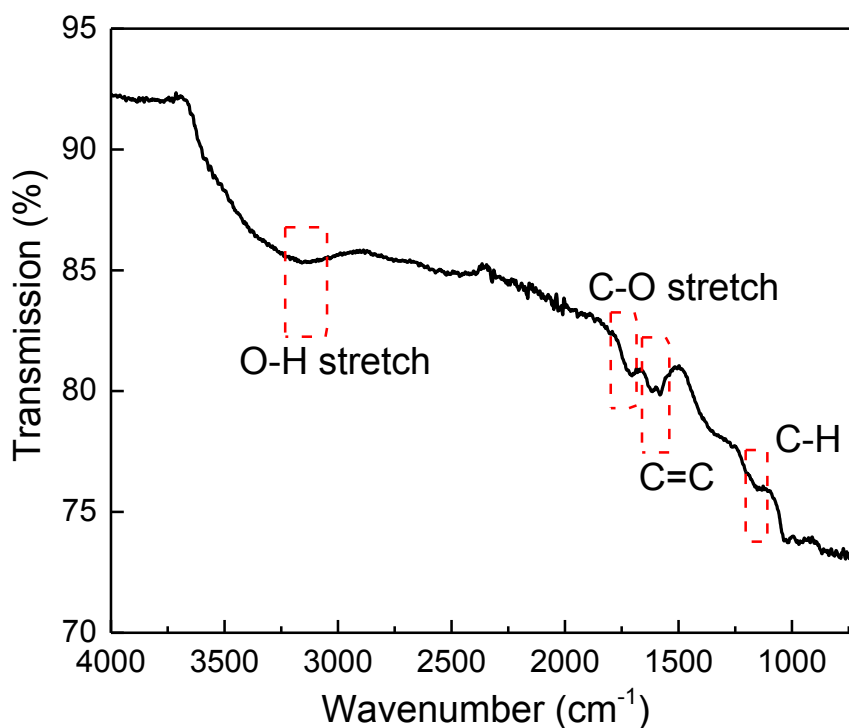


Figure 3.4: FT-IR spectra for GO.

3.4.2. XRD

GO samples were heated to $800\text{ }^{\circ}\text{C}$ at the rate of $10\text{ }^{\circ}\text{C}/\text{min}$ and 50 cc of air flow. XRD was carried out using Bruker D2 fitted with a $\text{Co K}\alpha$ X-ray source. The scans were analysed in the

range of 7° to -90° at a rate of $5^\circ/\text{min}$. The XRD scan is shown in Figure 3.5. The first absorbance peak appears in 2θ equal to 13.75° in the plane Carbon (002) [163]. If compared to the general well known peaks from the graphite, the peak C (002) is dislocated. In graphite the spacing between the graphene layers (d-spacing) is 0.34 nm [164, 165]. When the oxidation of graphite occurs, the oxygen groups are introduced between the graphene layers. Consequently, the spacing between the layers increased to 0.747 nm shifting the absorbance peak. The peak at 2θ of 31.17° is C (002) from the graphite [165, 166], according to this the oxidation was only partial and not complete. The peak at 2θ equal to 38.72° is due the Si base and has no influence from the GO sample. The peaks in this work are shifted from the large amount of the XRD scans found in the literature [163-166] because Co was used as X-ray source and not the regular Cu.

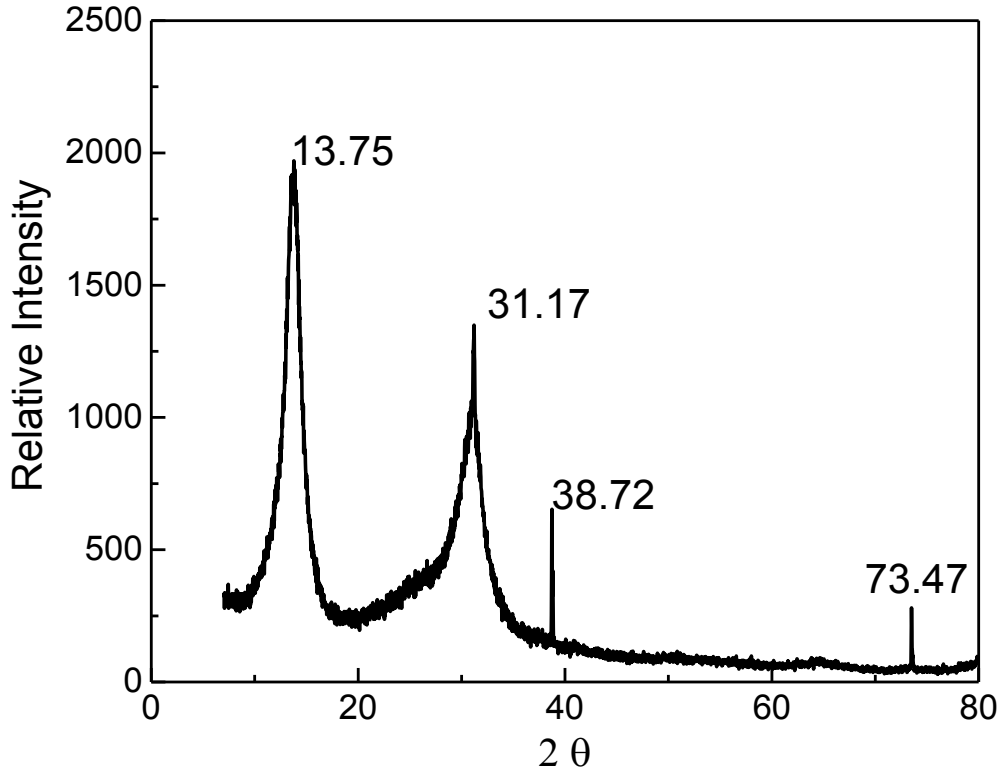


Figure 3.5: XRD scan of GO.

3.4.3. XPS

X-ray photoemission spectroscopy was carried out using an Al K α ($h\nu = 1486.6$ eV) source to identify if the oxidation of graphite occurred. Graphene oxide was successfully synthesized as is shown in the XPS curve of Figure 3.6. In the fitting process for C1s, the peak sp² was found in position 284.52 eV of binding energy (BE) [166]. This peak is common for graphite and represents the larger portion of the sample (~52% from the area). The peak at the position 286.66 eV is related to the C-O-C band, while the peak at the position 286.20 eV refers to C-OH. The peak at 287.79 eV is related to C=O and the peak 289.04 is related to COOH [107, 167]. These four last peaks are only present in GO and not in graphite, showing that the synthesis reaction occurred.

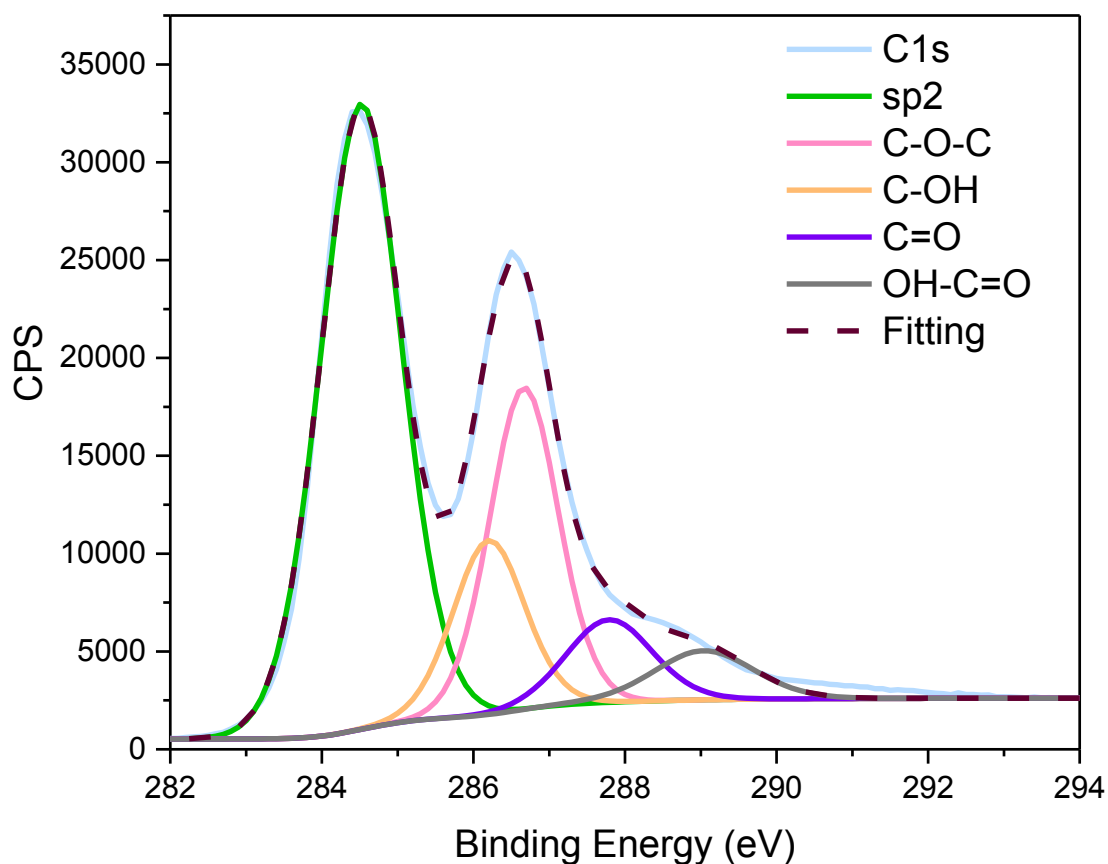


Figure 3.6: XPS fitting curve of synthesized GO.

3.5. Thermal behaviour

Both SPInd and GO were evaluated related to their thermal behaviour with Thermogravimetric analysis (TGA). Differential scanning calorimetry (DSC) analysis was carried out only on SPInd. Three samples of each material were analysed. Details of the experimental protocols are in the Appendix.

3.5.1. TGA

PInd and SPInd were characterised by TGA (2050, TA Instruments) with N₂ at a heating rate of 20 °C per min. The scans are shown in Figure 3.7. The curves show the superior thermal stability and around 8% higher water content of the SPInd sample due to the addition of the sulphonic group. Both these characteristics are ideal for use in fuel cells with operating temperature ranging from 80 to 120 °C. The mass loss and derivative curves show that the pristine polymer presents only one degradation event recorded above 300 °C with a maximum rate at 383.7 °C and a residue of 0.7% after undergoing full oxidation. The TGA crucible was found to be clean after the test, proving that practically none residue was left. On the other hand, when sulphonated, SPInd presents at least three significant events before it undergoes carbonization (400 °C onwards) and degrades slowly, leaving a residue of 3.7% at 950 °C. The first event, with mass loss of 8%, corresponds to water trapped by the sulphonic groups, since the SPInd is a hydrophilic polymer. Water loss occurs in the interval of 25 °C to 120 °C. This is contributed by initial loss of weakly linked molecules followed by the loss of hydrogen bonded water linked to the sulphonic groups, with a maximum evaporation rate at 56 °C. The water percentage in the electrolyte changes according to the degree of sulphonation [158] of the polymer.

The second event, a shoulder in the thermogram at 301 °C, denotes the decomposition of the sulphonic groups. This was followed by a partial decomposition of the polymer chains (third event) with a maximum rate at 350 °C. The loss of the sulphonic groups from the phenylene rings enhances chain condensation leading to carbonization [168]. Following this, above 400 °C, the carbonized material goes through slow oxidation producing higher residue content compared to the pristine polymer. The TGA evaluation showed that SPInd retained water up to 100 °C and no decomposition or degradation was observed until 200 °C confirming its potential suitability for use as an electrolyte for IT-PEFC.

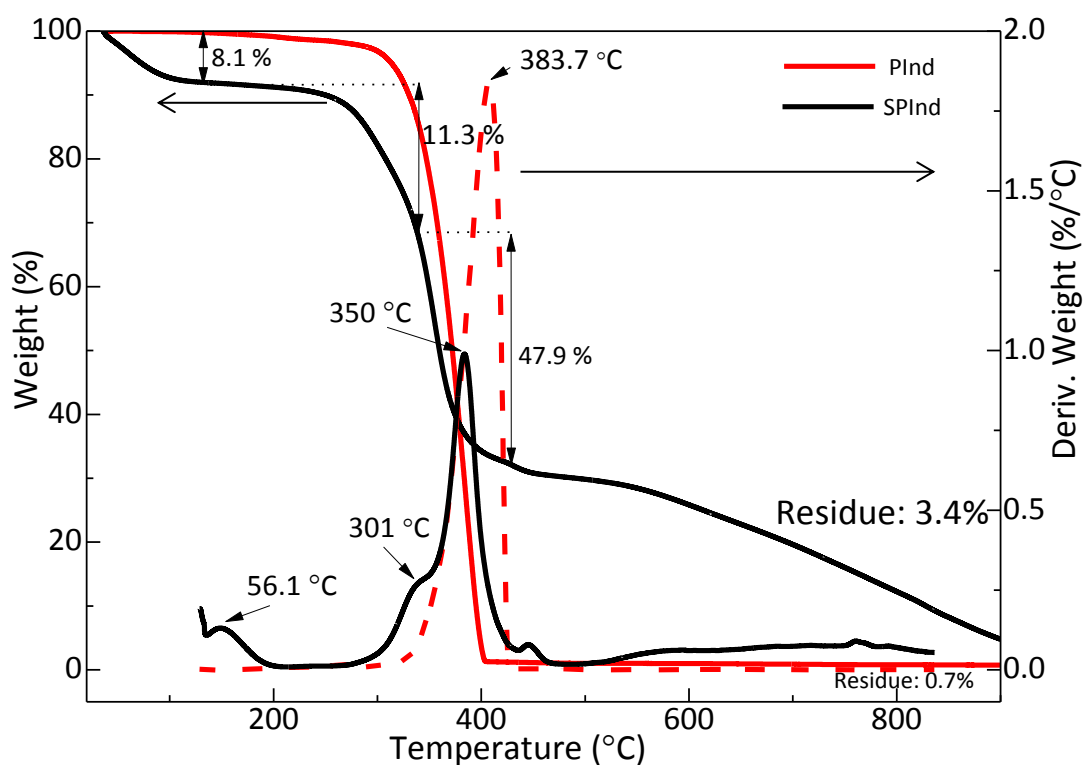


Figure 3.7: PInd and SPInd thermogram curves by TGA

Graphene oxide TGA was performed by the TG 209 F1. GO samples were heated to 800 °C at the heating rate of 10 °C/min and 50 cc of air flow. TGA and its first derivate (DTG) curves for GO are shown in Figure 3.8. The first mass loss in the DTG peak at 80 °C is related to water

and solvents evaporation. This loss starts at ~ 50 °C and terminates at ~ 120 °C. First, free water and low ebullition point solvents are evaporated. As temperature increases, internal water in GO (by hydrogen bonds) is eliminated, until the total dryness revealed at ~ 120 °C. The mass loss was 6%; however, the sample had already been dried in the oven at 80 °C overnight and, thus, this value cannot be related to the total absorbed water in GO. The second peak was found to be between ~ 150 °C and ~ 240 °C, with a mass loss of 22%. It is due to the loss of oxygen from the functional groups such as OH, COOH, CO, etc [169, 170]. Subsequently, the oxidation of graphite was 22%. The third mass loss, which starts at ~ 510 °C and ends at ~ 730 °C, is just present due to the oxygen flow. In the analysis from literature with only nitrogen or argon flow [171, 172], this degradation ramp is not present. Accordingly, it is the oxidation of the main carbon chain, remaining residues of $\sim 1.69\%$ which are associated to impurities in the GO. It is also associated to the loss of more stable oxygen present in the GO [172].

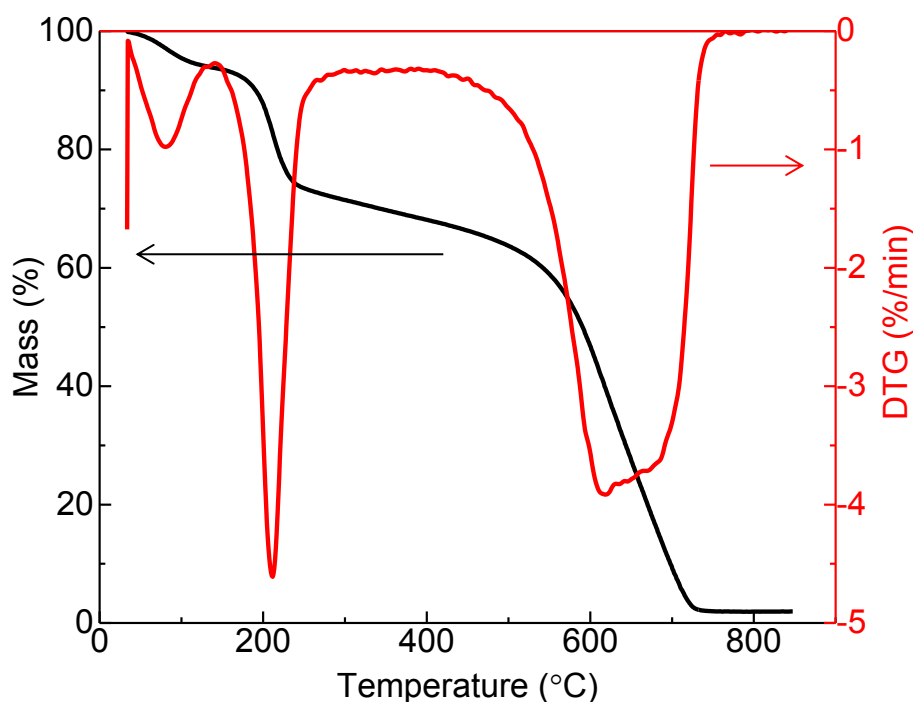


Figure 3.8: TGA curves of GO.

3.5.2. DSC

DSC was carried out in a DSC Q20, TA Instruments, for PInd and SPInd samples with a heating rate of 10 °C/min. Figure 3.9 shows the endothermic curves of the SPInd from first and second run in DSC and the curve obtained from the second run of the PInd. Comparing the curves obtained in second run, it can be seen that PInd reached its glass transition temperature (T_g) at 204 °C, whereas the T_g for the SPInd curve is not clear. The endothermic curve for the SPInd in the first run shows a large peak ($T_{\text{onset}} = 25$ °C; $T_{\text{andset}} = 175$ °C) due to water evaporation with a maximum rate at 102 °C. The enthalpy of vaporization, which is related to water content released from the membrane, was found to be 288 J/g. These results corroborate that SPInd is a suitable polymer electrolyte for membranes operating at 120 °C such as in an IT-PEFC.

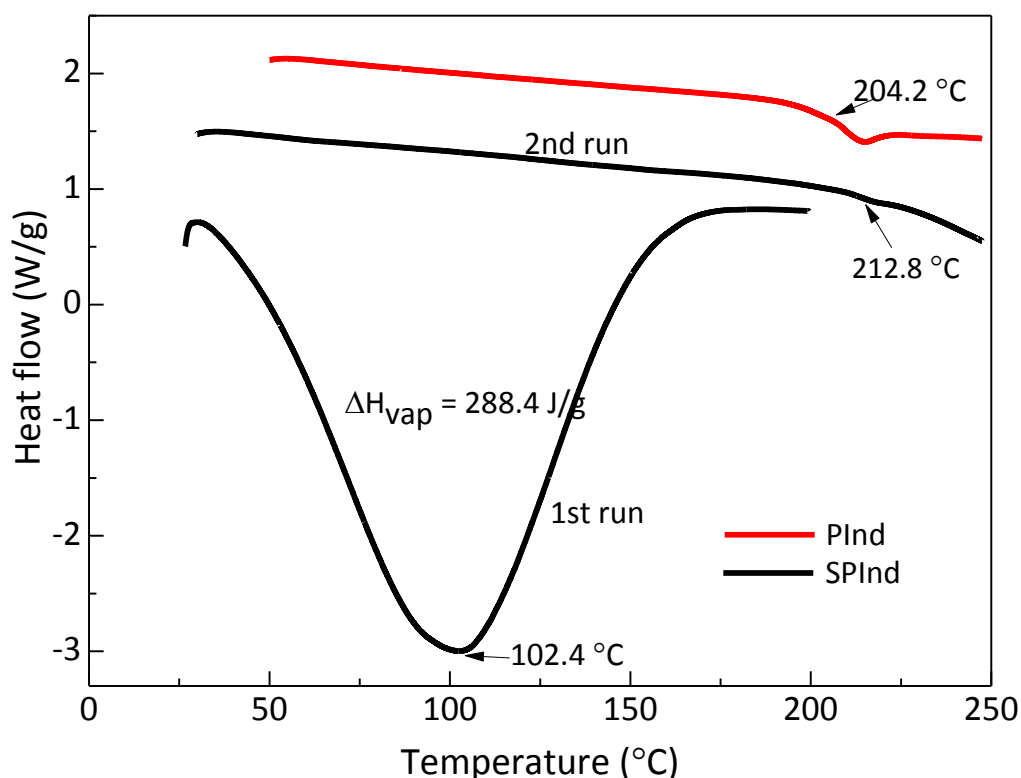


Figure 3.9: DSC curves for PInd and SPInd.

3.6. Conclusions

PIInd synthesis and the sulphonation reaction were successful. The resulting SPIInd can be easily identified by the sulphonic groups bond in the FT-IR analysis at the absorbance peaks 1150 and 1000 cm^{-1} . SPIInd does not have any major loss in mass at temperature as high as 200 °C. The SPIInd Tg was not possible to identify, but up to 120 °C, SPIInd does not suffer modifications. Accordingly, SPIInd is applicable in IT-PEFC without any thermal degradations issues. GO was successfully synthesized from graphite powder as is proved by the chemical analysis. Thermal analysis demonstrated a major event of mass loss only at 200 °C. Thus, GO is also suitable for use in IT-PEFC.

CHAPTER IV – MEMBRANES PREPARATION

Graphene oxide and sulphonated polyindene synthesized and characterized in the previous chapter were used in the membranes preparation prior to single cell testing in intermediate temperature mode. Together with Nafion, they were assembled to multilayer membranes by different methods for further IT-PEFC evaluation. Membranes prepared in this work are classified into three types: I) membranes with Nafion polymer only; II) membranes including SPInd, and III) membranes including GO. Group I contains Nafion single layer membranes, commercial or cast in lab, and Nafion bilayers prepared with commercial single layers or cast single layers. Single layer membranes were assembled to multilayer membranes by hot pressing (HP) or casting. The second group comprises SPInd single layer membranes and Nafion-SPInd-Nafion multilayer membranes which were prepared by HP and casting. Nafion-GO-Nafion membranes prepared by HP and casting constitute group III.

The membrane nomenclature is $[A_X/B_Y/C_Z]_W$ where A and C are the external layer materials, and B is the inner layer material. If the membrane is a bilayer, it is labelled as $[A_X/B_Y]_W$ and if the membrane is a single layer it is defined as A_X . The subscripted letters X, Y, Z are relative to the preparation method of each layer, which can be C (casting) or F (filtration). The subscripted W is the method with which the membrane layers were assembled (C or HP) into a multilayer membrane. For example, the bilayer membrane $[N_C/N_C]_C$ contains two layers of cast Nafion assembled by casting. The prepared membranes are detailed in Table 4.1.

Table 4.1: Layer structure of the membranes prepared.

	Membrane nomenclature	Bottom layer	Inner layer*	Top layer	Assembling method
Group I	N212	Nafion 212	--	--	--
	N_c	cast Nafion	--	--	--
	$[N_{211}/N_{211}]_{HP}$	Nafion 211	Nafion 211	--	Hot pressing
	$[N_c/N_c]_{HP}$	cast Nafion	cast Nafion	--	Hot pressing
	$[N_c/N_c]_c$	cast Nafion	cast Nafion	--	Casting
Group II	$SPInd_c$	cast sulphonated polyindene	--	--	--
	$[N_c/SPInd_c/N_c]_{HP}$	cast Nafion	cast sulphonated polyindene	cast Nafion	Hot pressing
	$[N_c/SPInd-5N_c/N_c]_c$	cast Nafion	cast sulphonated polyindene with 5 wt.% of Nafion	cast Nafion	Casting
	$[N_c/SPInd-10N_c/N_c]_c$	cast Nafion	cast sulphonated polyindene with 10 wt.% of Nafion	cast Nafion	Casting
	$[N_c/SPInd-20N_c/N_c]_c$	cast Nafion	cast sulphonated polyindene with 20 wt.% of Nafion	cast Nafion	Casting
Group III	$[N_c/GO_F/N_c]_{HP}$	cast Nafion	filtered GO film	cast Nafion	Hot pressing
	$[N_c/GO-10N_F/N_c]_{HP}$	cast Nafion	filtered GO film with 10 wt.% of Nafion	cast Nafion	Hot pressing
	$[N_c/GO-20N_F/N_c]_{HP}$	cast Nafion	filtered GO film with 20 wt.% of Nafion	cast Nafion	Hot pressing
	$[N_c/GO-30N_F/N_c]_{HP}$	cast Nafion	filtered GO film with 30 wt.% of Nafion	cast Nafion	Hot pressing
	$[N_c/0.5GO_c/N_c]_c$	cast Nafion	cast 0.5 wt.% GO	cast Nafion	Casting
	$[N_c/0.5GO-5N_c/N_c]_c$	cast Nafion	cast 0.5 wt.% GO with 5 wt.% of Nafion	cast Nafion	Casting
	$[N_c/0.5GO-20N_c/N_c]_c$	cast Nafion	cast 0.5 wt.% GO with 20 wt.% of Nafion	cast Nafion	Casting
$[N_c/2.5GO_c/N_c]_c$	cast Nafion	cast 2.5 wt.% GO	cast Nafion	Casting	

Membrane nomenclature	Bottom layer	Inner layer*	Top layer	Assembling method
$[N_c/2.5GO-5N_c/N_c]_c$	cast Nafion	cast 2.5 wt.% GO with 5 wt.% of Nafion	cast Nafion	Casting
$[N_c/2.5GO-20N_c/N_c]_c$	cast Nafion	cast 2.5 wt.% GO with 20 wt.% of Nafion	cast Nafion	Casting
$[N_c/4.5GO_c/N_c]_c$	cast Nafion	cast 4.5 wt.% GO	cast Nafion	Casting
$[N_c/4.5GO-5N_c/N_c]_c$	cast Nafion	cast 4.5 wt.% GO with 5 wt.% of Nafion	cast Nafion	Casting
$[N_c/4.5GO-20N_c/N_c]_c$	cast Nafion	cast 4.5 wt.% GO with 20 wt.% of Nafion	cast Nafion	Casting
$[N_c/6.5GO_c/N_c]_c$	cast Nafion	cast 6.5 wt.% GO	cast Nafion	Casting
$[N_c/6.5GO-5N_c/N_c]_c$	cast Nafion	cast 6.5 wt.% GO with 5 wt.% of Nafion	cast Nafion	Casting
$[N_c/6.5GO-20N_c/N_c]_c$	cast Nafion	cast 6.5 wt.% GO with 20 wt.% of Nafion	cast Nafion	Casting

*Nafion content in Group II and III is referred to SPInd and GO weight respectively. For example, in $[N_c/SPInd-10N_c/N_c]_c$, 10 wt% of Nafion with respect to the total SPInd weight. GO content in Group III is related to the total multilayer membrane without Nafion in the inner layer. For example in $[N_c/6.5GO-5N_c/N_c]_{HP}$, there are 6.5 wt.% of GO in the total membrane weight (not considering Nafion in the inner layer) and 5 wt.% of Nafion with respect to the total GO weight.

This chapter presents the membrane preparation methods: hot pressing, casting and filtration. It further discusses the optimization parameters for the processes and compositions. The following sections are divided according to the single layer membranes, and then by multilayer preparation method: hot pressed membranes and cast membranes.

4.1. Single layer membranes

Nafion and SPInd single layer membranes, for evaluation on their own or for further hot pressing into a multilayer membrane (MM), were prepared by casting. Casting is the process of formation of a film or membrane on a flat surface by the evaporation of the solvent.

4.1.1. Nafion single layers

To prepare N_C, 2.5 to 7 mL of Nafion solution 10 v/v% (D1021, Ion Power) was poured on a flat petri dish, varying the amount of Nafion proportional to the target thickness of the final membrane. Table 4.2 summarises the thickness and the volume of the Nafion solution required. The petri dish with the solution was placed for drying in an oven at 100 °C for 2 h and at 120 °C for further 1 h for annealing the polymer.

Table 4.2: Volume of Nafion solution required to achieve the target thickness.

Nafion solution (mL)	Target thickness (µm)	Actual thickness
7	50	55 ± 2
3.5	25	24 ± 1
2.8	20	20 ± 2
2.1	15	16 ± 2
1.4	10	13 ± 3

The parameters to cast Nafion have been widely discussed in literature [173-175]. To prepare membranes from polymer solutions, the slower the evaporation of solvent, the

lower the number of visible defects, such as pin holes. However, the membrane formed by solution casting is mechanically weak [173, 175], which is not desirable in a PEFC. A heat treatment can increase the mechanical stability of cast membrane. This heat treatment can be done by two methods, either with boiling solvents or by annealing at higher temperature with subsequent solvent evaporation. Unlike regular evaporation, in the boiling technique, the solvent is only removed after boiling. Vengatesan *et al.* [173, 175] affirmed that cast Nafion films at low temperature (i.e. room temperature) have a micellar structure, with PTFE in the backbone and sulphonic groups in the outside structure. This structure is similar to Nafion polymer in solution [176]. However, with the heat treatment, the structure is inverted and the PTFE migrates to the external part of the micelles and the sulphonic groups migrate to the internal part [173, 177] which is more analogous to N212 and N211 commercial membranes. These sulphonic groups inside the structure form ionic clusters that are the passageways for the protons in the PEFC. Jung *et al.* [178] found that the crystallinity of the polymer increases with the heat treatment, increasing the membrane water uptake. Nevertheless, if the crystallinity increases beyond a certain limit, the ionic cluster will shrink more than desired and the ionic conductivity will decrease. Vengatesan *et al.* [173] found that to achieve the maximum crystallinity with the best performance in a FC, Nafion should be submitted to 150 °C for 6 h. The increase in crystallinity also reduces the membrane solubility in solvents after casting, since perfluorosulphonate ionomer films cast at room temperature are soluble in most polar solvents [176]. Gebel *et al.* [177] annealed the polymer at 120 °C while casting Nafion, producing stronger and more resistant membranes. Similarly, in the present study, lower temperatures than in the other reported work were

chosen to reduce the formation of pinholes in the membrane. Still, heat treatment (without boiling solvents) was carried out to improve the proton conductivity.

Single layer Nafion membranes N212 and N211 have different properties from N_c . For example, they are insoluble in solvents while cast Nafion can be solubilised depending on the casting temperature. Moore *et al.* [176] have proven that with heat treatment at 200 °C and boiling solvents, N_c becomes insoluble in most solvents. In addition to this, the rate of evaporation and the temperature during casting are important in avoiding cracking and brittle polymers. The lower the temperature, the brittle the final membrane. With temperatures around 120 – 200 °C [176, 177], this can be avoided. The treatment increases the density of the membranes [175] making them similar to the as-received membranes N212 and N211. Due to the formation of an intense ionic cluster in N_c , the water content in those membranes should be higher than in N212 and N211.

4.1.2. SPInd single layers

SPInd_c membranes with 50 µm thickness were prepared by dissolving the polymer in powder form in 5 mL of dimethyl sulphoxide (DMSO). DMSO has a high boiling point (189 °C) which can produce a more uniform and higher quality membrane due to the slow solvent evaporation [179]. The choice of solvent is essential in the casting method. It is necessary that the polymer dissolves uniformly in the solvent to obtain a uniform membrane. The degree of crystallinity, as described for Nafion above, depends on the solvent, as this characteristic completely changes the properties of a membrane. Traditional amine solvents for casting, such as dimethylformamide (DMF), reduce the proton mobility due to the hydrogen bonds formed with sulphonic groups in the polymer, even at low temperatures,

consequently, reducing the proton conductivity [180]. Therefore, the most suitable solvent for SPInd is DMSO if compared with amine solvents with high boiling point.

To obtain a less brittle membrane, Nafion (in solution form) was added to the SPInd solution and then cast at 80 °C for 2 h and annealed at 100 °C for further 2 h. The content of Nafion varied between 20, 30 and 40 wt.% with respect to the SPInd content and is described in Table 4.3. The membrane with 20 wt.% of Nafion was less brittle and easier to remove from the petri dish and it was selected for use as reference SPInd_c for comparison purposes.

Table 4.3: Approaches to cast single layer of SPInd with 50 μm of thickness.

SPInd weight (g)	Volume of Nafion solution (10 v/v.%) (mL)	Concentration of Nafion in the membrane (wt.%)
0.096	0.24	20
0.084	0.36	30
0.072	0.48	40

The layer of SPInd to be used as inner layer in the [N_c/SPInd_c/N_c]_{HP} should be thinner than the SPInd_c single layer membrane. As such, to reduce the thickness, 0.06 g of SPInd were dissolved in 5 mL of DMSO with 150 μL of Nafion solution (to obtain 20 wt.% of Nafion). Then, the membrane was cast as described above for a SPInd_c single layer. However, this membrane was difficult to handle and due to its fragile nature, cracked while peeled off from the petri dish. To resolve this, a thin layer of Nafion was cast on the bottom of the petri dish and the layer of SPInd above it (Figure 4.1(a)). Figure 4.2(b) shows the micrograph image of the SPInd_c layer cross section. The porous structure present in the membrane is due the evaporation of the solvent and characteristic of the SPInd polymer. The uniformity in the porosity shows that the evaporation was fast (high temperature). When the solvent leaves the polymer slowly, the bottom part of the membrane has time to seal down the

pores, while the top of the membrane remains porous due to the continuous evaporation of the solvent.

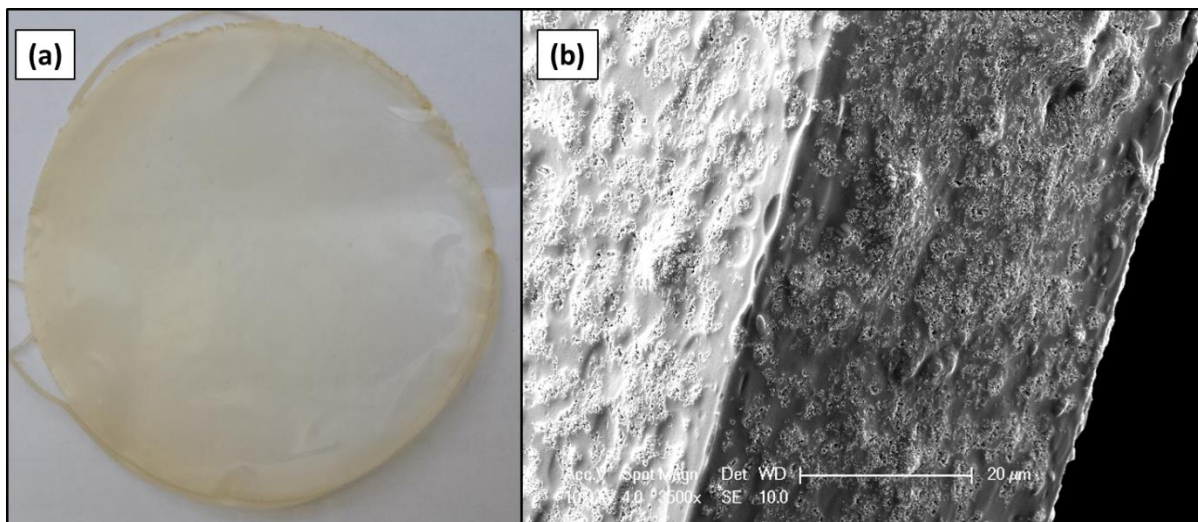


Figure 4.1: (a) Thin SPInd membrane cast over Nafion layer to use as inner layer in $[N_c/SPInd_c/N_c]_{HP}$. (b) Micrograph image of the cross-section of the SPInd_c membrane, 3500x magnification, 20 μ m scale.

4.1.3. GO single layers

To prepare a thin film of GO, vacuum assisted filtration was used, which in recent years has become a popular method to produce these films [171, 181-185]. This technique can produce films as thin as 2- 10 μ m, allowing an entire new set of applications. 3 mL of the aqueous GO solution, as prepared in Chapter III, was diluted in 200 mL of deionized (DI) water. The solution was then vacuum filtrated (Figure 4.2(a)) through the Anodisc 47 (purchased from Whatman, pore-size 0.02 μ m and diameter of 47 mm). The film with the filter was dried in an oven at 60 °C overnight. Afterwards, the film (highlighted in Fig 4.2(a)) was peeled off from the filter and used for further hot pressing with Nafion single layer membranes.

These films of GO are formed by a semi-ordered mechanism as discussed by Putz *et al.* [186] and shown in Figure 4.2(b). At the first moment, GO remains dispersed in water while there is still plenty of solvent. As the solvent is being removed, GO solubility starts to reach the limit. Consequently, GO basal planes begin to align more orderly. However, the space between those planes is bigger than the final spaces between them in the filtered film. When most of the water is removed, the pressure from the air column and vacuum completely align the GO sheets in an ordered way. Nevertheless, water is still present between the sheets and must be removed by drying the film overnight to form highly packed films as shown in the micrograph image of the cross-section in Figure 4.3(a).

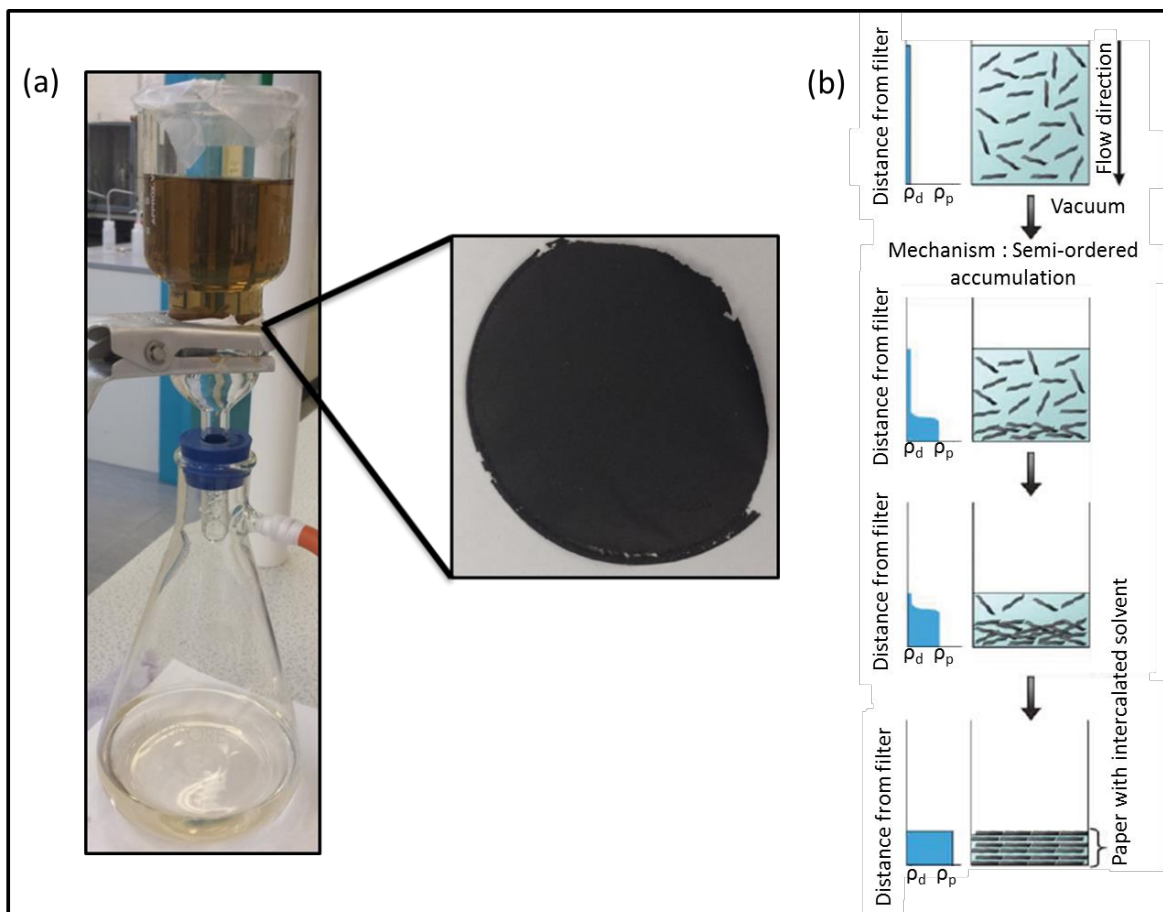


Figure 4.2: (a) Vacuum assisted filtration to produce GO film. Inset: thin filtrated GO film. (b) Semi-ordered mechanism to form the GO film by filtration, where ρ_d is the density of the dispersion and ρ_p is the density of the paper, adapted from [186].

GO films formed by vacuum assisted filtration were more brittle than the ones formed by casting, as Huang *et al.* [187] reported in their hybrid films of GO/CNTs or Chen *et al.* [188] in their GO films by free standing evaporation of solvents. In both those cases, the slow solvent removal allows the formation of long fragments of GO sheets, which leads to softness in the film. In the case of vacuum assisted filtration, the water removal is aggressive and fast, resulting in the formation of short fragments of GO that can be seen in Figure 4.3(b). This kind of microstructure makes the film more brittle, but it also has some advantages. In GO, the concentration of ketones and carboxyl groups is higher at the edge planes, and that of epoxides and alcohols is higher in the basal planes [166, 189]. With small fragments, the surface area is larger, exposing the oxygen groups, which may increase the water retention in the structure.

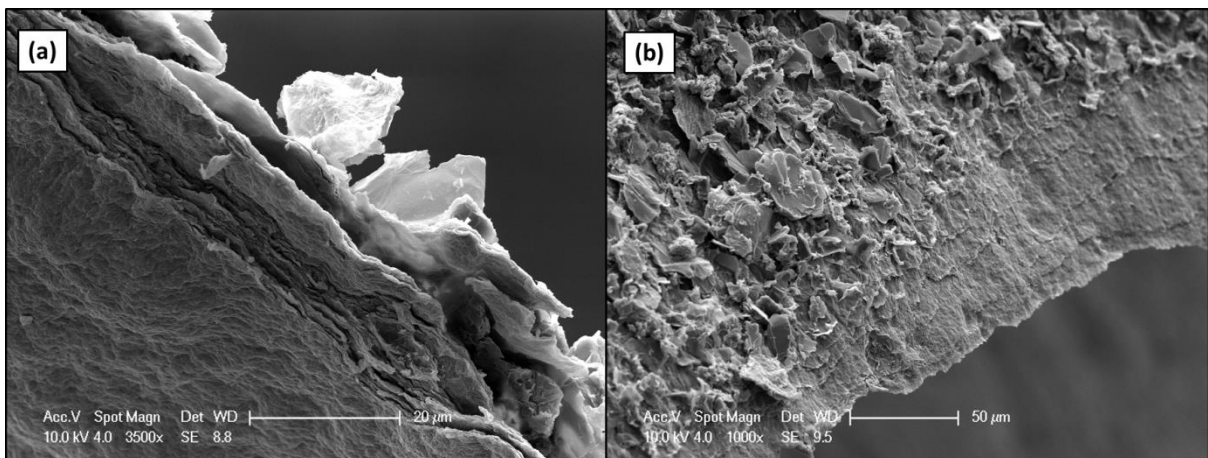


Figure 4.3: GO filtered films (a) cross section, 3500x magnification, 20 μm scale and (b) surface 1000x magnification, 50 μm scale.

To reduce the GO film brittleness due to vacuum filtration, Nafion was added during the filtration. It is a common method to add a polymer to an oxide film to give plasticity to the final composite film [190-194]. The resultant composite will show properties balanced between the properties of both materials. Accordingly, it will have the plasticity of the

polymer and the characteristics of GO such as hydrophilicity. The vacuum assisted filtration technique for the fabrication of GO composite films has already been reported with different polymers such as poly(vinyl alcohol) (PVA) [182, 183], or silk [184]. In this study, Nafion has been chosen as the polymer to be added because the thin GO_F film will be the inner layer in the [N_C/GO_F/N_C]_{HP} membrane. Accordingly, the interaction between the inner layer and external layers can be improved by adding Nafion. This interaction is an important factor in the optimization of the hot pressing process, which will be discussed in the next section of this chapter.

Nafion was added to the GO film in the ratios of 10, 20 and 30 wt.% with respect to GO weight, with Nafion solution volumes of 9, 18 and 27 µL. The polymer addition was made when there was 100 mL remaining of the GO/water solution to be filtered. Thus, there still were spaces between the GO planes for Nafion to pass into and settle as described in the semi-ordered mechanism of the film formation [182, 186]. Energy dispersive X-ray spectroscopy (EDS) was carried out to confirm that Nafion was retained in the film and did not pass through the filter. Comparative EDS spectra of GO_F and GO-30N_F are shown in Figure 4.4(a) and (b) respectively. Considering the elements present in Nafion and GO, sulphur and fluorine should be present only in Nafion. However, sulphur was a contamination found in all the membranes because it was not completely eliminated in the GO purification process and it is a common impurity in the lab environment. On the other hand, fluorine was present only in Nafion. Fluorine, thereby, was chosen to be the comparative element. As can be seen, fluorine was not present in the GO_F and it was in the GO-30N_F, suggesting that Nafion was retained in the film. Figure 4.4(c) shows the elemental mapping and distribution in the GO-30N_F film, by order from the top to the bottom: fluorine,

carbon, oxygen and sulphur. Fluorine was observed throughout the film, showing a uniform distribution of Nafion.

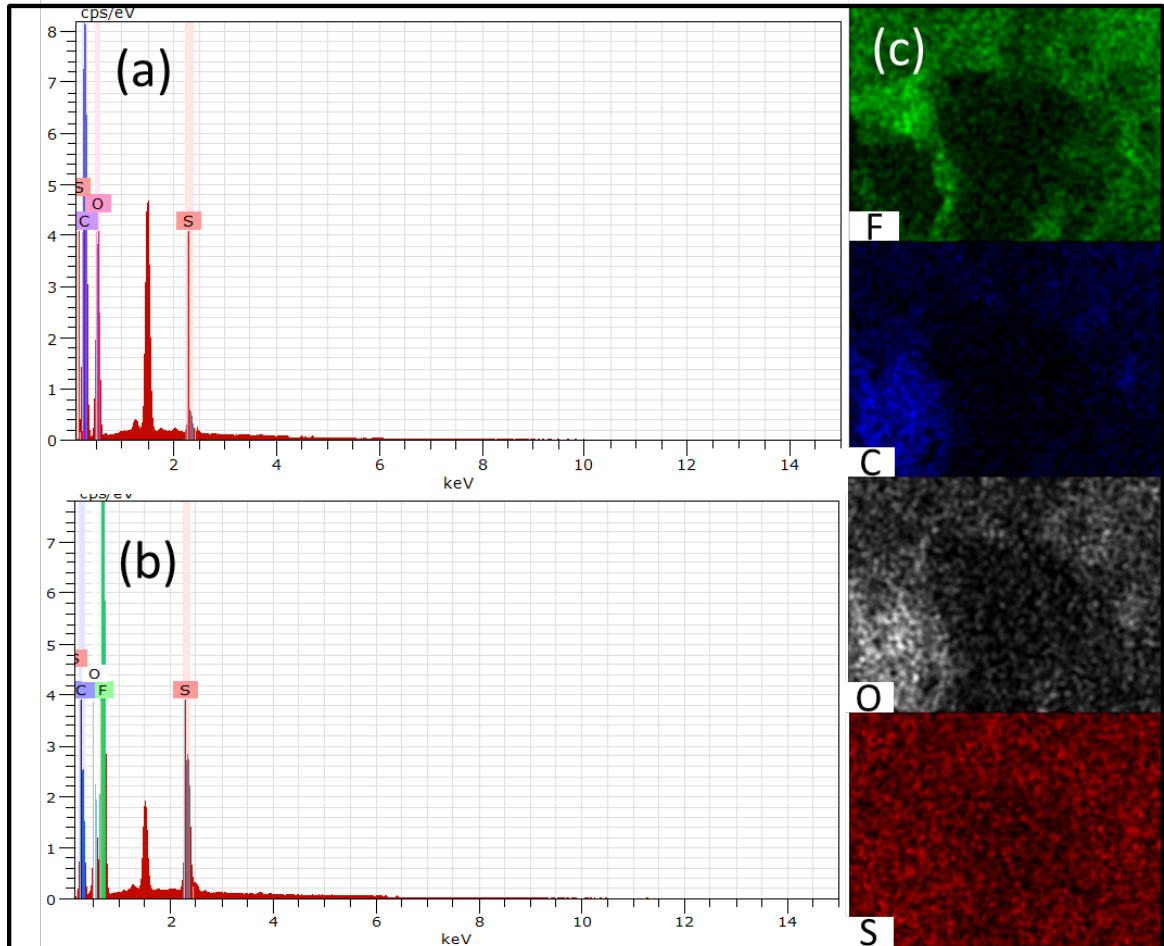


Figure 4.4: (a) EDS spectrum for the GO_F film, (b) EDS spectrum for the GO-30N_F film and (c) elemental mapping for the GO-30N_F film for the elements fluor, carbon, oxygen, and sulphur (top to bottom).

4.2. Hot pressed membranes

Although there are hot pressed membranes in all the three groups of membranes described in Table 4.1, the interaction between the layers to keep the adhesion intact is unique for each case. In the first group, Nafion bilayers have the same equivalent polymer in both layers, enabling an easy adhesion and interaction. In the second group, the layers still consist of polymers. However, the inner layer is an aromatic hydrophilic polymer (SPInd), different

from the external layers of Nafion non-aromatic PFSA polymer. Nafion has a hydrophilic surface due to the sulphonic groups while its backbone has hydrophobic fluorine groups. As such, the interface SPInd-Nafion will not be as strong as in the bilayers of Nafion. In the third case, the inner layer is not a polymer but a layer of graphene oxide, which has lower attraction with the external layers of Nafion than SPInd. However, it is a highly hydrophilic material that even in a dry state can keep water molecules trapped inside the structure, weakening the adhesion. Therefore, the optimization of hot pressing conditions varies for each case, which is discussed in the following.

N_c membranes with a thickness of approx. 25 μm were chosen to identify the HP parameters for the bilayers. The membranes were positioned between two aluminium foils and hot pressed. The HP conditions including pressure, temperature and time are detailed in Table 4.4. In summary, Nafion bilayers posed no problem with respect to adhesion if hot pressed for the period of 5 min with a pressure of 6.9 MPa (1000 psi) at 125 or 130 °C. With shorter periods than 5 min, the membrane layers did not adhere to each other, while with pressing longer times, the membrane stuck to the aluminium foil. At temperatures above 130 °C the membrane adhered more to the aluminium foil and could not be removed without damage. The glass transition temperature (T_g) for Nafion is ~ 125 °C [195] due to the movement of the main chain. It is known that water acts as a plasticizer, increasing the mobility of the main chain and lowering Nafion's T_g [195]. As a result, if there is some water in the membrane, it will decrease the T_g and increase the adherence between polymer and aluminium foil. If the temperature is increased during hot pressing, the temperature gradient for the T_g is higher, causing polymer softening and higher adhesion to the foil. Besides, the aluminium foil oxide layer has a very irregular roughness surface [196]. Due to

this surface characteristic, the polymer, at temperatures higher than its T_g or at extended pressing times, can deform and adhere to the peaks and valleys of the aluminium foil surface, making it more difficult to peel the membrane off.

Nafion single layers can adhere to each other at these low temperatures due to the high affinity between the layers (same material). However, N_c single layers must be dried before hot pressing the assemblies. Water trapped between the layers can force its way out from the membranes as the temperature and pressure increase, creating holes on the membrane surface.

Table 4.4: Hot pressing parameters for $[N_c/N_c]_{HP}$ membrane sandwiched between aluminium foil.

	Temperature (°C)	Time (min)	Pressure (MPa) ²	Outcome
Aluminium Foil	125	5	6.9	√
	130	2.5	6.9	X
	130	5	6.9	√
	130	7.5	6.9	X
	135	5	6.9	X
	140	5	6.9	X

The membranes $[N_c/SPInd_c/N_c]_{HP}$ were hot pressed following the parameters detailed in Table 4.5. Although $SPInd_c$ and N_c are polymer membranes, their properties differ considerably. As discussed in Chapter III, the $PInd$ has a $T_g \sim 204$ °C. For the $SPInd$ T_g is not clear, but is believed to be higher than Nafion. The difference in the T_g causes differential behaviour during hot pressing. At 125 °C, Nafion chains gain a certain mobility, while the $SPInd$ chains are still frozen. Consequently, the adhesion between the layers is

² 6.9 MPa= 1000 psi

compromised. Besides, this different thermal behaviour leads to expansion and contraction by the polymers at different temperatures. These differences can cause small spacing between the layers, making the adhesion poor or even difficult. The roughness of the polymer layers is also different which adds to problems in adhesion and thus in the multilayer properties and their applicability.

Table 4.5: Hot pressing parameters detailed for the multilayer membranes $[N_C/SPInd_C/N_C]_{HP}$ sandwiched between aluminium foils.

	Temperature (°C)	Time (min)	Pressure (MPa)	Outcome
Aluminium Foil	125	5	6.9	X
	130	5	6.9	X
	130	4	6.9	√
	130	3	6.9	√

Peng *et al.* [129] hot pressed a bilayer of Nafion 212 and Aquivon E_{79-05s} in two steps. First, at 170 °C for 2.5 min with 0.05 MPa (=7.2 psi) and a second step at the same temperature for 3.5 min with 3.5 MPa (=507.5 psi). This was the temperature used because it is higher than the Aquivon mechanical relaxation temperature, which is higher than Nafion.

In this work, the membranes $[N_C/SPInd_C/N_C]_{HP}$ were hot pressed between two aluminium foils, at different conditions. The one that presented the best adhesion was 130 °C, 6.9 psi for 4 min. In this condition the layers adhered to each other but did not stick to the aluminium foil. This temperature, being higher than the Nafion T_g, can enhance diffusion between the polymers [197], improving the interfacial interaction. Although the essence of the interfacial adhesion between two polymers in the HP process is mainly limited to

mechanical interaction [18], with a temperature above the T_g there is some chemical attachment through diffusion.

The high number of polar sulphonic groups in the SPInd tend to be a factor in improving the interface adhesion [198]. However, while casting the Nafion single layer membrane, with the heat treatment, the micellar structure is inverted, as described above. Therefore, on the Nafion inverted structure surface, the presence of the PTFE backbone is more pronounced in the external structure than in the centre, where the ionic clusters of sulphonic groups are located. This inversion aggravates the poor adhesion between Nafion and SPInd, considering that otherwise the polar groups would attach to each other strengthening the interface.

The parameters used to define the optimization process for hot pressing $[N_C/GO-xN_F/N_C]_{HP}$ were tested with a membrane with $x=0$, *i.e.* no Nafion in the inner layer, and applied to the whole series. These are detailed in Table 4.6. The membranes, as in the case of Nafion bilayers and multilayer SPInd, were hot pressed between two aluminium foils. Unlike Nafion bilayers, these membranes showed assembly problems at temperatures below 130 °C.

Although there are many reports about Nafion-GO composite membranes [107, 199], multilayer membranes with GO [131] are still a new field with minimal discussion about the manufacturing and optimizing process. The first attempt to assemble the membranes by hot pressing was carried out by placing (between two aluminium foils) cast Nafion, a thin filtered film of GO, and cast Nafion, in this order, and hot press at 125 °C, 6.9 psi for 5 min. However, there was no adherence between the layers, even with the GO film diameter smaller than the Nafion membrane diameter. The diameter of the Nafion membrane must be larger than that of the GO, because Nafion shows more interlayer interaction to Nafion than to an

inorganic oxide such as GO. As GO is not a polymer, it has no Tg, unlike Nafion or SPInd, and consequently no chains to move at this temperature. GO, as seen in Chapter III, does not undergo any main change in the structure at 125 °C that could aid the adhesion. Therefore the GO layer needs to be dropped between the two Nafion layers that seal along the rim around it.

Table 4.6: Hot pressing parameters for the membranes $[N_C/GO_F/N_C]_{HP}$.

	Temperature (°C)	Time (min)	Pressure (MPa)	Outcome
Aluminium Foil	125	5	6.9	X
	125	7.5	6.9	X
	130	2	10.35	X
	130	2.5	10.35	X
	130	3	6.9	X
	130	3	10.35	X
	130	4	5.52	X
	130	5	10.35	X
	135	2	10.35	X
	140	5	6.9	X
	125	2	6.9	X
	130	2	6.9	X
	130	1	3.45	X
	130	2	6.9	X
	130	2	3.45	√
	130	3	6.9	√
	130	2	5.52	√
	130	3	6.9	√
	130	2	5.52	√
	135	1	6.9	√

GO, different from polymers such as Nafion, is extremely hydrophilic due the high number of oxygen groups. Thus, the water trapped inside the internal structure by hydrogen bonds is

difficult to eliminate. GO was dried as much as possible before the hot pressing. Nevertheless, the water attached by hydrogen bonds remains in the GO structure and, with the pressure and heating, finds a way through the Nafion membrane, causing visible holes. Consequently, a two-step method for the HP was developed: 1st) Hot pressing at lower temperature to eliminate the water and 2nd) Hot pressing at higher temperature to complete adhesion of the membranes together and to improve the interface.

When hot pressing $[N_C/GO_F/N_C]_{HP}$, the presence of water in the GO film substantially influences HP parameters. As explained above, for Nafion, water acts as a plasticizer and reduces Nafion's T_g . Thus, even though Nafion is dried before the HP process, water molecules in the GO membrane will be free at these conditions and will migrate to the external layers due to the pressure. At this moment this will lower Nafion's T_g and will ensure that it adheres to the aluminium foil as shown in Figure 4.5. Accordingly, increasing the temperature is an attempt to complete water elimination. Especially the two-step process, because at low temperature water starts to migrate to the external layer. As there still is space between the layers, water can leave through this space and does not cause pinholes. Consequently, the final temperature to assemble the membrane can be increased.



Figure 4.5: GO multilayer membrane after HP with each external layer of Nafion stuck on the aluminium foil.

For hot pressing, the parameters 1st step – 130 °C, 5.52 MPa, 2 min; 2nd step – 135 °C, 6.9 MPa, 1 min for [N_C/GO_F/N_C]_{HP} and 130 °C, 6.9 MPa, 4 min for [N_C/SPInd_C/N_C]_{HP} with aluminium foil were succeeded. Nevertheless, increasing the HP temperature may increase Nafion performance as a proton conductor. Likewise, higher temperatures can lead to better adhesion between the layers. As Liang *et al.* [200] reported, during the hot pressing, sulphur in the Nafion surface is reduced if compared with the amount of fluorine groups. This happens because the sulphur is not as stable at this temperature as the fluorine and can be eliminated. This interpretation can mislead to an impression that the proton conductivity will be reduced due to the lower number of sulphonic groups. However, the ratio between both (sulphur and fluorine) is not reduced. The temperature allows the sulphur from the bulk of the membrane to move to the surface, increasing the proton conduction activity. Accordingly, the increase in the temperature during HP can be a positive factor in assisting the three-layer membrane to act as a PEM. It can activate the sulphur, which at low temperature would not participate as active site.

Increasing the temperature during the hot pressing, does not allow to use aluminium foil. As seen in Table 4.4, the Nafion membrane adhered to the aluminium at temperatures ~140 °C. Thus, the external material had to be changed. PTFE sheets were chosen to be the base for the membrane hot pressing, which is exemplified in Figure 4.6. The process is equivalent for all materials, as is specified in (a) with [N_C/SPInd_C/N_C]_{HP}, (b) with [N_C/GO_F/N_C]_{HP} and (c) with [N/N]_{HP}.

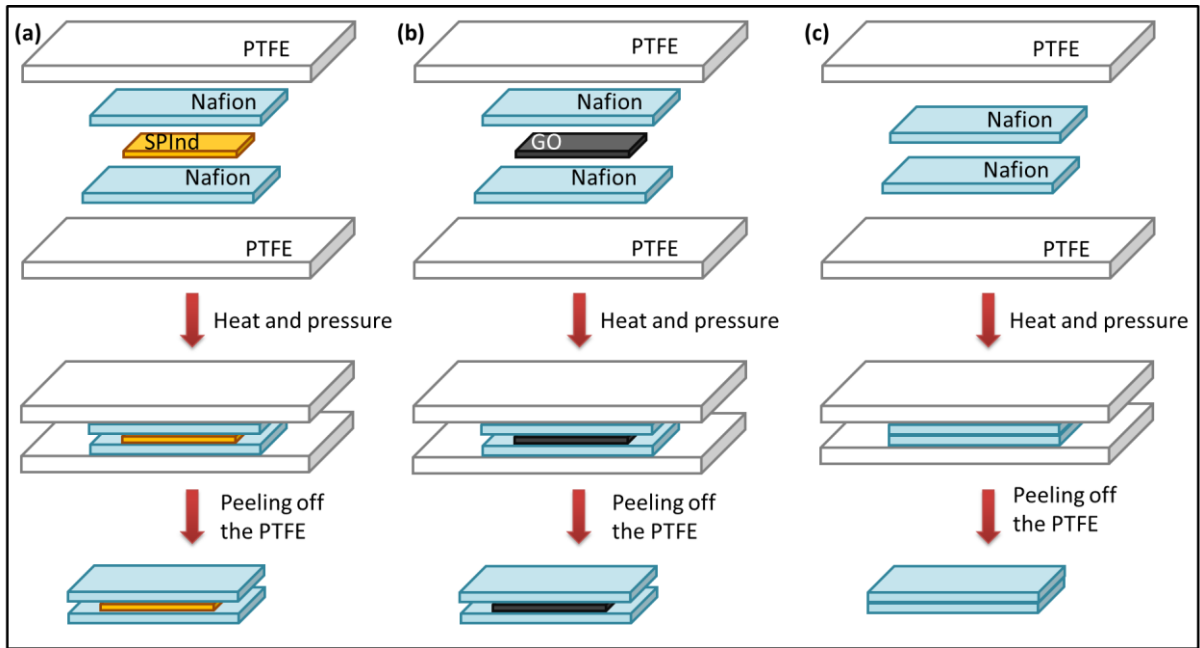


Figure 4.6: Schematic illustration of the hot pressing procedure to obtain the multilayer membranes (a) $[N_c/SPIInd_c/N_c]_{HP}$, (b) $[N_c/GO_c/N_c]_{HP}$ and (c) $[N/N]_{HP}$.

The parameters for PTFE hot pressing used for each group of membranes are specified in Table 4.7. As mentioned before, Peng *et al.* [129] reported hot pressing at 170 °C with Nafion 212. Accordingly, the hot pressing for $[N_c/N_c]_{HP}$ was tested at this temperature at 6. MPa for 5 min. The membrane showed a good adhesion between the layers but did not stick to the PTFE sheet. This was unlike $[N_c/SPIInd_c/N_c]_{HP}$, which at these conditions was not able to be peeled off from the PTFE without damage. As such, to standardize the hot pressing conditions for both series of membranes, Nafion bilayers and SPIInd multilayers were assembled at 160 °C, 6.9 MPa for 5 min. On the other hand, for $[N_c/GO_c/N_c]_{HP}$ one step pressing even at high temperature was not effective, allowing water escape through holes. Therefore, this membrane was assembled in two steps to allow water elimination (1st step) and to complete adhesion (2nd step). The parameters used in all $[N_c/GO_c/N_c]_{HP}$ series from this point and beyond were 1st step – 125 °C, .6.9 MPa for 1 min, and 2nd step – 160 °C, 6.9 MPa for 2 min.

Table 4.7: Hot pressing parameters for the multilayer membranes with PTFE sheets cover.

	Membrane	Temperature (°C)	Time (min)	Pressure (MPa)	Outcome
	[N _C /N _C] _{HP}	160	5	6.9	√
	[N _C /N _C] _{HP}	170	5	6.9	√
PTFE sheet	[N _C /SPInd _C /N _C] _{HP}	160	5	6.9	√
	[N _C /SPInd _C /N _C] _{HP}	170	5	6.9	X
	[N _C /GO _F /N _C] _{HP}	160	5	6.9	X
	[N _C /GO _F /N _C] _{HP}	170	5	6.9	X
	[N _C /GO _F /N _C] _{HP}	125	1	6.9	√
	[N _C /GO _F /N _C] _{HP}	160	2	6.9	√

PTFE is a polymer with very low surface roughness, thus reducing the adhesion of a second polymer such as Nafion to it. It actually has lower roughness than aluminium. Besides, PTFE is hydrophobic and due to this has been used to reduce adhesion in many fields, such as for medical studies [201, 202]. This hydrophobicity limits any interaction with the hydrophilic Nafion, whose polar sulphonic groups need polar groups to be attached to. Even water eliminated from the membranes during the hot pressing will not increase the attraction between Nafion and hydrophobic PTFE [203]. For all these reasons, PTFE proved to be a better base for the membranes during the hot pressing. The resultant membranes with SPInd and GO are presented in Figure 4.7(a) and (b) respectively.

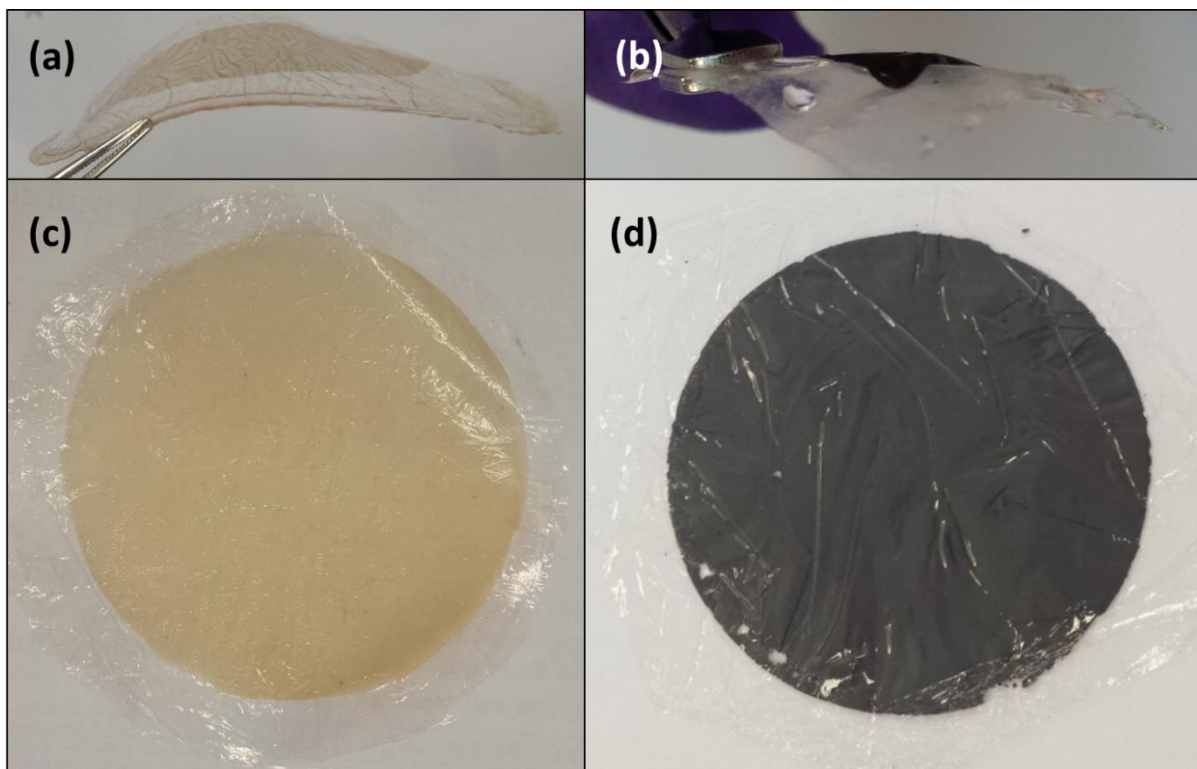


Figure 4.7: Lateral view of (a) $[N_C/SPInd_C/N_C]_{HP}$ and (b) $[N_C/GO_F/N_C]_{HP}$ membranes. Front view (c) $[N_C/SPInd_C/N_C]_{HP}$ and (d) $[N_C/GO_F/N_C]_{HP}$ membranes.

4.3. Cast membranes

Cast membranes are also present in the groups I, II and III (from Table 4.1) and can be divided into Nafion bilayers, multilayer membranes with SPInd and multilayer membranes with GO. The process of casting a membrane is very commonly used. Single layer cast polymeric films and membranes have been used in many applications as filtration system [204], medical [205], optical [206], energy [207] and others [208, 209] over the past century. Casting can be used to prepare composite membranes as well. This method consists of solvent evaporation by utilising time and/or temperature. After the evaporation, the polymer remains on the flat surface, forming a membrane or film. To cast a multilayer or a bilayer, the process is similar to that of the single layer and is exemplified in Figure 4.8 for SPInd and GO multilayer membranes. For the three-layer membranes, the process is as

follows. 1st layer: pour Nafion solution in a flat petri dish, then dry the membrane in the oven, but without annealing. 2nd layer: pour the solution of GO in water or the solution of SPInd in DMSO over the 1st layer in the petri dish and dry it in the oven. 3rd layer: pour Nafion solution over the 2nd layer and dry it in the oven with annealing. After that, peel off the membrane from the petri dish with the assistance of water.

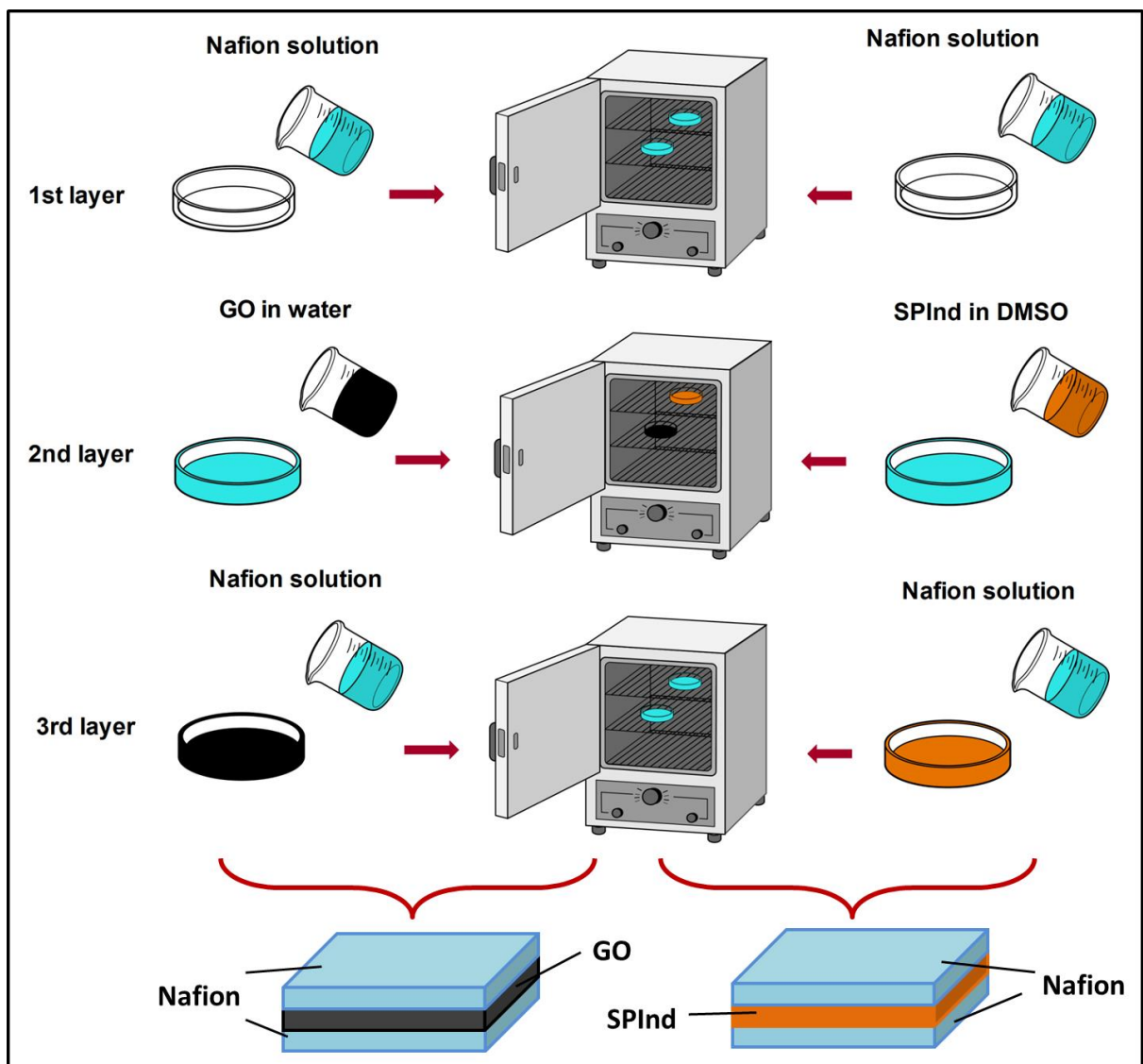


Figure 4.8: Schematic illustration of the casting process to produce $[N_c/GO_c/N_c]_c$ and $[N_c/SPInd_c/SPInd_c]_c$.

Cast Nafion bilayers were simple to produce and had no problem to adhere to each other. The parameters used were to dry the 1st layer at 100 °C for 2 h then to drop the second solution of Nafion and dry at 100 °C for 2 h plus 1 h at 120 °C to anneal it. This membrane was easily removed from the surface and apparently had a good interaction between the layers. The properties affected due to the layers interaction will be discussed in the Chapter V and VI related to cast membranes.

4.3.1. Nafion/sulphonated polyindene/Nafion multilayer membranes

Multilayer membranes with SPInd as inner layer were not as reliably to cast as Nafion bilayers. The first layer of Nafion was easily cast. However, the second layer of SPInd affected the first layer of Nafion. Nafion is a chemically and thermally resistant polymer, but these characteristics are enhanced only when annealed as typical polymers [210, 211]. As a result, if the second layer was cast before the annealing process, the solvent and the temperature could affect the bottom layer, which could partially dissolve or get mixed with the second layer. However, if the second solution is dropped after annealing the first layer, the interaction between the layers tends to be reduced. After all, to have a stronger interface, the polymers must chemically bond to each other. Accordingly, the annealing would prevent that the polar groups of SPInd form bonding with the polar groups of Nafion. In Table 4.8, the parameters to dry each layer of the $[N_c/SPInd_c/N_c]_c$ membranes are detailed.

Table 4.8: Parameters to dry each layer of the membrane [N_c/SPInd_c/N_c]_c.

Attempt	1 st layers casting	2 nd layer casting	3 rd layer casting
A	100 °C, 2 h	100 °C, 2 h	100 °C, 2 h 120 °C, 1 h
B	100 °C, 2 h	80 °C, 2 h 100 °C, 2 h	100 °C, 2 h 120 °C, 1 h
C	100 °C, 2 h 50 °C, 0.5 h	80 °C, 2 h 100 °C, 2 h 50 °C, 0.5 h	100 °C, 2 h 120 °C, 1 h
D	100 °C, 2 h 120 °C, 1 h 50 °C, 0.5 h	100 °C, 2 h 120 °C, 1 h 50 °C, 0.5 h	100 °C, 2 h 120 °C, 1 h

The first attempt (A) (Figure 4.9(a)) to cast the multilayer membrane with SPInd consisted of the same process used to cast Nafion bilayers. However, SPInd was dissolved in DMSO, which is a heavier solvent and has a higher evaporation point than water. The slower the DMSO evaporates, the less porous the membrane become. In attempt B, the evaporation of DMSO from SPInd was the same as with casting SPInd single layers. Nevertheless, when casting SPInd single layer, the solution was poured in the petri dish in which the surface was at room temperature. In the case of attempt B, the Nafion surface was as hot as 100 °C. Thus, DMSO started to evaporate at 100 °C and not 80 °C as desired. To reduce the rate of DMSO evaporation, in attempt C, the first and the second layer were cooled to 50 °C for 0.5 h after casting. As a result, a smoother membrane was achieved as can be seen in Figure 4.9(b). When the second layer was poured over the first before annealing, it was expected that some chains of the second layer would penetrate the first layer [212], improving the adhesion and interaction between the two. A parallel can be drawn between these parameters and Zhong *et al's*. [146] work. In their study, the solution additions over the

previous layers were carried out before any crosslinking and only after dropping the last layer, the membrane underwent crosslinking. Polymer annealing can reduce the bonding capacity similar as crosslinking inside a single layer can reduce it, weakening the interfacial interaction.

In attempt D, the first Nafion layer was annealed before the addition of the second layer which caused a poor interaction between the layers. Furthermore, after annealing, Nafion contracted and was peeled off from the surface in the presence of a solvent. This behaviour generated an uneven surface on which the SPInd was cast resulting in a rough and highly corrugated membrane surface as shown in Figure 4.9(c). In all multilayer membranes, part of the solvent of the second solution leaked into the first layer through the rims. This aggravated as the amount of solvent was increased. As such, the amount of DMSO was minimised to 5 mL. Consequently, the most suitable membrane was the one of attempt C and all further $[N_c/SPInd_c/N_c]_c$ membranes were cast with those parameters.

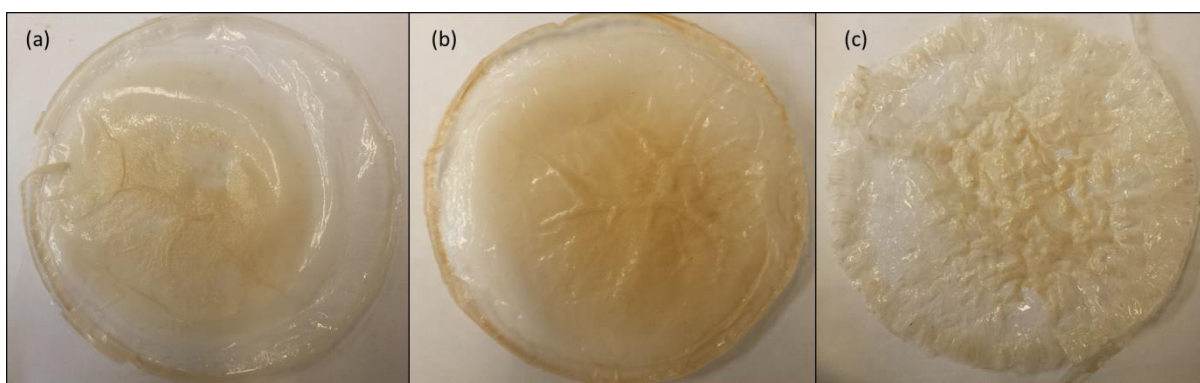


Figure 4.9: $[N_c/SPInd_c/N_c]_c$ membranes by cast parameters attempt: (a) attempt A, same conditions as Nafion bilayer; (b) attempt C, lower temperature casting SPInd; (c) attempt D, annealing before the addition of the third layer.

Similar to the process used in hot pressed membranes, to make the inner layer of SPInd less brittle, more homogeneous and to have a better attraction to the external layers, some content of Nafion was added. 5, 10 and 20 wt.% of Nafion in respect to SPInd weight was

added in the SPInd while it was solubilizing in DMSO. As can be seen in Figure 4.10, all resultant membranes apparently had more homogeneous spread of the SPInd on the first layer. The yellow/light brown colour is characteristic of SPInd and makes it easy to observe where the polymer is in the membrane. While the membranes from Fig. 5.9 have a darker colour in the centre suggesting that SPInd is concentrated at the centre of the membranes, the membranes in Fig. 4.10 have a lighter colour suggesting a more even distribution on the entire surface, including the edges.

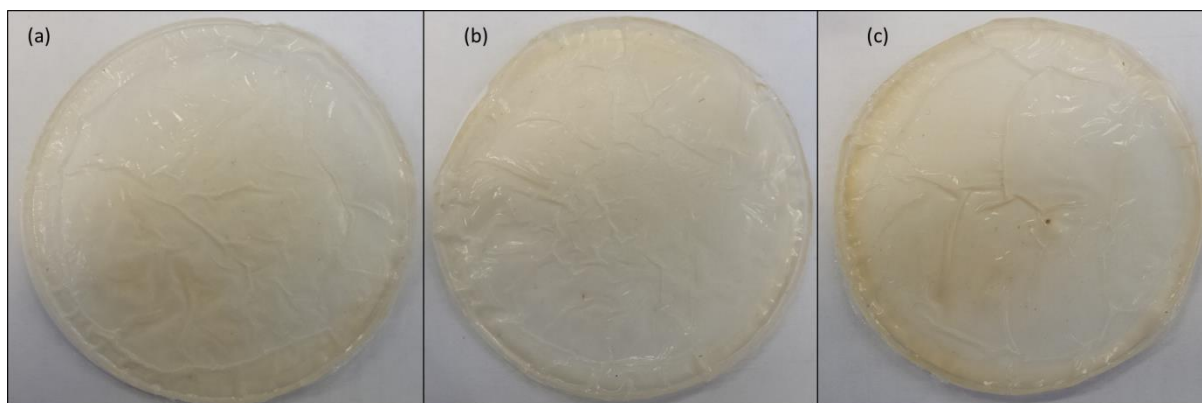


Figure 4.10: $[N_c/SPInd_c/N_c]_c$ with (a) 5 wt.%, (b) 10 wt.% and (c) 20 wt.% of Nafion in the inner layer.

To evaluate the prepared membranes, water uptake (WU) and ion exchange capacity (IEC) studies were performed on all of them (from Fig 4.10) and the results are shown in Table 4.9. The WU was higher in the membranes following the sequence 10> 20>5 wt.% of Nafion content in the inner layer, while the IEC was higher in the sequence 5>20>10 wt.%. This means that the sequence was inversely proportional. To define which membrane has the best set of properties, a balance between WU and IEC must be found. For that, $WU \times IEC$ was calculated. However, the results were equivalent to 0.23 for all the membranes. Therefore, it can be assumed that to increase IEC with addition of Nafion in the inner layer, the WU must be compromised, reciprocally, IEC will be reduced on improvement of WU.

The middle point for both properties was with 20 wt.% of Nafion, the same value used in the hot pressed membranes. Besides, the reproducibility in this case was more effective. As a result, the following membranes were manufactured with this composition. The results for water uptake and IEC were very similar for all the cast membranes. The difference between them was well within the error range and it cannot be affirmed that actually there is a difference. As such, the hot pressed and cast membranes can be compared due to their equivalent layer composition.

Table 4.9: Properties of $[N_c/SPInd_c/N_c]_c$ varying the content of Nafion in the inner layer of SPInd.

Membrane	WU (%)	IEC (mequiv/g)	Ratio (WU*IEC)
$[N_c/SPInd-5N_c/N_c]_c$	24.99 ± 2.67	0.93 ± 0.024	0.23
$[N_c/SPInd-10N_c/N_c]_c$	26.94 ± 0.58	0.88 ± 0.031	0.23
$[N_c/SPInd-20N_c/N_c]_c$	26.05 ± 1.49	0.90 ± 0.018	0.23

Unlike hot pressed membranes, the chemical composition was not the only aspect evaluated for the cast ones. The thickness of each layer was found to have an influence on the final properties. This chapter, though, only discusses the different layer proportions and sequences.

Casting a multilayer membrane brings some difficulties that are not present while casting a single layer membrane. The thickness of each layer is a challenge, and it can affect the achievement of properties, such as proton conductivity, and final thickness desired, in this case at most 50 μm [213]. The thickness of the constituent cast single layers and the total thickness of a multilayer membrane do not necessarily match. This is caused by the interaction, mixing and migration between adjacent layers. The mixing can be accentuated

when the layers are made of polar polymers and are dissolved in solvents which are hostile for the other polymer, as is the case with these cast SPInd multilayer membranes.

The starting composition of $[N_c/SPInd_c/N_c]_c$ layers was in the proportion 2:1:2 (detailed values for each layer are exposed in Table 4.10). However, this membrane had an extremely high thickness of $115 \pm 10.5 \mu\text{m}$, which can compromise the proton conductivity. Therefore, to reduce the general thickness, the proportion of the layers was changed to 1:1:1.5, 1.5:1:1 and 1:1:2. The idea was to not reduce the amount of SPInd, because it enhances the IEC of the membrane. Nafion, on the other hand, gives stability, but decreases the IEC to the minimum value when there is 100% of Nafion. Comparing both 1:1:1.5 and 1.5:1:1 compositions, the difference is in the sequence of addition. In the first one, the top layer (third layer) has a higher proportion of Nafion compared to the 1.5:1:1 membrane, while in the second one the bottom layer (the layer in contact with the flat surface) has the higher content of Nafion. The interaction and evaporation rate between these membranes is different. It is expected that the inner layer had more interaction with the bottom layer than with the top layer. When the inner layer is added, DMSO (an aggressive solvent) can penetrate into the Nafion, creating an interface between both polymers and facilitating the mixing. When the third layer is added, the solvent is water, not as strong as DMSO which has been evaporated. Thus, the migration to the previous layer is not the same. However, both membranes have an acceptable final thickness for use in the PEFC.

Another difference between the sequence of additions is that each layer must completely cover the previous layer. For the first layer, it is very simple, since on the bottom there is just the petri dish. The second layer is the same. However, for the third layer there is a

difference. The surface of the inner layer is not regular, and therefore a higher volume of liquid is necessary to completely cover this layer before drying. Nevertheless, it has to be a higher volume of the polymer and not just the solvent (water), because water can easily penetrate under the bottom layer (through the sides of petri dish) and lift it, making the membrane non-uniform. As such, the membrane 1:1:1.5 seems to be more promising and uniform, not because the increase in amount of solution for the third layer creates a thicker membrane, but because it helps to fill the rough surface. A membrane with the composition 1:1:2 was prepared to check if its uniformity would be higher as well. However, the thickness was $86.7 \pm 6.2 \mu\text{m}$, which is too high for this PEFC.

Table 4.10: Detailed layers composition of $[\text{N}_c/\text{SPInd}_c/\text{N}_c]_c$ membranes.

Layers proportion	Thickness (μm)	First layer (mL of Nafion Solution)	Second layer (g of SPInd)	Third layer (mL of Nafion Solution)
1:1:1.5	55.9 ± 4.9	1.4	0.06	2.1
1.5:1:1	50.7 ± 4.64	2.1	0.06	1.4
2:1:2	115 ± 10.5	2.8	0.06	2.8
1:1:2	86.7 ± 6.2	1.4	0.06	1.4

4.3.2. Nafion/graphene oxide/Nafion multilayer membranes

To cast a multilayer membrane with GO as inner layer has some similarities to casting a multilayer with SPInd. However, GO is not a polymer and the kind of interaction expected for SPInd is not the same for GO. For example, as seen in Chapter III, GO undergoes no alteration at 120°C other than losing water. Other than with SPInd membranes, GO does not have any annealing stage. Therefore, defining the parameters for casting the membranes was simpler. The membranes were cast in the following sequence by layer: 1st) 100°C for 2 h, 50°C for 0.5 h; 2nd) 100°C for 2 h, 50°C for 0.5 h; 3rd) 100°C for 2 h, 120°C for 1 h.

The first layer was similar to that of the $[N_c/SPInd_c/N_c]_c$ membrane, but with a higher amount of Nafion solution, 2.8 mL. This is due the fact that the GO layer would be much thinner than the SPInd. To have the same thickness of SPInd, the content of GO would be massive and it could completely block the passageway of protons. Yuan *et al.* [147] prepared a multilayer membrane of Nafion with bilayers of poly(diallyldimethylammonium chloride) (PDDA) and GO for DMFC. The membranes with 2 bilayer had better performance than the membranes with 4 bilayers. The authors claimed that 4 bilayers drastically reduced the methanol crossover but reduced as well the proton transport. The 2 bilayers membranes had a better balance between these properties. Similarly, in the membranes in the present study, increasing the thickness of the GO layer could block the protons, since GO does not have the same proton conductivity as Nafion.

The GO content that must be added in a membrane to improve the water retaining properties and to not reduce the proton conductivity remains controversial in literature. Xue *et al.* [162] prepared composite membranes for high temperature PEFC (HT-PEFC) with PBI and GO, in which the content of GO was 1, 3 and 5 wt.%. The one with higher proton conductivity in all range of temperatures was the 5 wt.%. Wang *et al.* [199], on the other hand, claimed that the membrane with 3 wt.% of GO in a composite membrane with Nafion has better mechanical properties. Lee *et al.* [107] also found that the composite membrane with Nafion and 3 wt.% of GO had the highest performance. The optimum GO content in the Nafion/GO composite membrane for DMFC was 0.5 wt.% as stated by Choi *et al.* [98]. Many other studies are still discussing the best values for Nafion/GO composites. However, all concluded that low levels of GO are necessary. This discrepancy may be caused by issues such as the GO synthesis, the low dispersion of GO in the polymer and the final testing

parameters. Each batch of GO synthesised and purified has slight differences in the oxygen content which may affect the mixing with the polymer. Besides, dried GO tends to agglomerate, which makes the homogenous dispersion in the polymer difficult. Finally, DMFC and PEFC can operate in a vast range of temperatures, humidification, pressure, etc. These parameters are affected differently by the varying GO content.

Therefore, in this work four values of GO content in the multilayer membranes were selected: 0.5, 2.5, 4.5 and 6.5 wt.% of GO. The prepared membranes are shown in Figure 4.11 (a) to (d) respectively. As can be seen, the darker the membrane, the higher the GO content. GO in water solution spreads uniformly over the bottom layer. Nevertheless, the amount of water had to be controlled. In Fig 4.11(b) it is highlighted that a non-uniform region in the membrane forms, which is caused by water from the inner layer that moves under the bottom layer. Thus, Nafion is lifted and grooves are formed. The GO inner layer will coat this part, as the third layer will coat the GO layer. Due to the irregularity in this area, it is not suitable to be applied in a PEFC. Accordingly, the amount of water to solubilize GO was optimized to 4 mL.

The interaction between GO and Nafion was not as strong as in the case of SPInd. Before adding the third layer, GO coated the bottom layer but it was not completely chemically bonded. If the surface was scratched, the GO powder was removed from the surface. Some oxygen groups from the GO can bond with the polar groups of Nafion, but the low temperature is too low to cause stronger adherence and interaction. At this temperature, GO does not suffer any significant modification to chemically bond with Nafion. However, if the temperature was increased to improve the interaction, Nafion would anneal and would

not link to any GO. Therefore, GO was physically trapped between the two layers of Nafion. And as the GO content is low, Nafion from the top layer enters in contact with the Nafion in the bottom layer, strengthening the interface and restraining the GO. To improve interaction between the GO layer and Nafion and avoid delamination, membranes with 5 and 20 wt.% of Nafion in the GO inner layer for each GO content were prepared, as in the case of SPInd.

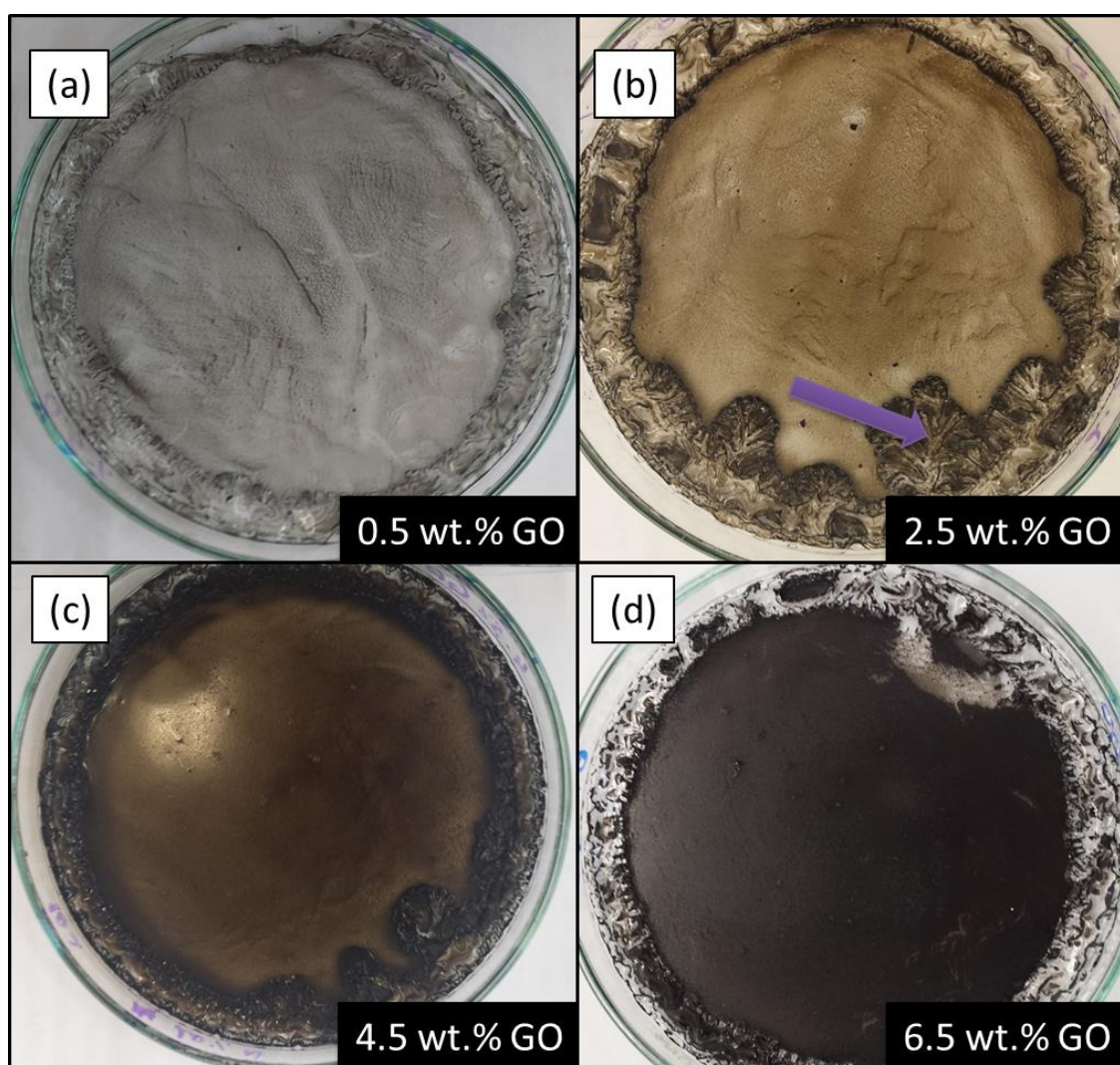


Figure 4.11: $[N_c/xGO_c/N_c]_c$ membranes with x equal to (a) 0.5wt.%, (b) 2.5wt.%, (c) 4.5wt.% and (d) 6.5wt.%.

The $[N_c/6.5GO_c/N_c]_c$ membrane delaminated when cut to small samples as show in the images of Figure 4.12. In this membrane, there is a high amount of GO which forms a compacted film, blocking any kind of contact between the external layers. Thus, Nafion layers do not have space for bonding, weakening the membrane sealing. All the membranes with Nafion content in the inner layer were more resistant to cutting. However, the more Nafion content, the lower the water retention. Therefore, the content of Nafion was limited to 20 wt.%. Both membranes, with and without Nafion, were used for fuel cell tests which will be discussed in the Chapters V and VI.

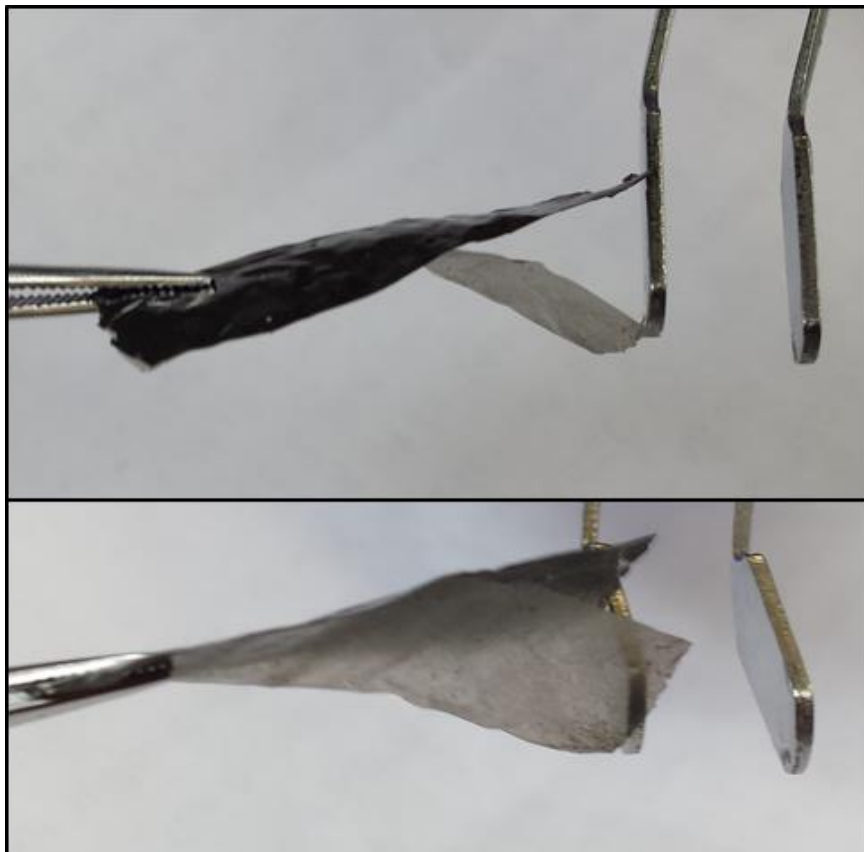


Figure 4.12.: Two views of $[N_c/6.5GO_c/N_c]_c$ membrane delaminated after cutting.

4.4. Membrane activation

The membranes were treated at 80 °C by immersion in the following sequence for 1 h each: in water, in 3% hydrogen peroxide, in water, in 0.5 M sulphuric acid and in water. After washing, the desired membrane sample was immersed in water for at least 24 hours.

4.5. Conclusions

Nafion single and bilayers were cast and hot pressed with no major issues following procedures found in the literature. The heat treatment which Nafion was subjected to during the casting process modified its structure, inverting the micelles configuration. This characteristic reduced the adhesion to the other layers, such as SPInd and GO. On the other hand, pure SPInd membranes presented a porous and brittle structure when alone. Similarly, GO films prepared by filtration were brittle. The addition of Nafion in both layers (SPInd and GO) increased the malleability and the adhesion to the Nafion external layers in both casting and hot pressed multilayer membranes.

The adherence between SPInd and Nafion layers in HP membranes was stronger than Nafion with GO. The GO hydrophilicity caused problems in the HP assembly. A two-step method was developed to remove the retained water. On the other hand, the adherence between the layers in the cast membranes was better for all membrane configurations than for the HP membranes. This was because in the casting method the layers are chemically bonded and not only mechanically attached as in HP. The best parameters found for preparing membranes are in Table 4.11. These procedures were applied in all further membranes.

Table 4.11: Summary of the membranes preparation methods.

Membrane	First layer	Cast condition	Second layer	Cast condition	Third layer	Cast condition	Hot press condition
N_c	Nafion	100 °C, 2 h 120 °C, 1 h	NA*	NA	NA	NA	NA
SPInd_c	Sulphonated polyindene	80 °C, 2 h 100 °C, 2 h	NA	NA	NA	NA	NA
[N_c/N_c]_{HP}	Nafion	100 °C, 2 h 120 °C, 1 h	Nafion	100 °C, 2 h 120 °C, 1 h	NA	NA	160 °C + 6.9 MPa, 5 min
[N_c/N_c]_c	Nafion	100 °C, 2 h	Nafion	100 °C, 2 h 120 °C, 1 h	NA	NA	NA
[N_c/SPInd_c/N_c]_{HP}	Nafion	100 °C, 2 h 120 °C, 1 h	Sulphonated polyindene	80 °C, 2 h 100 °C, 2 h	Nafion	100 °C, 2 h 120 °C, 1 h	160 °C + 6.9 MPa, 5 min
[N_c/SPInd_c/N_c]_c	Nafion	100 °C, 2 h 50 °C, 0.5 h	Sulphonated polyindene	80 °C, 2 h 100 °C, 2 h 50 °C, 0.5 h	Nafion	100 °C, 2 h 120 °C, 1 h	NA
[N_c/GO_F/N_c]_{HP}	Nafion	100 °C, 2 h 120 °C, 1 h	Graphene oxide	NA	Nafion	100 °C, 2 h 120 °C, 1 h	125 °C + 6.9 MPa, 1 min 160 °C + 6.9 MPa, 2 min
[N_c/GO_c/N_c]_c	Nafion	100 °C, 2 h	Graphene oxide	100 °C, 2 h	Nafion	100 °C, 2 h 120 °C, 1 h	NA

*Not applicable

CHAPTER V – THE INFLUENCE OF SPIIND ON THE MEMBRANE PERFORMANCE

SPInd is a promising material to use in PEM due to the high number of sulphonic groups available to bond with water and transport protons. However, SPInd as a single material has low mechanical strength, thus it has been tested for PEFC in blends with PVA [214, 215]. Different from Nafion, PVA has extremely high water uptake [216], which can be above 100%. Therefore, the membrane SPInd/PVA still presents low mechanical stability and is not suitable for PEFC application. On the other hand, SPInd displays high ion exchange capacity, which is essential to be an excellent proton conductor. Therefore, it was attempted in this study to fabricate a multilayer membranes with SPInd as inner layer and Nafion membranes as external layers as explained in the previous chapter.

The performance of the multilayer membranes *in-situ* and *ex-situ* will be discussed in this chapter. It is divided in two sections, first hot pressed membranes, and second cast membranes. Each section discusses the influence of SPInd on the properties such as conductivity and microstructure. At the end, a summary comparing both groups of membranes will be presented to evaluate the effect of the preparation method.

5.1. Hot-pressed membranes

As Yang *et al.* [127] reported, one of main problems of hot pressing a multilayer membrane (MM) is delamination. This can affect the final properties and performance of the MM. Thus,

the preparation method was extensively discussed in the previous chapter to find the best parameters, which were identified as 160 °C, 6.9 MPa for 5 min and were used to fabricate the membranes used in the following. The next sections discuss the ex-situ properties such as microstructure and water uptake.

5.1.1. Microstructure

The microstructure and cross-sections of the membranes were studied using a Phillips XL-30 FEG Environmental Scanning Electron Microscope (ESEM). The membranes were freeze-cracked using liquid nitrogen before inspection in the ESEM.

SEM images reveal the microstructure and morphology of the $[N_C/SPInd_C/N_C]_{HP}$ multilayers in Figure 5.1 (a-d). No visible pores were seen in the Nafion layer of the MM structure. As seen in the SEM images, only two layers, one more porous (identified as SPInd) and one with a less porous/solid structure (identified as Nafion) were observed. The third layer (Nafion) seemed missing. It was concluded that delamination of the third Nafion layer occurred at some point during the SEM sample preparation in liquid nitrogen, which was used for freeze fracturing the membranes. Hot-pressing simply allows mechanical interaction between the layers and a lack of chemical interaction leads to weak adhesion. As predicted in the thermal analysis of SPInd (Chapter III), water evaporation from the electrolyte, which occurs at 160 °C, prejudices a good interfacial-interaction between the layers. The problem of layer delamination for multilayer membranes is consistent with literature reports [217]. However, it must be appreciated that liquid nitrogen, given its freezing properties, is more aggressive [218] compared to any other elements/conditions found in a PEFC. Moreover, the PEFC working set-up creates a completely different environment with the compressional forces

holding the MEA, bipolar plates and the entire cell together. A free MM faces a very different environment when immersed in liquid N₂. As the liquid N₂ freezes the water content, it leads to size change of the individual layers in the MM. In a case where the layers do not have a good adherence and interfacial interaction, the layers can easily delaminate as a result of loss of physical contact between them. Thus, this freeze drying process is not only a requirement for performing SEM tests but also helps develop an understanding of the interlayer interaction in the MM. DeLongchamp *et al.* [219] found that their multilayer membranes delaminated in the presence of flowing water due to the poor adhesion between the layers. However, the membranes were still suitable for electronic applications. Similarly, the membranes presented here are suitable for PEFC applications, although they show delamination in sample preparation.

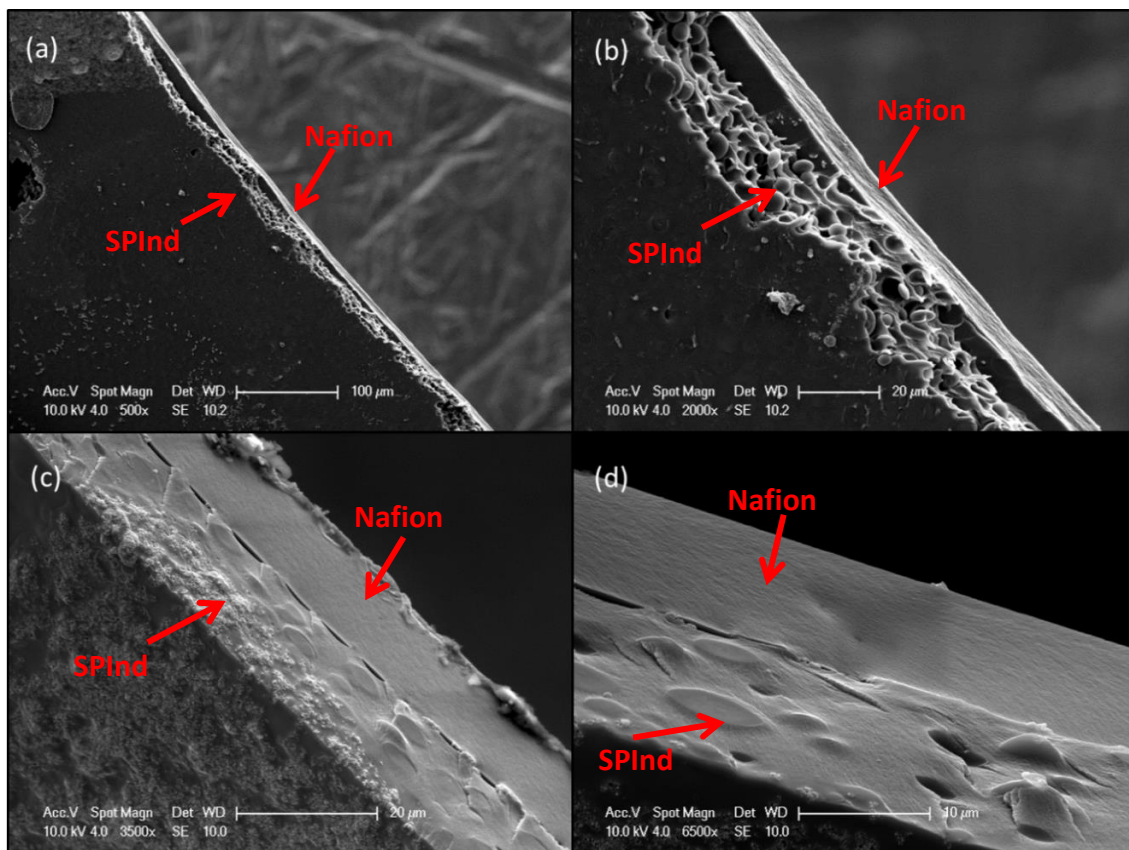


Figure 5.1: Micrographic images from [N_C/SPInd_C/N_C]_{HP} membranes with zoom of (a) 500x, (b) 2000x, (c) 3500x and (d) 6500x.

The membranes [N_C/SPInd_C/N_C]_{HP} were successfully assembled. However, the interaction between the layers was weak, only being mechanical, which weakened the final membrane by allowing delamination. Even when the membrane was well assembled, in some conditions, such as cryogenic temperature, the poor adherence led to delamination. Thus, the surface of the SPInd inner layer would be exposed to water and the environment in general, which is the opposite of the purpose of a multilayer system. If the whole surface of SPInd comes into contact with water, with no Nafion protection, part of the SPInd can be lixiviated from the PEFC.

The poor adherence between the two polymers further underlines the necessity and suitability of the chosen multilayer design within this study with larger diameter Nafion outer layers, so that Nafion can seal the outer rim of the MM.

5.1.2. Water uptake and ion exchange capacity

Water uptake (WU) was determined gravimetrically by recording the wet and dry mass of the membranes using the following steps. Details of the experimental protocols are in the Appendix. Three membranes samples were placed in water at room temperature for 24 h, and then their wet weight was measured three times each sample. After this the wet membrane samples were dried at 100 °C (until no more weight variation was detected) and their dry weight was recorded three times each sample. The water uptake (WU) was measured using Equation 5.1 with the mean value of the recorded weights, where W_w and W_d denote the wet weight and the dry weight, respectively.

$$WU = \frac{W_w - W_d}{W_d} \quad (\text{Equation 5.1})$$

The WU and IEC results for all membranes are compiled in Figure 5.2. The single layer SPInd showed the highest water uptake of $(26.8 \pm 1.59)\%$ among the single and bilayer membrane samples. SPInd showed nearly 6 and 8 percentage points higher water uptake than cast Nafion $(20.8 \pm 0.77)\%$ and the commercial Nafion 212 $(17.9 \pm 2.25)\%$ membranes. The enhanced WU in the SPInd membrane was attributed to the larger number of free sulphonic acid groups in SPInd that allow increased water retention. The commercial and in-situ cast Nafion bilayer membranes $[N_c/N_c]_{HP}$ and $[N211/N211]_{HP}$ displayed similar behaviour to each other with water uptake values of $(17.79 \pm 0.88)\%$ and $(18.53 \pm 0.87)\%$, respectively. This suggests that in case of a Nafion bilayer, the multilayer manufacturing process was effective (both in cast and commercial materials) as Nafion can adhere to Nafion allowing good interfacial interaction. Moreover, the HP temperature of $160\text{ }^\circ\text{C}$, which was used for the bilayer manufacturing, is above the Nafion T_g , facilitating the bonding between the layers. There was no external element (such as SPInd or other material) to negatively influence the interfacial interaction and hot-pressing method. The WU was similar for both Nafion bilayers as well as for the Nafion single layer 212. The water uptake of N_c was higher than that for commercial N212. This is attributed to the efficiency of the casting process as discussed in the previous chapter.

The $[N_c/SPInd_c/N_c]_{HP}$ membrane showed the highest water uptake of $(41.2 \pm 3.39)\%$ among all samples. This is almost double the WU value of a single SPInd membrane. The fact that the multilayer membrane showed higher WU than its constituent layers led to further scrutiny of this multilayer system. The optical picture of a small piece of the $[N_c/SPInd_c/N_c]_{HP}$ membrane while still soaked in water (24 h) can be seen in Figure 5.3. It is evident from this picture that small water bubbles were formed between the constituent SPInd and Nafion

layers. The Nafion bilayers, unlike the SPInd multilayer system, did not show such bubble formation. While SPInd can surely have a positive influence on the WU especially considering the WU performance of single layer SPInd, the presence of the bubbles in the $[N_C/SPInd_C/N_C]_{HP}$ evidences that part of the high WU value for the $[N_C/SPInd_C/N_C]_{HP}$ is due to partial delamination forming gaps between the layers following loss of adhesion and poor interaction between the Nafion and SPInd layers.

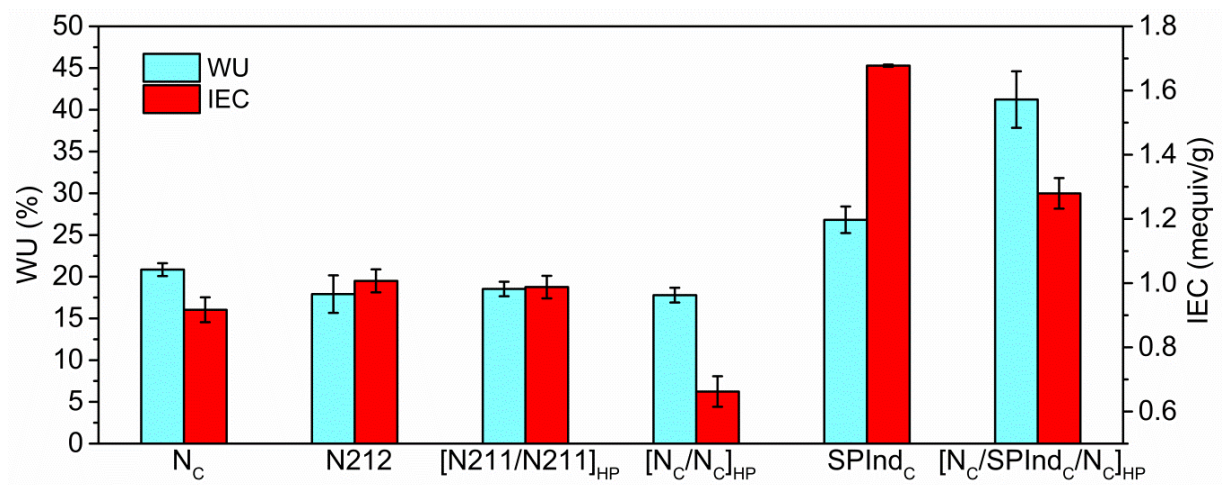


Figure 5.2: Water uptake and ion exchange capacity of the membranes, at room temperature.

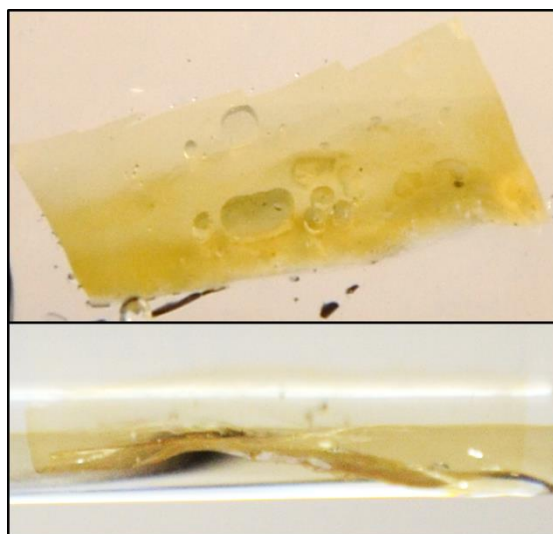


Figure 5.3: Bubbles in the $[N_C/SPInd_C/N_C]_{HP}$ membrane when soaked in water.

Membrane Ion Exchange Capacity (IEC) was evaluated by the acid-base titration method. Three samples of each membrane were soaked in 0.1 M HCl for 24 h. After thoroughly rinsing the membranes with water, they were immersed in saturated NaCl for 72 h to exchange the H⁺ ions for Na⁺ ions. Then, the proton release was evaluated by titrating the solution with 0.01 M NaOH at room temperature with phenolphthalein as indicator. The IEC was obtained by using Equation 5.2 with the mean value of the samples.

$$IEC = \frac{V_{NaOH} \times M_{NaOH}}{W_d} \quad (\text{Equation 5.2})$$

Where, V_{NaOH} is the volume of NaOH titrated, M_{NaOH} is the molar mass of NaOH and W_d is the sample dry weight.

The IEC values of the membranes are shown in Figure 5.2 and included in Table 5.1. The cast SPInd revealed the highest IEC value of 1.68 ± 0.003 mequiv/g, while cast Nafion revealed a value of 0.92 mequiv/g. The high IEC for SPInd was as expected and is attributed to the large number of free sulphonic groups in SPInd structure. The membrane $[N_C/N_C]_{HP}$ displayed the lowest IEC value of 0.66 ± 0.048 mequiv/g among all the samples. This value is even lower than that of the single layer cast Nafion (0.916 ± 0.039) of equivalent thickness which showed nearly a 40% higher IEC value. The comparison between N_C and $[N_C/N_C]_{HP}$ highlights the vital role an interface can play on the performance of a multilayer membrane. Despite better interaction between Nafion-Nafion layers compared to Nafion-SPInd, the interface formed during the hot-pressing process is not good enough to lead to a IEC performance similar to that of a single (interface free) membrane. Thus, it can be safely assumed that the interface between the layers has a negative effect on the IEC. Remarkably, in spite of the

negative influence of the interface and a poor inter-layer interaction (as seen in the SEM preparation and Figure 5.3) the multilayer $[N_C/SPInd_C/N_C]_{HP}$ system was able to show a very good performance and revealed an IEC value of 1.28 ± 0.048 mequiv/g which is nearly 28% higher than the IEC value for commercial N212. It is emphasised at this stage that water trapped in the gaps between the multilayers cannot contribute to IEC values for the membrane. This further affirms our assumption that the high water uptake in $[N_C/SPInd_C/N_C]_{HP}$ was not entirely due to gaps in the interface. Similarly, the low IEC value for $[N_C/N_C]_{HP}$ despite its reasonably good WU values (similar to those of N212 and N_C) suggests that there could be some gaps on the micro and nanoscale in the $[N_C/N_C]_{HP}$ multilayer that lead to excess trapped water at interfaces which would not contribute to its IEC performance.

Table 5.1: Detailed physical properties of the membranes.

Membrane	WU (%)	IEC (mequiv/g)	Hydration Number
N_C	20.85 ± 0.77	0.916 ± 0.039	12.8 ± 0.1
N212	17.91 ± 2.25	1.007 ± 0.036	8.8 ± 0.7
$[N211/N211]_{HP}$	18.53 ± 0.87	0.988 ± 0.035	10.4 ± 0.5
$[N_C/N_C]_{HP}$	17.79 ± 0.88	0.662 ± 0.048	14.9 ± 0.7
SPInd_C	26.82 ± 1.59	1.677 ± 0.003	8.8 ± 0.5
$[N_C/SPInd_C/N_C]_{HP}$	41.23 ± 3.39	1.280 ± 0.048	16.4 ± 0.3

Another interesting observation was that the IEC value for $[N211/N211]_{HP}$ was similar to that of commercial, single layer N212 and is approximately 1.5 times higher than that of $[N_C/N_C]_{HP}$. Keeping in mind, that apart from the manufacturing of the initial single layers, all the following hot pressing steps are equivalent, this performance, apparently unaffected by

the interface, may be attributed to the higher homogeneity and chemical stability in the commercial extruded-cast Nafion membrane. Thus, suggesting that the preparation process of the constituent single layers will have a significant impact on the behaviour of the resultant MM [220].

The hydration number (λ , Table 5.1) is defined as the number of water molecules per sulphonic group as shown in Equation 5.3, where M_{H_2O} is the water molar mass.

$$\lambda = \frac{W_w - W_d}{IEC \times W_d \times M_{H_2O}} \quad (\text{Equation 5.3})$$

Calculations revealed the highest value for the $[N_C/SPInd_C/N_C]_{HP}$ membrane. All the single layer membranes presented a lower hydration number than the bilayers and multilayers. Based on this, it can be commented that in multilayer membranes, the accessibility of sulphonic groups to reach the water molecules appears to be facilitated. This increases the suitability of the membrane for PEM applications. For the Nafion membrane series, the membrane preparation method has more influence on the λ , as previously discussed. The heat treatment inverts the micellar structure, allowing ionic clusters in the centre. As such, more water molecules are trapped by sulphonic groups. The hot-pressing seems to be effective in increasing the hydration number. It can be seen that all membranes submitted to hot pressing have a higher hydration number than their analogue single layer, which can be the influence of the trapped water.

5.1.3. Proton conductivity

Membrane samples with size of 3x1 cm were immersed in water 24 hours prior to testing for proton conductivity. A four-probe system fitted with platinum electrodes and connected to the Scribner 850e Fuel Cell Test System (shown in Figure 5.4) was used to measure the in-plane proton conductivity of the membrane at three temperatures (80, 100 and 120 °C) and five different relative humidity (RH – 20, 40, 60, 80 and 100%) conditions. The proton conductivity (σ) for the membranes was calculated by using the Equation 5.3.

$$\sigma = \frac{L}{RxA} \quad (\text{Equation 5.3})$$

Where L is the distance between the two inner probes, R is the ohmic resistance and A is the membrane cross-sectional area. Three samples of each type of membrane were measured in the proton conductivity test. Although the same type was used for the three samples, they were originated from different membranes to evaluate the reproducibility of the preparation method. Each sample was measured three times.

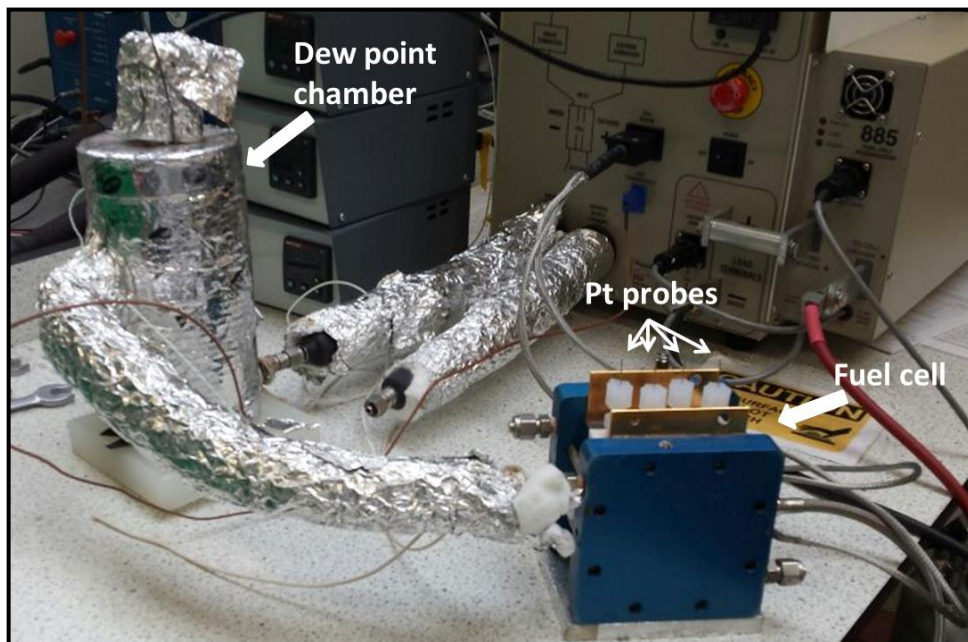


Figure 5.4: Proton conductivity test in the Scribner 850e Fuel Cell system.

Proton conductivity studies were carried out on $[N_C/SPInd_C/N_C]_{HP}$, $[N_C/N_C]_{HP}$ and N_C as shown in Figure 5.5. At 80 °C (Figure 5.5(a)) and at higher relative humidity (80-100%), N_C revealed the highest proton conductivity, while $[N_C/SPInd_C/N_C]_{HP}$ revealed higher proton conductivity at lower relative humidity (20-60%). A similar trend was seen for higher relative humidity at 100 °C, as seen in Figure 5.5(b). At 120 °C (and at RH \geq 40%), as shown in Figure 5(c), the proton conductivity for N_C was higher than that for the other membranes. On the other hand, the $[N_C/SPInd_C/N_C]_{HP}$ appeared to perform similar or better than the $[N_C/N_C]_{HP}$ at all the relative humidity and temperature conditions. While the N_C seem to be performing similar or better than the $[N_C/SPInd_C/N_C]_{HP}$ system, these results were contrary to the IEC and WU results. The possible reasons for this have been discussed below.

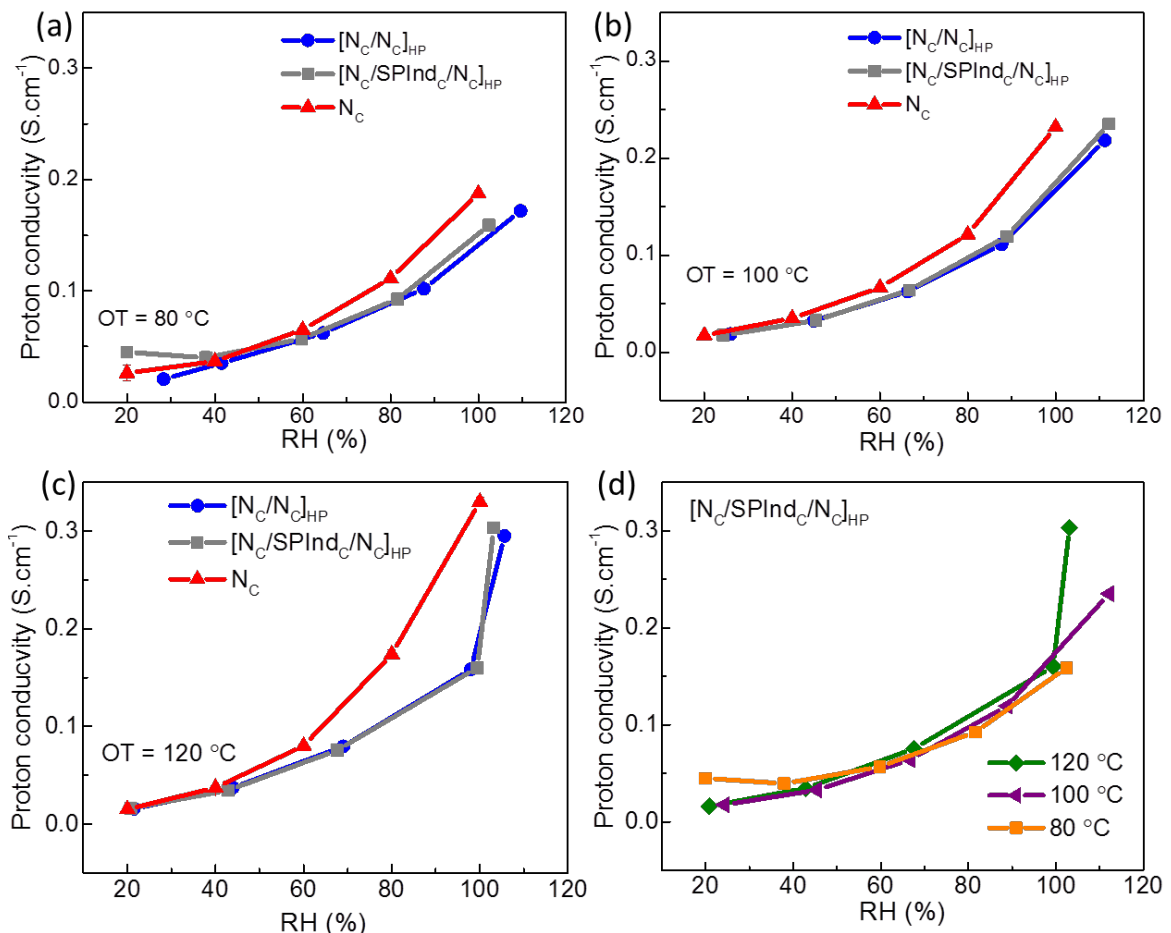


Figure 5.5: Proton conductivity at (a) 80 °C, (b) 100 °C and (c) 120 °C. (d) Proton conductivity of multilayer membrane N/SPInd/N at different temperatures; OT: Operating temperature.

Marrony *et al.* [137] suggested in their study about SPEEK bilayer membranes that the proton conductivity is dependant and proportional to the hydration number in the MM, but this is not necessarily the case in the single layers. This was also observed in this study. This, however, does not shed any light on the poor proton conductivity performance of the $[N_C/SPInd_C/N_C]_{HP}$ MM. It is understood that the ionic resistance (inversely proportional to proton conductivity) in the MMs increases because of the increase in the number of interfaces, the resistance between the layers and interface voids [221]. Jiang *et al.* [222] have also found that resistance in multilayer membranes is higher due to the interface effect. In the present study, the proton conductivity performance of the SPInd MM, containing two interfaces, i.e. $[N_C/SPInd_C/N_C]_{HP}$ was similar or better than that of a single interface Nafion system, i.e. $[N_C/N_C]_{HP}$. On comparison, the single interface Nafion system showed a significantly poorer performance compared to an interface-free N_C membrane. Thus, it is speculated that, attributes such as the higher WU and IEC of the SPInd and the resultant $[N_C/SPInd_C/N_C]_{HP}$ could sufficiently compensate for the disadvantage of double the interfacial resistance, enabling a performance equivalent to that of $[N_C/N_C]_{HP}$. However, these attributes were not sufficient enough to surpass the proton conductivity performance of a Nafion single layer.

It is also worth noting that $[N_C/N_C]_{HP}$ and N_C membranes gain some advantage due to their lower thicknesses compared to $[N_C/SPInd_C/N_C]_{HP}$ MM, leading to better values of proton conductivity. In principle proton conductivity ($S\text{cm}^{-1}$) is a normalised quantity, independent of area and hence comparable for all samples. However, it must be appreciated that the variation in thickness especially in different layers made of different materials leads to variable overall water uptake. Water uptake, as is well known, plays a profound effect on the

proton conductivity of a PEM. Considering that $[N_C/SPInd_C/N_C]_{HP}$ displayed results similar to that of cast Nafion at 120 °C and low humidity despite being 25% thicker (75 μm) than cast Nafion (60 μm) and 29% thicker than $[N_C/N_C]_{HP}$ (58 μm), a comparative future study would need to test membranes with the same thickness. This was not possible to achieve by hot-pressing method used in this study despite achieving the correct thickness for the constituent single layers. Perhaps the weak interfacial interaction between Nafion and SPInd during hot pressing contributes to this variation in thickness. This would also explain the lower thickness of $[N_C/N_C]_{HP}$ and $[N211/N211]_{HP}$ (compared to $[N_C/SPInd_C/N_C]_{HP}$), when the total thickness of the constituent layers in all cases is identical as the Nafion-Nafion interaction is better than Nafion-SPInd interaction when subjected to hot pressing, as discussed earlier. Moreover, the low mechanical stability of SPInd makes it extremely difficult to handle a thin (< 10 μm) layer of SPInd with the hot-pressing method. The results and observations above underline the importance of the choice of layer materials as well as manufacturing process when preparing multilayer membranes.

Figure 5.5(d) compares the performance of $[N_C/SPInd_C/N_C]_{HP}$ at different temperatures. The results for intermediate relative humidity ($40 \leq RH \leq 80\%$) are comparable at all the temperatures. This confirmed that the $[N_C/SPInd_C/N_C]_{HP}$ retains its properties and is a promising and has potential to be a sturdy multilayer membrane system for IT-PEFC, especially at low and intermediate humidity conditions.

The proton conductivities at the lower values of relative humidity ($RH < 60\%$) were found to be very similar for all samples making it difficult to observe them in the graphs of Figure 5.5. Therefore, these values are detailed in Table 5.2. These similar results could be associated to

the fact that the in-plane measurements consider the opposite direction from the thickness and may not consider the interface, especially for thicker membranes.

Table 5.2: Comparison between the membranes proton conductivity with low humidity at 80, 100 and 120 °C.

Membrane	Temperature (°C)	Relative Humidity (%)	Proton conductivity (S cm ⁻¹)
[N _C /SPInd _C /N _C] _{HP}	80	20	0.045 ± 6x10 ⁻⁴
		40	0.040 ± 6x10 ⁻³
	100	20	0.018 ± 2x10 ⁻³
		40	0.033 ± 2x10 ⁻³
	120	20	0.016 ± 3x10 ⁻³
		40	0.035 ± 2x10 ⁻⁴
[N _C /N _C] _{HP}	80	20	0.021 ± 1x10 ⁻³
		40	0.035 ± 2x10 ⁻³
	100	20	0.019 ± 4x10 ⁻⁴
		40	0.032 ± 1x10 ⁻³
	120	20	0.016 ± 3x10 ⁻⁴
		40	0.037 ± 2x10 ⁻⁴
N _C	80	20	0.026 ± 5x10 ⁻³
		40	0.037 ± 2x10 ⁻⁴
	100	20	0.018 ± 2x10 ⁻³
		40	0.035 ± 9x10 ⁻⁴
	120	20	0.015 ± 1x10 ⁻⁴
		40	0.037 ± 7x10 ⁻⁵

In these particular conditions [N_C/SPInd_C/N_C]_{HP} presented similar or superior proton conductivity compared to that of N_C and [N_C/N_C]_{HP}. Surprisingly, Nafion continued to perform well even at 120 °C, suggesting that if it is properly humidified, good performance can be achieved in high humidity conditions. However, at low humidity and high temperature conditions (120 °C, RH=20% or 40%) Nafion is unable to retain water leading to loss of

proton conductivity and its performance was similar to that of the MMs. Impressively, in these conditions the multilayer membrane performed at par with the N_C despite the negative influence of the interfaces, as discussed above. These trends are clearly visible in Table 5.2.

5.2. Cast Membranes

As extensively discussed in Chapter II, multilayer membranes fabricated by casting should present stronger interaction between the layers than hot pressed membranes. In this section the main results for cast SPInd multilayer membranes will be discussed. Besides the comparison with Nafion membranes, the multilayers were evaluated with respect to the composition of each individual layer (see Chapter IV). All SPInd multilayer membranes were cast in the following conditions:

- 1st layer - N_C : 100 °C for 2 h + 50 °C for 0.5 h
- 2nd layer - SPInd_C: 80°C for 2 h + 100 °C for 2 h + 50 °C for 0.5 h
- 3rd layer - N_C : 100 °C for 2 h + 120 °C for 1 h.

5.2.1. Multilayer membrane microstructure

The structure of three layers can clearly be seen in the 1:1:1.5 [N_C /SPInd_C/ N_C]_C membrane cross section shown in Figure 5.6(a). The porosity found in the inner layer is a characteristic of SPInd membranes and cannot be observed in Nafion single layer membranes (Figure 5.6(b)). In the [N_C /SPInd_C/ N_C]_C membrane, the left layer represents the top layer and the right layer represents the bottom layer in the casting process. The difference in the thickness of both layers is mainly due to the difference in the amount of Nafion used. However, the

casting process has its own contribution for differences in the thickness. The intensity of DMSO aggressiveness allowed the penetration and interaction of SPInd in the bottom layer. Especially because the membrane was not yet annealed. The penetration of SPInd in the bottom layer created large pores in the interface, which can negatively impact on some properties such as proton conductivity. The penetration of Nafion from the top layer to the inner layer was subtler. The large pores cannot be seen in this interface. Water, as the solvent for the top layer, did not allow deeper penetration of the Nafion.

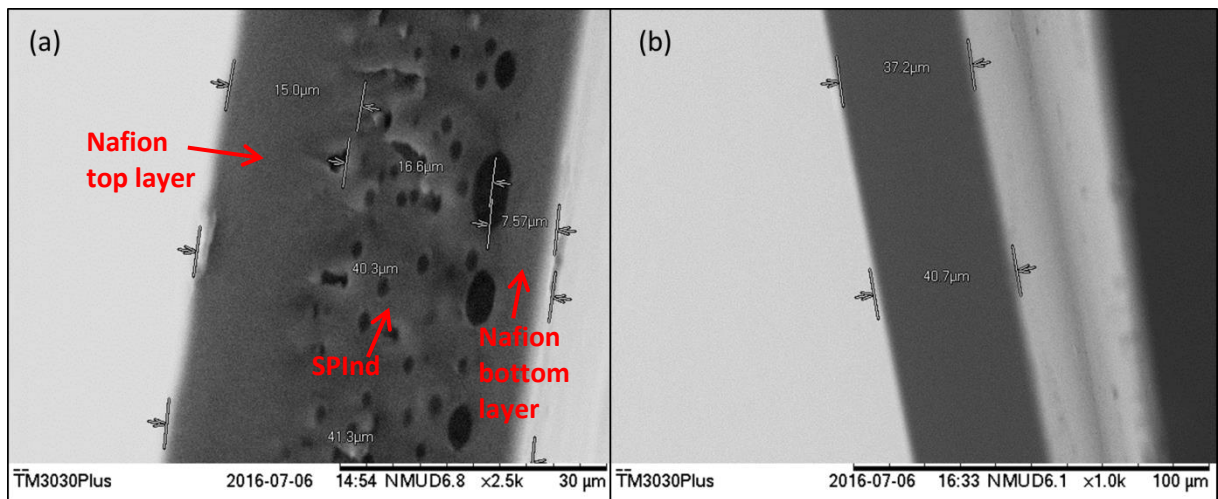


Figure 5.6: Cross-section SEM images of (a) 1:1:1.5 $[N_c/SPInd_c/N_c]_c$ membrane and (b) N_c membrane.

The inner SPInd layer presents densely distributed and symmetric pores. In this layer, the formation of the polymeric membrane started by phase separation due to the solvent vapour. Following this, the solvent was completely evaporated leaving the thin membrane on the substrate. The porosity is known to increase with low polymer concentration and high humidity [223]. This porosity found in the SPInd would be a major issue for fuel cell operation if the membrane was a single layer. However, in the MM, Nafion is expected to seal the membrane structure, avoiding hydrogen crossover.

Comparing with the hot pressed MM (equivalent to 2:1:2 [N_c/SPInd_c/N_c]_c), the structure is significantly different. The gap associated to the interlayer space found in the HP membrane is not evident in the cast one. This difference is due to the assembling of the separate layers in HP happening after each layer has been annealed. Whereas in casting the membranes, the assembly takes place before the annealing. Thus, each layer is able to penetrate and chemically contact the previous layer. The difference in the structure was also found by Kamiya *et al.* [224], when these authors compared bilayer membranes prepared by casting and hot pressing, although the materials were different from the present study. This structure found in the cast membrane is expected to improve properties such as proton conductivity because interlayer spaces would add protonic flow resistance to the membranes. Accordingly, the overall resistance is higher in HP, resulting in lower proton conductivity and performance. At the same time, WU does not necessarily decrease. This is due to the water retained in the interlayer space which can create the false idea that more is retained by the sulphonic groups. However, this water is accumulated in the pores and has no effect during fuel cell operation.

5.2.2. Water uptake and ion exchange capacity

Following the imaging and the analysis of the microstructures, the membranes were characterised by their water uptake which is represented in Figure 5.7. [N_c/SPInd_c/N_c]_c membranes showed higher water uptake than Nafion single and bilayer. Nafion single layer presented higher WU than Nafion bilayer, (20.85 ± 0.8)% and (12.46 ± 1.6)%, respectively. Thus, the increase in WU in the multilayer membranes is associated to the presence of SPInd and its sulphonic groups. Besides, it can be assumed that the interface has a negative effect

on the WU. Unlike with HP, the well assembled bi or tri layer structure in the cast membranes does not allow any void in the interface, reducing the space for unwanted water.

Between the multilayer membranes, the 2:1:2 showed lower water uptake than the other membranes. However, the WU value was similar to the SPInd single layer, ($26.05 \pm 1.49\%$ and $(26.82 + 1.59)\%$ respectively. While for all other layer ratios in the MM, the WU was higher than in the SPInd_c. In the 2:1:2 MM the difference between the amounts of Nafion to the SPInd is the largest. As Nafion has a lower WU than SPInd, the MM with the highest amount of Nafion has lower WU, as expected. The other multilayer membranes showed higher WU due to the presence of the sulphonic groups and porous structure from SPInd. Similar to this situation, the WU was higher for the MM 1:1:1.5 than for the MM 1:1:2. The ratio of Nafion is higher in the second membrane, lowering the WU. However, the difference between the component ratios is distinguished lower in this case (MM 1:1:1.5) than in the 2:1:2, approximating the WU values.

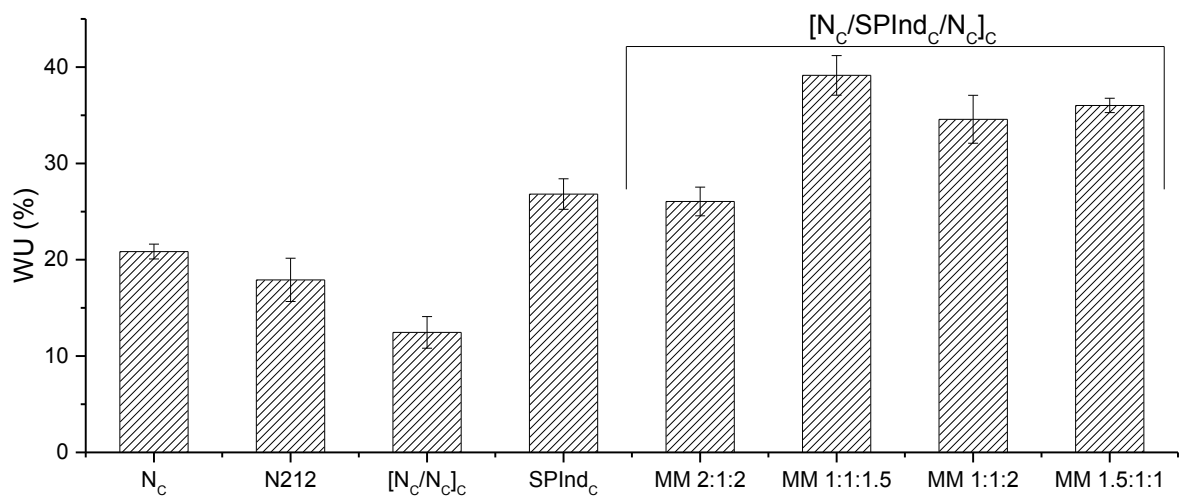


Figure 5.7: Water uptake of multilayer membranes by composition of each layer.

Besides the WU characteristics, SPInd showed higher IEC and lower λ than Nafion single layer, and higher IEC and λ than the bilayers as shown in Figure 5.8 and previously discussed. The IEC for all multilayer membranes was similar and lay between 0.9 and 0.96 mequiv/g, considerably lower than the 1.68 mequiv/g for SPInd. Thereby, the presence of Nafion has a negative effect on the IEC. While the interface did not affect the IEC as it affected the WU, and cast Nafion single and bilayer membranes showed similar IEC.

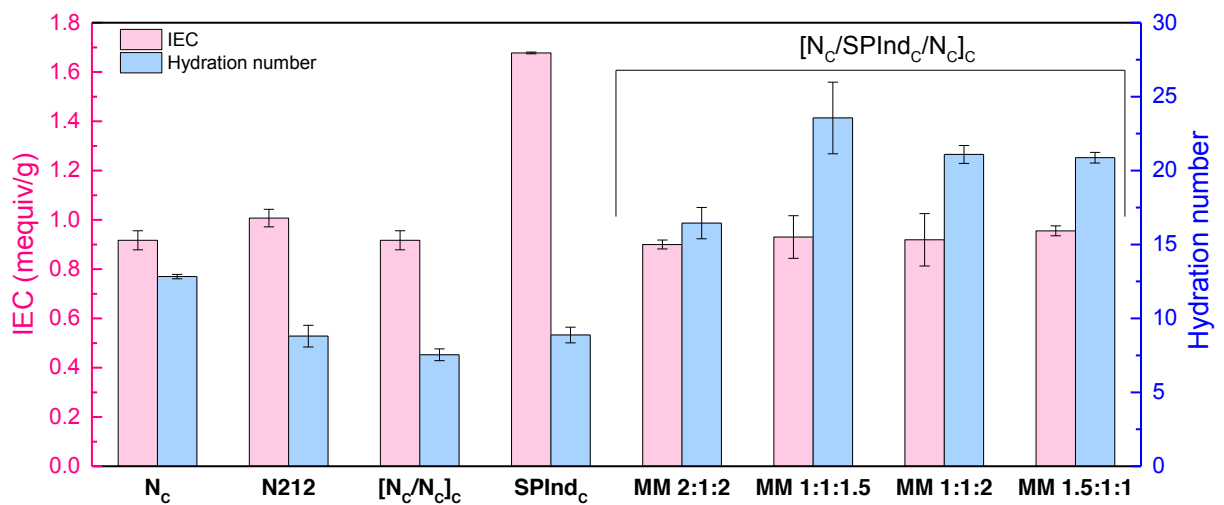


Figure 5.8: Ion exchange capacity and hydration number of the cast SPInd multilayer membranes.

On the other hand, λ was significantly higher in the multilayer membranes than in any other membrane. λ is associated with the number of water molecules per of sulphonic group. In other words, the hydration number can be interpreted as the efficiency of the sulphonic group in catching water. The higher the λ , the less sulphonic groups are necessary to retain the same amount of water. Therefore, the sulphonic groups presented in the multilayer membranes are able to retain more water molecules and, consequently, facilitate the proton transport. Among the SPInd multilayer membranes, the highest λ was found in the 1:1:1.5,

such as with the WU. The λ for this membrane was 23.56 ± 2.42 molecules of water per sulphonic group, while for N_c it was 12.83 ± 0.15 molecules of water per sulphonic group. As such, the membrane 1:1:1.5 was the most promising membrane after the ex-situ tests. The interface in MM was found by Li *et al.* [138] to reduce the IEC and WU, unlike this study that only identified a significant difference in WU. Nevertheless, Li *et al.* proved that the external layers (sulphonated polyimide) provided the mechanical structure and limited the expansion of the highly hydrophilic inner layer (SPEEK). All values of WU, IEC, and hydration number for cast MM are detailed in Table 5.3.

Table 5.3: Detailed properties of single and cast multilayer membranes.

Membrane	WU (%)	IEC (mequiv/g)	λ (molecules of water per $-\text{SO}_3$)
N_c	20.85 ± 0.77	0.917 ± 0.039	12.83 ± 0.15
N212	17.91 ± 2.25	1.007 ± 0.036	8.80 ± 0.73
$[N_c/N_c]_c$	12.46 ± 1.64	0.917 ± 0.039	7.54 ± 0.40
SPInd_c	26.82 ± 1.59	1.667 ± 0.003	8.88 ± 0.53
$[N_c/\text{SPInd}_c/N_c]$ 2:1:2	26.05 ± 1.49	0.900 ± 0.018	16.45 ± 1.06
$[N_c/\text{SPInd}_c/N_c]$ 1:1:1.5	39.14 ± 2.05	0.930 ± 0.086	23.56 ± 2.42
$[N_c/\text{SPInd}_c/N_c]$ 1:1:2	34.58 ± 2.49	0.919 ± 0.106	21.09 ± 0.61
$[N_c/\text{SPInd}_c/N_c]$ 1.5:1:1	36.02 ± 0.74	0.955 ± 0.020	20.87 ± 0.36

The IEC values for the cast MM were lower than for the HP membranes, which are shown in Figure 5.9. Similarly to the case of WU, the HP membranes showed interlayer spaces which mask the values of IEC. However, the hydration number was significantly higher for the cast membranes. SPInd MMs, cast and hot pressed, showed higher ex-situ properties than Nafion single layer, highlighting the positive influence of the SPInd layer.

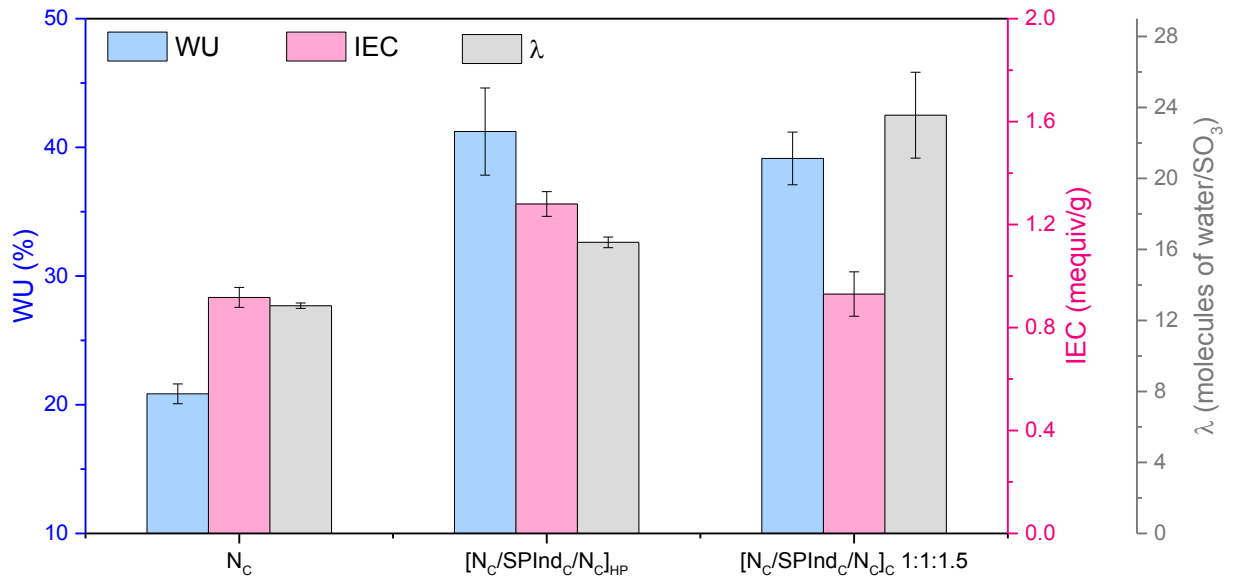


Figure 5.9: Comparison between hot pressed and cast SPInd multilayer membranes.

5.2.3. Conductivity

The most successful multilayer membrane in the previous tests, $[N_c/SPInd_c/N_c]_{1:1:1.5}$, was tested in a fuel cell set up to measure the proton conductivity. It was compared with N_c , N212, $[N_c/N_c]_c$ and $[N_c/SPInd_c/N_c]_c$ 2:1:2. The results are shown in Figure 5.10. All membranes showed the same trend: proton conductivity increased when relative humidity increased. As the amount of water is increased, the distance between activated sites is reduced. It means that each sulphonic group has water or another sulphonic group next to it. Thus, protons have a smooth path to follow through the membrane with conductor sites all along. Nafion membranes N_c , $[N_c/N_c]_c$ and N212 showed similar proton conductivity behaviour under all conditions. Accordingly, the interface in the cast membrane did not present any significant influence on this property. This equality in the proton conductivity validates the cast preparation method used in this study, as there is not decrease in this property for these membranes.

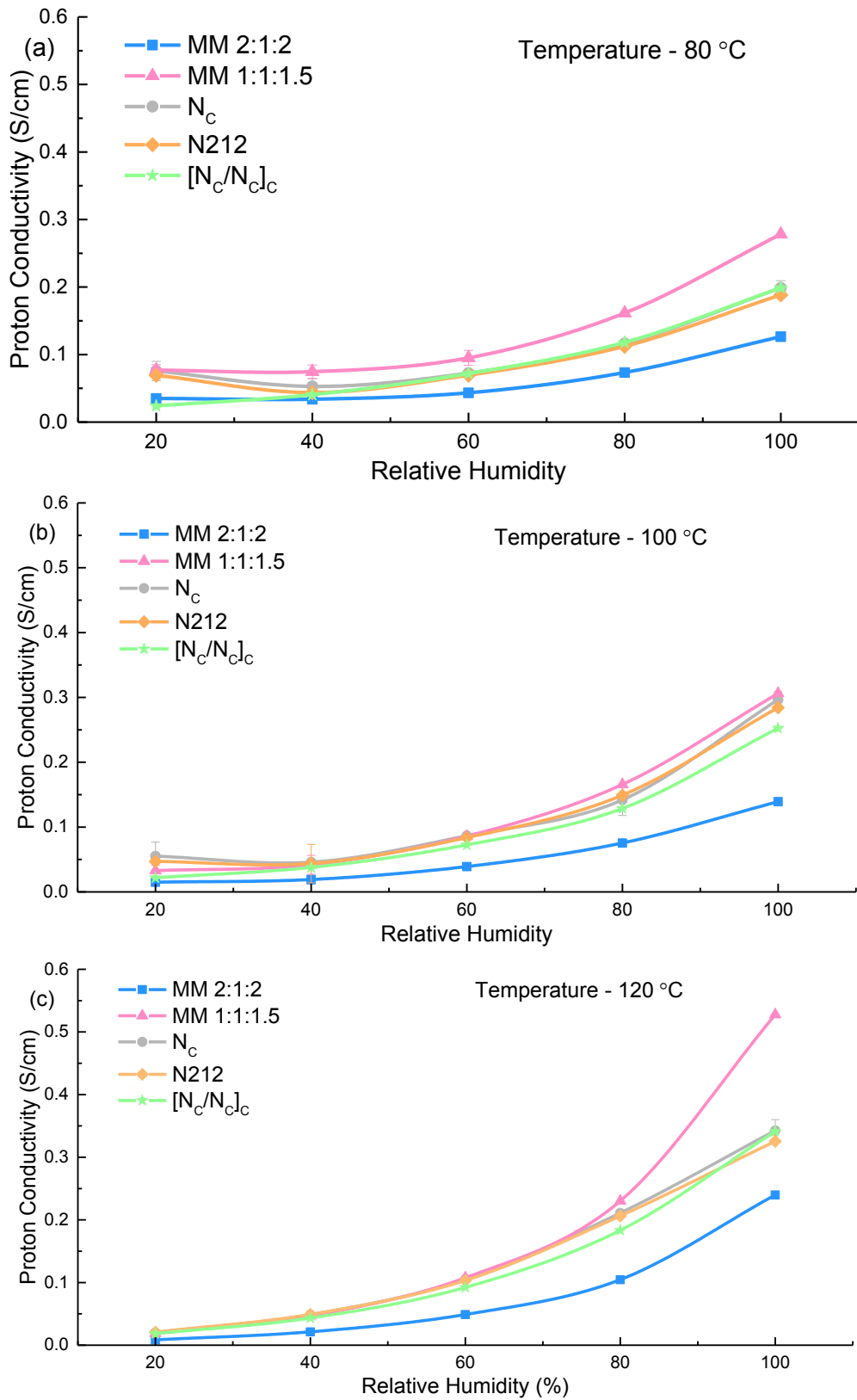


Figure 5.10: Cast MM proton conductivity curves at (a) 80 °C, (b) 100 °C and (c) 120 °C.

Between $[N_c/SPInd_c/N_c]_c$ multilayer membranes, the 1:1:1.5 presented higher proton conductivity than the 2:1:2 at all conditions of humidity and temperatures. The difference in the ratio of SPInd/Nafion is a significant parameter for proton conductivity. When comparing the IEC values of SPInd and Nafion single layers, SPInd showed 1.8 times the IEC value of Nafion. Although IEC results cannot be assumed to exactly match proton conductivity, the higher IEC found in the SPInd is a good indicative to assure this higher value.

Comparing with Nafion, $[N_c/SPInd_c/N_c]_c$ 1:1:1.5 showed higher values of proton conductivity at 80 °C with $RH \geq 40\%$. At 120 °C, the MM presented higher proton conductivity values than Nafion with high humidity and equal at low humidity.

Arrhenius plots of the membranes conductivity with humidity equal to or lower than 80% are shown in Figure 5.11 and with $RH = 100\%$ shown in Figure 5.12. The Arrhenius plot is the representation of the proton conductivity natural logarithm ($\ln \sigma$) versus the inverse of the temperature ($1/T$), which should follow a linear trend. This plot is important to evaluate if the proton transport through the membrane is kinetic favourable or not, and to analyse the effect of the temperature in the proton conductivity. However, the membranes do not represent Arrhenius behaviour with low humidity. With Arrhenius behaviour, the membranes should show the decreasing $\ln \sigma$ as $1000/T$ increases. Therefore, activation energy (E_a) for the proton conductivity was calculated assuming Arrhenius behaviour only for relative humidity of 100% and is detailed in Table 5.4. The E_a could be calculated for low humidity conditions. However the E_a would demonstrate that the proton transport is not favourable in these conditions even for Nafion. It is known that the proton transport

depends on the water availability. Thus, there is no goal in calculating the E_a for these low values of RH. The activation energy is calculated following equation 5.4 below.

$$E_a = slope \times R \quad \text{(Equation 5.4)}$$

Where R is the universal gas constant and the slope is found in the linear regression in Arrhenius plots, calculated following equation 5.5 below.

$$slope = \frac{\Delta \ln \sigma}{\Delta 1/T} \quad \text{(Equation 5.5)}$$

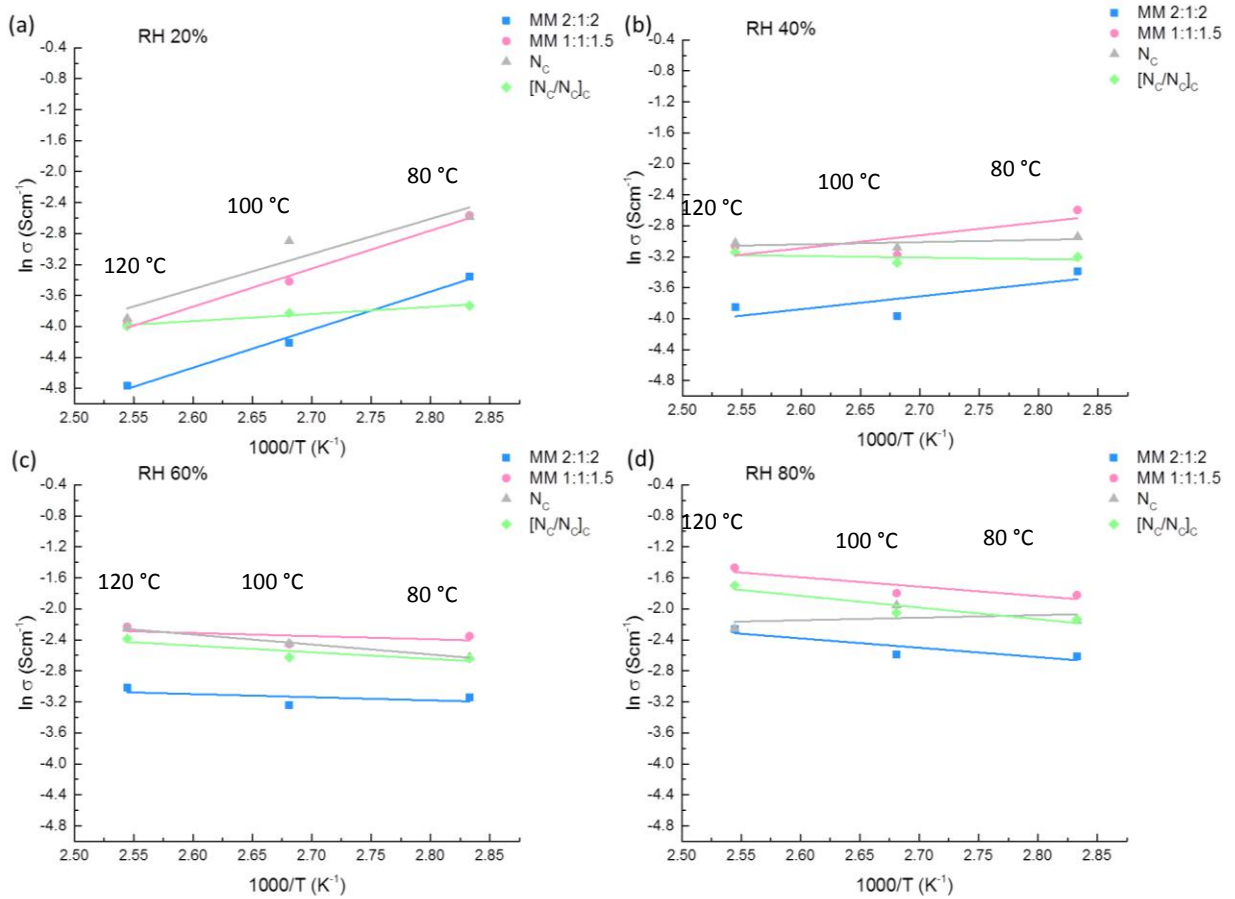


Figure 5.11: Arrhenius plot with RH of (a) 20%, (b) 40%, (c) 60% and (d) 80%

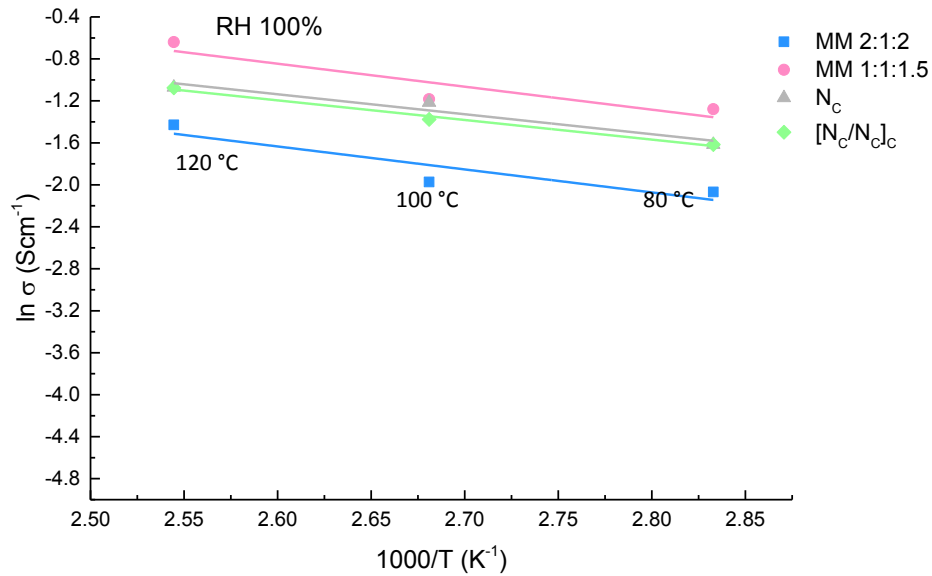


Figure 5.12: Arrhenius plot with 100 % of RH.

Table 5.4: Membranes activation energy at the temperature range of 80-120 °C and with 100% of relative humidity.

Membrane	Activation Energy (kJ/mol)
$[N_c/SPInd_c/N_c]_c$ 2:1:2	18.2033
$[N_c/SPInd_c/N_c]_c$ 1:1:1.5	18.2039
N_c	15.819
$[N_c/N_c]_c$	15.539

The activation energy is higher for the multilayer membranes than for Nafion membranes, ~18 and ~15.5 kJ/mol, respectively. These energies were calculated based on Figure 5.12. Accordingly, the barrier for proton transport is higher for SPInd multilayer membranes than for Nafion. This is expected since the complexity of these membranes is higher, adding two new interfaces and difference of the materials. This value found for Nafion was similar to the activation energy found in the literature (14.2 kJ/mol) with 100% of relative humidity [105]. Although higher activation energy than Nafion, the MMs showed a negative slope with RH = 100% and the proton conductivity is kinetically favourable.

5.2.4. Single cell test

The single cell test was carried out in the 850e High Temperature Scribner Associates Incorporated Test Stand which had a 885 Fuel Cell Potentiostat. The potentiostat, humidifiers, mass flow control, and pressurised water supply were integrated into the system. The maximum load current and power were 100 A and 100 W, respectively. The reference electrode had a range of input voltage of -3 to +3 V. Bipolar plates were composed of graphite with single serpentine flow channels to allow the gas distribution. Current collectors were made of copper coated with gold. Prior to the test, the membranes were immersed in water for 24 h.

MEAs had an active area of 6.25 cm². The gas diffusion electrode (GDE) with carbon paper support and the catalyst platinum was acquired from Johnson Matthey with a catalyst loading of 0.4 mg Pt/cm². A solution with Nafion and isopropyl alcohol (1:2) was used as binder and painted on the GDE. Thereafter, the membranes were cut into 16 cm² squares, placed between the electrodes and hot pressed at 125 °C for 5 min.

The MEAs were tested in the fuel cell single cell sample holder. The i-V curve was recorded 3 times for each sample, and was tested 3 samples for each membrane. The three samples were originated from three different membranes from the same type to evaluate the reproducibility of the membranes preparation method. The back pressure was 1.8 bar. The anode was supplied with hydrogen and the cathode with compressed air at a rate of 1 and 2.5 L/min, respectively.

The resultant curves of potential and power for membranes in the fuel cell test are exhibited in Figures 5.13 to 5.20. With low humidity of 20%, the $[N_c/SPInd_c/N_c]_c$ 1:1:1.5 membrane showed higher potential and power at low currents than all other membranes. At 80 °C (Fig. 5.13(a)), the Nafion bilayer equalized the potential only at $\sim 400 \text{ mA/cm}^2$, while at 100 °C (Fig. 5.15(b)) it was never equal. At 120 °C (Fig. 5.18(b)), N_c matched the value only at $\sim 600 \text{ mA/cm}^2$. On the other hand, $[N_c/SPInd_c/N_c]_c$ 2:1:2 showed lower potential and power than N_c in all these conditions. Thus, SPInd indeed holds water at low humidity, while Nafion tends to dry. When the ratio of Nafion to SPInd was increased, the potential was reduced. As such, SPInd is a promising material to be applied in PEFC at low humidity at all temperatures.

Unlike the previous conditions, with 40% RH, $[N_c/SPInd_c/N_c]_c$ 1:1:1.5 only showed advantage related to $[N_c/N_c]_c$ at temperature over 80 °C (Fig. 5.13(b)) and advantage to N_c at 100 °C (Fig. 5.16(a)) and 120 °C (Fig. 5.18(b)) at low and medium currents. Increasing the humidity allows Nafion to retain more water, even at higher temperature, due the continuous flow of water. Thus, Nafion performance improves when the humidity increases even at intermediate temperature. As the temperature and humidity increase, so does Nafion conductivity as Alberti *et al.* [225] confirmed in their study. At 120 °C with 20 and 40% RH, $[N_c/N_c]_c$ showed practically zero performance, which means that the interface between both layers of Nafion is detrimental to the performance at these conditions. At lower temperature and high humidity, the interface did not show the same negative effect, whilst at 120 °C, only with 100% RH (Fig. 5.20) the bilayer demonstrated similar performance to the single layer.

With humidity as high as 60% and 80%, N_c showed the best performance. However, at 100 °C, all four membranes approximated the performances. Nafion has an ideal performance at low temperature (80 to 100 °C) and high humidity (~80%) (Figs. 5.14(b) and 5.17(a)). Thus, with these conditions Nafion layers in all membranes stand out to the others. And as shown, Nafion does not demonstrate any issue to retain water in this situation.

Both $[N_c/SPInd_c/N_c]_c$ 1:1:1.5 and $[N_c/SPInd_c/N_c]_c$ 2:1:2 membranes showed severe voltage losses due to mass transport above currents $>400 \text{ mA/cm}^2$, which are not seen in Nafion membranes. This might be associated to the flooding of the membrane and, consequently, the gas flow channels. This behaviour is noticed at 80 and 120 °C with different RHs. The only case at 100 °C is with 100% RH (Fig. 6.17(b)), but it is expected. In this particular fuel cell unit, when the humidity reaches 100%, the membrane is flooded. $[N_c/N_c]_c$ only presented losses due to mass transport at 120 °C, unlike the SPInd membranes. Therefore, the losses cannot be attributed to the interfaces, if so it would have this effect on the Nafion bilayer as well. The presence of SPInd increases the water uptake, which can retain the water in the inner layer. In contrast, at low humidity the water may find it more difficult to diffuse to the external layers of Nafion, decreasing the potential. The flooding can also be attributed to a mismatch of membranes properties with GDL and test rig setup. However, this was not further pursued in this study.

The power curves have the same trend of polarization curves. $[N_c/SPInd_c/N_c]_c$ 1:1:1.5 presented higher power at low humidity, while Nafion presented higher power at medium and high humidity. Not all membrane achieved the maximum power at all conditions.

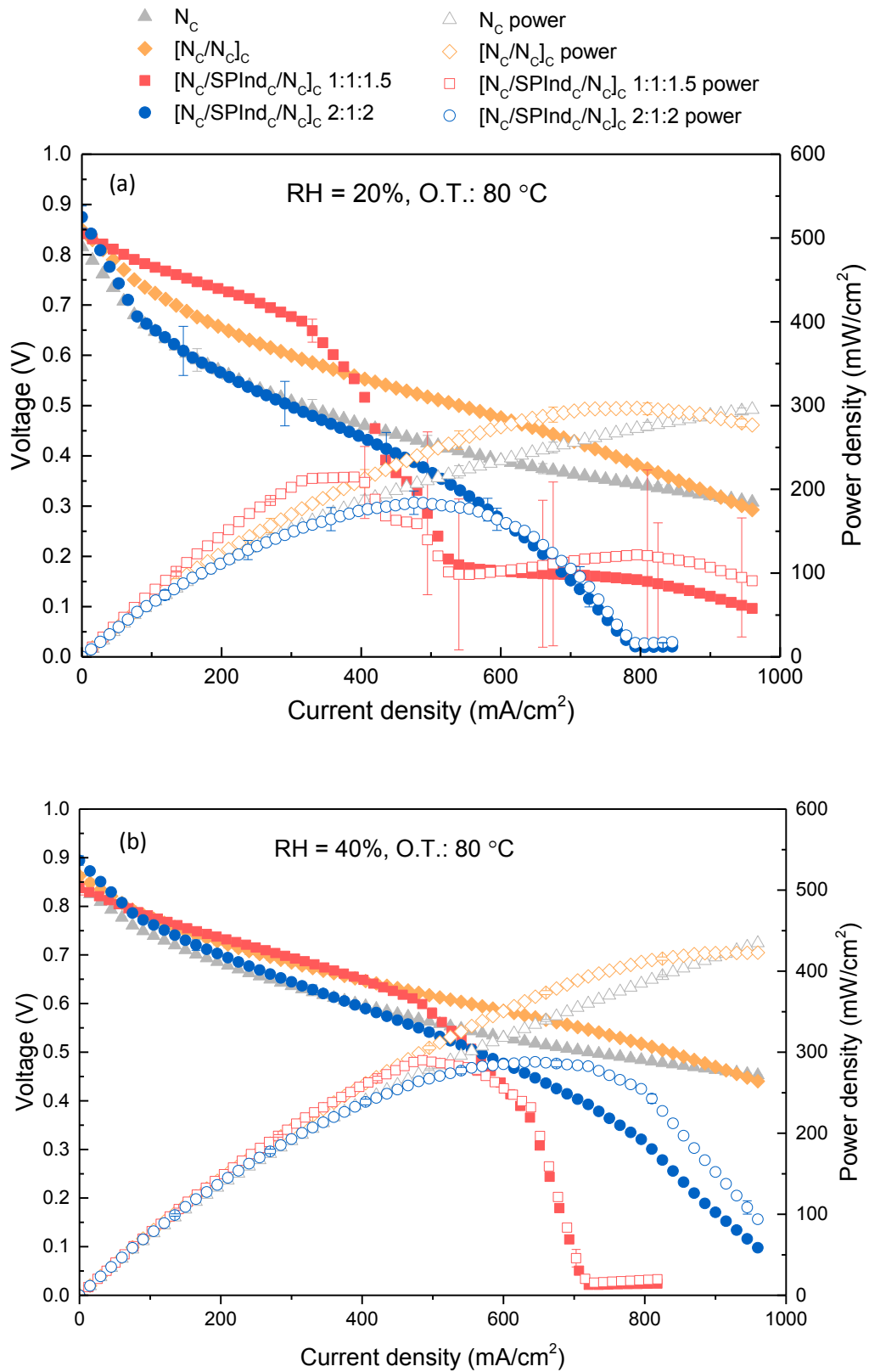


Figure 5.13: Polarization and power curves with (a) 20% of relative humidity and 80 °C of operation temperature, (b) 40% of relative humidity and 80 °C of operation temperature. Back pressure 0.18 MPa, H₂/Air at rate of 1 and 2.5 L/min respectively.

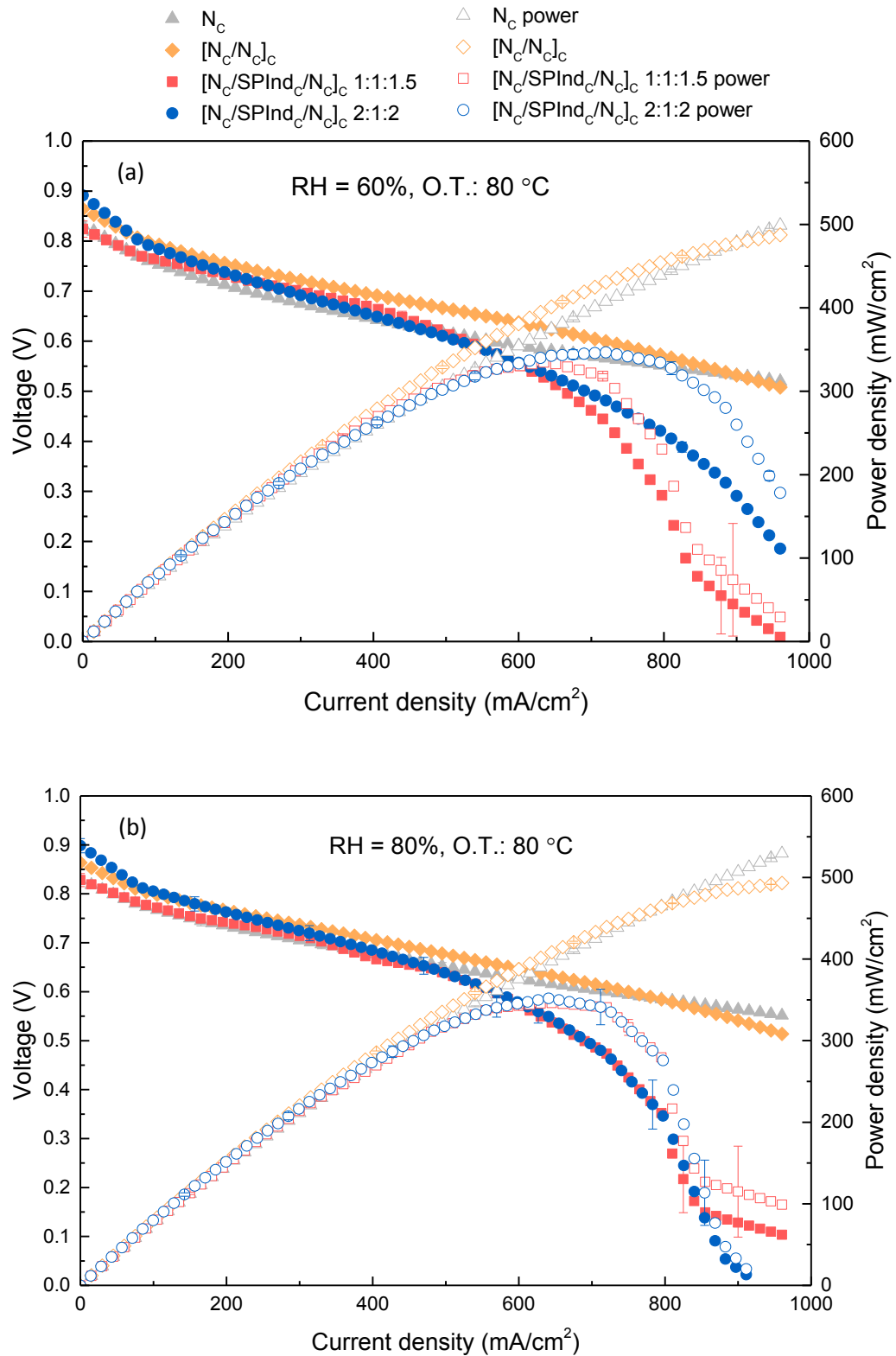


Figure 5.14: Polarization and power curves with (a) 60% of relative humidity and 80 °C of operation temperature, (b) 80% of relative humidity and 80 °C of operation temperature. Back pressure 0.18 MPa, H₂/Air at rate of 1 and 2.5 L/min respectively.

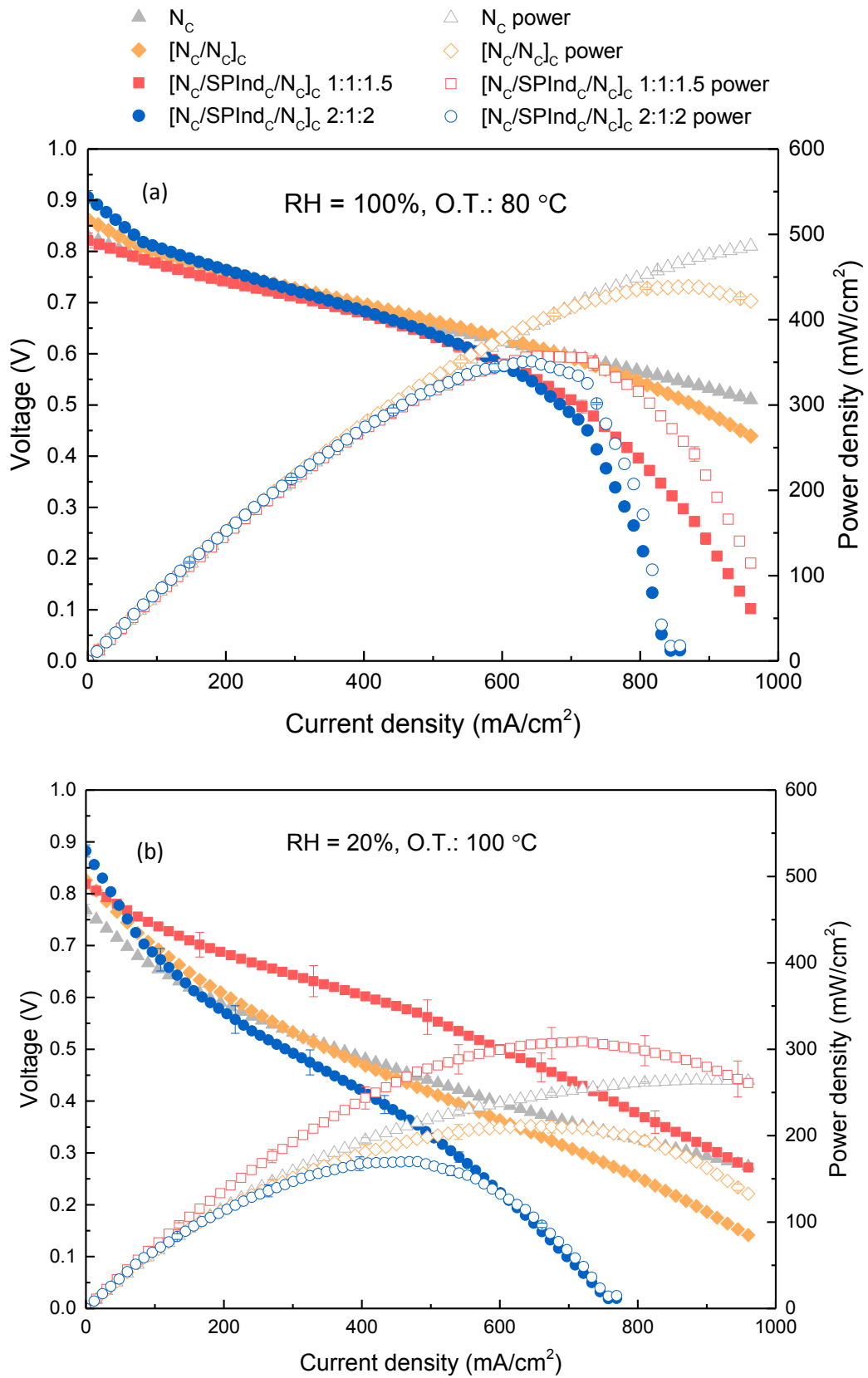


Figure 5.15: Polarization and power curves with (a) 100% of relative humidity and 80 °C of operation temperature, (b) 20% of relative humidity and 100 °C of operation temperature. Back pressure 0.18 MPa, H₂/Air at rate of 1 and 2.5 L/min respectively.

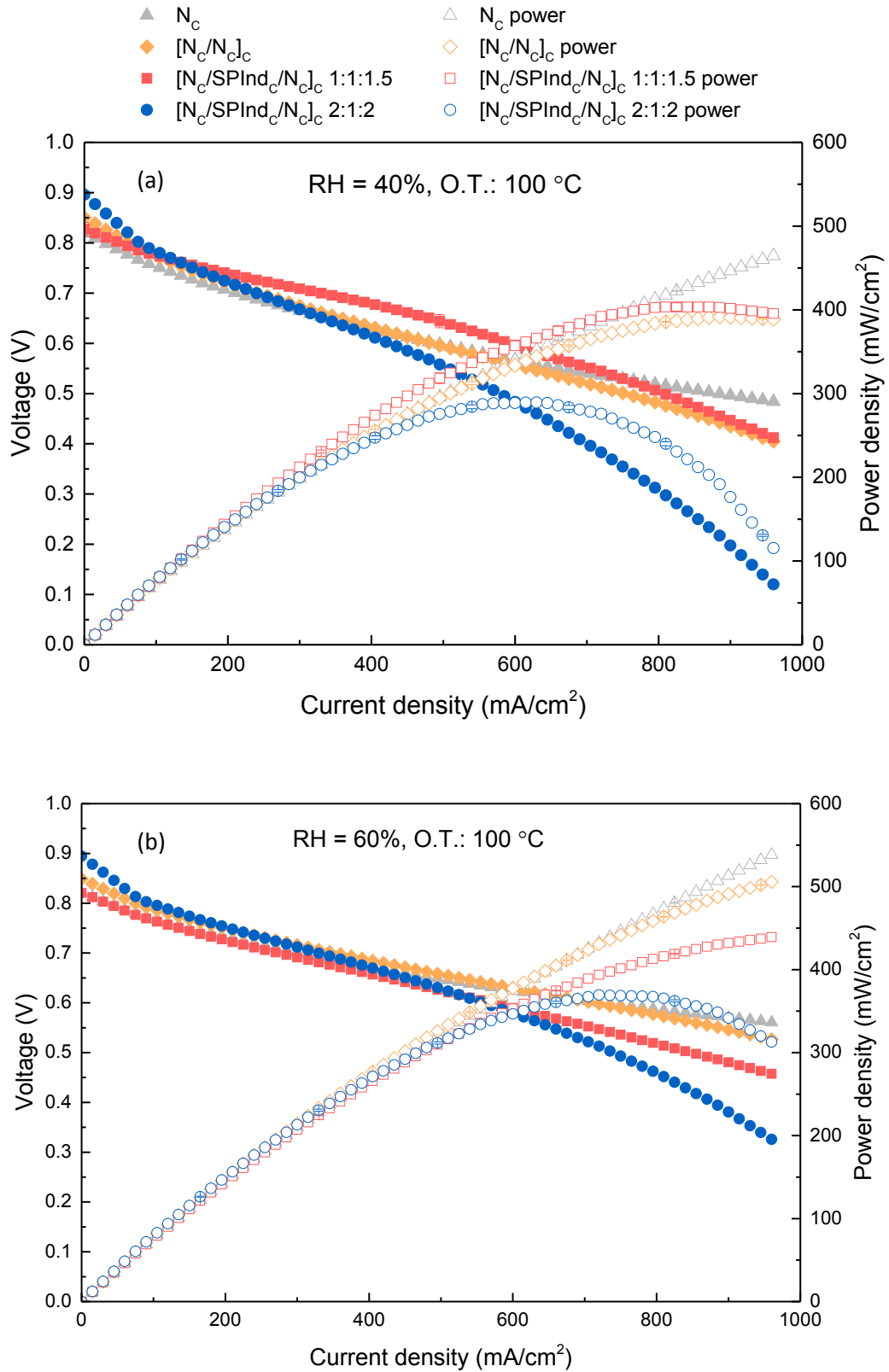


Figure 5.16: Polarization and power curves with (a) 40% of relative humidity and 100 °C of operation temperature, (b) 60% of relative humidity and 100 °C of operation temperature. Back pressure 0.18 MPa, H₂/Air at rate of 1 and 2.5 L/min respectively.

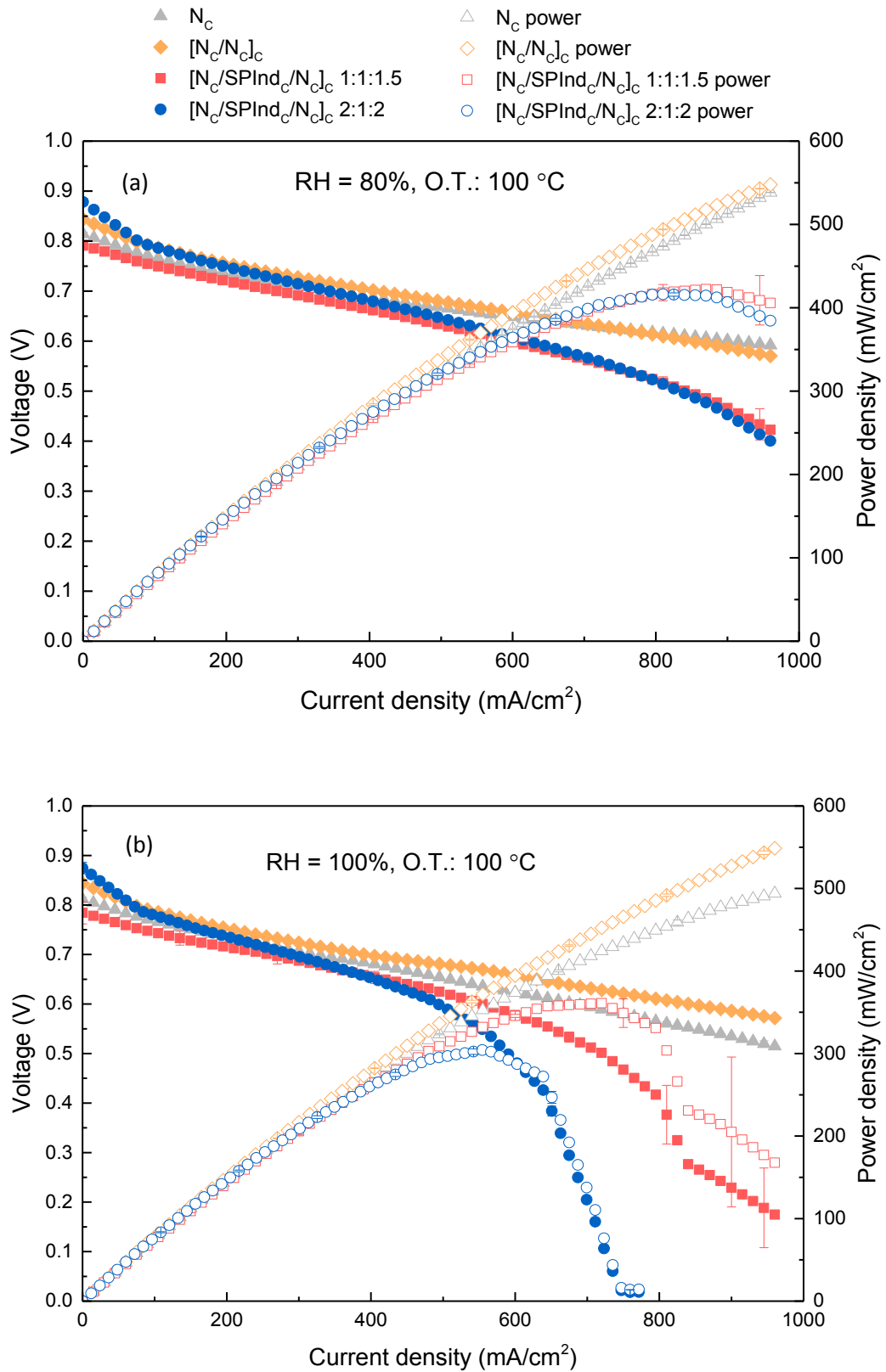


Figure 5.17: Polarization and power curves with (a) 80% of relative humidity and 100 °C of operation temperature, (b) 100% of relative humidity and 100 °C of operation temperature. Back pressure 0.18 MPa, H₂/Air at rate of 1 and 2.5 L/min respectively.

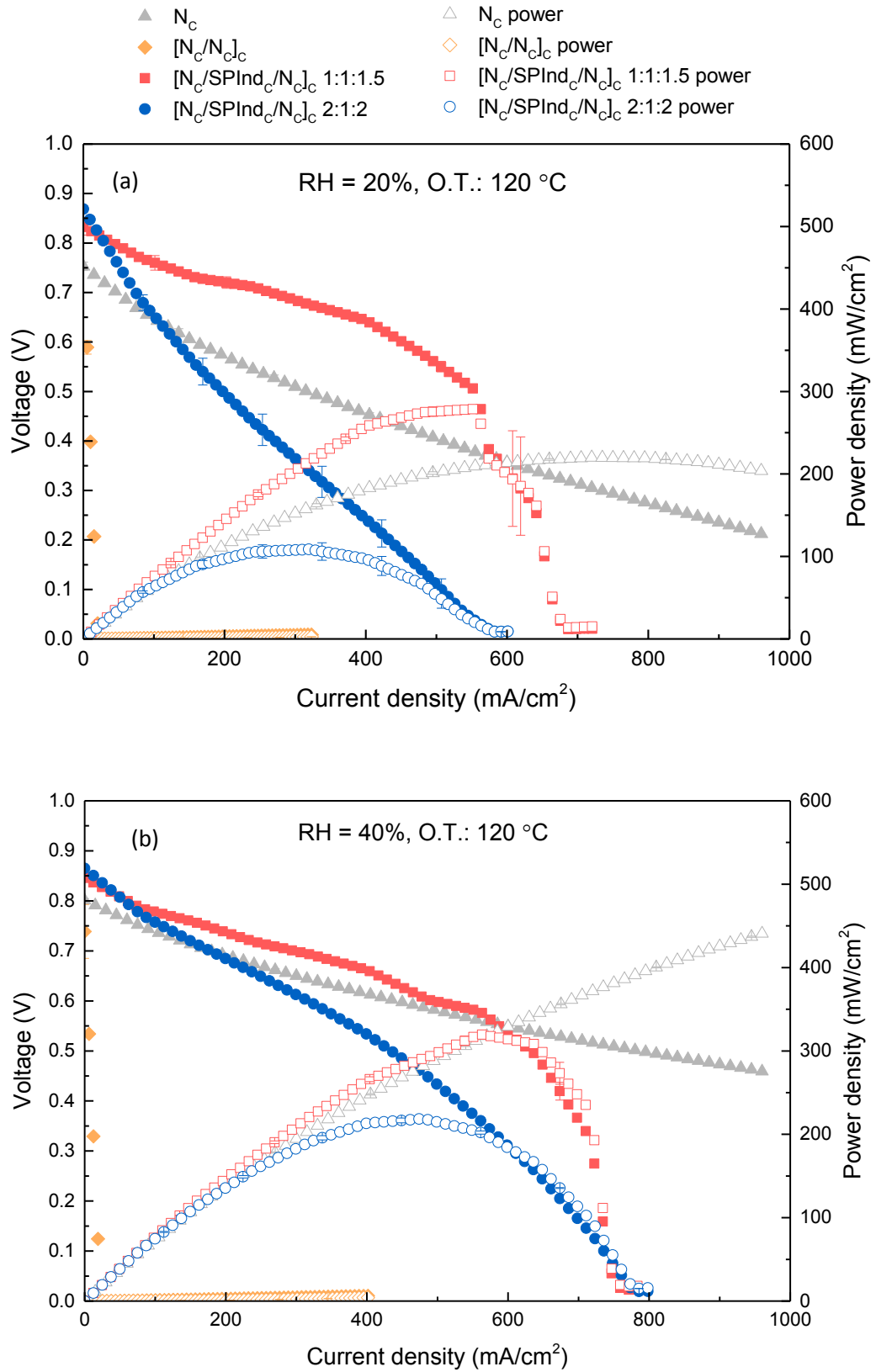


Figure 5.18: Polarization and power curves with (a) 20% of relative humidity and 120 °C of operation temperature, (b) 40% of relative humidity and 120 °C of operation temperature. Back pressure 0.18 MPa, H₂/Air at rate of 1 and 2.5 L/min respectively.

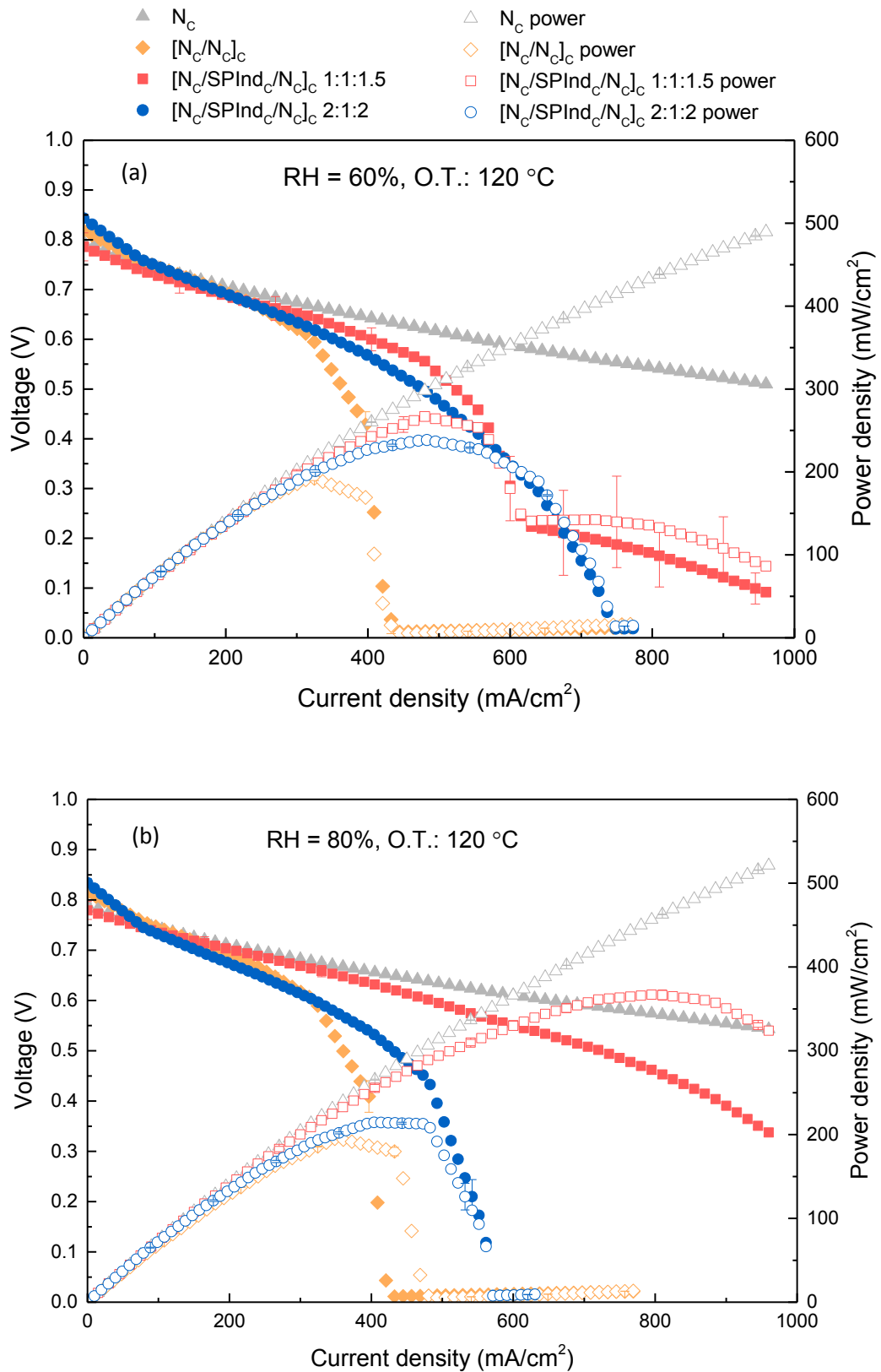


Figure 5.19: Polarization and power curves with (a) 60% of relative humidity and 120 °C of operation temperature, (b) 80% of relative humidity and 120 °C of operation temperature. Back pressure 0.18 MPa, H₂/Air at rate of 1 and 2.55 L/min respectively.

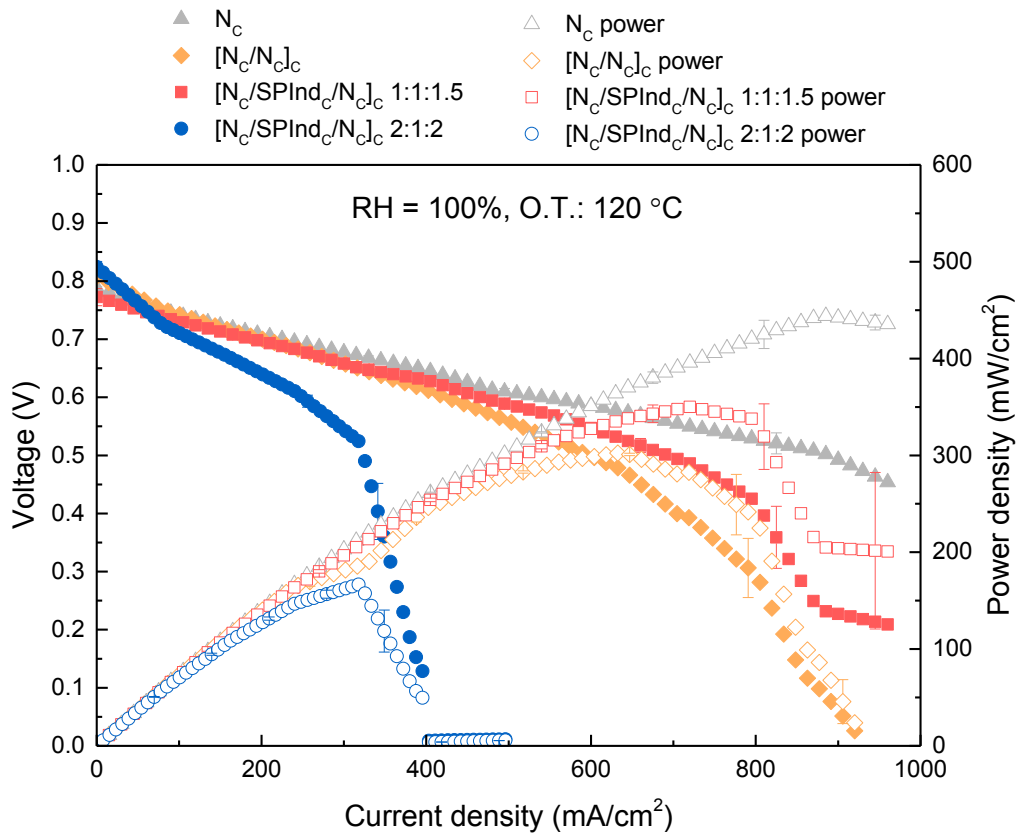


Figure 5.20: Polarization and power curves with 100% of relative humidity and 120 °C of operation temperature. Back pressure 0.18 MPa, H₂/Air at rate of 1 and 2.5 L/min respectively.

In Table 5.5 the voltage and power values for low current density (400 mA/cm²) and medium current density (600 mA/cm²) are detailed. Besides, the maximum power reached by each membrane at each condition of RH and temperature is listed. In bold and blue are highlighted the power values for MM which are higher than the respective N_c membrane. It is clear to note that for low current values the MM has a higher performance than at high current. Furthermore, $[N_c/SPInd_c/N_c]_{1:1:1.5}$ improved the power values at low humidity, as it was the initial goal for the membranes. However, this membrane did not hold the power and potential at high current.

Table 5.5: Membranes detailed voltages and power.

Membrane	Temperature (°C)	RH (%)	at 0.400 mA/cm ²		at 0.600 mA/cm ²		Maximum Power (mA/cm ²)
			Voltage (V)	Power (mA/cm ²)	Voltage (V)	Power mA/cm ²	
N _c	80	20	0.4599	186.12	0.3911	234.22	295.41
		40	0.5946	240.69	0.5304	317.79	434.63
		60	0.6429	260.28	0.5909	354.23	498.91
		80	0.6769	274.05	0.6263	375.42	529.51
		100	0.6818	277.08	0.6244	373.99	486.00
	100	20	0.4811	194.70	0.9308	237.48	264.06
		40	0.6274	253.99	0.5667	339.59	464.66
		60	0.6722	272.15	0.6246	374.46	538.31
		80	0.6873	274.92	0.6482	388.92	538.30
		100	0.6802	275.41	0.6235	373.69	493.97
	120	20	0.4527	183.17	0.3569	213.41	219.87
		40	0.6125	247.94	0.5492	329.08	440.83
		60	0.6425	260.11	0.5884	352.64	489.47
		80	0.6560	265.59	0.6106	366.07	521.22
		100	0.6451	261.13	0.5856	350.95	438.93
[N _c /N _{cl}] _c	80	20	0.5526	212.75	0.4757	274.6	296.93
		40	0.6465	261.71	0.5851	350.68	422.74
		60	0.6911	278.92	0.6371	380.82	487.45
		80	0.7054	285.58	0.6466	387.50	493.21
		100	0.8627	0.6950	0.6304	377.68	437.89
	100	20	0.4682	180.75	0.3634	209.21	211.27
		40	0.6304	255.18	0.5573	333.82	391.52
		60	0.6843	277.50	0.6298	377.49	505.80
		80	0.7013	283.95	0.6570	393.86	547.80
		100	0.6970	282.18	0.6580	394.37	548.83
	120	20	x	x	x	x	2.70
		40	0.0105	4.20	x	x	4.20
		60	0.4281	168.20	0.0164	9.85	192.24
		80	0.4090	189.85	0.0164	9.84	194.89
		100	0.6970	282.18	0.6580	394.37	548.83

Membrane	Temperature (°C)	RH (%)	at 0.400 mA/cm ²		at 0.600 mA/cm ²		Maximum Power (mA/cm ²)
			Voltage (V)	Power (mA/cm ²)	Voltage (V)	Power mA/cm ²	
[N _c /SPInd _c /N _c] _c 1:1:1.5	80	20	0.5164	208.22	0.1709	91.90	214.68
		40	0.6410	257.09	0.4373	255.17	289.97
		60	0.6636	269.73	0.5510	330.61	334.70
		80	0.6661	269.71	0.5733	342.70	346.09
		100	0.6755	274.57	0.5703	347.77	356.95
	100	20	0.6020	243.68	0.5002	299.18	309.12
		40	0.6771	274.11	0.5965	357.16	403.47
		60	0.6568	265.87	0.5895	353.15	439.09
		80	0.6618	267.92	0.5988	358.73	422.28
		100	0.6537	264.65	0.5779	345.59	361.05
	120	20	0.6396	258.78	0.3439	202.01	278.55
		40	0.6594	266.17	0.5358	314.00	317.78
		60	0.5999	242.73	0.3049	179.89	262.04
		80	0.6317	255.69	0.5506	329.75	367.01
		100	0.6276	254.02	0.5471	327.47	350.04
[N _c /SPInd _c /N _c] _c 2:1:2	80	20	0.4398	174.15	0.2790	164.24	184.09
		40	0.5894	238.52	0.4768	285.03	288.06
		60	0.6489	262.65	0.5571	333.36	346.69
		80	0.6850	273.05	0.5790	345.18	351.86
		100	0.6825	274.32	0.5759	346.18	351.09
	100	20	0.4226	167.51	0.2231	132.20	169.94
		40	0.6113	247.38	0.4834	288.82	289.37
		60	0.6696	271.05	0.5792	346.70	369.43
		80	0.6793	275.00	0.6083	364.37	416.26
		100	0.6538	260.01	0.4804	287.17	304.15
	120	20	0.2377	95.60	0.0151	9.05	108.59
		40	0.5341	213.11	0.3117	184.55	218.34
		60	0.5687	226.55	0.3443	205.69	238.51
		80	0.5322	214.62	0.0141	8.47	214.62
		100	0.0089	3.60	x	x	166.54

As shown previously, the $[N_c/SPInd_c/N_c]_c$ 1:1:1.5 membrane displayed a thickness of $\sim 41 \mu\text{m}$. This membrane suffered a compression when the MEA was prepared and further compression when tested in the fuel cell. Figure 5.21(a) shows the membrane before the MEA preparation and Figure 5.21(b) shows the membrane in the MEA after the PEFC test. With the images, the reduction in the thickness due to these compressions is evident. The final thickness of the post-used membrane was $\sim 23 \mu\text{m}$, which means a reduction of 44% in the thickness.

The thickness reduction can increase proton conductivity. However, it also increases the gas crossover. Consequently, this crossover reduces the OCV. This situation is confirmed by the low OCV values presented by the membranes. Finally, reducing the OCV, the energetic efficiency is reduced too. The reduction in thickness can be avoided using inorganic oxides with high mechanical properties, such as graphene oxide.

Although there was a reduction in thickness, no further change in the membranes structure could be distinguished in the post PEFC test membrane.

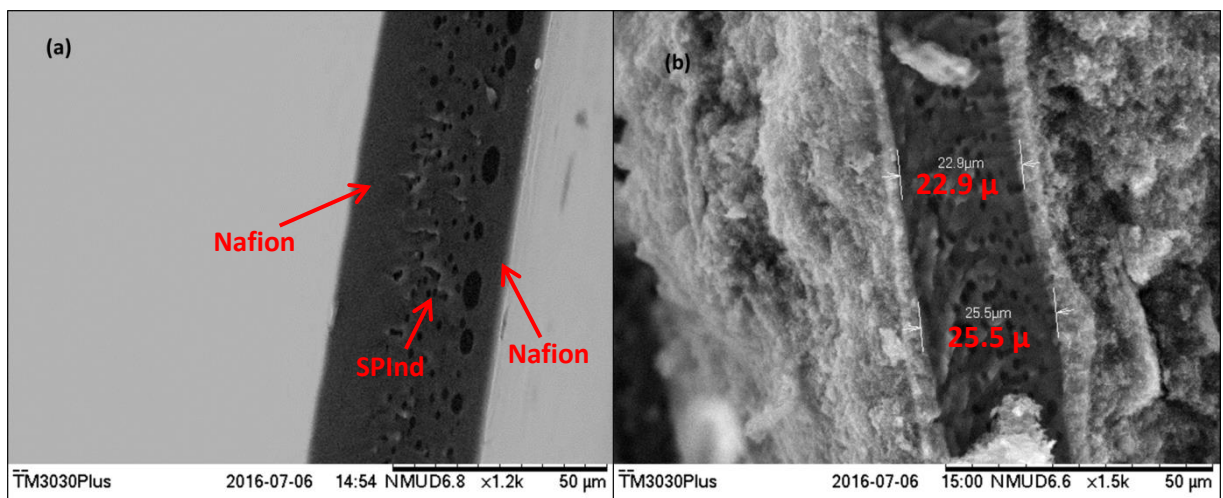


Figure 5.21: $[N_c/SPInd_c/N_c]_c$ 1:1:1.5 membrane (a) before and (b) after PEFC single cell test.

5.3. Conclusions

As-prepared HP and cast membranes were analysed by SEM, which revealed delamination and insufficient interfacial interaction between the constituent Nafion and SPInd layers in hot pressed membranes, while the interaction was satisfactory and no delamination was presented in casting membranes. WU studies further highlighted the effect of weak interlayer interactions in $[N_C/SPInd_C/N_C]_{HP}$ and $[N_C/N_C]_{HP}$ membranes, because the high WU value is masked by the water trapped between the layers. $[N_C/N_C]_C$ presented lower WU than a Nafion single layer. On the other hand, $[N_C/SPInd_C/N_C]_C$ membranes showed higher WU than both Nafion bi and single layer. Since there was no delamination in the membrane, this WU can be assumed as a real value, demonstrating the potential of this membrane for PEFC application.

$[N_C/SPInd_C/N_C]_{HP}$ showed higher IEC value compared to that of single and bilayer Nafion as well as commercial Nafion 212 overcoming the negative effect of the interface. The equivalent cast membrane $[N_C/SPInd_C/N_C]_C$ 2:1:2 showed lower IEC value than the HP. However both presented the same hydration number. The cast multilayer membranes with less Nafion in the composition also presented lower IEC than the HP. Nevertheless, these membranes $[N_C/SPInd_C/N_C]_C$ 1.5:1:1, 1:1:2 and 1:1:1.5 showed higher hydration number than the other membranes. Thus, a reduced amount of these membranes is necessary than with the other membranes to retain the same volume of water. This characteristic is due to the free active sites on the SPInd, which in Nafion are not present to the same extent.

Proton conductivity studies showed $[N_C/SPInd_C/N_C]_{HP}$ performance to be similar or slightly higher compared to $[N_C/N_C]_{HP}$ in all conditions. In comparison to interface-free N_C ,

$[N_c/SPInd_c/N_c]_{HP}$ showed higher proton conductivity at low humidity and high temperature conditions. However, the $[N_c/SPInd_c/N_c]_{HP}$ membrane formed in this study was 25% thicker than cast Nafion. The in-plane proton conductivity is affected by the water uptake potential of the material used. It is, therefore, imperative to compare multilayer membranes (involving different materials) of equal thickness. Casting a membrane with the same composition of the hot pressed membrane (2:1:2) also presented lower proton conductivity than Nafion. However, when the ratio of Nafion was reduced, the casting membrane presented higher or equivalent proton conductivity to Nafion and a Nafion bilayer. Unlike HP, in casting methods, the adhesion between the layers occurs before the polymer annealing, facilitating the adhesion between the layers and, consequently, reducing the interface challenges. As such, $[N_c/N_c]_c$ presented higher proton conductivity and general properties than the equivalent hot pressed. Another challenge in the HP that was not present in the cast membranes was that in the HP it was difficult to reduce the thickness of Nafion layers and, then, work with the ratio 1:1:1.5. This occurred because to hot press the membranes, each layer is handled separately, while in casting only the final membrane is handled.

With the success of the cast membranes with respect to the properties discussed here, only these were submitted to single cell test. Between all multilayer membranes, $[N_c/SPInd_c/N_c]_c$ 1:1:1.5 was highlighted as the best performing. The fuel cell tested confirmed this affirmation and this membrane showed a higher performance than Nafion at low RHs at all temperatures, though not at high RH. Therefore, $[N_c/SPInd_c/N_c]_c$ 1:1:1.5 is a good membrane for start-up to use in low humidity PEFC between 80 to 120 °C. If the problems of

mass transport hydration can be overcome, the $[N_c/SPInd_c/N_c]_c$ 1:1:1.5 could display excellent properties over all conditions.

CHAPTER VI – THE INFLUENCE OF GO ON THE MEMBRANE PERFORMANCE

Graphene oxide (GO), also known as graphite oxide, is drawing attention from the scientific community around the world since the identification of single layers of graphene by Novoselov, Geim and co-workers [226]. GO is a single layer of graphite which can be produced by different methods. In this study it was prepared by a modified Hummer's method [93, 159] as explained in Chapter III. The extraordinarily high strength compared with its light weight has led GO to be integrated into polymer composites [227, 228]. Graphene is an excellent electron conductor and for this reason has been used in electronic devices [229, 230]. On the other hand, GO, due to the oxygen groups, is an electronic insulator. GO is stable at high temperature and the carboxyl groups give it hydrophilic properties.

Unlike the membranes with SPInd from the previous chapter, the dispersion and interaction between GO and Nafion is not as effective as between SPInd and Nafion. SPInd and Nafion are both organic materials with polar characteristics. In contrast, GO is an inorganic nanomaterial which has a tendency to agglomerate, interfering with the homogeneous spreading on a substrate.

In this chapter are presented the main results for GO membranes prepared by hot pressing and casting. Their performance will be discussed based on the evaluation of properties, such as water uptake, IEC, and conductivity.

6.1 Hot pressed membranes

The GO content in the membrane can act as a water catcher at intermediate conditions and as gas barrier. GO has been dispersed in Nafion polymers and used as a loading in composite membranes to provide mechanical structure [199], water retention, and self-humidifying properties when functionalized with Pt [107]. Composites with Nafion were not the only attempts to use GO in PEFCs. Xue *et al.* [162] applied GO in polybenzimidazole (PBI) membranes. Therefore, Nafion would not be a limitation to the temperature, since both PBI and GO can operate at high temperatures such as 160 °C. Functionalized GO, especially with sulphonic groups, in polymer matrix such as poly(ether ether ketone) [231, 232], or Nafion [233, 234] is another approach to composite membranes. The functionalized groups can also act as water catcher and, consequently, proton transporter.

Despite GO has been used more as a loading in composite membranes for PEFCs, there were some attempts to use GO as a film for such applications. Gao *et al.* [131] prepared a membrane by hot pressing Nafion/GO/Nafion, where GO was a film, either ozonated or not. As such, the authors compared the effect of GO film ozonation in PEFC. In these films, external Nafion layers were Nafion 212, and they were only used to prevent GO coming in contact with the hydrogen flow. Unlike commercial PEFC, Gao *et al.* only tested the membranes at 35 °C, which is extremely low for commercial applications. In their study, the ozonated GO showed a higher performance than GO. However, there was no comparison with Nafion, since the aim was to evaluate the effect of ozonation and not to develop a higher performing PEFC. Paneri *et al.* [235] developed a sandwich design Nafion/GO/Nafion for a direct methanol fuel cell (DMFC), where GO was a thin film produced by a vacuum

assisted filtration system. GO was selected to reduce the methanol crossover. In their study, Nafion was used as a binder between the GO film and the electrode ink. Therefore, Nafion 211 (25 μm thick) was used as external layers. Nafion as external layer provides mechanical structure to GO layer and increases the proton conductivity due to the activate site of sulphonic groups. The DMFC performance was higher for the multilayer membrane than for a Nafion single layer.

Following Panieri's report, in this present study, a systematic study of a three layer membrane similar to Paneri's configuration was carried out, but for a PEFC with hydrogen as fuel. However, the external layers were cast Nafion membranes and in the inner layer of GO film, Nafion polymer was added to achieve better adherence with the external layers. This membrane was hot-pressed (HP) together and prepared as discussed in Chapter IV. The optimized membranes were evaluated with respect to proton conductivity at low and high temperature in the complete range of humidities (20 -100%).

6.1.1. Structural analysis

The formation of a three-layer structure is proved in images Figure 6.1(a) and (b), which represent $[\text{N}_\text{C}/\text{GO}-20\text{N}_\text{F}/\text{N}_\text{C}]_{\text{HP}}$ and $[\text{N}_\text{C}/\text{GO}_\text{F}/\text{N}_\text{C}]_{\text{HP}}$, respectively. In the $[\text{N}_\text{C}/\text{GO}-20\text{N}_\text{F}/\text{N}_\text{C}]_{\text{HP}}$ image, the compacted GO film in the inner layer is revealed. Although it is not possible to visualise Nafion in the inner layer, its presence was confirmed as explained in Chapter IV.

GO fragments migrated to the Nafion external layers during hot pressing assembly. Those fragments and migration were aggravated by the fragmented GO film formation during filtration. After HP, the surface of the internal GO layer became less homogenous with spikes along all the length. From the image of $[\text{N}_\text{C}/\text{GO}_\text{F}/\text{N}_\text{C}]_{\text{HP}}$, the GO inner layer thickness can be

measured as approximately 6.5 μm . The thickness of the GO film before hot pressing and after filtration (and after the drying step) was 9 μm , showing a contraction of 27.8%. The contraction is due to the elimination of water and interlayer space during the hot pressing, consequently, compacting the GO film.

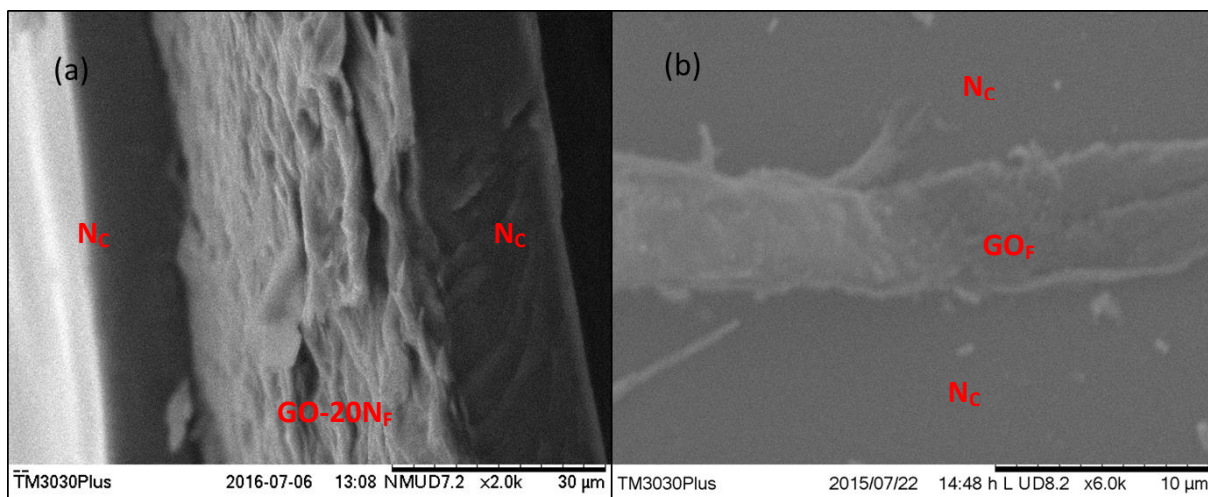


Figure 6.1: SEM images of the cross-section of (a) $[\text{N}_c/\text{GO-20N}_f/\text{N}_c]_{\text{HP}}$ and (b) $[\text{N}_c/\text{GO}_f/\text{N}_c]_{\text{HP}}$ membranes.

6.1.2. Water uptake and ion exchange capacity

Water uptake (WU) and Ion Exchange Capacity (IEC) are important properties to characterise a membrane as proton exchange membrane due to the influence of water on the proton transport [129, 236, 237]. The mechanisms of proton transport hopping and Grotthuss are water dependant. Thus, in PEFCs, water content has an important role. Both tests were carried out as described in the previous chapter in the section 5.1.2 and details of the experimental protocols are in the Appendix.

GO multilayer membranes presented higher water uptake than Nafion single layers or Nafion bilayer membranes, as shown of Figure 5.2. The WU for Nafion membranes were

similar, even for the bilayers. $[N_{211}/N_{211}]_{HP}$ and $[N_C/N_C]_{HP}$ did not demonstrate any difference in the behaviour with WU values of $(18.53 \pm 0.87)\%$ and $(17.79 \pm 0.88)\%$ respectively. The interaction between Nafion layers in the bilayer membrane, therefore, was enough to seal the membrane and did not allow water to stagnate at the interface. If interface interaction and adherence between the layers was poor, a gap would appear and an amount of water would be held, considerably increasing the WU. The WU values for N212 and N_C were $(17.91 \pm 2.25)\%$ and $(20.85 \pm 0.77)\%$ respectively, comparable with the bilayers. In the bilayers, the materials involved, i.e. cast Nafion and Nafion 211, are chemically equivalent. Thereby, any difference in the WU is related to the single layer manufacturing process, which cannot be noticed. As detailed in Chapter IV, Nafion has adherence to itself and good interaction, minimising the effects of the interface.

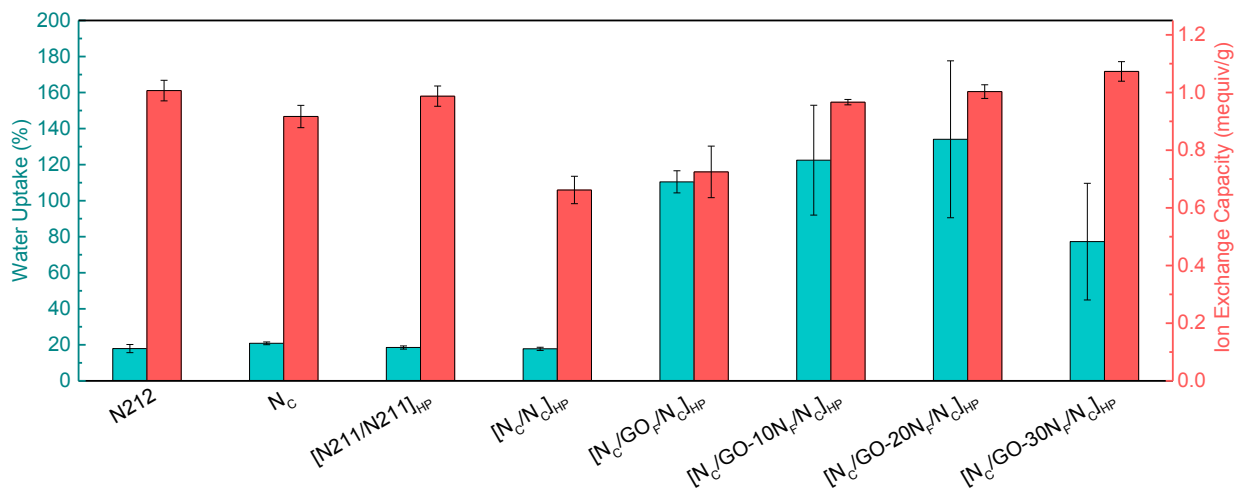


Figure 6.2: Multilayer membrane water uptake (left bar) and IEC (right bar) plots.

The small fragments of GO formed in the film filtration stage are influential on the GO film WU. GO shows a duality in its water attraction behaviour, where there is COOH and other oxygen groups it is hydrophilic. In the aromatic structure the predominance of C=C and C-C bonds leads to a hydrophilic structure [238]. Accordingly, with the smaller flakes of GO

sheets, the GO surface is larger, increasing the water uptake of the GO hot pressing membranes series. The poor interface between GO/Nafion is highly responsible for the high WU. As can be seen in the Figure 6.3(a) and (b), the membrane after soaked in water showed some bubbles in the interface, swelling the membrane. Besides swelling, the inner GO film cracked. However, these effects were observed to be more intense in $[N_C/GO_F/N_C]_{HP}$ and $[N_C/GO-10N_F/N_C]_{HP}$. When the content of Nafion increased to 20%, there was no cracking or swelling. Meanwhile, in $[N_C/GO-30N_F/N_C]_{HP}$, cracking and swelling reappeared, but in much lower intensity. In the extreme case, of long hours exposed to water (more than 72 h, for 0, 10 and 30% of Nafion), the GO inner layer partially dissolved in the water trapped between the Nafion layers. However, apparently the GO does not leak from the membrane and is kept in place as inner layer by the two external Nafion membranes. GO bonds with water, forming bigger structures [93], which are large enough to not penetrate the interface spacing, while water alone can penetrate those spaces. Finally, for applications in constant humidification, as PEFC, $[N_C/GO-20N_F/N_C]_{HP}$ shows to be the best suitable GO multilayer membrane.

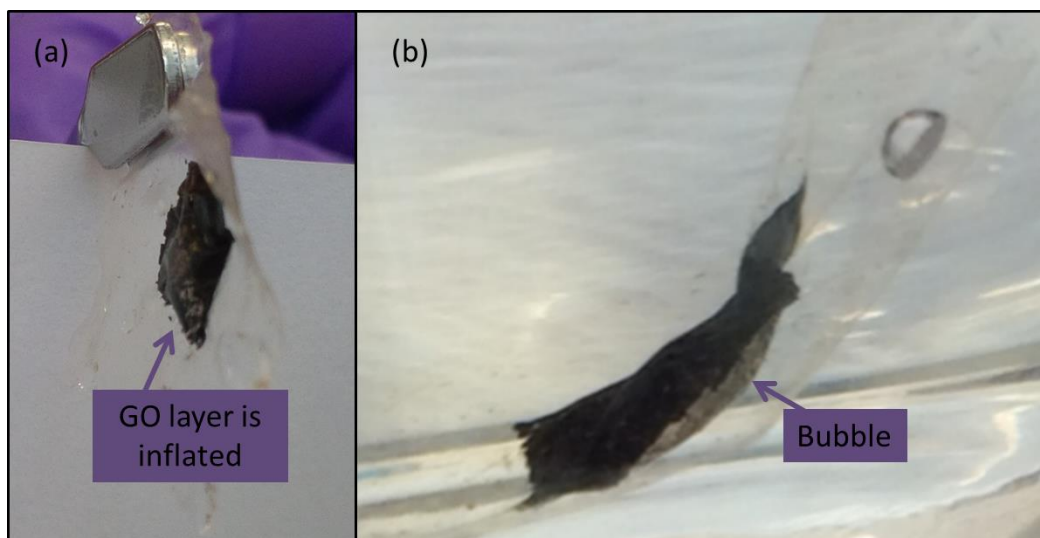


Figure 6.3: $[N_C/GO_F/N_C]_{HP}$ soaked in water to emphasize the formation of bubbles and swelling.

On the other hand, the IEC of $[N211/N211]_{HP}$ and $[N_C/N_C]_{HP}$ (Fig. 6.2) showed differences. The IEC for the bilayers $[N211/N211]_{HP}$ and $[N_C/N_C]_{HP}$ are 0.99 ± 0.03 and 0.66 ± 0.05 mequiv/g, while for the single layers N212 and N_C it is 1.01 ± 0.03 and 0.92 ± 0.04 mequiv/g, respectively. The significant difference between the bilayer membranes shows that for the commercial membranes N211 and N212, the interface and hot pressing process does not affect the IEC. However, for the cast membranes, those parameters considerably affect the IEC. The surface of a N_C single layer differs from the surface of N211. An in-lab membrane does not have the smooth surface of a commercial membrane. The hot pressing is affected by this roughness. Even though there is no significant gap to allow trapped water at the interface, some space is existent due to the roughness. Proton transport from one to the other layer is hampered by those spaces.

The IEC for the $[N_C/GO-xN_F/N_C]_{HP}$ membranes increased with the content of Nafion as expected. The tests were held at room temperature, in such case, Nafion is an excellent proton conductor. The IEC found for the membranes $[N_C/GO_F/N_C]_{HP}$, $[N_C/GO-10N_F/NC]_{HP}$, $[N_C/GO-20N_F/N_C]_{HP}$ and $[N_C/GO-30N_F/N_C]_{HP}$ were 0.725 ± 0.089 , 0.967 ± 0.009 , 1.003 ± 0.023 and 1.073 ± 0.034 mequiv/g, respectively. In the GO nanosheet films, nanocapillaries are formed [235], which allows water pathways, and, consequently, proton pathways. Therefore, it is expected that due to the high water retention of GO membranes, the negative influence of the interface on the IEC can be suppressed. This factor is highlighted when Nafion is added in the inner layer because the adherence in those membranes is higher than with GO alone.

6.1.3. Proton conductivity

Before a proton conductivity test is performed, membranes usually are activated as described in Chapter IV. However, HP GO membranes were not successfully activated. Figures 6.4(a) and (b) display the $[N_C/GO-20N_F/N_C]_{HP}$ membrane before and after activation, respectively. The GO inner layer cracked and delaminated from the Nafion external layers due to the poor interlayer adhesion. This membrane was the sample that suffered least damage to its structure. In the other $[N_C/GO-xN_F/N_C]_{HP}$ membranes, the GO inner layer disintegrated completely becoming a suspension and not a film any longer. Thus, it is confirmed that $[N_C/GO-20N_F/N_C]_{HP}$ membranes demonstrated the best interface between GO membranes. In the activation process, besides water that already affected the membrane structure as explained in the previous section, there was the presence of sulphuric acid. The acid is strongly aggressive and polar, affecting the GO layer. Therefore, $[N_C/GO-xN_F/N_C]_{HP}$ membranes could not be activated. The following tests of proton conductivity and single cell were carried out without activation. To evaluate these membranes in a fair manner, Nafion membranes were also tested without any activation. However, individual layers of Nafion were activated before the hot pressing step.

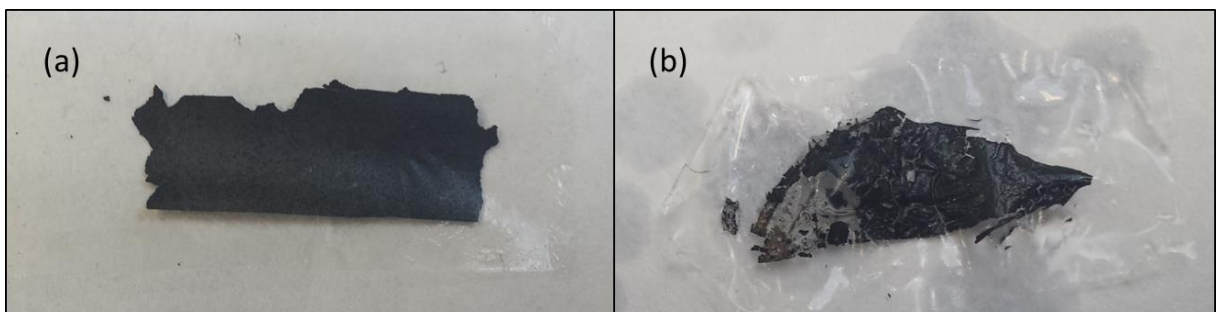


Figure 6.4: $[N_C/GO-20N_F/N_C]_{HP}$ membrane (a) before and (b) after the activation.

The cracking and swelling of the internal GO layer in the $[N_C/GO-30N_F/N_C]_{HP}$ membrane limits the applicability in the fuel cell. The resistance and conductivity depend on the membrane thickness. If a membrane swells such as the $[N_C/GO-30N_F/N_C]_{HP}$ MM, the proton conductivity is compromised. Besides, the cracking and the low integrity of the internal layer in this membrane can generate a non-homogenous performance of the membrane in the fuel cell. As a result, $[N_C/GO-20N_F/N_C]_{HP}$ was chosen to be tested in the fuel cell due to the stability of its internal layer in the presence of water.

To evaluate the applicability of $[N_C/GO-20N_F/N_C]_{HP}$ in a real system of IT-PEFC, the proton conductivity at 80, 100 and 120 °C was tested as shown in Figure 6.5. The test was carried out as described in the previous chapter in section 5.1.3. Proton conductivity was higher for $[N_{211}/N_{211}]_{HP}$ than for N_C and $[N_C/GO-20N_F/N_C]_{HP}$ for relative humidity 60% or higher. At low humidity (<60%), $[N_C/GO-20N_F/N_C]_{HP}$ presented slightly higher proton conductivity than N_C , while at high humidity (>60%) it was lower. GO has a higher WU than Nafion, thus, the low humidity affects GO less. Even though water is not being supplied for the membrane in higher amounts, it attaches to GO due to the high hydrophilicity. Similar to the WU, water bonded to the GO face is difficult to remove from the membrane. Therefore, the proton conductivity does not decay as much as with Nafion. At high humidity, this phenomenon is not noted. Nafion, when confronted constantly with high humidity in the hydrogen flow, has enough sulphonic groups to catch water and transport the protons.

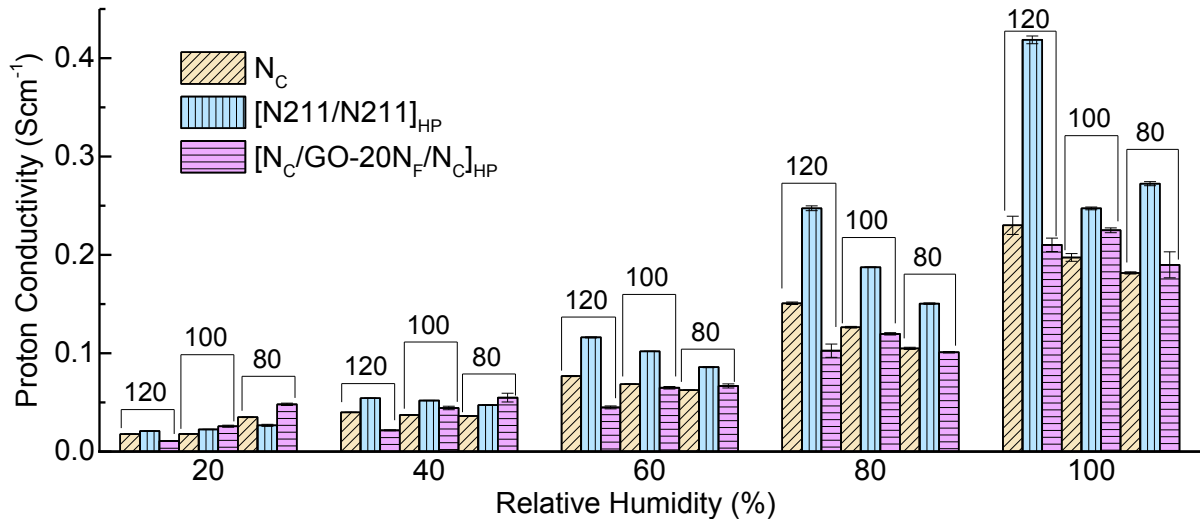


Figure 6.5: Membranes proton conductivity, where the number over the brackets represents temperature.

6.1.4. Single cell test

Single cell testing was carried out following the steps discussed in the previous chapter in section 5.2.4. The test was carried out at three temperatures 80, 100 and 120 °C shown in Figures 6.6, 6.7 and 6.8, respectively, with relative humidity (RH) of 20, 40, 60, 80 and 100%. As in the proton conductivity test, the membranes were not washed. The performance in all conditions of temperature and humidity was acceptable only for N_C . Thus, the common hot pressing for the other two membranes is not effective for membranes for PEFC applications. The interface clearly has a negative effect on the performance. The commercial Nafion 212, equivalent to 211 but thicker, has already been amply tested and has shown satisfactory performance at 80 and 100 °C. The poor performance of $[N_{211}/N_{211}]_{HP}$ can therefore only be caused by the interface. As can be observed in the three graphs, the $[N_C/GO-20N_F/N_C]_{HP}$ performance is much lower than N_C , but it is still slightly higher than $[N_{211}/N_{211}]_{HP}$ at all conditions. Thus, GO can improve the performance of a standard multilayer, but it is still not

able to suppress the effect of the interface. This improvement can be attributed to the high water uptake found in the $[N_C/GO-20N_F/N_C]_{HP}$ comparing to $[N211/N211]_{HP}$ as discussed in the previous section. The extremely high WU causes mass transport problems, which lowers the voltage at very low currents.

Although the proton conductivity is acceptable for $[N_C/GO-20N_F/N_C]_{HP}$, this value is calculated based on the stable dimensions of the membrane. Even when the system is under pressure, the water held in the membrane changes the membrane dimensions. Consequently, the proton conductivity decays relative to the original value. The real proton conductivity is lower than the proton conductivity found in Fig 6.5. Therefore, the membrane performance is poor as well. However, if refining the fabrication method produce method, such as modifying the process parameters, the membrane $[N_C/GO-20N_F/N_C]_{HP}$ might should operate with better performance than the displayed in this study.

From the results discussed above, it can be concluded that the interlayer interfaces have a negative effect on the bilayer and multilayer membranes. The adhesion between the layers was predominantly mechanical. At hot pressing conditions and with no water present, the GO film is not chemically modified to do chemical bonds with the Nafion membrane. Thus, the bonds were easily broken by the water flow, gas flow, or any kind of force. When the layers were slightly separated from each other, the pathway for the protons is interrupted. At that time, the proton conductivity and, consequently, the performance dropped.

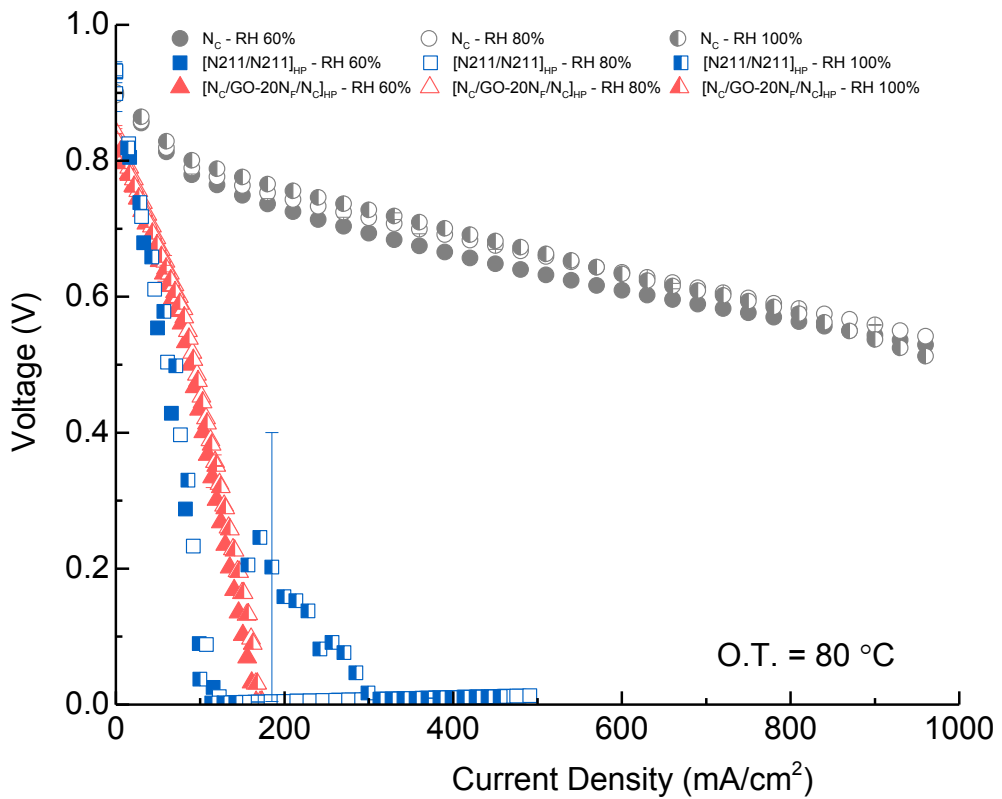
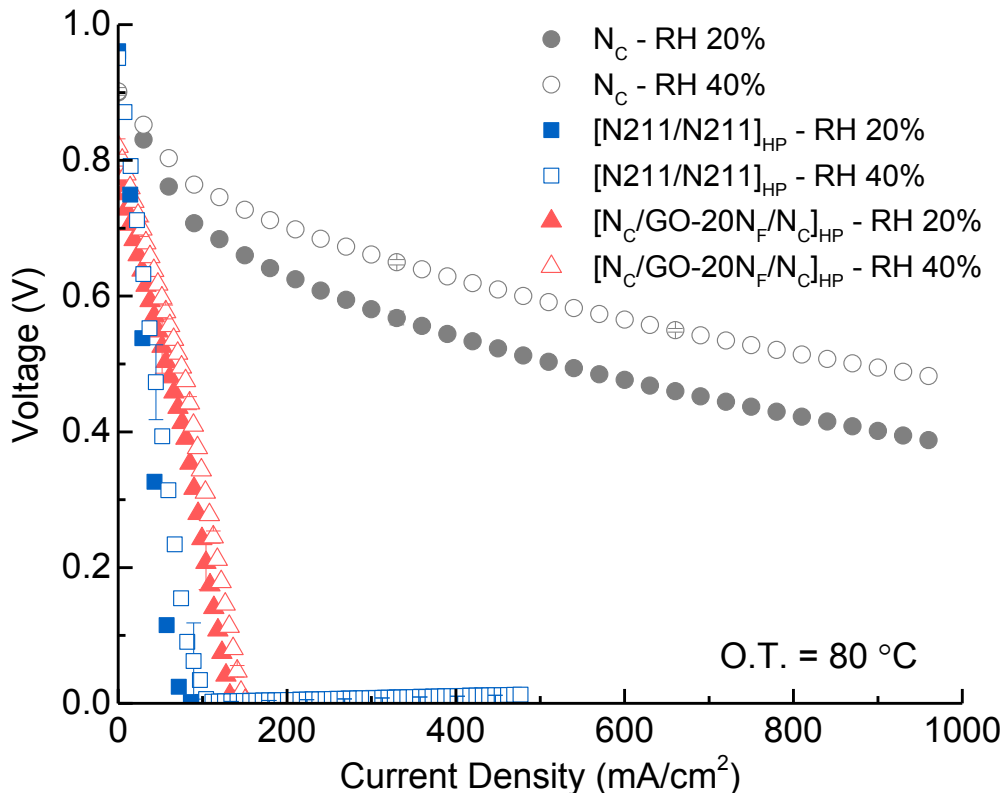


Figure 6.6: Polarization curves at 80 °C with (a) low humidity and (b) high humidity. Back pressure 0.18 MPa, H₂/Air at rate of 1 and 2.5 L/min respectively.

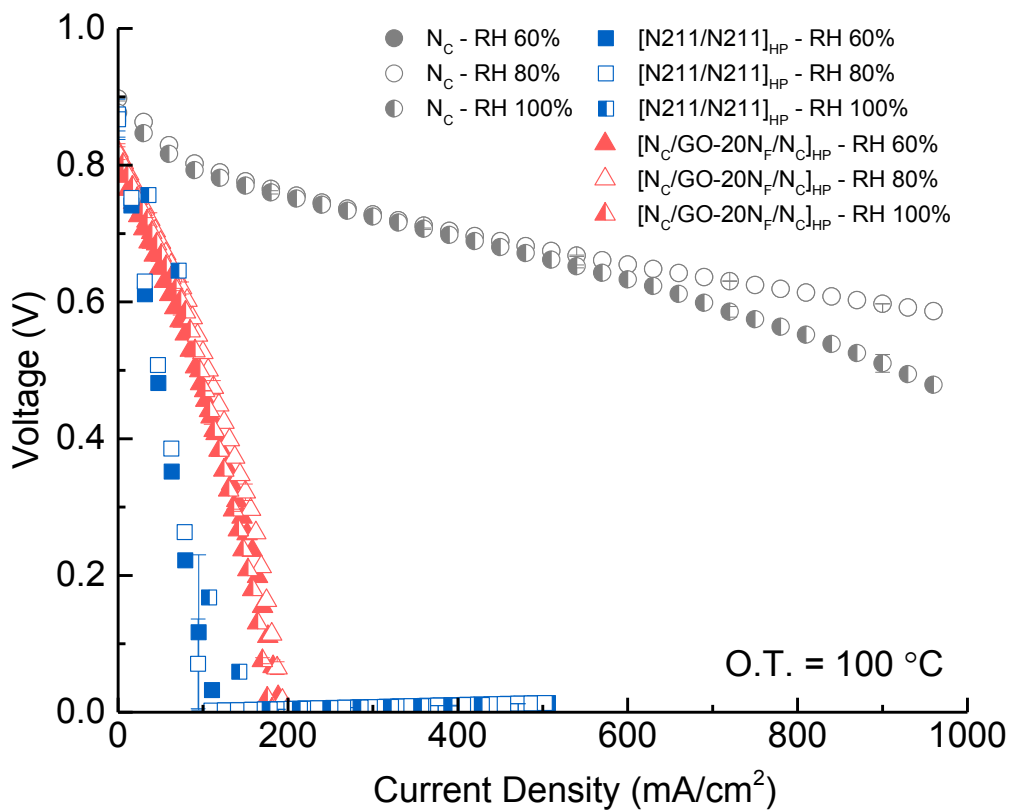
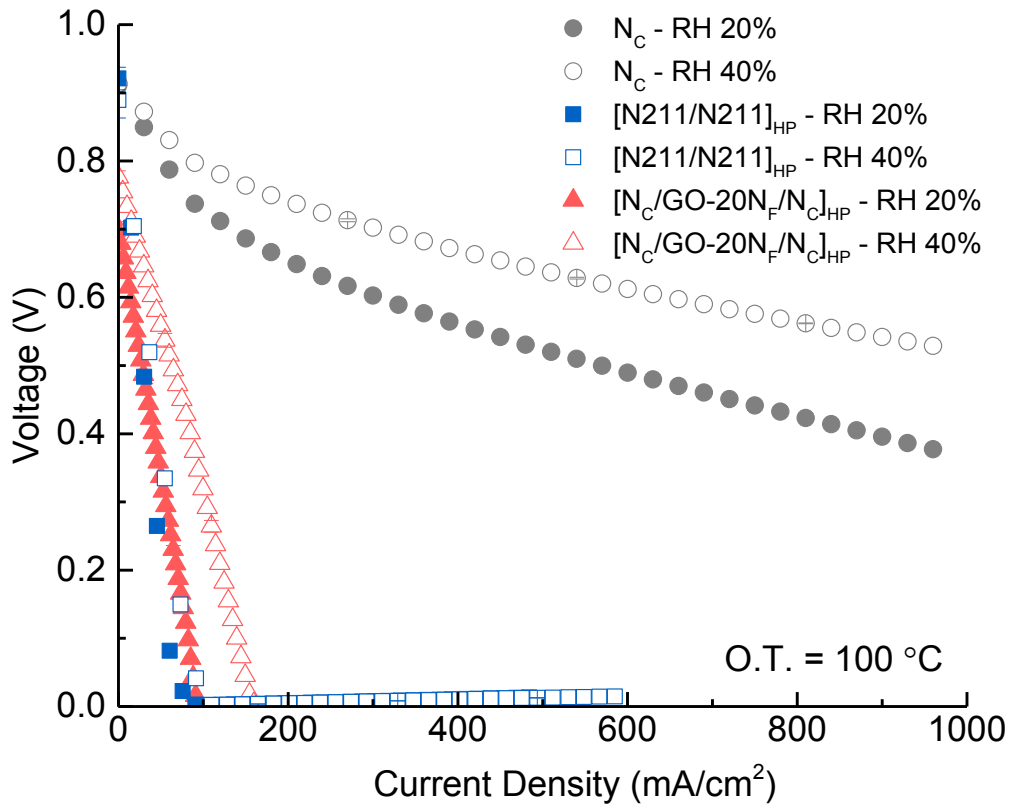


Figure 6.7: Polarization curves at 100 °C with (a) low humidity and (b) high humidity. Back pressure 0.18 MPa, H₂/Air at rate of 1 and 2.5 L/min respectively.

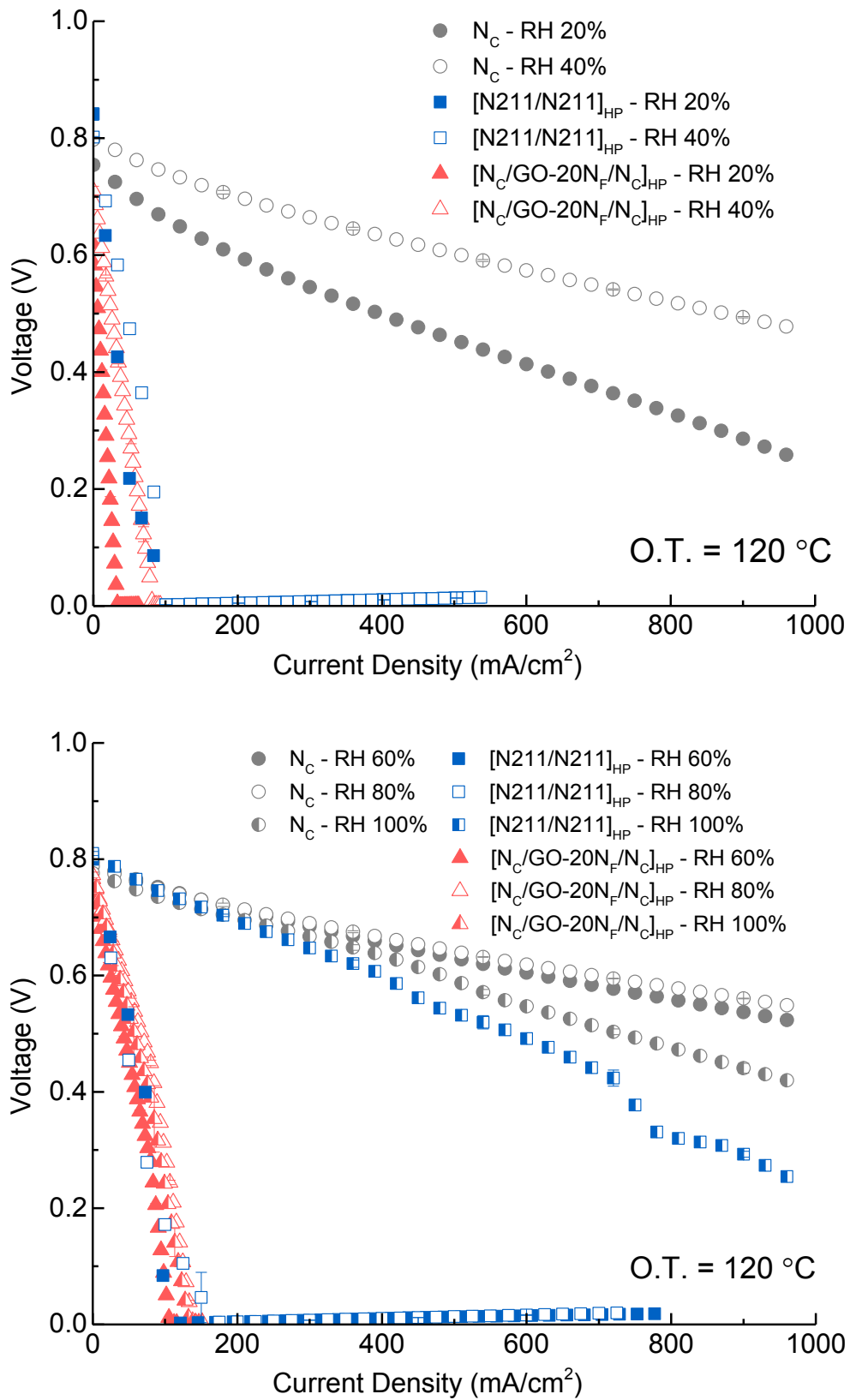


Figure 6.8: Polarization curves at 120 °C with (a) low humidity and (b) high humidity. Back pressure 0.18 MPa, H₂/Air at rate of 1 and 2.5 L/min respectively.

To analyse the interface and inner layer behaviour in $[N_C/GO-20N_F/N_C]_{HP}$, the membrane was soaked in water and freeze-cracked. Figure 6.9(a) and (b-d) show the membrane before and after soaking, respectively. Before immersing the membrane in water, the structure was homogeneous. Clearly, three layers are observed which keep the same thickness along the entire length. Liquid nitrogen did not expand the GO enough to separate the layers. In Fig. 6.9(b) water separated the layers and the GO bulged away from the compacted sheets, as is highlighted with the arrows. In Figs 6.9(c) and (d) in the interlayer interface there are vacancies left by water bubbles.

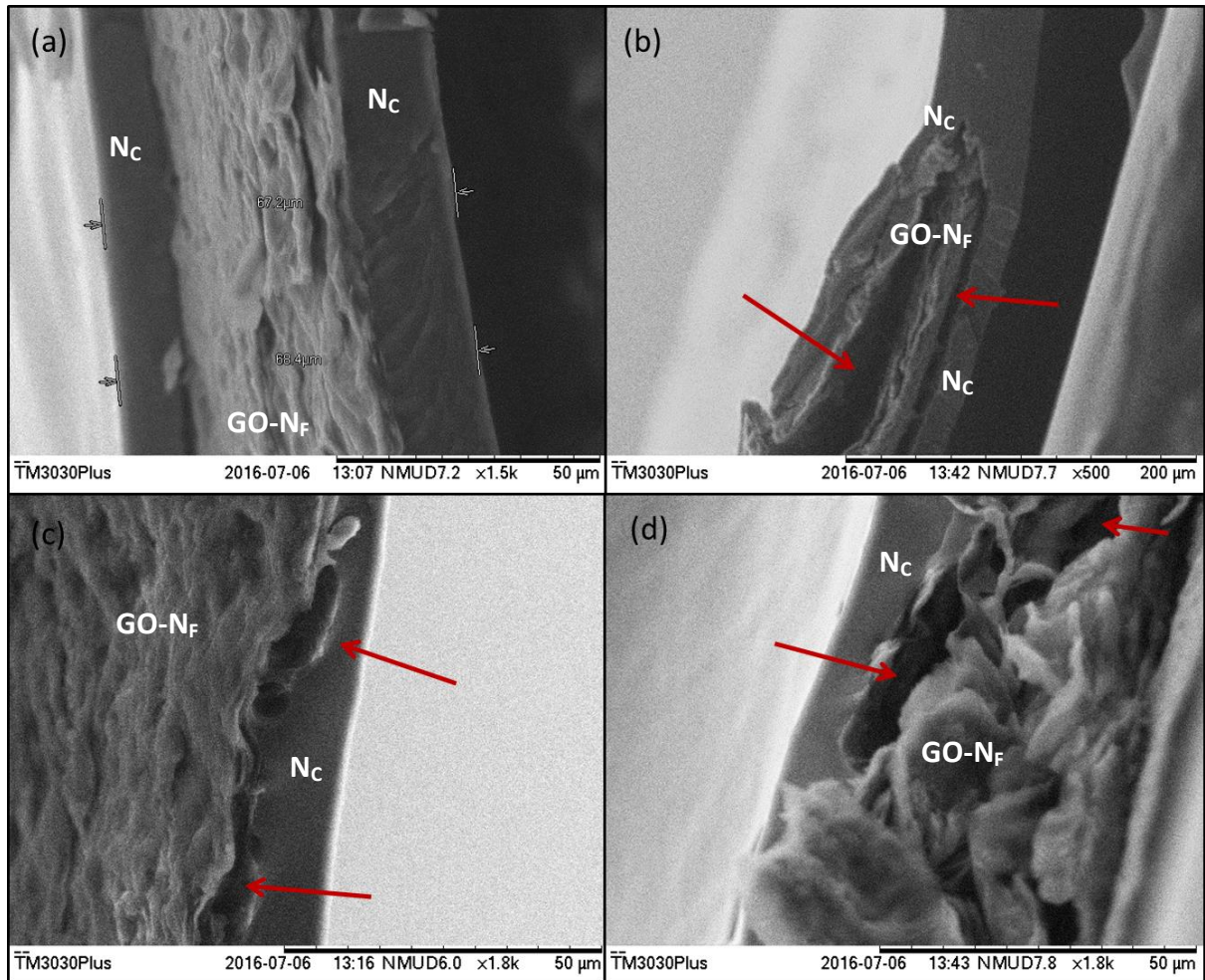


Figure 6.9: Freeze-cracked $[N_C/GO-20N_F/N_C]_{HP}$ cross-section (a) before and (b-d) after soaking in water. Arrows highlight voids and delamination due to water bubbles.

6.2. Cast membranes

The mechanical interaction between membrane layers in hot pressed membranes was stated as the main drawback. For this reason these membranes were not suitable for PEFC application. Therefore, cast membranes were prepared and characterised. The casting process permits chemical interaction between the layers, strengthening the interfaces. Thus, delamination can be avoided. This section will cover all tests carried out for cast GO membranes.

6.2.1 Structural analysis

SEM analysis of the membranes revealed the three layer structure as seen in the SEM images of Figure 6.10 (a) $[N_c/0.5GO_c/GO_c]_c$ and (b) $[N_c/2.5GO_c/GO_c]_c$. The thickness of the membrane inner layer varied between 7 and 10 μm depending on the GO content. GO solutions with lower concentrations spread more uniformly forming a homogenous layer on the bottom Nafion as compared to those with higher concentrations. The GO layer also revealed small voids similar to those reported by Lee *et al.* [139] in the silica layer in their multilayer membrane. However, these voids are not comparable with HP membranes. The size is far smaller and expected to be compacted during MEA fabrication. The packed structure of layers in GO sheets increases the path tortuosity, which is expected to decrease the fuel crossover.

The casting method resulted in membranes with smoother layer transition than with the hot pressing method. Although the difference in the layers is evident, no spaces can be observed between the layers.

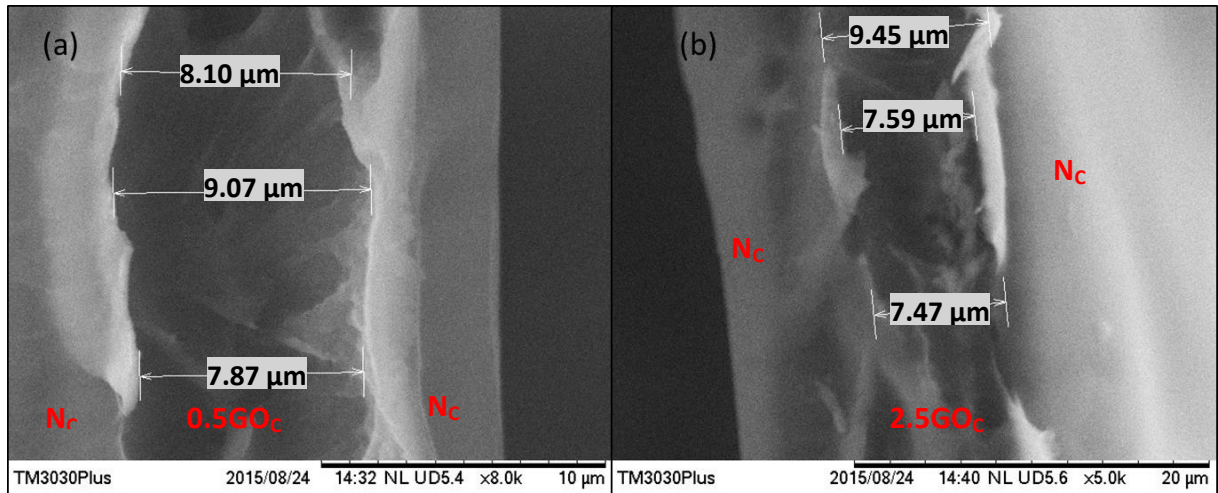


Figure 6.10: SEM image of (a) $[N_c/0.5GO_c/GO_c]_c$ and (b) $[N_c/2.5GO_c/GO_c]_c$ membranes.

6.2.2. Water uptake and ion exchange capacity

Graphene oxide is highly hydrophilic due to the high amount of oxygen groups present in the structure [93] as shown in the XPS (Chapter III). As a result, it is expected that the WU of GO based membranes is higher as compared to Nafion membranes [239-243]. All GO multilayer membranes, but for $[N_c/0.5GO_c/N_c]N_c$, showed a higher WU than Nafion (Figure 6.11, where Nafion is plotted as GO content = 0). First water uptake was reduced with 0.5 wt.% of GO, showing that low content has a negative effect on the membrane. The value of WU increased up to a medium content of GO of 2.5 w.t% (WU = 31.56%). Then, the WU decreased with the increase in GO content for 4.5 wt.% (WU = 26.79%) and increased again for the maximum WU value of 42.12% with 6.5 wt.% of GO. A similar trend was also reported by Peng *et al.* [240] who prepared single layer composite membranes of Nafion/GO-Nafion with different loadings of GO-Nafion. The authors found that independent of the GO-Nafion content, composite membranes had higher WU than recast Nafion. However, the 0.10 w.t% GO-Nafion had the highest value (~57%) in the range of 0-0.15 wt.% of loading content.

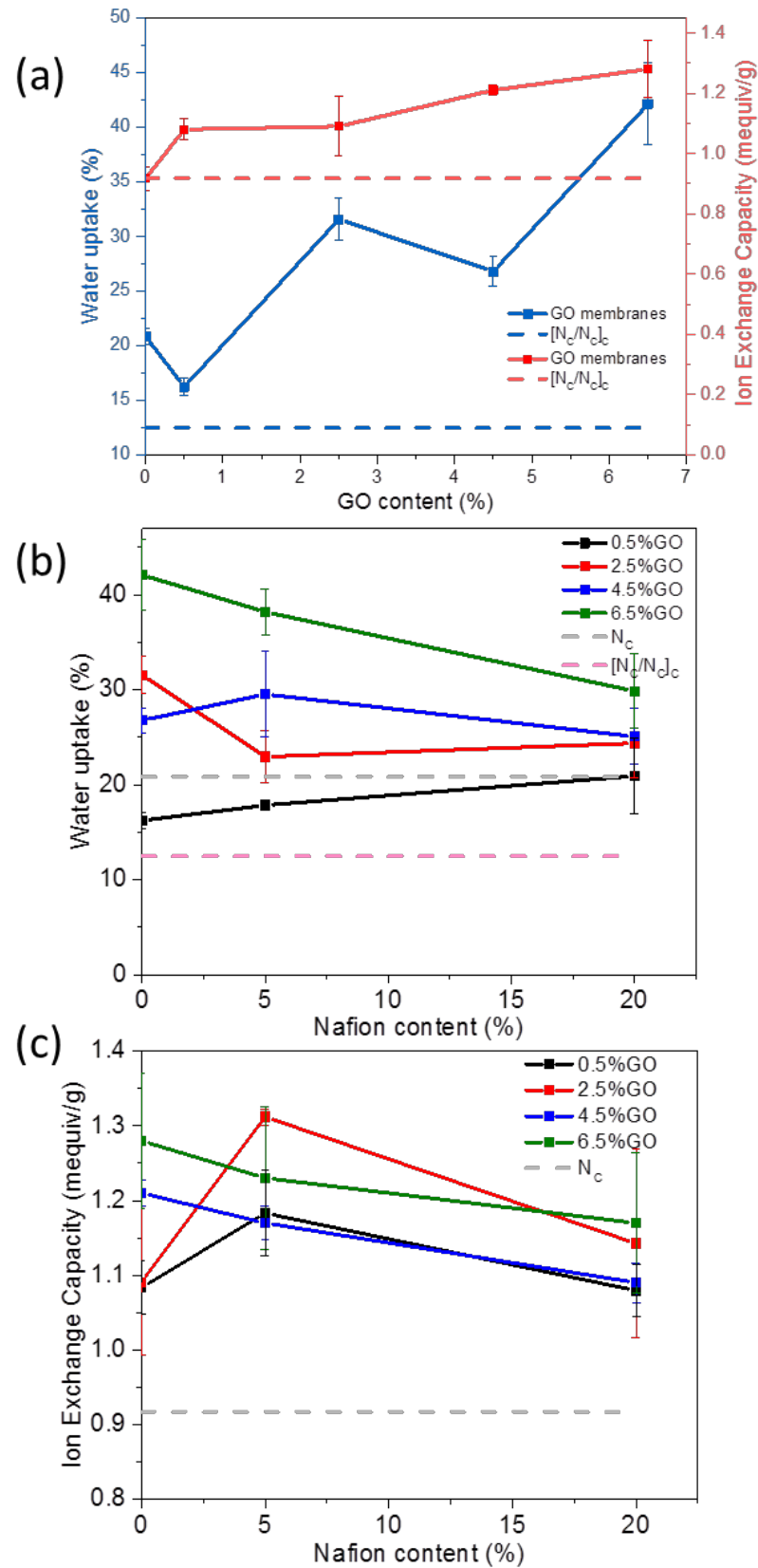


Fig 6.11: WU (blue line) and IEC (red line) with respect to GO content in the MM without Nafion in the inner GO layer. (b) WU and (c) IEC of the multilayers with respect to Nafion content in the inner GO layer.

The presence of water is essential to the proton transport, since the proton transport mechanisms, hopping and diffusion, are water dependant. However, high WU can cause severe dimensional changes in the membrane during FC operation. This can affect the membrane performance and properties, such as mechanical resistance and proton conductivity. The thicker the membrane, the higher the protonic resistance. Thus, if water content considerably increases the thickness, it reduces the proton conductivity. GO, in a single layer membrane, can minimise the loss in mechanical structure, but in the multilayer is not expected to affect the mechanical structure of the Nafion external layers. Thereby, the $[N_c/6.5GO_c/N_c]_c$ membrane that showed the highest WU can lose quality in the performance due to this thickness change.

Moreover, it is known that GO can migrate from the inner layer to the external layers during the membrane preparation and thus increase the WU [239]. This GO increases the WU of the external layer, facilitating the transport of protons from the anode to the cathode. In the current study, GO migrates more easily towards the top Nafion layer than the bottom one. When the solution to cast the top layer is poured, the solvent (water) can slightly dissolve the GO, resulting in some of this GO to be trapped in the external layer. This also helps to improve the interface. While adding the GO solution on the petri dish, the bottom Nafion is already dried so migration of GO towards the bottom layer does not occur.

When Nafion was added in the inner layer of GO, as a general trend, the WU values were found to decrease, Figure 6.11(b). The most significant reduction was observed in the $[N_c/6.5GO-20N_c/N_c]_c$ membrane where the WU value reduced from 42.12% to 29.87% when comparing to its Nafion free inner layer counterpart, $[N_c/6.5GO_c/N_c]_c$. On the other hand,

for the membranes with less GO content, $[N_c/0.5GO-20N_c/N_c]_c$, the WU loss was almost insignificant as compared with the Nafion free-inner layer (NFIL) membranes. In general, the membranes with 20 wt.% of Nafion in the inner layer had lower WU than the membranes with 5 wt.% of Nafion. i.e. higher Nafion content led to higher loss in WU as compared to NFIL membranes. This decrease in WU can be attributed to the fact that Nafion has a lower WU than GO. Thus, adding Nafion (with lower WU) in GO, a material with higher WU, reduces the overall WU.

It is also worth pointing out that since Nafion acts as a binder, it will limit the GO movement, reducing its migration from the inner to the external layers unlike that in NFIL membranes. Thus, contributing to the lower WU in the membranes with Nafion in the inner layer.

The IEC of the membranes increased with increase of GO content (Fig. 6.11(a)) reaching the values of 1.21 ± 0.02 and 1.28 ± 0.09 mequiv/g for $[N_c/4.5GO_c/N_c]_c$ and $[N_c/6.5GN_c/N_c]_c$, respectively. These results are similar to the reported values for single layer Nafion/GO membranes [105]. The IEC values of the respective membranes with Nafion in the inner layer decreased with the addition of any content of Nafion as shown in Fig. 6.11(c). Meanwhile, the IEC of the membranes with low GO content, $[N_c/0.5GO-yN_c/N_c]_c$ and $[N_c/2.5GO-yN_c/N_c]_c$, increased for $y = 5$ wt.%, followed by a decrease when $y = 20$ wt.%. The high WU of the GO membranes justified the increase in the IEC of the same membranes. Finally, as reported in Chapter V for SPInd cast membranes, Nafion single and bilayer showed the same IEC. Unlike with the WU, the IEC was not affected by the interfaces. All IEC and WU values are included in Table 6.1.

Table 6.1: Detailed values of water uptake and ion exchange capacity.

Membrane	WU (%)	IEC (mequiv/g)
N_c	20.85 ± 0.77	0.92 ± 0.039
$[N_c/N_c]_c$	12.46 ± 1.64	0.92 ± 0.039
$[N_c/0.5GO_c/N_c]_c$	16.23 ± 0.80	1.08 ± 0.036
$[N_c/0.5GO-5N_c/N_c]_c$	17.85 ± 0.53	1.18 ± 0.057
$[N_c/0.5GO-20N_c/N_c]_c$	20.92 ± 4.03	1.07 ± 0.035
$[N_c/2.5GO_c/N_c]_c$	31.56 ± 1.96	1.09 ± 0.098
$[N_c/2.5GO-5N_c/N_c]_c$	22.96 ± 2.77	1.31 ± 0.011
$[N_c/2.5GO-20N_c/N_c]_c$	21.38 ± 3.65	1.14 ± 0.126
$[N_c/4.5GO_c/N_c]_c$	26.79 ± 1.33	1.21 ± 0.017
$[N_c/4.5GO-5N_c/N_c]_c$	29.54 ± 4.49	1.17 ± 0.023
$[N_c/4.5GO-20N_c/N_c]_c$	25.08 ± 2.96	1.09 ± 0.026
$[N_c/6.5GO_c/N_c]_c$	42.12 ± 3.74	1.28 ± 0.090
$[N_c/6.5GO-5N_c/N_c]_c$	38.22 ± 2.38	1.23 ± 0.095
$[N_c/6.5GO-20N_c/N_c]_c$	29.87 ± 3.81	1.17 ± 0.094

6.2.3. Proton conductivity

Proton conductivity measurements for $[N_c/xGO_c/N_c]_c$ or NFIL membranes (i.e. $0.5 \leq x \leq 6.5$ = GO content, y = Nafion content = 0) are shown in Figure 6.12 as recorded at 80 °C (a), 100 °C (b) and 120 °C (c). At all temperatures and with all membranes, the highest proton conductivity was observed for 100% of RH. The proton conductivity depends on the humidity level [244, 245] due to the approximation of the ionic clusters caused by water. At this humidity condition (RH= 100%), proton conductivity increased as the GO content increased from 0 to 2.5 wt.% and, then, decreased dramatically. As a result, the proton conductivity values were lowest for the $[N_c/6.5GO_c/N_c]_c$ membranes. This membrane, $[N_c/6.5GO_c/N_c]_c$, recorded the highest WU and IEC values due to the high amount of GO to hold the water. The poor proton conductivity for this sample could be attributed to this high WU in the in situ proton conductivity studies which caused the membrane to flood, decreasing proton

conductivity performance. Moreover, as the membrane demonstrated high water uptake, the membrane dimensions change as the RH increased, varying the thickness. As a result, effective proton conductivity decayed.

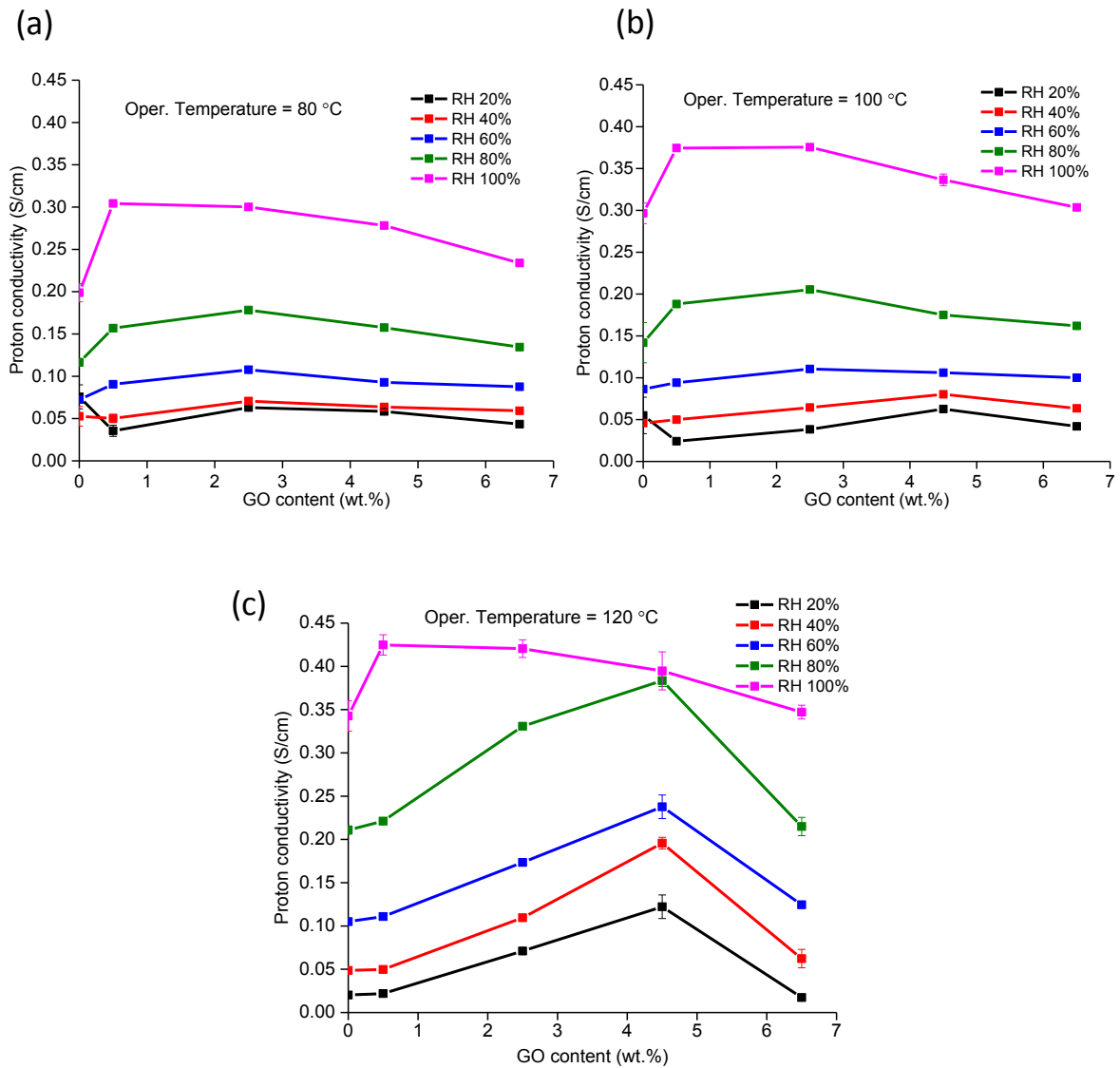


Figure 6.12: Proton conductivity curves of $[N/xGO/N]_c$ membranes varying the RH, at (a) 80 °C, (b) 100 °C and (c) 120 °C where the $x=0$ represents single layer cast Nafion membrane.

At 80 °C, with RH of 80%, $[N_c/0.5GO_c/N_c]_c$ showed a slight improvement in proton conductivity with respect to cast Nafion. For RH values $40\% \leq RH \leq 60\%$, proton conductivity was stable with the whole range of GO content. At RH=20%, proton conductivity decreased with 0.5 wt.% of GO and increased again with higher values of GO, achieving values similar to Nafion at RH of 40%. With RH of 20%, 0.5 wt.% of GO is not enough to increase the water uptake significantly to improve the proton conductivity. Thereby, the GO content cannot compensate the interface effect and the Nafion single layer showed higher proton conductivity. In comparison to the proton conductivity studies reported by Choi *et al.* [98], the membranes in this present work shows a different trend. This is because Choi *et al.* reported measurements at 25 °C, and at these conditions Nafion easily holds water and the presence of liquid water guarantees the proton conductivity. Moreover standard operating conditions for PEFC are above 75 °C. The problem of proton transport in Nafion starts at temperatures at which water starts evaporating [48, 246].

As the temperature increased to 100 °C, the proton conductivity increased for all values of GO content and for cast Nafion with RH>40%. Nafion and $[N_c/0.5GO_c/N_c]_c$ showed equivalent proton conductivity at all temperatures with RH of 40%. At this temperature with 20% of RH and this low content of GO, Nafion and $[N_c/0.5GO_c/N_c]_c$ dehydrated at a similar rate, equalizing the proton conductivity. At this temperature, all the membranes with GO did not present any significant improvement related to Nafion. The exceptions are 80 and 100% of RH for the membranes with GO content lower than 6.5 wt.%

On the other hand, Nafion showed lower proton conductivity with humidity of 20% at 120 °C. While at lower temperatures the sulphonic groups present on Nafion can hold water,

at 120 °C the interaction between those groups and water starts to weaken. Therefore, the membranes dehydrated and proton conductivity decayed. Even though, at 120 °C and any RH this phenomenon happens, with low values of humidity it is highlighted because the presence of water in the membrane is very low. In the multilayer membranes with the GO layer, Nafion external layers dehydrate as well. However, the GO layer can hold enough water to suppress Nafion dehydration and assist the proton transport. Water diffuses from GO to the external layers of Nafion. Thus the proton conductivity is kept the same or improved, depending on the content of GO.

At 120 °C, for RH below 100%, $[N_c/4.5GO_c/N_c]_c$ reached the highest proton conductivity amongst the membranes for all other humidity values, reaching the maximum value of 0.3836 Scm^{-1} with 80% RH. The observed trend for PC at 120 °C for RH = (20-80%) was $N_c \leq [N_c/6.5GO_c/N_c]_c < [N_c/0.5GO_c/N_c]_c < [N_c/2.5GO_c/N_c]_c < [N_c/4.5GO_c/N_c]_c$. However, at RH=100% the trend was $N_c \leq [N_c/6.5GO_c/N_c]_c < [N_c/4.5GO_c/N_c]_c < [N_c/2.5GO_c/N_c]_c < [N_c/0.5GO_c/N_c]_c$. Kumar *et al.* [105] in their single layer composite membranes also reported the highest proton conductivity for 4 wt.% GO membranes at all temperatures.

The presence of oxygen groups in the GO increases the water retained and the proton hopping, thus increasing the proton conductivity. Epoxy groups, which are present in the as-prepared GO (see XPS, Chapter III), are especially responsible for increasing the water uptake [247]. However, unlike composite single layer membranes, in multilayer membranes the decrease of proton conductivity after an optimum value of loading cannot be attributed to the breakdown of micellar structure of hydrophilic/hydrophobic sites [248] because GO is completely surrounded by Nafion. In the present study, the $[N_c/6.5GO_c/N_c]_c$ membrane

absorbed more water than the other GO membranes. At low temperature, water diffuses slower than at higher temperature to the Nafion external layers. Thus, with the high content of water trapped in the inner layer, this layer expands, induces delamination and, consequently, loss of proton conductivity. Therefore, $[N_c/6.5GO_c/N_c]_c$ showed this lower proton conductivity compared with the other multilayer membranes.

Compared with hot pressed membranes, the values for proton conductivity for cast membranes are higher. The interlayer interaction was stronger in the casting method. Accordingly, to force annealed membranes to interact with other annealed membranes was not as effective as interacting before annealing. Thus, it is expected that the cast membranes reveal higher performance in the single cell than the hot pressed.

Although the multilayer membranes above showed satisfactory proton conductivity, the interaction between the layers could be improved especially for the highest value of GO content (6.5 wt.%). The delamination occurred depending on how rough the environment was. Thus, the addition of Nafion in the inner layer can improve the interaction between the layers. Likewise, Padmavathi *et al.* [141] prepared multilayer membranes by casting with sulphonated polysulphone (SPSu) as external layers with silica in the inner layer, mixed with aminated polysulphone to strengthen the interface.

Proton conductivity trends for the membranes $[N_c/0.5GO-yN_c/N_c]_c$, $[N_c/2.5GO-yN_c/N_c]_c$, $[N_c/4.5GO-yN_c/N_c]_c$ and $[N_c/6.5GO-yN_c/N_c]_c$, are shown in Figure 6.13, 6.14 and 6.15. As in the NFIL membranes, it is increased proportional to the relative humidity. With the lowest level of GO (0.5 wt.%), the addition of Nafion resulted in no significant change in proton conductivity. The low content of GO leads to a membrane with a strong domain of Nafion

and the external layers can afford a high contact surface between them even without Nafion in the inner layer. All $[N_c/2.5GO-yN_c/N_c]_c$ and $[N_c/4.5GO-yN_c/N_c]_c$ membranes showed a higher proton conductivity without Nafion at 120 °C. As such, the addition of Nafion in these had a negative influence on the proton conductivity at 120 °C. While Nafion is also expected to improve interlayer interactions, it seems the water retention properties had stronger influence on the membrane behaviour at 120 °C. At lower temperatures, the values of proton conductivity were more similar between the membranes with Nafion and the NFIL. $[N_c/6.5GO-yN_c/N_c]_c$ membranes did not show any significant positive or negative influence with the addition of Nafion. The dispersion of Nafion in high content of GO, may not have been successfully done.

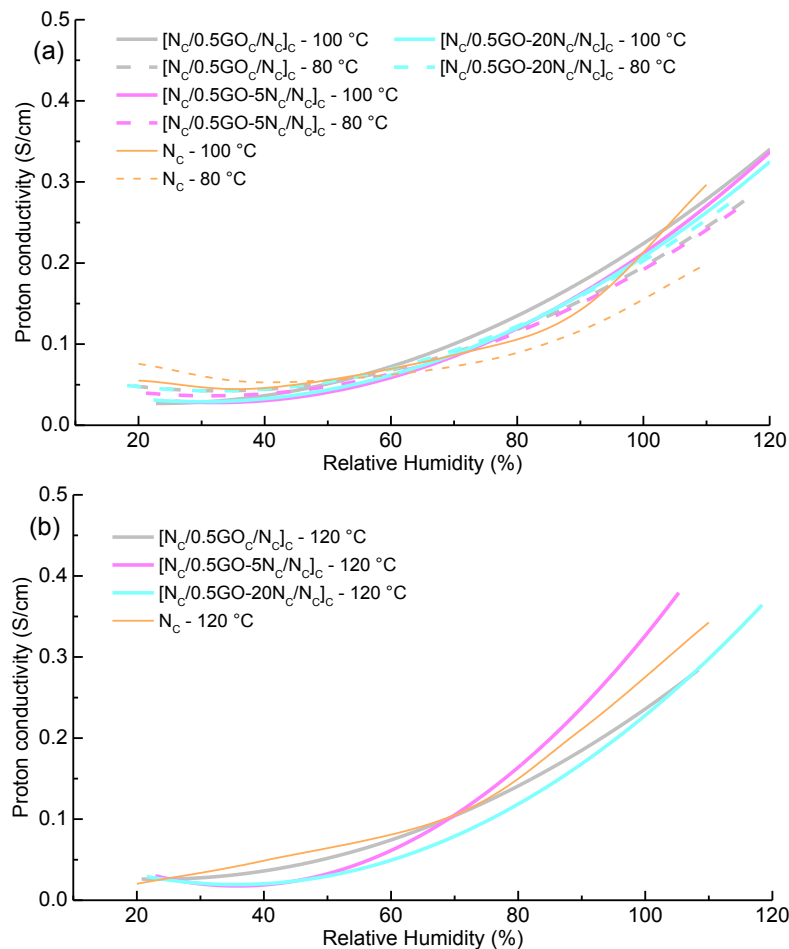


Figure 6.13: Proton conductivity of $[N_c/0.5GO-yN_c/N_c]_c$ at (a) 80 and 100 °C and (b) 120 °C.

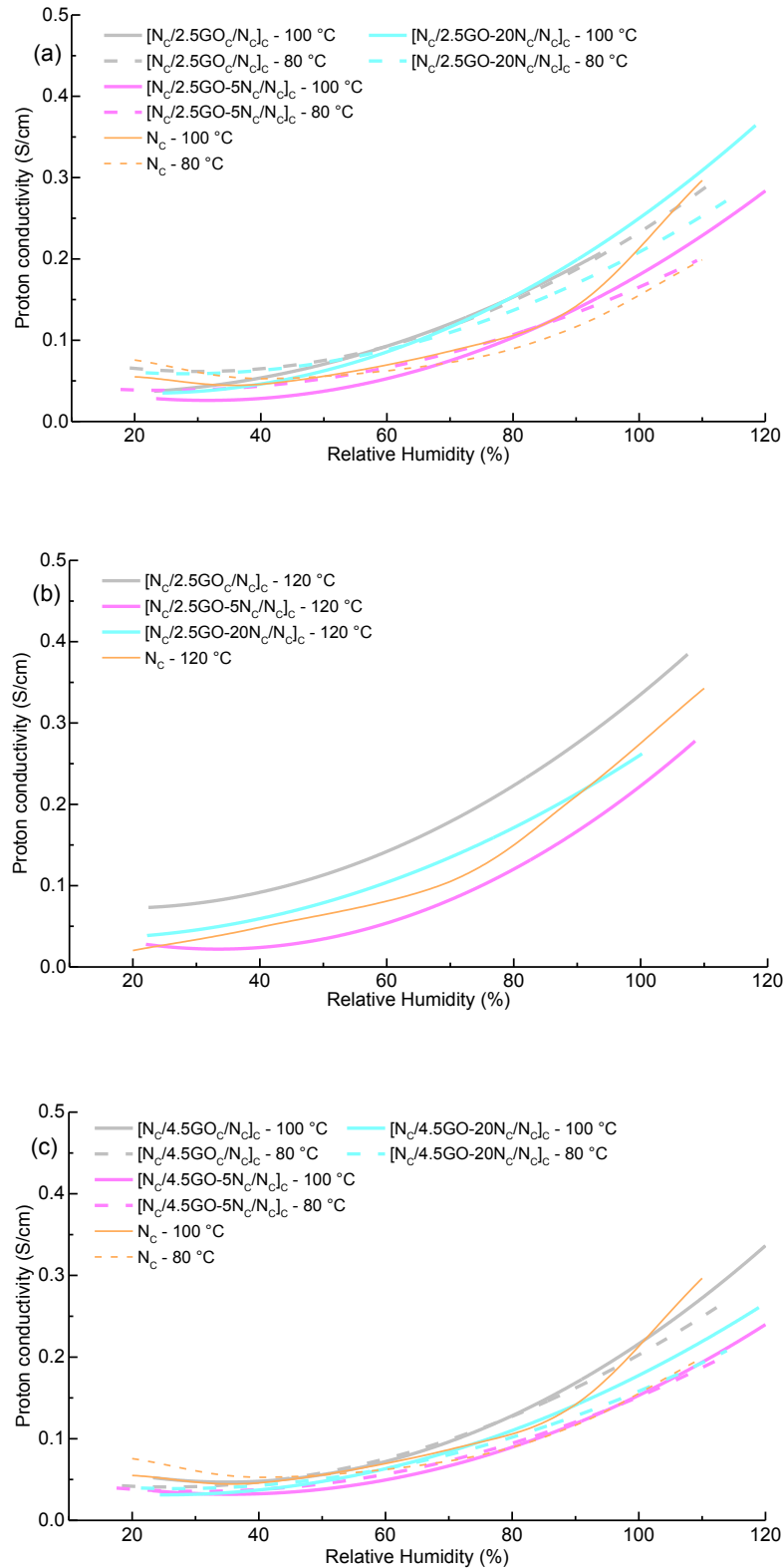


Figure 6.14: Proton conductivity of $[N_c/2.5GO-\gamma N_c/N_c]_c$ at (a) 80 and 100 °C and (b) 120 °C. (c) Proton conductivity of $[N_c/4.5GO-\gamma N_c/N_c]_c$ at 80 and 100 °C.

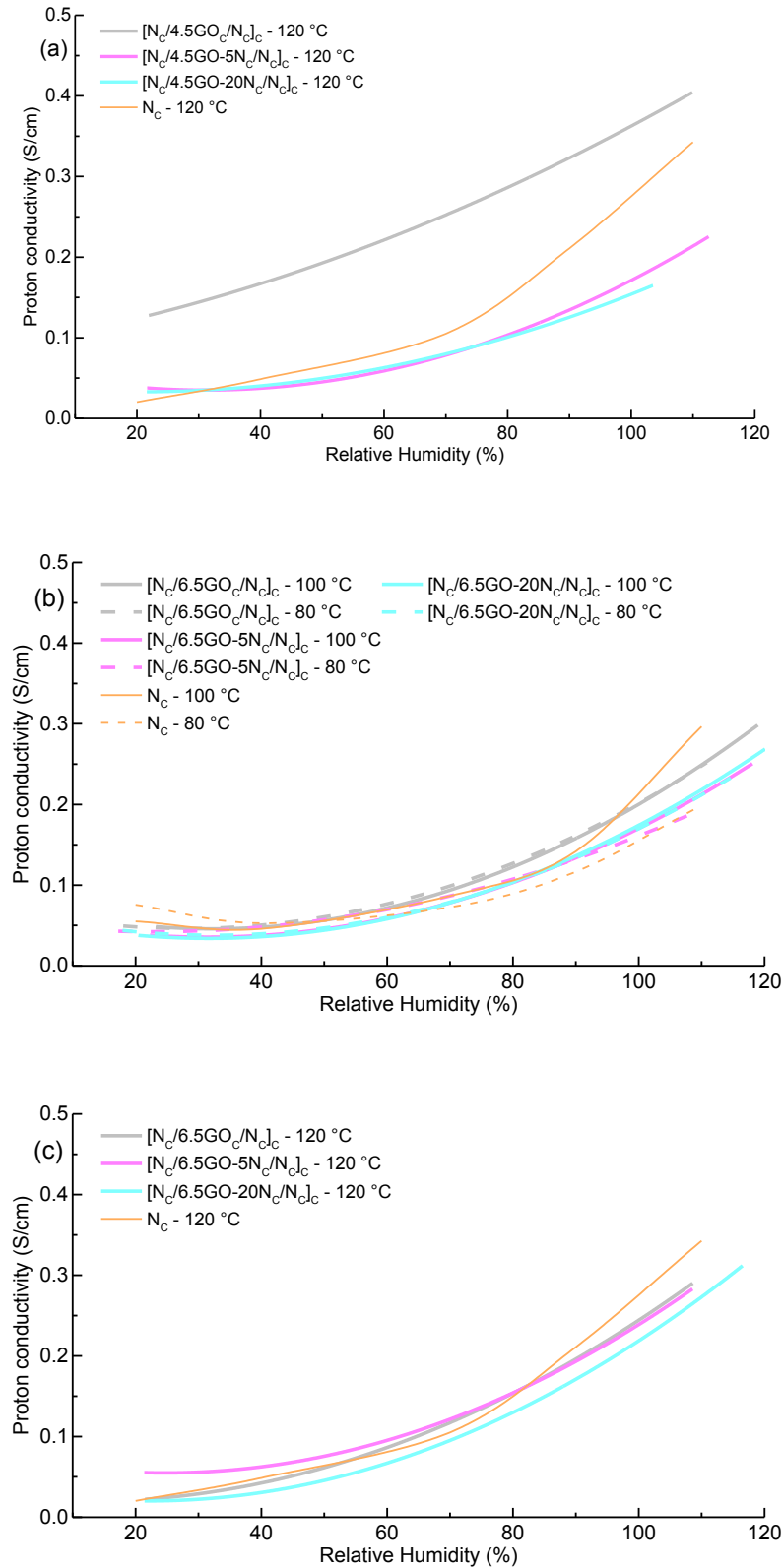


Figure 6.15: Proton conductivity of $[N_c/4.5GO-yN_c/N_c]_c$ at (a) 120 °C. Proton conductivity of $[N_c/4.5GO-yN_c/N_c]_c$ at (b) 80 and 120 °C and (c) 120 °C.

6.2.4. Single cell performance

The i-V characteristics obtained from single cell testing for NFIL membranes are presented in Figures 6.16 to 6.20, while the power curves are found in the Figures 6.21 and 6.22. At 80 and 100 °C, the Nafion bilayer $[N_c/N_c]_c$ showed better performance than various $[N_c/xGO_c/N_c]_c$ membranes at all humidities. This is expected, since Nafion has an outstanding conductivity at these conditions as water is retained. However, at intermediate temperature (120 °C), the performance of the bilayer was very poor at RH 80% and lower. The initial performance of $[N_c/N_c]_c$ was comparable with $[N_c/xGO_c/N_c]_c$ at RH equal to 60% and 80%. Nevertheless, the mass transport losses were intensified as the voltage dropped to ~ 0.6 V and current density around 370 mA/cm^2 , leading to a complete loss of voltage and failure close to 400 mA/cm^2 . At RH 40% and below, the $[N_c/N_c]_c$ membrane failed miserably. On the other hand, the $[N_c/xGO_c/N_c]_c$ membranes showed excellent performance at 120 °C for all humidities lower than 100%. This clearly highlights the role of GO in the inner layer in facilitating water retention at higher temperatures, and ensuring effective proton transport and cell performance. The lower performance of $[N_c/N_c]_c$ with respect to Nafion single layer (N_c) demonstrates the negative influence of the interface between the layers. This interface increases the ohmic resistance, making the proton transport difficult. The addition of GO in the inner layer overcomes this negative effect. In contrast, $[N_c/xGO_c/N_c]_c$ membranes only show higher performance than N_c at low currents. At high currents, N_c had the best performance, thus N_c achieved higher maximum power than $[N_c/xGO_c/N_c]_c$ membranes.

Among the $[N_c/xGO_c/N_c]_c$ membranes, while $[N_c/2.5GO_c/N_c]_c$ and $[N_c/4.5GO_c/N_c]_c$ closely compete, with $[N_c/4.5GO_c/N_c]_c$ delivering the best performance at 40% and 60% RH,

$[N_c/6.5GO_c/N_c]_c$ showed the poorest performance at all humidities at 120 °C. Interestingly, with 80% RH, $[N_c/2.5GO_c/N_c]_c$ showed a superior performance than $[N_c/4.5GO_c/N_c]_c$. This could be due to excessive water retention with higher amounts of GO. Hence at lower humidities, membranes with higher GO content are able to retain more water for longer enabling enhanced performance. As mentioned during the proton conductivity discussion, the value of 4.5 wt% GO appears to be the optimum GO content in these membranes, hence higher GO content (6.5%) leads to easy flooding and cell failure, especially at high RH values. The transfer of water from the inner layer to the external layers is limited. Consequently, the high content of water retained in samples with higher GO content ($x = 6.5$ wt.%) in the inner layer compromises the stability of the membranes and generates mass transport problems. For the membranes with lower content of GO ($x \leq 4.5$ wt.%) the water uptake is lower, thus the inner layer can keep a satisfactory humidification while transferring water to the external layers. On the other hand, the lower performance of the $[N_c/2.5GO_c/N_c]_c$ membrane compared to the $[N_c/4.5GO_c/N_c]_c$ membrane in many conditions can be explained by the insufficient water retention and the fact that GO at lower content generates a blocking effect of ionic clusters, while in higher concentration this blocking effect is overcome by the high presence of oxygen [107].

OCV values are higher for $[N_c/xGO_c/N_c]_c$ membranes than for Nafion membranes. As GO increases the membrane tortuosity, the gas crossover is reduced. In general, exceptions at few conditions, there was not observed significant difference in OCV between NFIL membranes.

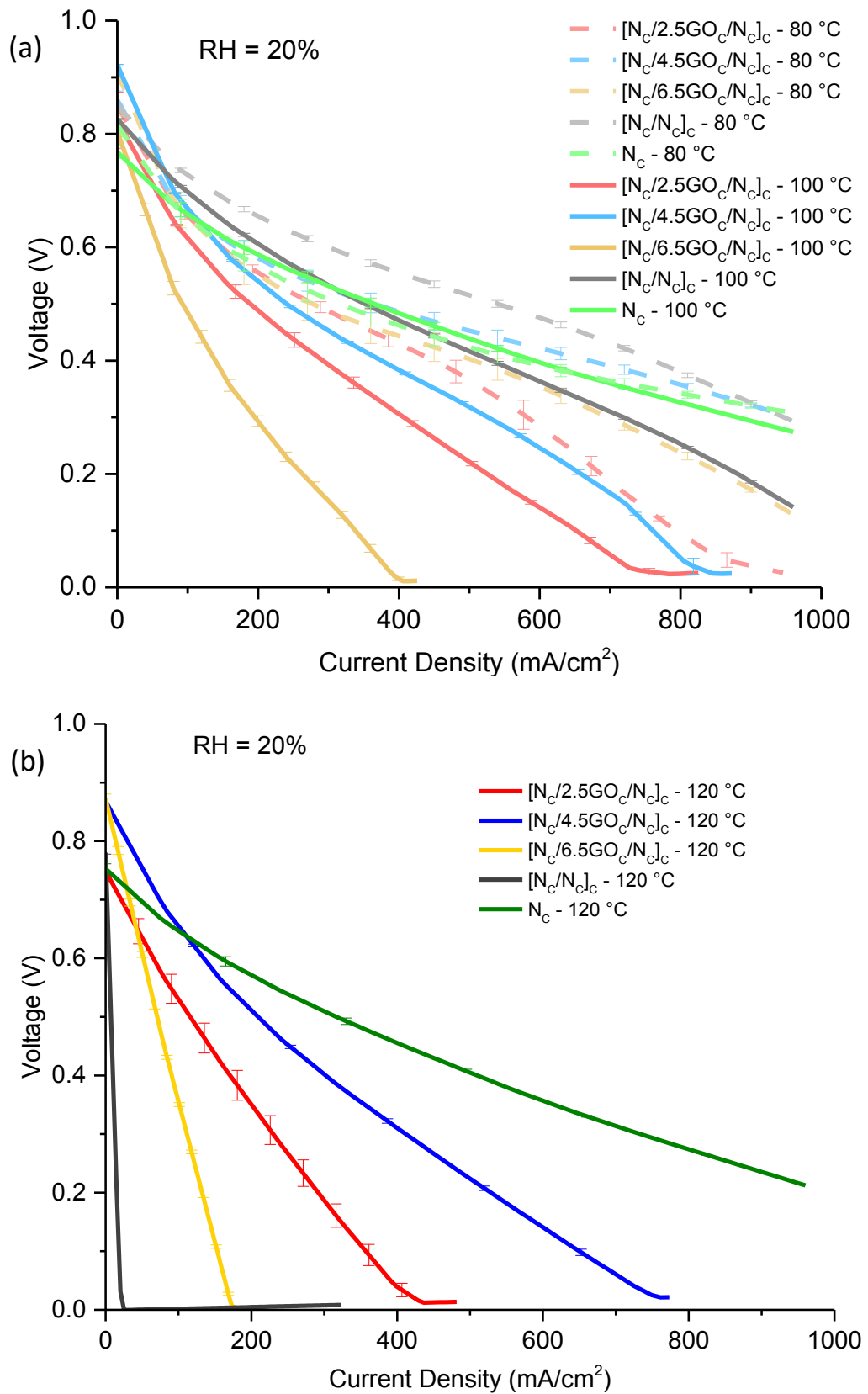


Figure 6.16: NFIL membranes polarization curves with 20% of RH at (a) 80 and 100 °C and (b) 120 °C. Back pressure 0.18 MPa, H₂/Air at rate of 1 and 2.5 L/min respectively.

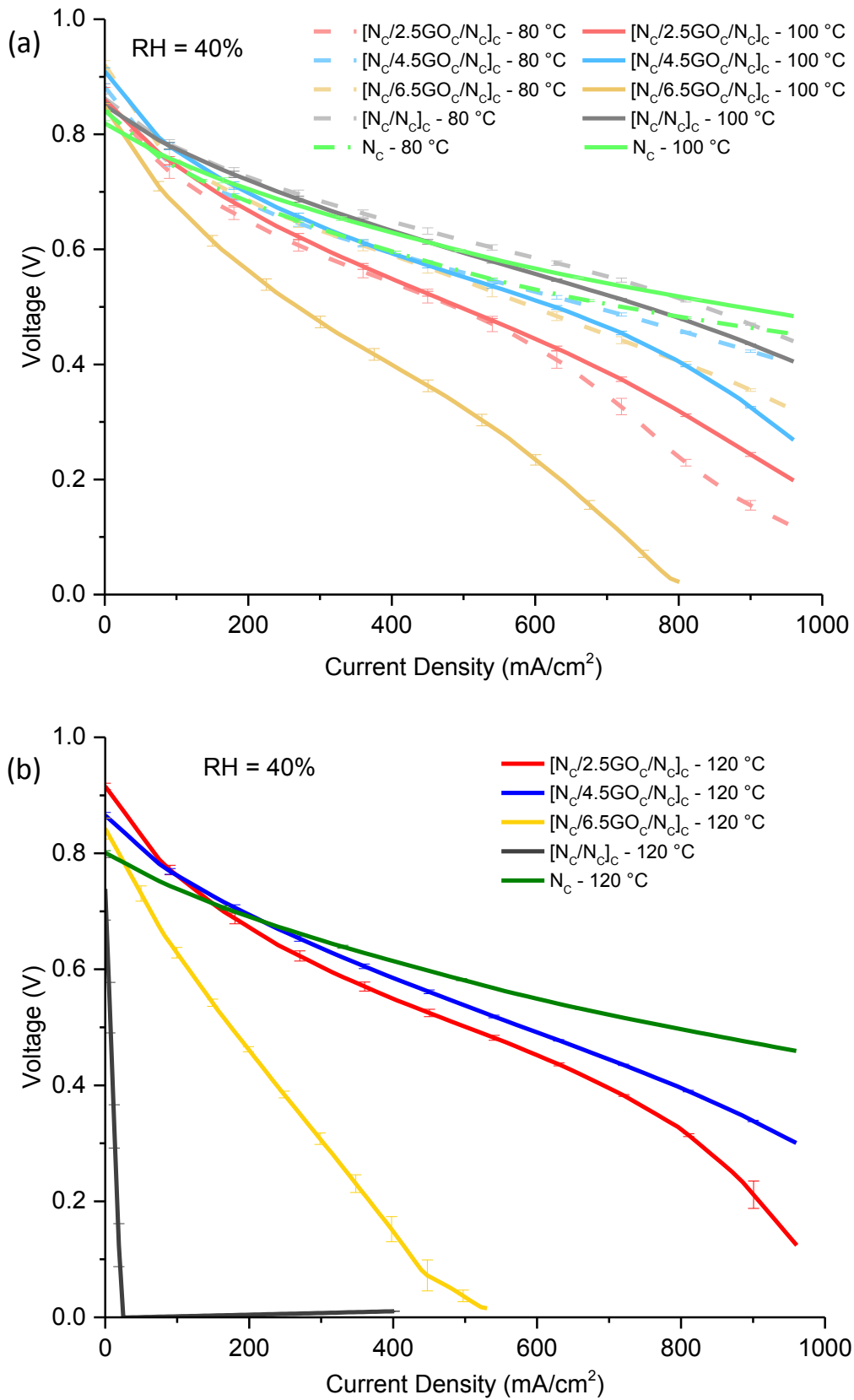


Figure 6.17: NFIL membranes polarization curves with 40% of RH at (a) 80 and 100 °C and (b) 120 °C. Back pressure 0.18 MPa, H₂/Air at rate of 1 and 2.5 L/min respectively.

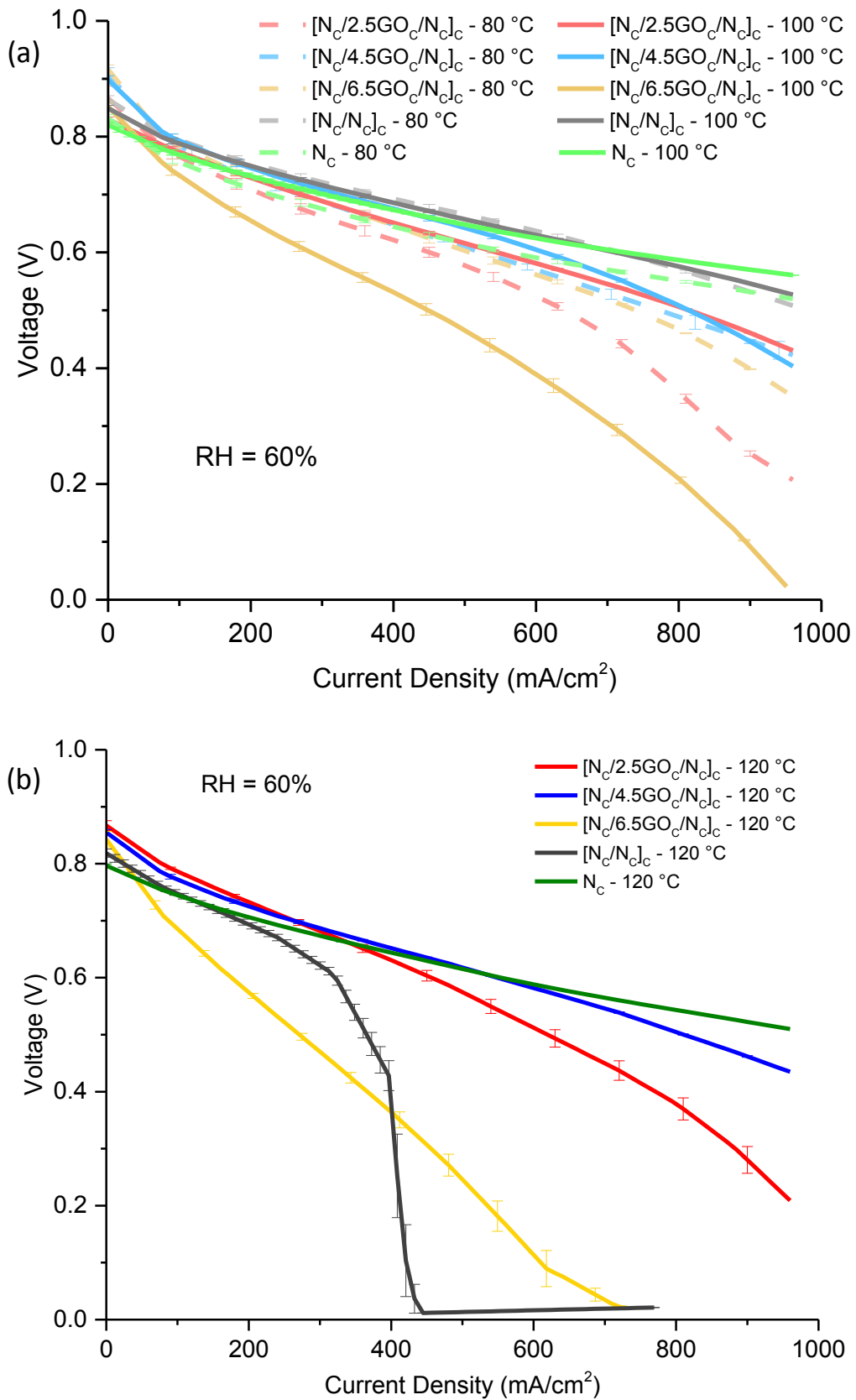


Figure 6.18: NFIL membranes polarization curves with 60% of RH at (a) 80 and 100 °C and (b) 120 °C. Back pressure 0.18 MPa, H₂/Air at rate of 1 and 2.5 L/min respectively.

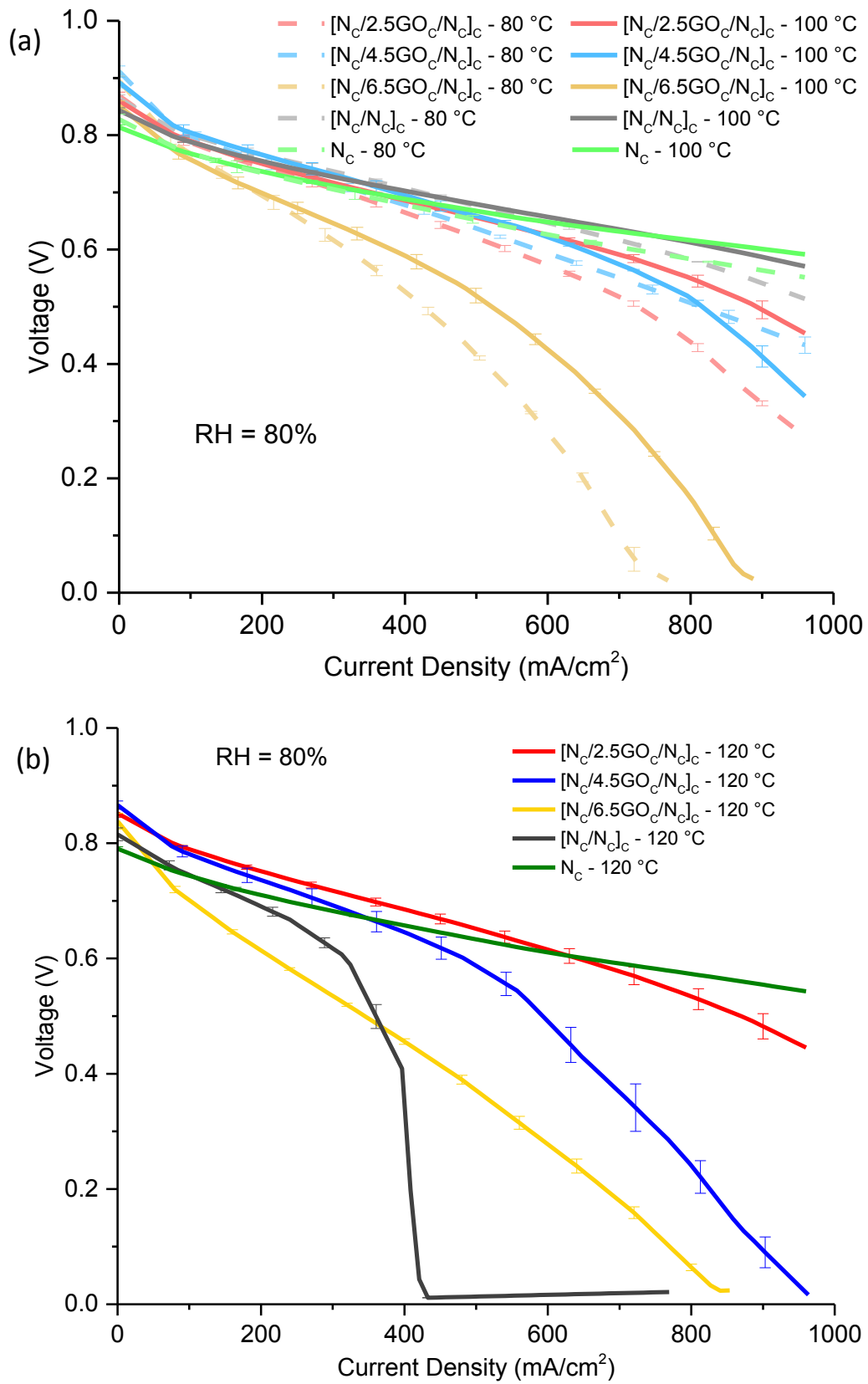


Figure 6.19: NFIL membranes polarization curves with 80% of RH at (a) 80 and 100 °C and (b) 120 °C. Back pressure 0.18 MPa, H₂/Air at rate of 1 and 2.5 L/min respectively.

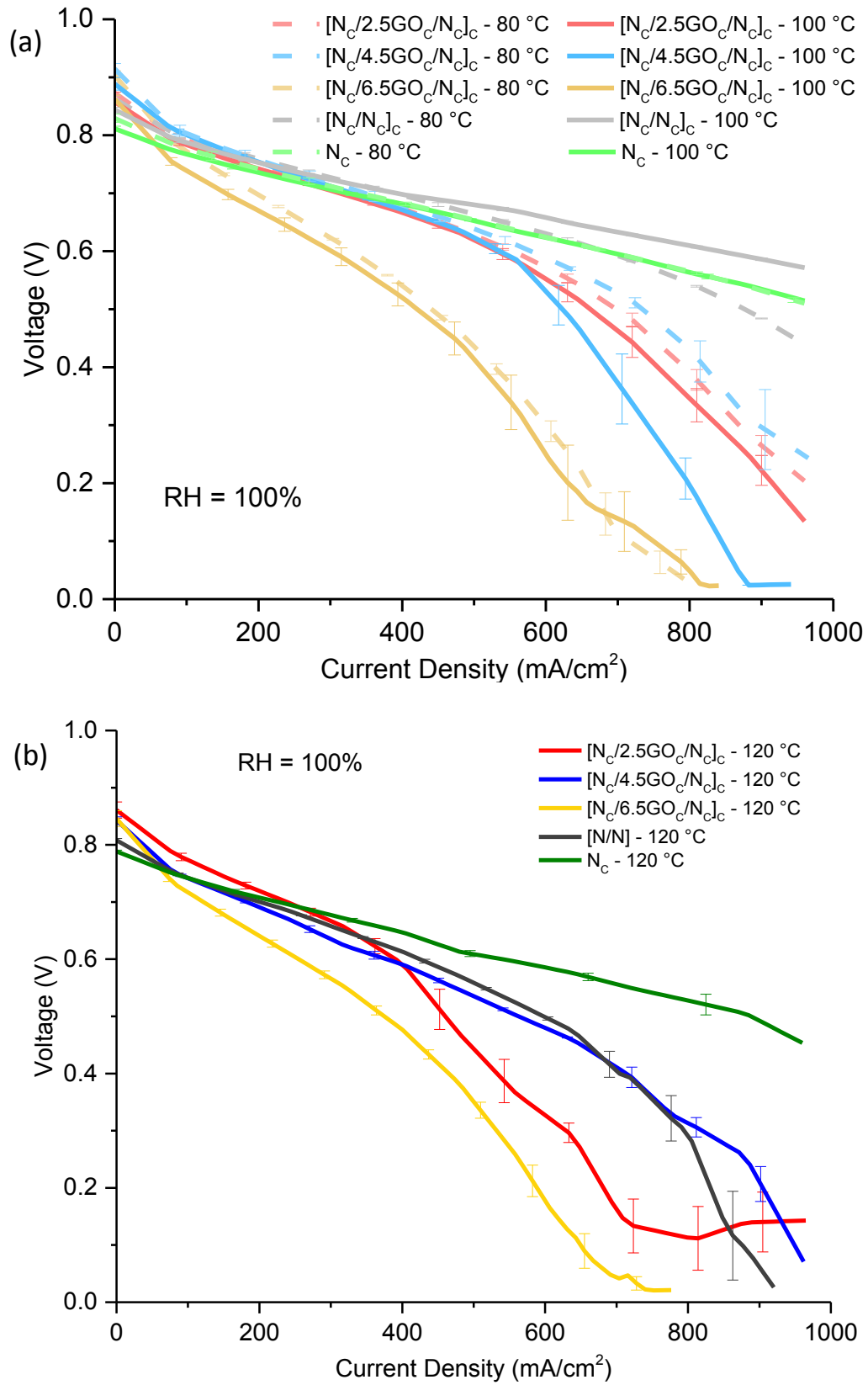


Figure 6.20: NFIL membranes polarization curves with 100% of RH at (a) 80 and 100 °C and (b) 120 °C. Back pressure 0.18 MPa, H₂/Air at rate of 1 and 2.5 L/min respectively.

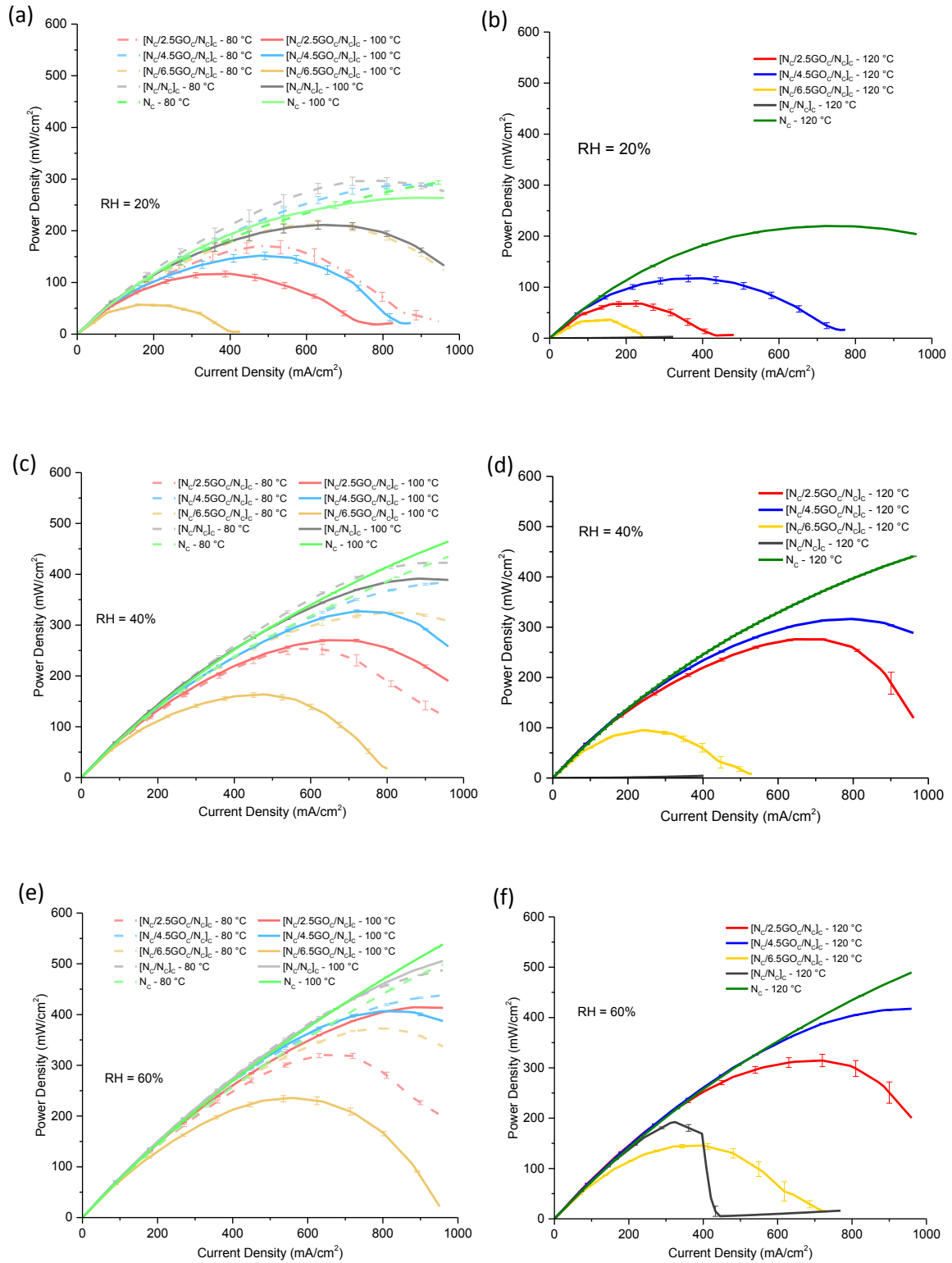


Figure 6.21: NFIL membranes power curves at (a) 80 and 100 °C, RH =20%; (b) 120 °C, RH =20%; (c) 80 and 100 °C, RH =40%; (d) 120 °C, RH =40%; (e) 80 and 100 °C, RH = 60% and (f) 120 °C, RH =60%. Back pressure 0.18 MPa, H₂/Air at rate of 1 and 2.5 L/min respectively.

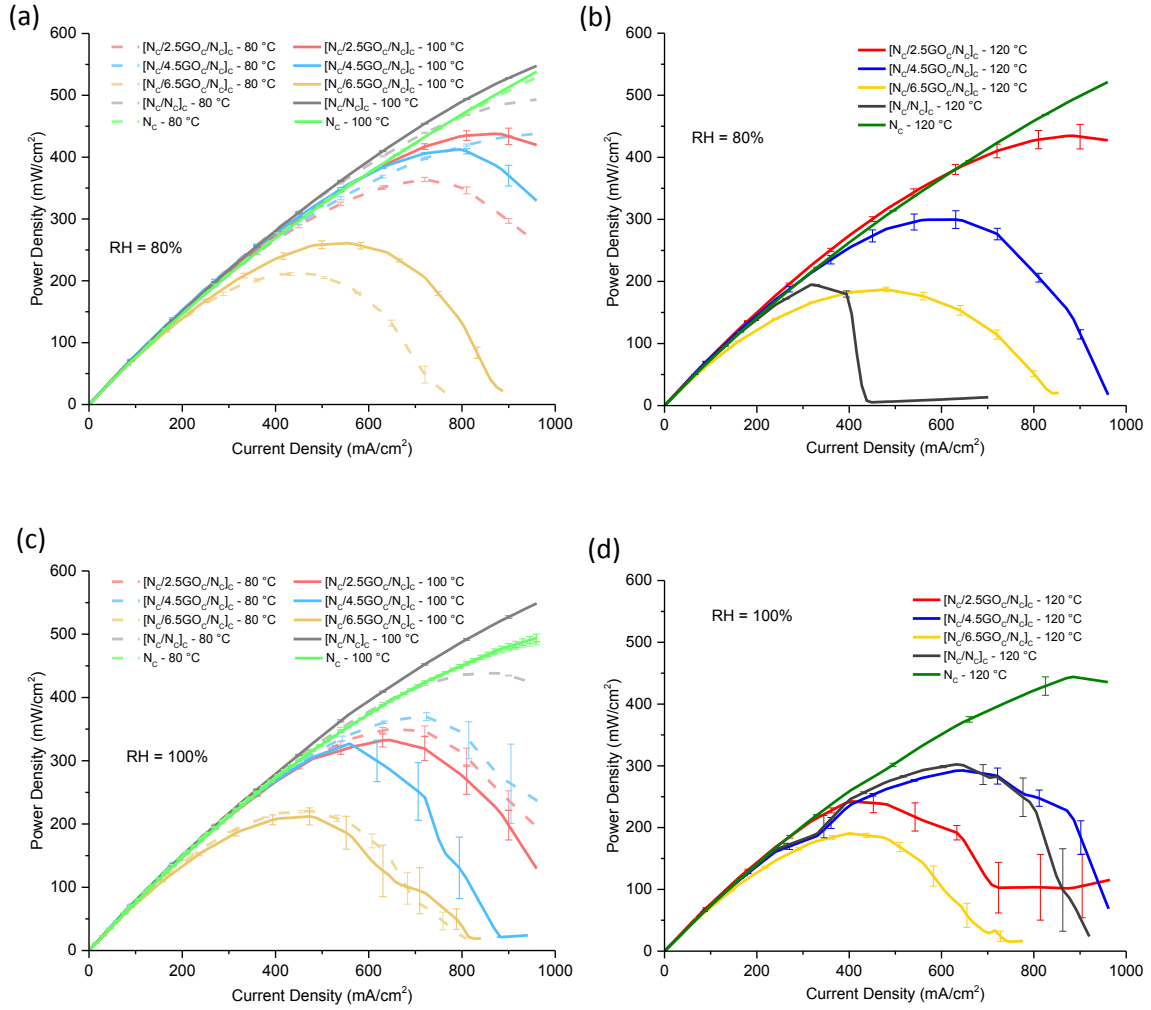


Figure 6.22: NFIL membranes power curves at (a) 80 and 100 °C, RH =80%; (b) 120 °C, RH =80%; (c) 80 and 100 °C, RH =100% and (d) 120 °C, RH =100%. Back pressure 0.18 MPa, H₂/Air at rate of 1 and 2.5 L/min respectively.

Figures 6.23 to 6.24 show the polarization curves for the [N_c/4.5GO- γ N_c/N_c]_c membranes, with γ = 0, 5 and 20 wt.% of Nafion and cast Nafion single layer membranes. In general, the performance was in the following order [N_c/4.5GO_c/N_c]_c > [N_c/4.5GO-5N_c/N_c]_c > [N_c/4.5GO-20N_c/N_c]_c. However, under selected conditions, the Nafion containing membranes showed better performance. These conditions were with 20% RH at 100 °C and 120 °C, and 40% RH at 100 °C, in which the membrane with 5 wt.% Nafion had the best performance. At the highest humidification of 100%, [N_c/4.5GO-20N_c/N_c]_c showed the best performance. Nafion

has extraordinary proton conductivity if in constant humidification, thus with 100% of RH it was not a negative addition to the membrane. The membranes did not show significant improvement in the performance with the addition of Nafion in the inner layer. This suggests that even though the interaction between the layers perhaps was improved, Nafion in the inner layer reduces the conductivity and consequently the performance.

Interestingly, $[N_c/4.5GO-yN_c/N_c]_c$ multilayer membranes (as the NFIL) showed notably higher OCV than Nafion and also higher potential at low current density value (up to ~ 600 mA/cm²) in many of the conditions tested. This behaviour of the OCV could be caused by the possible reduction in gas crossover due to the presence of GO. While in DMFC, GO minimises methanol crossover [141], in the PEFC GO can restrain hydrogen crossover by increasing the tortuosity in the MM structure. Besides, the interaction between the OH groups in GO and sulphonic groups in Nafion, reduces the interaction with the hydrogen, suppressing the crossover and hydrogen paths. While at higher values of current density, Nafion presented a higher potential.

Also, as demonstrated by Bayer *et al.* [167] the proton resistance reduces with the increase of humidity and temperature in GO single layer membranes. Thus, in the current study the internal layers both with and without Nafion are expected to have lower proton resistance with the increase in humidity and temperature, further increasing the proton conductivity. Nevertheless, the interface challenges are also highlighted in the extreme conditions. In these conditions the interlayer resistance can increase due to the presence of the interface. Therefore, it is essential to improve the interlayer interactions in order to avoid a brutal change in resistance inside the multilayer membranes.

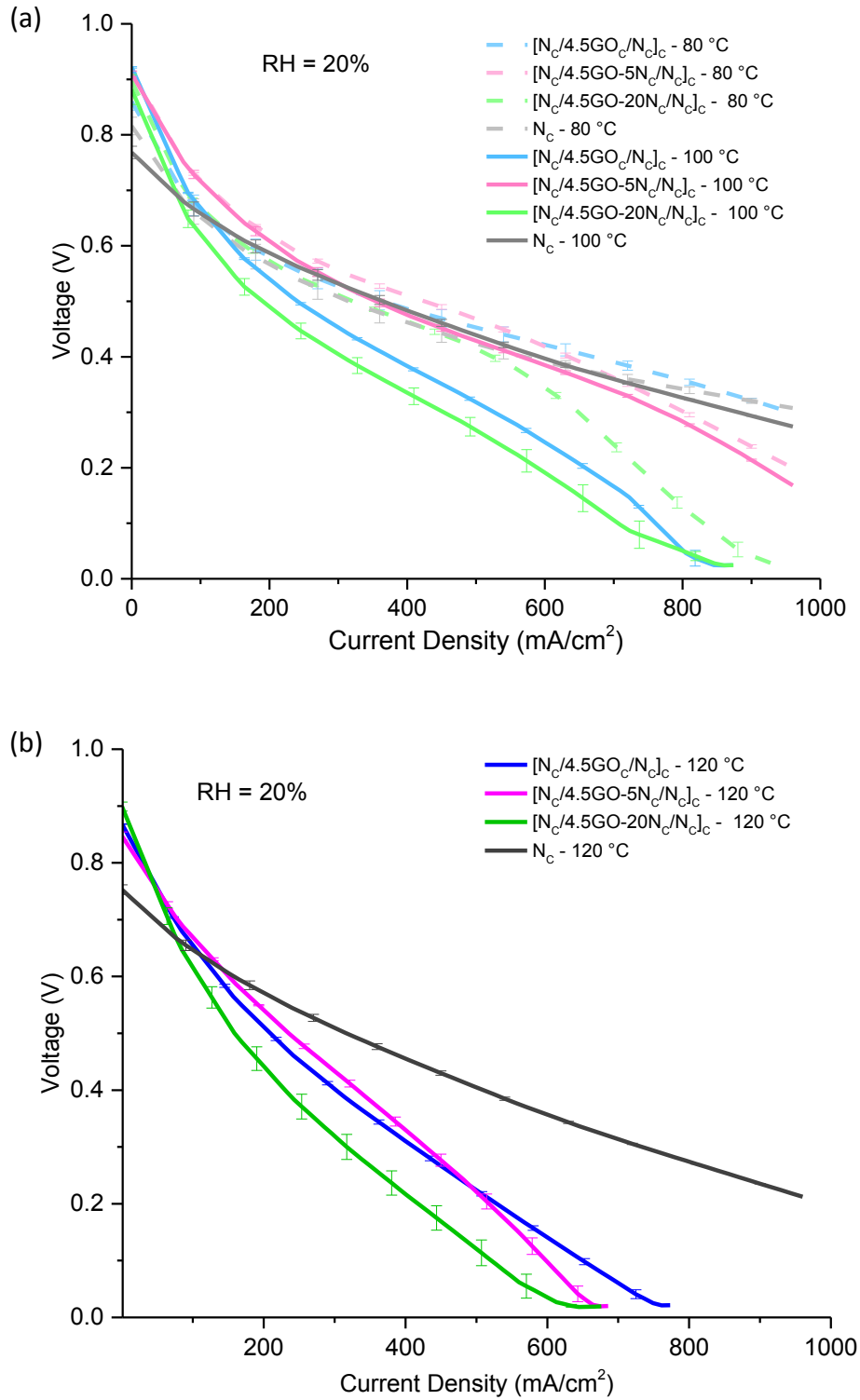


Figure 6.23: [N_c/4.5GO-yN_c/N_c]_c membrane polarization curves with RH of 20% at (a) 80 and 100 °C and (b) 120 °C. Back pressure 0.18 MPa, H₂/Air at rate of 1 and 2.5 L/min respectively.

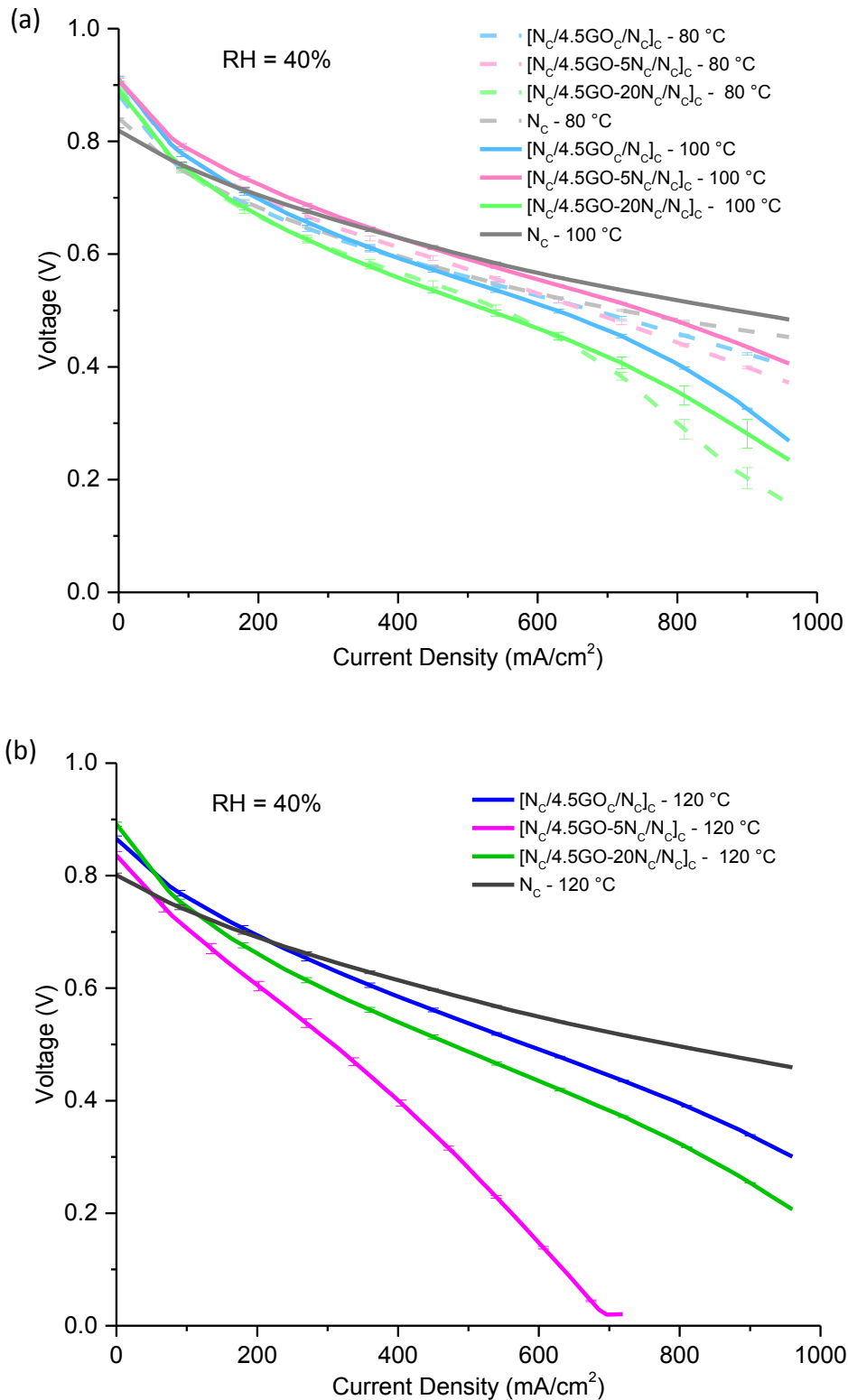


Figure 6.24: $[N_c/4.5GO-yN_c/N_c]_c$ membrane polarization curves with RH of 40% at (a) 80 and 100 °C and (b) 120 °C. Back pressure 0.18 MPa, H₂/Air at rate of 1 and 2.5 L/min respectively.

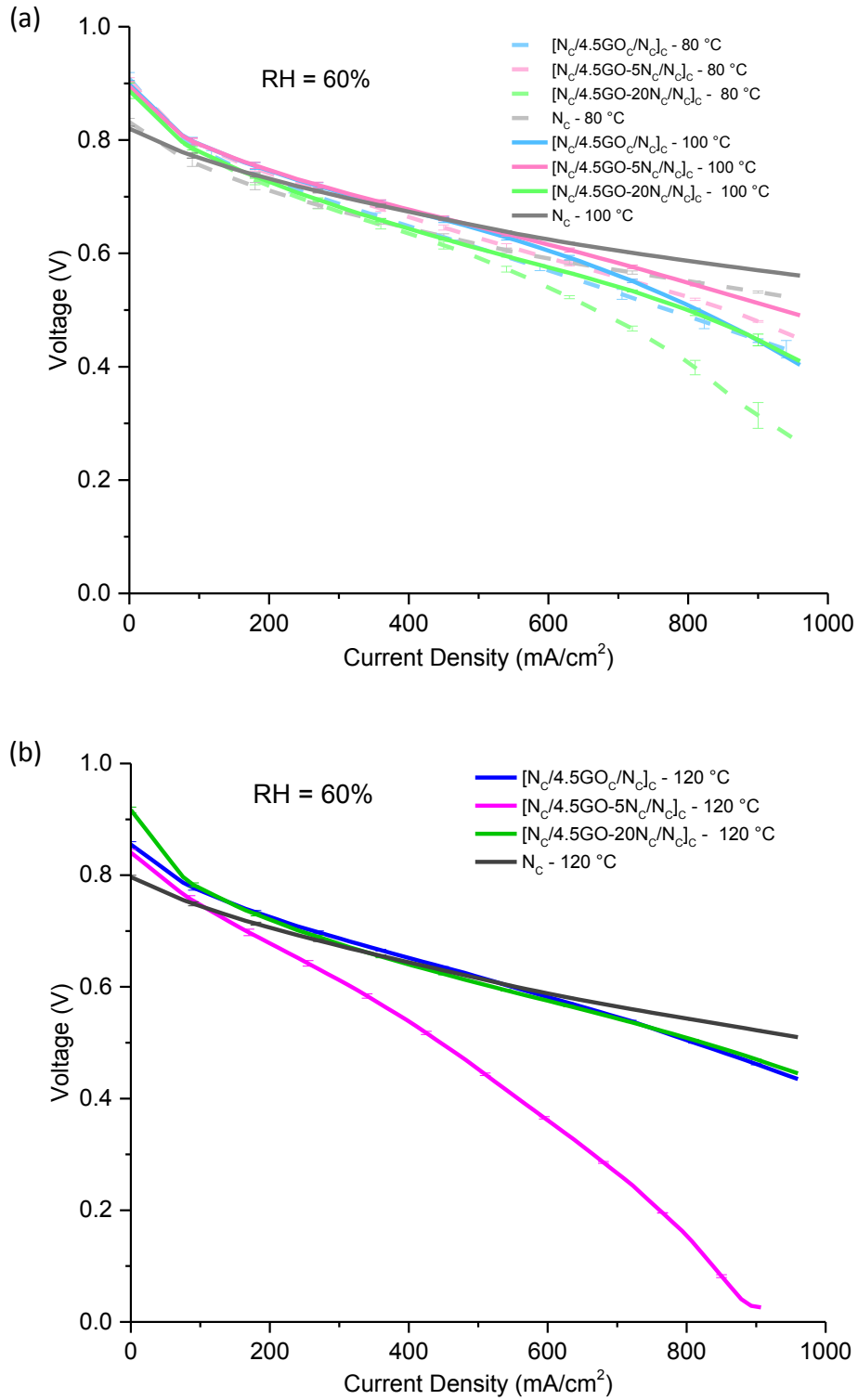


Figure 6.25: [N_c/4.5GO-yN_c/N_c]_c membrane polarization curves with RH of 60% at (a) 80 and 100 °C and (b) 120 °C. Back pressure 0.18 MPa, H₂/Air at rate of 1 and 2.5 L/min respectively.

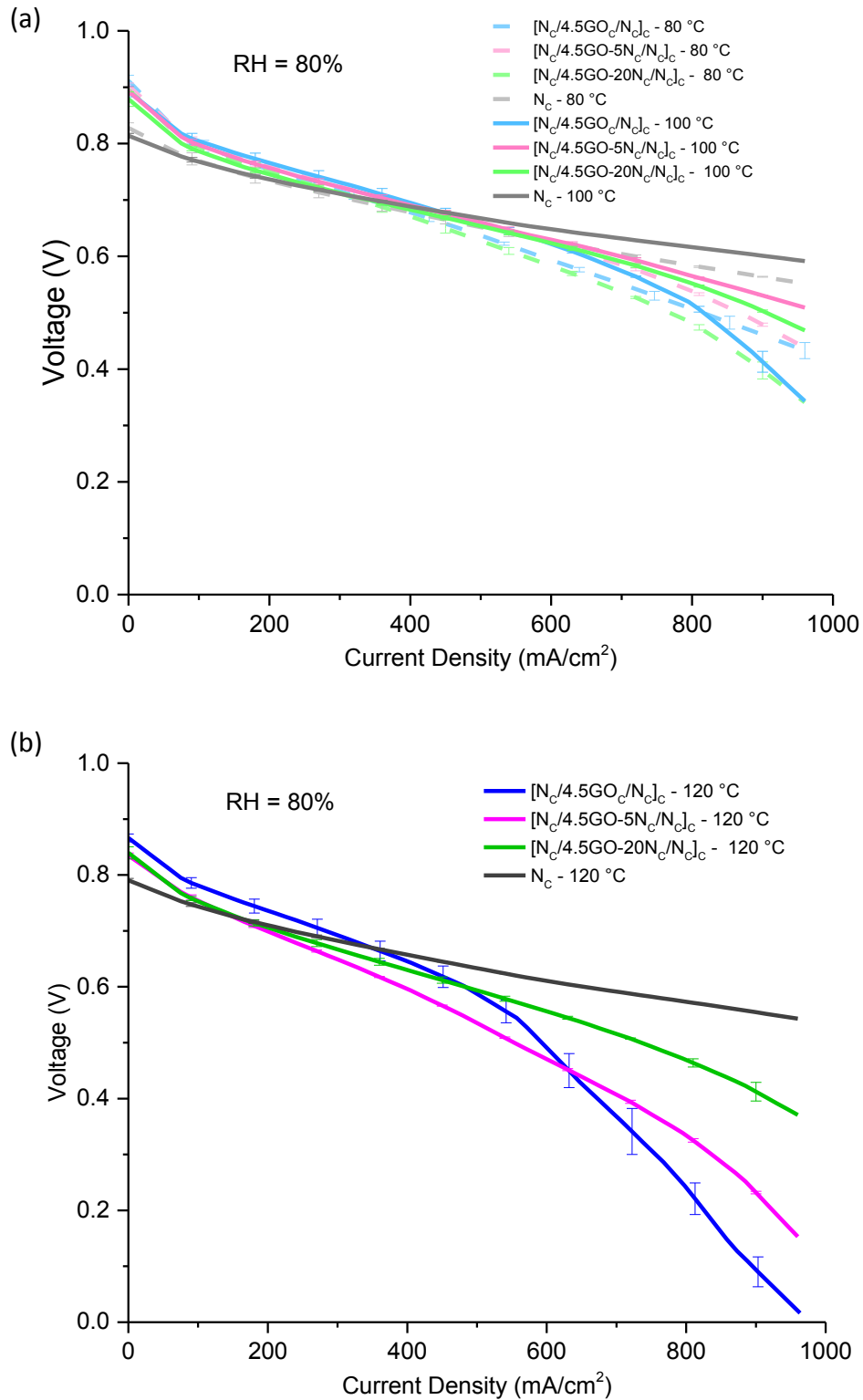


Figure 6.26: [N_c/4.5GO-yN_c/N_c]_c membrane polarization curves with RH of 80% at (a) 80 and 100 °C and (b) 120 °C. Back pressure 0.18 MPa, H₂/Air at rate of 1 and 2.5 L/min respectively.

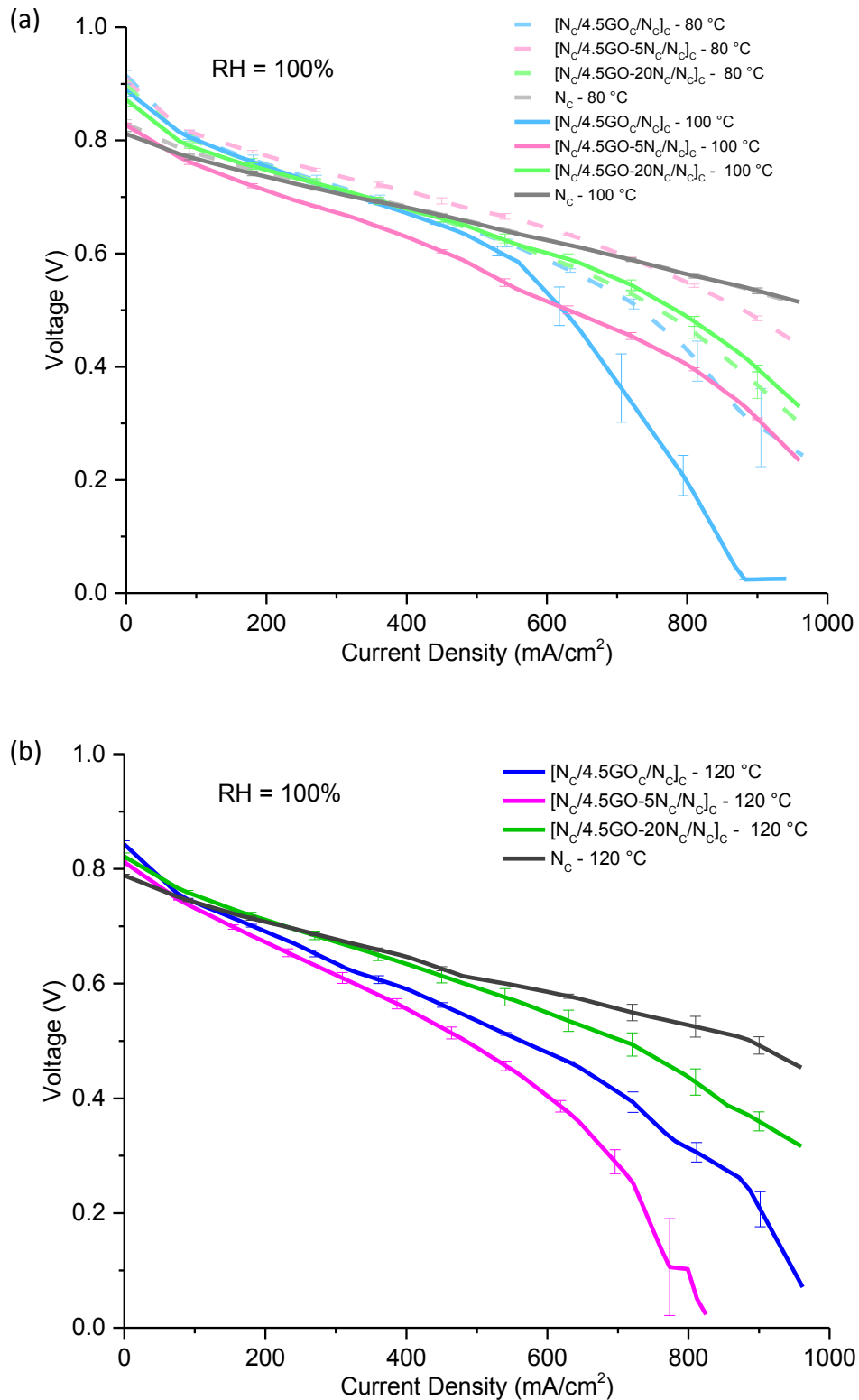


Figure 6.27: $[N_c/4.5GO-yN_c/N_c]_c$ membrane polarization curves with RH of 100% at (a) 80 and 100 °C and (b) 120 °C. Back pressure 0.18 MPa, H_2 /Air at rate of 1 and 2.5 L/min respectively.

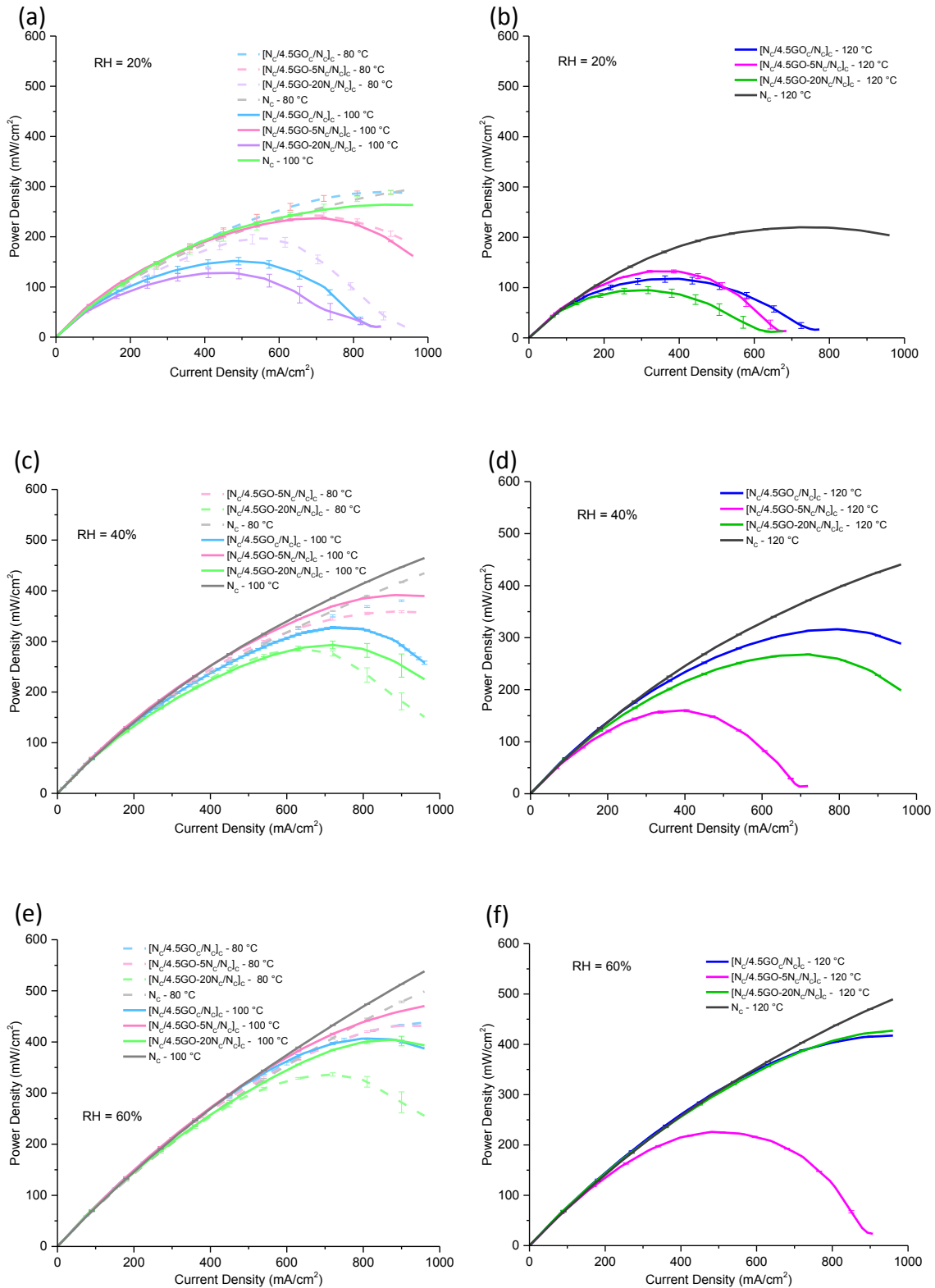


Figure 6.28: $[N_c/4.5GO-yN_c/N_c]_c$ membrane power curves at (a) 80 and 100 °C, RH = 20%; (b) 120 °C, RH = 20%; (c) 80 and 100 °C, RH = 40%; (d) 120 °C, RH = 40%; (e) 80 and 100 °C, RH = 60% and (f) 120 °C, RH = 60%. Back pressure 0.18 MPa, H₂/Air at rate of 1 and 2.5 L/min respectively.

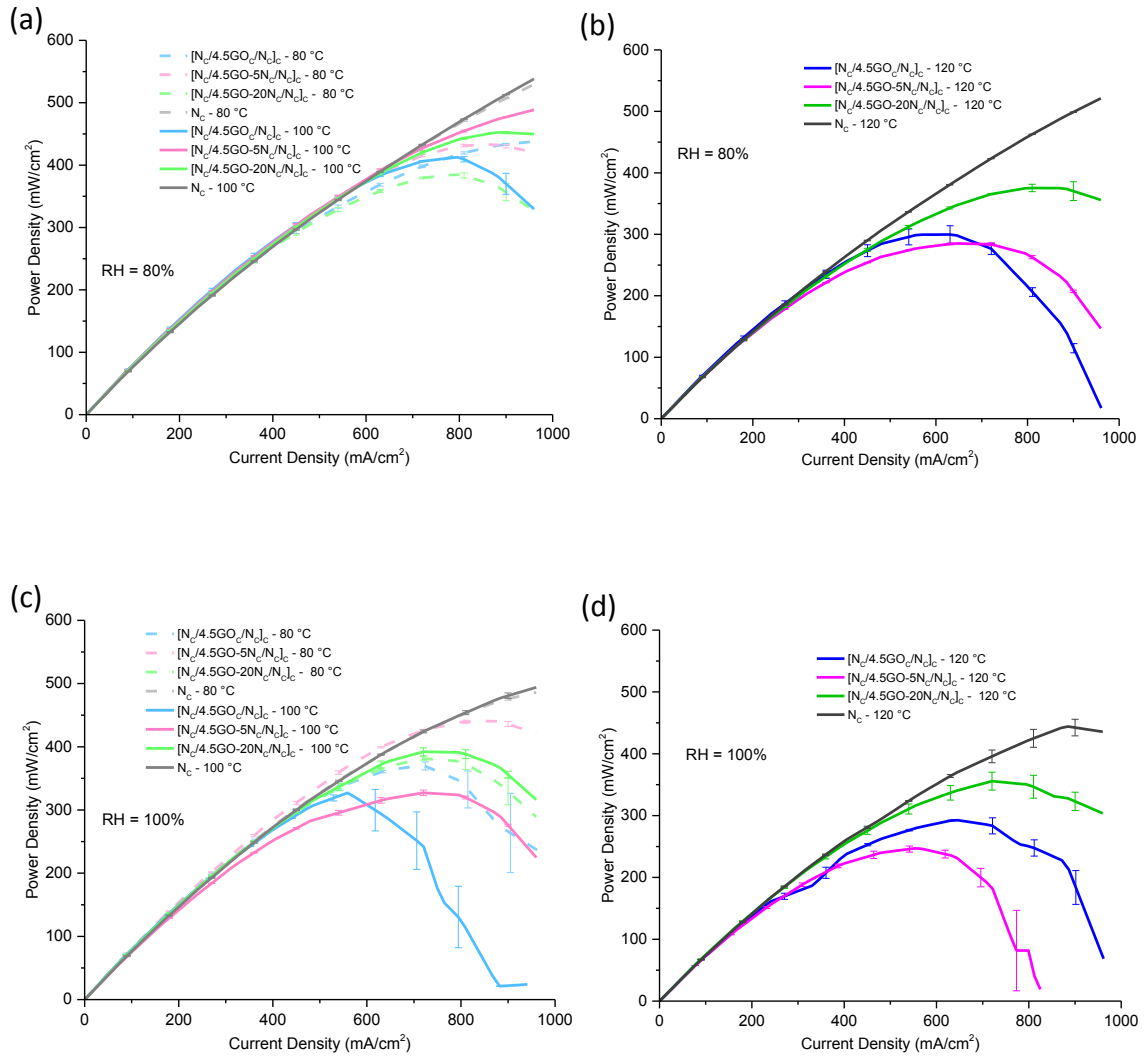


Figure 6.29: $[N_c/4.5GO-yN_c/N_c]_c$ membrane power curves at (a) 80 and 100 °C, RH = 80%; (b) 120 °C, RH = 80%; (c) 80 and 100 °C, RH = 100% and (d) 120 °C, RH = 100%. Back pressure 0.18 MPa, H₂/Air at rate of 1 and 2.5 L/min respectively.

The difference found in the proton conductivity and the single cell tests for the $[N_c/4.5GO-yN_c/N_c]_c$ membranes could also be associated to the direction of measurement in the proton conductivity. While in the proton conductivity is an in-plane measurement, the protons are transported through-plane in the single cell test.

6.2.5. Interface Analysis

To evaluate whether the interaction between the layers increased with the addition of Nafion in the inner layer, the $[N_c/4.5GO-yN_c/N_c]_c$ membranes were submitted to an accelerated delamination test. The membranes were soaked in methanol and then in water for 5 and 2 mins, respectively. This was done repeatedly in 2, 6 and 10 cycles [200]. Three samples of each membrane type were evaluated, and proton conductivity values were recorded three times for each sample. The proton conductivity of the membranes was measured at 120 °C and RH 60% before and after the soaking cycles. Any change in the proton conductivity was attributed to the delamination caused by the solvents soaking cycles. The results are shown in Figure 6.30.

Although methanol was not used in the single cell test, the solvent has the ability to penetrate into the membrane [133, 134, 249] and the interface, therefore it was used for this test. When the membrane is immersed into water after soaking in methanol, water penetrates into the space opened by methanol, expanding this interface further and leading to swelling of the layers. Each cycle further increases delamination, because after the expansion due to the water, methanol has even more space to penetrate inside the membrane [250]. Although this test does not exactly represent the conditions inside the fuel cell, it still demonstrates which membrane has the better interaction and adhesion between the layers.

The membrane with the highest loss in proton conductivity after 2 cycles was $[N_c/4.5GO_c/N_c]_c$, which dropped by 65% in proton conductivity as compared to the as-prepared membrane. On the other hand, $[N_c/4.5GO-5N_c/N_c]_c$ and $[N_c/4.5GO-20N_c/N_c]_c$

showed a reduction by 22 and 23%, respectively, after 2 cycles. After 6 cycles, the $[N_c/4.5GO_c/N_c]_c$ membrane presented a drop by 70% from the original membrane, while $[N_c/4.5GO-5N_c/N_c]_c$ dropped by 23%. The $[N_c/4.5GO-20N_c/N_c]_c$ membrane failed after 6 cycles and was it not possible to test the proton conductivity. Therefore, the addition of Nafion in the inner layer improved the interactions between the layers significantly. All the membranes failed after 10 cycles. The membranes delaminated completely separating the layers. The inset in Figure 6.30 shows this delaminated membrane, with arrows highlighting each layer.

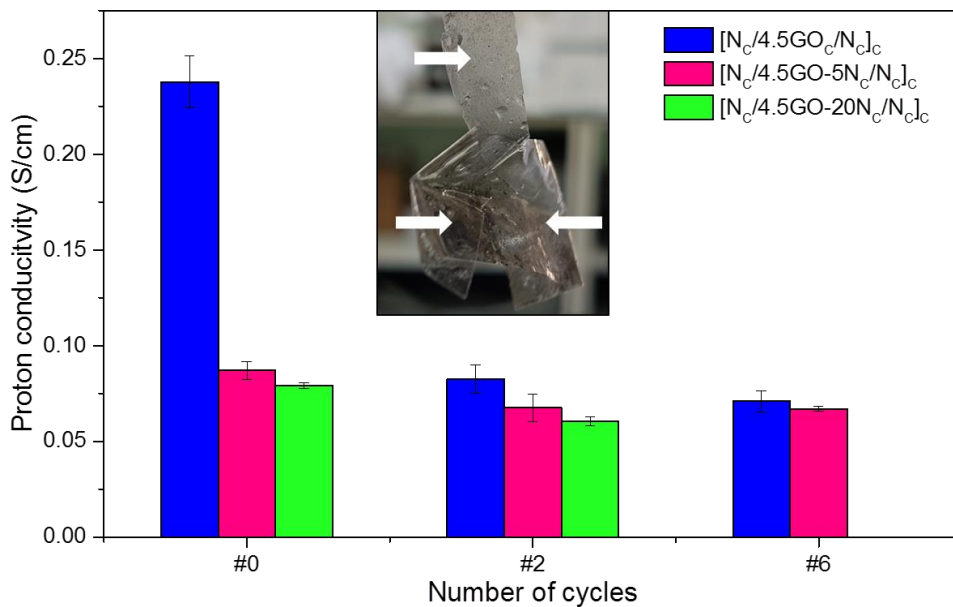


Figure 6.30: Proton conductivity of $[N_c/4.5GO-yN_c/N_c]_c$ membranes at 120 °C and RH 60% before and after delamination test. Inset: $[N_c/4.5GO-20N_c/N_c]_c$ membrane after the delamination cycles; the arrows highlight the three membrane layers.

6.2.4. Post-test of membranes

The multilayer membranes before MEA assembly and after use in the single cell test (with the MEA) were freeze-cracked. The images of the cross-section from $[N_c/4.5GO-5N_c/N_c]_c$

and $[N_c/6.5GO_c/N_c]_c$ are exhibited in Figure 6.31. The Figure (a) and (c) represent the membrane before the MEA assembly, while (d) and (e) represent the membrane after the single cell test. The three-layer structure can be seen in all membranes. However, it is notable that the membranes suffered compression in the MEA preparation and in the test. The GO layer was thinner and the interlayer spaces were reduced in the post use membranes. On the other hand, no other clear structure modifications were noticed which could have affected the performance.

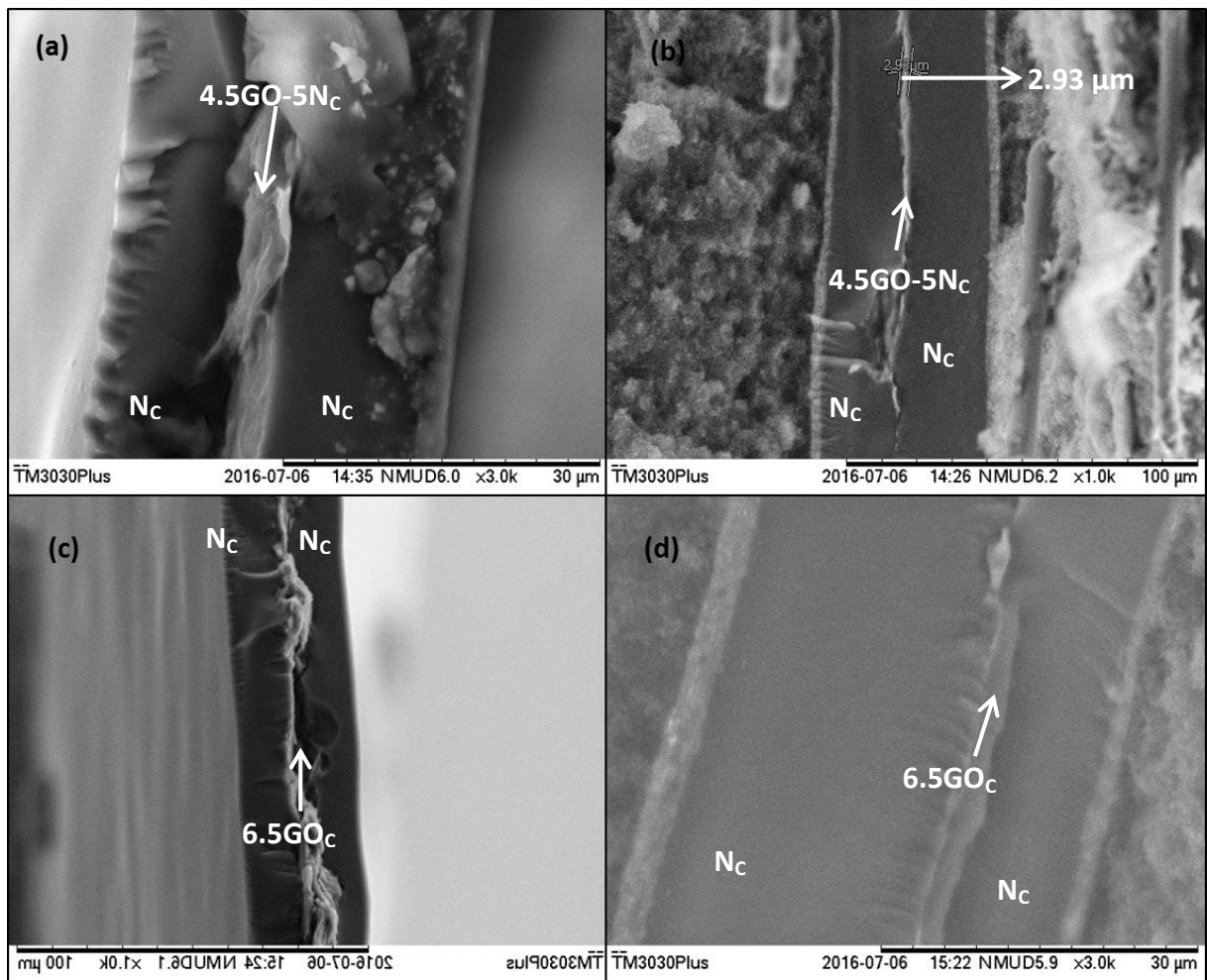


Figure 7.30: Cross-section of $[N_c/4.5GO-5N_c/N_c]_c$ membrane (a) before and (b) after single cell test. Cross-section of $[N_c/6.5GO_c/N_c]_c$ membrane (c) before and (d) after single cell test.

6.3. Conclusions

$[N_C/GO-20N_F/N_C]_{HP}$ was the only hot pressed GO membrane that did not show optical gaps between the layers, as the other GO membranes, and compensated the interface factor showing a higher ion exchange capacity and potential to be applied in PEFCs stacks. However, the in-situ tests proved that the hot pressing membranes allow gaps that are not visible to naked eye and the performance in a real fuel cell is poor. The bubbles left by water in the interlayer interface are discontinuities in the proton pathway. The membrane showed to be a potential PEM but not for PEFC systems.

On the other hand, proton conductivities of cast multilayer membranes have exceeded that of Nafion. $[N_C/4.5GO_C/N_C]_C$ showed the highest conductivity. Addition of Nafion in the inner layer reduced the proton conductivity values, although increasing the interaction between the layers. Higher content of GO led to flooding the membrane and, consequently, decreased the conductivity. The performances in the fuel cell prototype demonstrated the potential applicability of these membranes. Interfaces caused a negative effect on the membrane performance, as notable by the extremely lower performance of Nafion bilayer compared to a Nafion single layer. Nevertheless, GO overcame this effect by increasing the performance to equalise Nafion single layer performance at some conditions and suppress it at others. At intermediate temperature the difference between a Nafion bilayer and the multilayers was even more significant. While the bilayers start to demonstrate power at only 60% RH, the multilayer showed power RH from 20%.

It is evident that the casting method was more efficient preparing multilayer membranes than hot pressing method. Indeed, the interface interaction was stronger in the cast due to

the chemical bond between the layers. The IxV performance of both HP and cast emphasizes this difference.

CHAPTER VII – SUMMARY AND PERSPECTIVES

7.1. Conclusions

This study has delivered new multilayer membrane designs incorporating SPInd and GO cores and has contributed to detailed analysis of their behaviour and properties. The membrane preparation methods casting and hot pressing were discussed and optimised. Besides the multilayer membrane preparation, the study developed with respect to four objectives which are discussed below.

Both hot pressing and casting preparation methods were optimized for each group of multilayer membranes separately. The hot pressing method was more difficult with GO membranes, while casting presented more issues with SPInd membranes. The high water retention by GO through oxygen groups was the main drawback in the hot pressing. Thus, a two-steps hot press process was selected to be carried out. On the other hand, SPInd was successfully sandwiched between Nafion membranes in a one-step process. However, all these HP membranes were thicker than the target, which is prejudicial for fuel cell application. Unlike HP membranes, cast multilayer membranes achieved the target thickness. The individual membrane layers were cast on the surface of each other before annealing, ensuring the chemical bond between them.

In the hot pressed membranes, the main interaction between the layers was mechanical, weakening the interface. In contrast, in cast membranes the interaction is chemical. Thus, small interlayer spaces were found in HP membranes and not in cast. These spaces were

highlighted when the membranes were soaked in water. Thus, water retention was higher for HP membranes. However, this value was masked by the spaces. The water retained in these spaces was superficial and does not improve the fuel cell performance, because contributed for delamination. In both, SPInd and GO, membranes this situation occurred. On the other hand, all cast multilayer membranes showed higher water retention than the reference Nafion. Considering that the interface has a negative effect on holding water (compared to a Nafion bilayer), GO and SPInd not only surpassed this effect but also increased the water uptake. Oxygen and sulphonic groups were efficient catching and holding water in GO and SPInd respectively.

The interface was the main drawback in multilayer membranes as highlighted by general results from $[N_c/N_c]_c$ and $[N_c/N_c]_{HP}$ membranes. In the cases in which the interface was not strong enough, delamination occurred, such as with $[N_c/GO-xN_F/N_c]_{HP}$. In cast membranes, the delamination was not observed. Therefore, proton conductivity was higher for cast membranes. In $[N_c/GO-xN_c/N_c]_c$ membranes, the addition of Nafion in the inner layer improved the interaction between external and internal layers. However, Nafion is less hydrophilic than GO, thus the proton conductivity values were reduced and consequently the fuel cell performance. Although the interface was an issue in SPInd too, in general, delamination was avoided. The interaction between SPInd and Nafion is stronger than between GO and Nafion. Both SPInd and Nafion have a polar phase and are polymers that have a thermal behaviour more alike than GO.

The performance in the fuel cell was only acceptable for cast membranes. Thus, HP with these designs is not suitable to prepare membranes for PEFC application. The

$[N_c/SPInd_c/N_c]_c$ 1:1:1.5 membrane had the optimum performance and properties of all SPInd membranes. The low content of Nafion ensured high proton conductivity and ion exchange capacity, since the IEC was very high for SPInd single layers. Considering the performance in the PEFC, this membrane showed higher values of potential and power than a Nafion single layer with low humidity at all temperatures at low and medium current density. In particular, at 120 °C and 20% of relative humidity a significantly superior performance as shown to Nafion. This fuel cell condition, in which Nafion has the worst performance, was the initial goal for the multilayer membranes. The humidifiers can be simplified with a humidity as low as 20%, reducing the fuel cell cost and weight. Therefore, the cast SPInd multilayer membrane is a promising group to be applied in IT-PEFC.

Among the GO membranes, the best performance in the fuel cell varied between $[N_c/2.5GO_c/N_c]_c$ and $[N_c/4.5GO_c/N_c]_c$ membranes. However, considering all properties, such as proton conductivity, $[N_c/4.5GO_c/N_c]_c$ can be considered as the optimum composition. The interface showed a negative effect in the general performance and it was emphasized at 120 °C and low/medium humidity. GO in the inner layer overcame this effect and increased the membrane performance in comparison to a Nafion bilayer. However, GO membranes showed problems with mass transport, reducing the potential at high values of current density. Comparing with Nafion, GO has increased the OCV in the fuel cell performance for all humidities and temperatures tested, while SPInd kept the same or showed reduced OCV. GO increased the tortuosity of the membrane and thus reduced the gas crossover.

These multilayer membranes are not ready to be applied commercially in IT-PEFC, but this study is a starting point to develop further.

7.2. Suggested future work

As SPInd multilayer membranes showed high potential and power in IT-PEFC with low humidity and GO multilayer membranes showed high OCV, a combination between these materials could lead to an outstanding membrane. Thus, a multilayer $[N_c/SPInd-GO_c/N_c]_c$ would be the next step in future work. Although optimum compositions for $[N_c/SPInd_c/N_c]_c$ and $[N_c/GO_c/N_c]_c$ membranes were found, a new, detailed study in on composition would be necessary. However, the composition found in the present study could be the starting point of such research.

The SPInd used in the present study was 30% sulphonated. This value was chosen because studies in literature demonstrated that it was the ideal value for composite single layer membranes. However, considering multilayer membranes, a higher sulphonated degree can be applied. Therefore, the preparation and analysis of $[N_c/SPInd_c/N_c]_c$ and/or $[N_c/SPInd-GO_c/N_c]_c$ with SPInd with higher sulphonated degree is suggested. Since $[N_c/SPInd_c/N_c]_c$ membranes exhibit an excellent behaviour in IT-PEFC (with RH = 20%), increasing the number of sulphonic groups can lead to higher proton conductivity and water retention.

Considering that proton conductivity tests were carried out in-plane, impedance measurements, especially at high frequency, are suggested as future work. The proton conductivity in-plane and through-plane can be very different, especially for multilayer membranes due to the interface, which increases the resistance.

Finally, all the PEFC single cell tests carried out in the present study were not evaluated along time. Therefore, an investigation into the multilayer membrane durability needs to validate the membranes for commercial application.

APPENDIX

A. Detailed experimental procedures

A.1. Materials characterization

A.1.1. Fourier Transform Infrared Spectrometry (FT-IR)

Material samples were used as dried powder and placed in the PerkinElmer FT-IR Spectrum 100. The spectra were recorded between 4000 to 400 cm^{-1} . A background was recorded and the final spectra automatically considered the background values. The resolution was 2 cm^{-1} . Three samples were used for each material.

A.1.2. X-ray Diffraction (X-RD)

GO samples were solubilized in DI water. The solutions were drop and dried on a silicon substrate. Three samples were obtained. The samples were evaluated in a Bruker D2 XRD.

The parameters were:

- Final temperature: 800 °C.
- Heating rate: 10 °C/min.
- Air flow: 50 mL/min
- $\text{K}\alpha$ X-ray source: Co
- Scan range: 7 to – 90 °
- Angle rate: 5 °/min

A.1.3. X-ray Photoemission Spectroscopy (XPS)

GO samples were solubilized in DI water. The solutions were drop and dried on a silicon substrate. Three samples were obtained. The samples were evaluated in a Thermo Scientific K-Alpha™+ X-ray Photoelectron Spectrometer System with a K α Source of Al and $h\nu = 1486.6$ eV. The data was analysed in the CasaXPS software, Version 2.3.17PR1.1.

A.1.4. Thermogravimetric Analysis (TGA)

TGA was carried out for Plnd, SPInd and GO, three samples each. The samples were in powder format. GO samples were dried overnight in the oven at 60 °C. All tests were carried out in alumina crucibles. Plnd and SPInd were characterised by the TGA 2050, TA Instruments and the parameters were:

- N₂
- Flow: 50 mL/min
- Heating rate: 20 °C/min
- Final temperature: 900 °C

GO samples characterised by the TG 209 F1 and the parameters were:

- Air
- Flow: 50 mL/min
- Heating rate: 10 °C/min
- Final temperature: 850 °C

A.1.5. Differential Scanning Calorimetry (DSC)

Three samples of each PInd and SPIInd were characterised in the DSC Q20, TA Instruments in the powder format. Two runs were carried out for each sample. The first was to remove the water from the sample and the final temperature was 200 °C. While the second run final temperature was 250 °C. The heating rate was 10 °C/min. The system was purged with N₂ with a rate of 80 mL/min.

A.2. Tests on the Membranes

A.2.1. Water Uptake (WU)

Three samples for each set of membranes were cut in smaller pieces of 2 x 1 cm. The test was carried out using a gravimetric method [213, 251], as follow.

- The samples were immersed in DI water at room temperature for 24 h.
- The samples were pat dried.
- The wet weights (W_w) were recorded.
- The samples were immersed in water again for 30 min.
- The wet weights were recorded; this procedure was repeated 3 times.
- The samples were placed on a Petri dish over a paper filter and dried in an oven at 100 °C for 24 h.
- The dry weights (W_d) were record.
- The sample returned to the oven for another 30 min and the dry weight recorded again. This procedure was repeated 3 times.

Finally, the water uptake was obtained from the equation bellow:

$$WU = \frac{W_w - W_d}{W_d}$$

A.2.2. Ion Exchange Capacity (IEC)

The IEC test was carried out in the same samples from the WU test with the following method [105, 213]:

- The samples were soaked in HCl 0.1 M for 24h.
- The samples were rinsed.
- They were immersed in saturated NaCl for 72 h.
- The solutions were titrated with NaOH 0.01 M and phenolphthalein as indicator.

The IEC was obtained from the equation below, where V_{NaOH} and M_{NaOH} are the volume and molar mass of the NaOH titrated.

$$IEC = \frac{V_{NaOH} \times M_{NaOH}}{W_d}$$

A.2.3. Proton Conductivity

The membranes were cut in samples of 3 x 1 cm of area. After that, the membranes were soaked in water for 24 h. The sample that would be tested was fitted in the clamp BT-110 Conductivity Clamp from Scribner with four electrodes of platinum. The test was carried out in the Scribner 850e Fuel Cell test system with dew point chamber controller from Vaisala and the steps are as following:

- a. The system was stabilised at 80 °C and RH 20% for 2 h.
- b. The ixV was recorded.

- c. The system was stabilised for 5 min.
- d. The ixV was recorded. Procedures b to d were repeated 3 times.
- e. The RH changed for 40%.
- f. The system was stabilised for 30 min.
- g. The steps b to d were repeated.
- h. The same procedure followed for the RH of 60, 80 and 100%.
- i. The temperature changed 100 °C and the RH for 20%.
- j. The system was stabilised for 2 h.
- k. The same steps from b to h were repeated.
- l. The temperature changed for 120 °C and 20% of RH.
- m. The system was stabilised for 2 h.
- n. The same steps from b to h were repeated.

The ixV was measure between 0 to 0.8 V in a fixed rate of 10 points/s. The measurement was a linear sweep with 1 mV/s. The hydrogen flow was fixed at a rate of 0.5 L/min. The data was analysed in the FCView software from Scribner, where the resistance (R) was obtained. Then, the proton conductivity (σ) was calculated as follow, where L is distance between the inner probes and A is the thickness of the membrane.

$$\sigma = \frac{L}{RxA}$$

A.2.4. Single cell test

The MEAs were prepared with an area of 6.25 cm² with carbon paper as support and platinum as catalyst (0.4 mg Pt/cm², from Johnson Matthey). The MEA was assembled in a hot press at 125 °C and 6.8 MPa for 5 min.

The MEA were fitted in the fuel cell single cell holder and tested in the 850e High Temperature Scribner Associates Incorporated Test Stand, with the 885 Fuel Cell Potentiostat. Three MEAs for each type of membrane were prepared and tested. The test followed the steps bellow:

- a. The system was set up to 80 °C and 40% of RH.
- b. The system was stabilised with OCV for 1 h.
- c. Voltage applied from 0 to 0.6 V, follow by OCV step for 50 times.
- d. RH changed for 20%.
- e. The system was stabilised with OCV for 2 h.
- f. The ixV values were recorded 3 times with intervals of 30s.
- g. The steps d to f were repeated for the RH of 40, 60, 80 and 100%.
- h. The temperature changed for 100 °C and RH to 20%.
- i. The system was stabilised with OCV for 2 h.
- j. The ixV values were recorded 3 times with intervals of 30s.
- k. The steps d to f were repeated for the RH of 40, 60, 80 and 100%.
- l. The temperature changed for 120 °C and RH to 20%.
- m. The system was stabilised with OCV for 2 h.
- n. The ixV values were recorded 3 times with intervals of 30s.

- o. The steps d to f were repeated for the RH of 40, 60, 80 and 100%.

The ixV curves were measured between 0 and 6 V, linear with 0.5 amps/point. Each point was recorded for 60 s. The back pressure was 0.18 MPa (1.8 bar). The anode was supplied with hydrogen and the cathode with compressed air at a rate of 1 and 2.5 L/min respectively.

LIST OF PUBLICATIONS

- A. Branco, C.M., Sharma, S., Forte, M.M.C., Steinberger-Wilckens, R. *New approaches towards novel composite and multilayer membranes for intermediate temperature-polymer electrolyte fuel cells and direct methanol fuel cells*. Journal of Power Sources, 2016. **316**: p.139-159.*
- B. Sharma, S., Mclaughlin, J., Branco, C.M. *Preliminary Study on the Quick Synthesis of Manganese Oxide-Reduced Graphene Oxide Nano-hybrids and their Magnetic Properties*. Current Graphene Science, 2017. **1**.
- C. Branco, C.M., El-Kharouf, A., Du, Shangfeng. *Materials for Polymer Electrolyte Membrane Fuel Cell (PEMFCs): Electrolyte Membrane, Gas Diffusion Layers, and Bipolar Plates*. Chapter in the book: Reference Module in Materials Science and Materials Engineering. 2017. Elsevier.
- D. Sharma, S. and Branco, C.M. *Noble metal electrocatalysts for fuel cell anode and cathode*. Chapter in the book: Nanostructured Materials for Next Generation Storage and Conversion. Expected publish date: October 2017. Springer-Nature.

*Chapter II is based on the publication A.

REFERENCES

1. Andújar, J.M. and F. Segura, *Fuel cells: History and updating. A walk along two centuries*. Renewable and Sustainable Energy Reviews, 2009. **13**(9): p. 2309-2322.
2. Merle, G., M. Wessling, and K. Nijmeijer, *Anion exchange membranes for alkaline fuel cells: A review*. Journal of Membrane Science, 2011. **377**(1-2): p. 1-35.
3. Yoshida, T. and K. Kojima, *Toyota MIRAI Fuel Cell Vehicle and Progress Toward a Future Hydrogen Society*. The Electrochemical Society Interface, 2015: p. 45-49.
4. Garche, J. and L. Jörissen *Applications of Fuel Cell Technology: Status and Perspectives*. The Electrochemical Society Interface 2015: p. 39-43.
5. Mamlouk, M. and K. Scott, *A boron phosphate-phosphoric acid composite membrane for medium temperature proton exchange membrane fuel cells*. Journal of Power Sources, 2015. **286**: p. 290-298.
6. Tang, T.-H., P.-H. Su, Y.-C. Liu, and T.L. Yu, *Polybenzimidazole and benzyl-methyl-phosphoric acid grafted polybenzimidazole blend crosslinked membrane for proton exchange membrane fuel cells*. International Journal of Hydrogen Energy, 2014. **39**(21): p. 11145-11156.
7. Subianto, S., *Recent advances in polybenzimidazole/phosphoric acid membranes for high-temperature fuel cells*. Polymer International, 2014. **63**(7): p. 1134-1144.
8. Lucia, U., *Overview on fuel cells*. Renewable and Sustainable Energy Reviews, 2014. **30**: p. 164-169.
9. Mahato, N., A. Banerjee, A. Gupta, S. Omar, and K. Balani, *Progress in material selection for solid oxide fuel cell technology: A review*. Progress in Materials Science, 2015. **72**: p. 141-337.
10. Larmine, J. and A. Dicks, *Fuel Cell System Explained* 2003: John Wiley & Sons.
11. Neef, H.J., *International overview of hydrogen and fuel cell research* ☆. Energy, 2009. **34**(3): p. 327-333.
12. Taherian, R., *A review of composite and metallic bipolar plates in proton exchange membrane fuel cell: Materials, fabrication, and material selection*. Journal of Power Sources, 2014. **265**: p. 370-390.
13. Tawfik, H., Y. Hung, and D. Mahajan, *Metal bipolar plates for PEM fuel cell—A review*. Journal of Power Sources, 2007. **163**(2): p. 755-767.
14. Middelmann, E., W. Kout, B. Vogelaar, J. Lenssen, and E. de Waal, *Bipolar plates for PEM fuel cells*. Journal of Power Sources, 2003. **118**(1-2): p. 44-46.
15. Mehta, V. and J.S. Cooper, *Review and analysis of PEM fuel cell design and manufacturing*. Journal of Power Sources, 2003. **114**(1): p. 32-53.
16. Debe, M.K., *Electrocatalyst approaches and challenges for automotive fuel cells*. Nature, 2012. **486**(7401): p. 43-51.
17. Marcinkoski, J., J. Spendelow, A. Wilson, and D. Papageorgopoulos, *Fuel Cell System Cost - 2015 in Hydrogen and Fuel Cells Program Record* 2015, US DOE.
18. Branco, C.M., S. Sharma, M.M. de Camargo Forte, and R. Steinberger-Wilckens, *New approaches towards novel composite and multilayer membranes for intermediate temperature-polymer electrolyte fuel cells and direct methanol fuel cells*. Journal of Power Sources, 2016. **316**: p. 139-159.
19. Kim, D.J., M.J. Jo, and S.Y. Nam, *A review of polymer–nanocomposite electrolyte membranes for fuel cell application*. Journal of Industrial and Engineering Chemistry, 2015. **21**: p. 36-52.

20. Mauritz, K.A. and R.B. Moore, *State of Understanding Nafion*. Chemical Reviews, 2004. **104**(10): p. 4535-4585.
21. Chandan, A., M. Hattenberger, A. El-kharouf, S. Du, A. Dhir, V. Self, B.G. Pollet, A. Ingram, and W. Bujalski, *High temperature (HT) polymer electrolyte membrane fuel cells (PEMFC) – A review*. Journal of Power Sources, 2013. **231**: p. 264-278.
22. Shao, Y., G. Yin, Z. Wang, and Y. Gao, *Proton exchange membrane fuel cell from low temperature to high temperature: Material challenges*. Journal of Power Sources, 2007. **167**(2): p. 235-242.
23. Authayanun, S., K. Im-orb, and A. Arpornwichanop, *A review of the development of high temperature proton exchange membrane fuel cells*. Chinese Journal of Catalysis, 2015. **36**: p. 473–483.
24. Bose, S., T. Kuila, T.X.H. Nguyen, N.H. Kim, K.-t. Lau, and J.H. Lee, *Polymer membranes for high temperature proton exchange membrane fuel cell: Recent advances and challenges*. Progress in Polymer Science, 2011. **36**(6): p. 813-843.
25. Wang, J., X. Yue, Z. Zhang, Z. Yang, Y. Li, H. Zhang, X. Yang, H. Wu, and Z. Jiang, *Enhancement of Proton Conduction at Low Humidity by Incorporating Imidazole Microcapsules into Polymer Electrolyte Membranes*. Advanced Functional Materials, 2012. **22**(21): p. 4539-4546.
26. Kim, D.H., H.S. Park, S.J. Seo, J.S. Park, S.H. Moon, Y.W. Choi, Y.S. Jiong, and M.S. Kang, *Facile surface modification of anion-exchange membranes for improvement of diffusion dialysis performance*. J Colloid Interface Sci, 2014. **416**: p. 19-24.
27. Millet, P., D. Dragoë, S. Grigoriev, V. Fateev, and C. Etievant, *GenHyPEM: A research program on PEM water electrolysis supported by the European Commission*. International Journal of Hydrogen Energy, 2009. **34**(11): p. 4974-4982.
28. Fadhillah, F., S.M.J. Zaidi, Z. Khan, M.M. Khaled, F. Rahman, and P.T. Hammond, *Development of polyelectrolyte multilayer thin film composite membrane for water desalination application*. Desalination, 2013. **318**: p. 19-24.
29. Spohr, E., *Proton generation and transport in the fuel cell environment: atomistic computer simulations*. Journal of Computer-Aided Materials Design, 2008. **14**(S1): p. 253-258.
30. Zhao, Q., Q.F. An, Y. Ji, J. Qian, and C. Gao, *Polyelectrolyte complex membranes for pervaporation, nanofiltration and fuel cell applications*. Journal of Membrane Science, 2011. **379**(1-2): p. 19-45.
31. Sun, H., Z. Sun, and Y. Wu, *Proton transfer mechanism in perfluorinated sulfonic acid polytetrafluoroethylene*. International Journal of Hydrogen Energy, 2012. **37**(17): p. 12821-12826.
32. Peighambardoust, S.J., S. Rowshanzamir, and M. Amjadi, *Review of the proton exchange membranes for fuel cell applications*. International Journal of Hydrogen Energy, 2010. **35**(17): p. 9349-9384.
33. Zhang, H. and P.K. Shen, *Recent development of polymer electrolyte membranes for fuel cells*. Chem Rev, 2012. **112**(5): p. 2780-832.
34. Yoshida, T. and T. Tokumasu, *Molecular Dynamics Study of Proton Transfer including Grotthuss Mechanism in Polymer Electrolyte Membrane*. The Electrochemical Society, 2010. **33**(1): p. 1055-1065.
35. Collier, A., H. Wang, X. Ziyuan, J. Zhang, and D. Wilkinson, *Degradation of polymer electrolyte membranes*. International Journal of Hydrogen Energy, 2006. **31**(13): p. 1838-1854.
36. Chen, C., G. Levitin, D.W. Hess, and T.F. Fuller, *XPS investigation of Nafion® membrane degradation*. Journal of Power Sources, 2007. **169**(2): p. 288-295.
37. Chen, C. and T.F. Fuller, *The effect of humidity on the degradation of Nafion® membrane*. Polymer Degradation and Stability, 2009. **94**(9): p. 1436-1447.

38. Wu, J., X.Z. Yuan, J.J. Martin, H. Wang, J. Zhang, J. Shen, S. Wu, and W. Merida, *A review of PEM fuel cell durability: Degradation mechanisms and mitigation strategies*. Journal of Power Sources, 2008. **184**(1): p. 104-119.
39. Reimer, U., B. Schumacher, and W. Lehnert, *Accelerated Degradation of High-Temperature Polymer Electrolyte Fuel Cells: Discussion and Empirical Modeling*. Journal of The Electrochemical Society, 2014. **162**(1): p. F153-F164.
40. Angjeli, K., I. Nicotera, M. Baikousi, A. Enotiadis, D. Gournis, A. Saccà, E. Passalacqua, and A. Carbone, *Investigation of layered double hydroxide (LDH) Nafion-based nanocomposite membranes for high temperature PEFCs*. Energy Conversion and Management, 2015. **96**: p. 39-46.
41. Pinar, F.J., P. Cañizares, M.A. Rodrigo, D. Úbeda, and J. Lobato, *Long-term testing of a high-temperature proton exchange membrane fuel cell short stack operated with improved polybenzimidazole-based composite membranes*. Journal of Power Sources, 2015. **274**: p. 177-185.
42. Scott, K., C. Xu, and X. Wu, *Intermediate temperature proton-conducting membrane electrolytes for fuel cells*. Wiley Interdisciplinary Reviews: Energy and Environment, 2014. **3**(1): p. 24-41.
43. Yuan, X.-Z., H. Li, S. Zhang, J. Martin, and H. Wang, *A review of polymer electrolyte membrane fuel cell durability test protocols*. Journal of Power Sources, 2011. **196**(22): p. 9107-9116.
44. Kreur, K.D., S.J. Paddison, E. Spohr, and M. Schuster, *Transport in Proton Conductors for Fuel-Cell Applications: Simulations, Elementary Reactions, and Phenomenology*. Chemical Reviews, 2004. **104**: p. 4637-4678.
45. Feng, S. and G.A. Voth, *Proton solvation and transport in hydrated nafion*. J Phys Chem B, 2011. **115**(19): p. 5903-12.
46. Bai, H. and W.W. Ho, *Recent developments in fuel-processing and proton-exchange membranes for fuel cells*. Polymer International, 2010. **60**: p. 26-41.
47. Iojoiu, C., F. Chabert, M. Maréchal, N.E. Kissi, J. Guindet, and J.Y. Sanchez, *From polymer chemistry to membrane elaboration*. Journal of Power Sources, 2006. **153**(2): p. 198-209.
48. Zhang, H. and P.K. Shen, *Advances in the high performance polymer electrolyte membranes for fuel cells*. Chem Soc Rev, 2012. **41**(6): p. 2382-94.
49. Liu, Y.-L., *Developments of highly proton-conductive sulfonated polymers for proton exchange membrane fuel cells*. Polymer Chemistry, 2012. **3**(6): p. 1373.
50. Smitha, B., S. Sridhar, and A.A. Khan, *Solid polymer electrolyte membranes for fuel cell applications—a review*. Journal of Membrane Science, 2005. **259**(1-2): p. 10-26.
51. Cele, N. and S.S. Ray, *Recent Progress on Nafion-Based Nanocomposite Membranes for Fuel Cell Applications*, in *Macromolecular Materials and Engineering* 2009. p. 719-738.
52. Donnadio, A., M. Casciola, M.L. Di Vona, and M. Tamilvanan, *Conductivity and hydration of sulfonated polyethersulfone in the range 70–120°C: Effect of temperature and relative humidity cycling*, in *Journal of Power Sources* 2012. p. 145-150.
53. Park, J.-y., T.-H. Kim, K.H. Joong, J.-H. Choi, and Y.T. Hong, *Crosslinked sulfonated poly(arylene ether sulfone) membranes for fuel cell application*, in *International Journal of Hydrogen Energy* 2012. p. 2603-2613.
54. Jun, M.-S., Y.-W. Choi, and J.-D. Kim, *Solvent casting effects of sulfonated poly(ether ether ketone) for Polymer electrolyte membrane fuel cell*. Journal of Membrane Science, 2012. **396**: p. 32-37.
55. Silva, A.L.A., I. Takase, R.P. Pereira, and A.M. Rocco, *Poly(styrene-co-acrylonitrile) based proton conductive membranes*. European Polymer Journal, 2008. **44**(5): p. 1462-1474.
56. Wang, L., B.L. Yi, H.M. Zhang, Y.H. Liu, D.M. Xing, Z.G. Shao, and Y.H. Cai, *Sulfonated polyimide/PTFE reinforced membrane for PEMFCs*. Journal of Power Sources, 2007. **167**(1): p. 47-52.

57. Li, Q., R. He, J.O. Jensen, and N.J. Bjerrum, *Approaches and Recent Development of Polymer Electrolyte Membranes for Fuel Cells Operating above 100 °C*. Chemical Materials, 2003. **15**: p. 4896-4915.
58. Ahmed, M. and I. Dincer, *A review on methanol crossover in direct methanol fuel cells: challenges and achievements*. International Journal of Energy Research, 2011. **35**(14): p. 1213-1228.
59. Li, H., G. Zhang, J. Wu, C. Zhao, Q. Jia, C.M. Lew, L. Zhang, Y. Zhang, M. Han, and J. Zhu, *A facile approach to prepare self-cross-linkable sulfonated poly(ether ether ketone) membranes for direct methanol fuel cells*. Journal of Power Sources, 2010. **195**(24): p. 8061-8066.
60. Wu, B., M. Zhao, W. Shi, W. Liu, J. Liu, D. Xing, Y. Yao, Z. Hou, P. Ming, J. Gu, and Z. Zou, *The degradation study of Nafion/PTFE composite membrane in PEM fuel cell under accelerated stress tests*. International Journal of Hydrogen Energy, 2014.
61. Lu, S., R. Xiu, X. Xu, D. Liang, H. Wang, and Y. Xiang, *Polytetrafluoroethylene (PTFE) reinforced poly(ethersulphone)-poly(vinyl pyrrolidone) composite membrane for high temperature proton exchange membrane fuel cells*. Journal of Membrane Science, 2014. **464**: p. 1-7.
62. Alvarez, A., C. Guzmán, S. Rivas, L.A. Godinez, A. Saccà, A. Carbone, E. Passalacqua, L.G. Arriaga, and J. Ledesma-García, *Composites membranes based on Nafion and PAMAM dendrimers for PEMFC applications*. International Journal of Hydrogen Energy, 2014.
63. Lin, H.-L., T.L. Yu, L.-N. Huang, L.-C. Chen, K.-S. Shen, and G.-B. Jung, *Nafion/PTFE composite membranes for direct methanol fuel cell applications*. Journal of Power Sources, 2005. **150**: p. 11-19.
64. Lin, H.-L. and S.-H. Wang, *Nafion/poly(vinyl alcohol) nano-fiber composite and Nafion/poly(vinyl alcohol) blend membranes for direct methanol fuel cells*. Journal of Membrane Science, 2014. **452**: p. 253-262.
65. Hickner, M.A., H. Ghassemi, Y.S. Kim, B.R. Einsla, and J.E. McGrath, *Alternative Polymer Systems for Proton Exchange Membranes (PEMs)*. Chemical Reviews, 2004. **104**: p. 4587-4612.
66. Wu, X. and K. Scott, *A PFSA Composite Membrane with Sulfonic Acid Functionalized TiO₂Nanotubes for Polymer Electrolyte Fuel Cells and Water Electrolysers*. Fuel Cells, 2013. **13**(6): p. 1138-1145.
67. Mishra, P.S., J.N. Solanki, and Z.V.P. Murthy, *TiO₂nanoparticles synthesis for application in proton exchange membranes*. Crystal Research and Technology, 2013. **48**(11): p. 969-976.
68. Zapata, P., J.-H. Lee, and J.C. Meredith, *Composite proton exchange membranes from zirconium-based solid acids and PVDF/acrylic polyelectrolyte blends*. Journal of Applied Polymer Science, 2012. **124**(S1): p. E241-E250.
69. Chang, C.-M., H.-Y. Li, J.-Y. Lai, and Y.-L. Liu, *Nanocomposite membranes of Nafion and Fe₃O₄-anchored and Nafion-functionalized multiwalled carbon nanotubes exhibiting high proton conductivity and low methanol permeability for direct methanol fuel cells*. RSC Advances, 2013. **3**(31): p. 12895.
70. Adjemian, K.T., S.J. Lee, S. Srinivasan, J. Benziger, and A.B. Bocarsly, *Silicon Oxide Nafion Composite Membranes for Proton-Exchange Membrane Fuel Cell Operation at 80-140°C*, in *Journal of The Electrochemical Society*2002. p. A256-A261.
71. Ke, C.-C., X.-J. Li, S.-G. Qu, Z.-G. Shao, and B.-L. Yi, *Preparation and properties of Nafion/SiO₂ composite membrane derived via in situ sol-gel reaction: size controlling and size effects of SiO₂ nano-particles*. Polymers for Advanced Technologies, 2012. **23**(1): p. 92-98.
72. Kim, J.-Y., Y.-H. Ohn, K.-J. Ihn, and C. Lee, *Fabrication of inorganic/polymer nanocomposite membranes containing very high silica content via in situsurface grafting reaction and reactive dispersion of silica nanoparticles: Proton conduction, water uptake, and oxidative stability*. Journal of Applied Polymer Science, 2011. **119**(4): p. 2002-2009.

73. Thiam, H.S., W.R.W. Daud, S.K. Kamarudin, A.B. Mohamad, A.A.H. Kadhum, K.S. Loh, and E.H. Majlan, *Nafion/Pd-SiO₂ nanofiber composite membranes for direct methanol fuel cell applications*. International Journal of Hydrogen Energy, 2013. **38**(22): p. 9474-9483.
74. Tsai, C.-H., F.-L. Yang, C.-H. Chang, and Y.W. Chen-Yang, *Microwave-assisted synthesis of silica aerogel supported Pt nanoparticles for self-humidifying proton exchange membrane fuel cell*. International Journal of Hydrogen Energy, 2012. **37**(9): p. 7669-7676.
75. Peighambaroust, S.J., S. Rowshanzamir, M.G. Hosseini, and M. Yazdanpour, *Self-humidifying nanocomposite membranes based on sulfonated poly(ether ether ketone) and heteropolyacid supported Pt catalyst for fuel cells*. International Journal of Hydrogen Energy, 2011. **36**(17): p. 10940-10957.
76. Inaba, M., T. Kinumoto, M. Kiriake, R. Umebayashi, A. Tasaka, and Z. Ogumi, *Gas crossover and membrane degradation in polymer electrolyte fuel cells*. Electrochimica Acta, 2006. **51**(26): p. 5746-5753.
77. Devrim, Y., *Preparation and Testing of Nafion/Titanium Dioxide Nanocomposite Membrane Electrode Assembly by Ultrasonic Coating Technique*. Journal of Applied Polymer Science, 2014.
78. Zhang, G., J. Jiang, and J. Liu, *High proton conducting SPEEK/SiO₂/PWA composite membranes for direct methanol fuel cells*. Journal of Wuhan University of Technology-Mater. Sci. Ed., 2011. **26**(3): p. 417-421.
79. Lufrano, F., V. Baglio, O. Di Blasi, P. Staiti, V. Antonucci, and A.S. Arico, *Design of efficient methanol impermeable membranes for fuel cell applications*. Phys Chem Chem Phys, 2012. **14**(8): p. 2718-26.
80. Mustarelli, P., A. Carollo, S. Grandi, E. Quartarone, C. Tomasi, S. Leonardi, and A. Magistris, *Composite Proton-Conducting Membranes for PEMFCs*. Fuel Cells, 2007. **7**(6): p. 441-446.
81. Devrim, Y., S. Erkan, N. Baç, and I. Eroglu, *Nafion/titanium silicon oxide nanocomposite membranes for PEM fuel cells*. International Journal of Energy Research, 2013. **37**(5): p. 435-442.
82. Sangeetha Rani, G., M.K. Beera, and G. Pugazhenthii, *Development of sulfonated poly(ether ether ketone)/zirconium titanium phosphate composite membranes for direct methanol fuel cell*. Journal of Applied Polymer Science, 2012. **124**(S1): p. E45-E56.
83. Zhai, Y., H. Zhang, J. Hu, and B. Yi, *Preparation and characterization of sulfated zirconia (SO₄²⁻/ZrO₂)/Nafion composite membranes for PEMFC operation at high temperature/low humidity*. Journal of Membrane Science, 2006. **280**(1-2): p. 148-155.
84. Schlagenhaut, L., F. Nüesch, and J. Wang, *Release of Carbon Nanotubes from Polymer Nanocomposites*. Fibers, 2014. **2**(2): p. 108-127.
85. Oueiny, C., S. Berlioz, and F.-X. Perrin, *Carbon nanotube-polyaniline composites*. Progress in Polymer Science, 2014. **39**(4): p. 707-748.
86. Jandial, S. and P. Jindal, *Review of Carbon Nanotubes/Poly (methylmethacrylate) Composite Fabrication and Mechanical Characterization Techniques*. International Journal of Research in Advent Technology, 2014. **2**: p. 2321-9637.
87. Thostenson, E.T., Z. Ren, and T.-W. Chou, *Advances in the science and technology of carbon nanotubes and their composites: a review*. Composites Science and Technology, 2001. **61**: p. 1899-1912.
88. Kannan, R., P.P. Aher, T. Palaniselvam, S. Kurungot, U.K. Kharul, and V.K. Pillai, *Artificially Designed Membranes Using Phosphonated Multiwall Carbon Nanotube-Polybenzimidazole Composites for Polymer Electrolyte Fuel Cells*. The Journal of Physical Chemistry Letters, 2010. **1**: p. 2109-2113.
89. Asgari, M.S., M. Nikazar, P. Molla-abbasi, and M.M. Hasani-Sadrabadi, *Nafion®/histidine functionalized carbon nanotube: High-performance fuel cell membranes*. International Journal of Hydrogen Energy, 2013. **38**(14): p. 5894-5902.

90. Jiang, D., V. Cooper, and S. Dai, *Porous Graphene as the Ultimate Membrane for Gas Separation*. *Nano Letters*, 2009. **9**: p. 4019-4024.
91. Sun, Y. and G. Shi, *Graphene/Polymer Composites for Energy Applications*, in *Journal of Polymer Science* 2013. p. 231–253.
92. Ye, Y.-S., C.-Y. Tseng, W.-C. Shen, J.-S. Wang, K.-J. Chen, M.-Y. Cheng, J. Rick, Y.-J. Huang, F.-C. Chang, and B.-J. Hwang, *A new graphene-modified protic ionic liquid-based composite membrane for solid polymer electrolytes*. *Journal of Materials Chemistry*, 2011. **21**(28): p. 10448.
93. Dreyer, D.R., S. Park, C.W. Bielawski, and R.S. Ruoff, *The chemistry of graphene oxide*. *Chem Soc Rev*, 2010. **39**(1): p. 228-40.
94. Staudenmaier, L., *Verfahren zur Darstellung der Graphitsaure*. *Berichte der deutschen chemischen Gesellschaft*, 1898. **31**(2): p. 1481-1287.
95. Tang, Q., Z. Zhou, and Z. Chen, *Graphene-related nanomaterials: tuning properties by functionalization*. *Nanoscale*, 2013. **5**(11): p. 4541-83.
96. Pumera, M., *Electrochemistry of graphene, graphene oxide and other graphenoids: Review*. *Electrochemistry Communications*, 2013. **36**: p. 14-18.
97. Chiu, N.-F., T.-Y. Huang, and H.-C. Lai, *Graphene Oxide Based Surface Plasmon Resonance Biosensors*, in *Advances in Graphene Science*, M. Aliofkhazraei, Editor 2013.
98. Choi, B.G., Y.S. Huh, Y.C. Park, D.H. Jung, W.H. Hong, and H. Park, *Enhanced transport properties in polymer electrolyte composite membranes with graphene oxide sheets*. *Carbon*, 2012. **50**(15): p. 5395-5402.
99. Chien, H.-C., L.-D. Tsai, C.-P. Huang, C.-y. Kang, J.-N. Lin, and F.-C. Chang, *Sulfonated graphene oxide/Nafion composite membranes for high-performance direct methanol fuel cells*, in *International Journal of Hydrogen Energy* 2013. p. 13792-13801.
100. Zarrin, H., H. Drew, Y. Jun, Z. Chen, and M. Fowler, *Functionalized Graphene Oxide Nanocomposite Membrane for Low Humidity and High Temperature Proton Exchange Membrane Fuel Cells*, in *The Journal of Physical Chemistry C* 2011. p. 20774-20781.
101. Cao, Y.-C., C. Xu, X. Wu, X. Wang, L. Xing, and K. Scott, *A poly (ethylene oxide)/graphene oxide electrolyte membrane for low temperature polymer fuel cells*, in *Journal of Power Sources* 2011. p. 8377-8382.
102. Heo, Y., H. Im, and J. Kim, *The effect of sulfonated graphene oxide on Sulfonated Poly (Ether Ether Ketone) membrane for direct methanol fuel cells*, in *Journal of Membrane Science* 2013. p. 11-22.
103. Jiang, Z., X. Zhao, Y. Fu, and M. Manthiram, *Composite membranes based on sulfonated poly(ether ether ketone) and SDBS-adsorbed graphene oxide for direct methanol fuel cells*, in *Journal of Materials Chemistry* 2012.
104. Lin, C.W. and Y.S. Lu, *Highly ordered graphene oxide paper laminated with a Nafion membrane for direct methanol fuel cells*, in *Journal of Power Sources* 2013. p. 187-194.
105. Kumar, R., C. Xu, and K. Scott, *Graphite oxide/Nafion composite membranes for polymer electrolyte fuel cells*. *RSC Advances*, 2012. **2**(23): p. 8777-8782.
106. Paredes, J.I., S. Villar-Rodil, A. Martínez-Alonso, and J.M.D. Tascon, *Graphene Oxide Dispersions in Organic Solvents*. *Langmuir*, 2008. **24**: p. 10560-10564.
107. Lee, D.C., H.N. Yang, S.H. Park, and W.J. Kim, *Nafion/graphene oxide composite membranes for low humidifying polymer electrolyte membrane fuel cell*. *Journal of Membrane Science*, 2014. **452**: p. 20-28.
108. Choi, B.G., Y.S. Huh, Y.C. Park, D.H. Jung, W.H. Hong, and H. Park, *Enhanced transport properties in polymer electrolyte composite membranes with graphene oxide sheets*, in *Carbon* 2012. p. 5395-5402.
109. Huang, L.-N., L.-C. Chen, T.L. Yu, and H.-L. Lin, *Nafion/PTFE/silicate composite membranes for direct methanol fuel cells*. *Journal of Power Sources*, 2006. **161**(2): p. 1096-1105.

110. Chen, L.-C., T.L. Yu, H.-L. Lin, and S.-H. Yeh, *Nafion/PTFE and zirconium phosphate modified Nafion/PTFE composite membranes for direct methanol fuel cells*. Journal of Membrane Science, 2008. **307**(1): p. 10-20.
111. Choi, B.G., J. Hong, Y.C. Park, D.H. Jung, W.H. Hong, P.T. Hammond, and H.S. Park, *Innovative Polymer Nanocomposite Electrolytes: Nanoscale Manipulation of Ion Channels by Functionalized Graphenes*. ACS Nano, 2011. **5**: p. 5167–5174.
112. Lee, D.C., H.N. Yang, S.H. Park, K.W. Park, and W.J. Kim, *Self-humidifying Pt-graphene/SiO₂ composite membrane for polymer electrolyte membrane fuel cell*. Journal of Membrane Science, 2015. **474**: p. 254-262.
113. Ketpang, K., B. Son, D. Lee, and S. Shanmugam, *Porous zirconium oxide nanotube modified Nafion composite membrane for polymer electrolyte membrane fuel cells operated under dry conditions*. Journal of Membrane Science, 2015. **488**: p. 154-165.
114. Jana, R.N., B. Maity, S. Mallick, A. Majumdar, and P. Singh, *Nanostructured Ionomeric Membranes for Direct Methanol Fuel Cell*. Indian Chemical Engineer, 2015. **57**(2): p. 103-114.
115. Padilha, J.C., J. Basso, L.G. da Trindade, E.M.A. Martini, M.O. de Souza, and R.F. de Souza, *Ionic liquids in proton exchange membrane fuel cells: Efficient systems for energy generation*. Journal of Power Sources, 2010. **195**(19): p. 6483-6485.
116. Xu, C., X. Liu, J. Cheng, and K. Scott, *A polybenzimidazole/ionic-liquid-graphite-oxide composite membrane for high temperature polymer electrolyte membrane fuel cells*. Journal of Power Sources, 2015. **274**: p. 922-927.
117. Lee, S.-Y., T. Yasuda, and M. Watanabe, *Fabrication of protic ionic liquid/sulfonated polyimide composite membranes for non-humidified fuel cells*. Journal of Power Sources, 2010. **195**(18): p. 5909-5914.
118. Malik, R.S., P. Verma, and V. Choudhary, *A study of new anhydrous, conducting membranes based on composites of aprotic ionic liquid and cross-linked SPEEK for fuel cell application*. Electrochimica Acta, 2015. **152**: p. 352-359.
119. Liu, S., L. Zhou, P. Wang, F. Zhang, S. Yu, Z. Shao, and B. Yi, *Ionic-liquid-based proton conducting membranes for anhydrous H₂/Cl₂ fuel-cell applications*. ACS Appl Mater Interfaces, 2014. **6**(5): p. 3195-200.
120. Shan, W., P. Bacchin, P. Aimar, M.L. Bruening, and V.V. Tarabara, *Polyelectrolyte multilayer films as backflushable nanofiltration membranes with tunable hydrophilicity and surface charge*. Journal of Membrane Science, 2010. **349**(1-2): p. 268-278.
121. Hong, S.U., R. Malaisamy, and M.L. Bruening, *Separation of Fluoride from Other Monovalent Anions Using Multilayer Polyelectrolyte Nanofiltration Membranes*. Langmuir, 2007. **23**.
122. Sheng, C., S. Wijeratne, C. Cheng, G.L. Baker, and M.L. Bruening, *Facilitated Ion Transport through Polyelectrolyte Multilayer Films Containing Metal-binding Ligands*. Journal of Membrane Science, 2014.
123. Ouyang, L., R. Malaisamy, and M.L. Bruening, *Multilayer polyelectrolyte films as nanofiltration membranes for separating monovalent and divalent cations*. Journal of Membrane Science, 2008. **310**(1-2): p. 76-84.
124. Stanton, B.W., J.J. Harris, M.D. Miller, and M.L. Bruening, *Ultrathin, Multilayered Polyelectrolyte Films as Nanofiltration Membranes*. Langmuir, 2003. **19**.
125. Malaisamy, R. and M.L. Bruening, *High-Flux Nanofiltration Membranes Prepared by Adsorption of Multilayer Polyelectrolyte Membranes on Polymeric Supports*. Langmuir, 2005. **21**.
126. Mulyati, S., R. Takagi, A. Fujii, Y. Ohmukai, and H. Matsuyama, *Simultaneous improvement of the monovalent anion selectivity and antifouling properties of an anion exchange membrane in an electrodialysis process, using polyelectrolyte multilayer deposition*. Journal of Membrane Science, 2013. **431**: p. 113-120.

127. Yang, B. and A. Manthiram, *Multilayered membranes with suppressed fuel crossover for direct methanol fuel cells*. *Electrochemistry Communications*, 2004. **6**(3): p. 231-236.
128. Chen, S.-L., A.B. Bocarsly, and J. Benzinger, *Nafion-layered sulfonated polysulfone fuel cell membranes*, in *Journal of Power Sources* 2005. p. 27-33.
129. Peng, A.Z., A. Morin, P. Hugué, Y. Lanteri, and S. Deabate, *Asymmetric bi-layer PFSA membranes as model systems for the study of water management in the PEMFC*. *Physical Chemistry Chemical Physics*, 2014.
130. Wu, Q.X., T.S. Zhao, R. Chen, and L. An, *A sandwich structured membrane for direct methanol fuel cells operating with neat methanol*. *Applied Energy*, 2013. **106**: p. 301-306.
131. Gao, W., G. Wu, M.T. Janicke, D.A. Cullen, R. Mukundan, J.K. Baldwin, E.L. Brosha, C. Galande, P.M. Ajayan, K.L. More, A.M. Dattelbaum, and P. Zelany, *Ozonated Graphene Oxide Film as a Proton-Exchange Membrane*. *Angewandte Chemie*, 2014. **126**: p. 3662–3667.
132. Li, W. and A. Manthiram, *Sulfonated poly(arylene ether sulfone) as a methanol-barrier layer in multilayer membranes for direct methanol fuel cells*. *Journal of Power Sources*, 2010. **195**(4): p. 962-968.
133. Jiang, S.P. and H. Tang, *Methanol crossover reduction by Nafion modification via layer-by-layer self-assembly techniques*. *Colloids and Surfaces A: Physicochemical and Engineering Aspects*, 2012. **407**: p. 49-57.
134. Argun, A.A., J.N. Ashcraft, and P.T. Hammond, *Highly Conductive, Methanol Resistant Polyelectrolyte Multilayers*. *Advanced Materials*, 2008. **20**(8): p. 1539-1543.
135. Yang, T., S.X. Zhang, Y. Gao, F.C. Ji, and T.W. Liu, *Multilayer Membranes Based on Sulfonated Poly(Ether Ether Ketone) and Poly(Vinyl Alcohol) for Direct Methanol Membrane Fuel Cells*. *The Open Fuel Cells Journal*, 2008. **1**: p. 4-8.
136. Luo, Q.T., H.M. Zhang, J. Chen, D.J. You, C.X. Sun, and Y. Zhang, *Preparation and characterization of Nafion/SPEEK layered composite membrane and its application in vanadium redox flow battery*. *Journal of Membrane Science*, 2008. **325**(2): p. 553-558.
137. Marrony, M., J. Roziere, D.J. Jones, and A. Lindheimer, *Multilayer Sulfonated Polyaromatic PEMFC Membranes*. *Fuel Cells*, 2005. **5**.
138. Li, X., Y. Song, Z. Liu, P. Feng, S. Liu, Y. Yu, Z. Jiang, and B. Liu, *Triple-layer sulfonated poly(ether ether ketone)/sulfonated polyimide membranes for fuel cell applications*. *High Performance Polymers*, 2013. **26**(1): p. 106-113.
139. Lee, J.-R., J.-H. Won, K.-S. Yoon, Y.T. Hong, and S.-Y. Lee, *Multilayer-structured, SiO₂/sulfonated poly(phenylsulfone) composite membranes for proton exchange membrane fuel cells*. *International Journal of Hydrogen Energy*, 2012. **37**(7): p. 6182-6188.
140. Hasani-Sadrabadi, M.M., E. Dashtimoghadam, N. Mokarram, F.S. Majedi, and K.I. Jacob, *Triple-layer proton exchange membranes based on chitosan biopolymer with reduced methanol crossover for high-performance direct methanol fuel cells application*. *Polymer*, 2012. **53**(13): p. 2643-2651.
141. Padmavathi, R., R. Karthikumar, and D. Sangeetha, *Multilayered sulphonated polysulfone/silica composite membranes for fuel cell applications*. *Electrochimica Acta*, 2012. **71**: p. 283-293.
142. Hasani-Sadrabadi, M.M., E. Dashtimoghadam, F.S. Majedi, S. Hojjati Emami, and H. Moaddel, *A high-performance chitosan-based double layer proton exchange membrane with reduced methanol crossover*. *International Journal of Hydrogen Energy*, 2011. **36**(10): p. 6105-6111.
143. Wang, L., B.L. Yi, H.M. Zhang, and D.M. Xing, *Pt/SiO₂ as addition to multilayer SPSU/PTFE composite membrane for fuel cells*. *Polymers for Advanced Technologies*, 2008. **19**(12): p. 1809-1815.
144. Wang, L., B.L. Yi, H.M. Zhang, Y.H. Liu, D.M. Xing, Z.G. Shao, and Y.H. Cai, *Novel multilayer Nafion/SPI/Nafion composite membrane for PEMFCs*. *Journal of Power Sources*, 2007. **164**(1): p. 80-85.

145. Lin, C.-C., W.-F. Lien, Y.-Z. Wang, H.-W. Shiu, and C.-H. Lee, *Preparation and performance of sulfonated polyimide/Nafion multilayer membrane for proton exchange membrane fuel cell*. Journal of Power Sources, 2012. **200**: p. 1-7.
146. Zhong, S., X. Cui, C. Sun, S. Dou, and W. Liu, *Crosslinked organic/inorganic proton exchange membranes with multilayer structure*. Solid State Ionics, 2012. **227**: p. 91-95.
147. Yuan, T., L. Pu, Q. Huang, H. Zhang, X. Li, and H. Yang, *An effective methanol-blocking membrane modified with graphene oxide nanosheets for passive direct methanol fuel cells*. Electrochimica Acta, 2014. **117**: p. 393-397.
148. Liu, W., S. Wang, M. Xiao, D. Han, and Y. Meng, *A proton exchange membrane fabricated from a chemically heterogeneous nonwoven with sandwich structure by the program-controlled co-electrospinning process*. Chem Commun (Camb), 2012. **48**(28): p. 3415-7.
149. Li, S., S. Zhang, Q. Zhang, and G. Qin, *Assembly of an unbalanced charged polyampholyte onto Nafion(R) to produce high-performance composite membranes*. Chem Commun (Camb), 2012. **48**(100): p. 12201-3.
150. Zhao, C., H. Lin, Q. Zhang, and H. Na, *Layer-by-layer self-assembly of polyaniline on sulfonated poly(arylene ether ketone) membrane with high proton conductivity and low methanol crossover*. International Journal of Hydrogen Energy, 2010. **35**(19): p. 10482-10488.
151. Yilmaztürk, S., H. Deligöz, M. Yilmazoğlu, H. Damyan, F. Öksüzömer, S.N. Koç, A. Durmuş, and M.A. Gürkaynak, *A novel approach for highly proton conductive electrolyte membranes with improved methanol barrier properties: Layer-by-Layer assembly of salt containing polyelectrolytes*. Journal of Membrane Science, 2009. **343**(1-2): p. 137-146.
152. Yang, M., S. Lu, J. Lu, S.P. Jiang, and Y. Xiang, *Layer-by-layer self-assembly of PDDA/PWA-Nafion composite membranes for direct methanol fuel cells*. Chem Commun (Camb), 2010. **46**(9): p. 1434-6.
153. Son, H.D., M.S. Cho, J.D. Nam, S.M. Cho, C.H. Chung, H.G. Choi, and Y. Lee, *Depression of methanol-crossover using multilayer proton conducting membranes prepared by layer-by-layer deposition onto a porous polyethylene film*. Journal of Power Sources, 2006. **163**(1): p. 66-70.
154. Lin, H., C. Zhao, W. Ma, H. Li, and H. Na, *Layer-by-layer self-assembly of in situ polymerized polypyrrole on sulfonated poly(arylene ether ketone) membrane with extremely low methanol crossover*. International Journal of Hydrogen Energy, 2009. **34**(24): p. 9795-9801.
155. Lin, H., C. Zhao, W. Ma, H. Li, and H. Na, *Low water swelling and high methanol resistant proton exchange membrane fabricated by cross-linking of multilayered polyelectrolyte complexes*. Journal of Membrane Science, 2009. **345**(1-2): p. 242-248.
156. Smit, M.A., A.L. Ocampo, M.A. Espinosa-Medina, and P.J. Sebastián, *A modified Nafion membrane with in situ polymerized polypyrrole for the direct methanol fuel cell*. Journal of Power Sources, 2003. **124**(1): p. 59-64.
157. Brum, F.J.B., F.N. Laux, and M.M.C. Forte, *Synthesis of hydrocarbon polymers by cationic polymerization and their thermal properties*. Designed Monomers and Polymers, 2013. **16**(3): p. 291-301.
158. Brum, F.J.B., F.G. Zanatta, E.S. Marczyński, M.M.C. Forte, and B. Pollet, *Synthesis and characterisation of a new sulphonated hydrocarbon polymer for application as a solid proton-conducting electrolyte*. Solid State Ionics, 2014. **263**: p. 62-70.
159. Hummers, W.S. and R.E. Offeman, *Preparation of Graphitic Oxide*. J Am Chem Soc, 1958. **80**: p. 1339.
160. Chen, J., B. Yao, C. Li, and G. Shi, *An improved Hummers method for eco-friendly synthesis of graphene oxide*. Carbon, 2013. **64**: p. 225-229.
161. Wu, L.-L., J.-j. Wang, X. He, T. Zhang, and H. Sun, *Using Graphene Oxide to Enhance the Barrier Properties of Poly(lactic acid) Film*. Packaging Technology and Science, 2014: p. n/a-n/a.

162. Xue, C., J. Zou, Z. Sun, F. Wang, K. Han, and H. Zhu, *Graphite oxide/functionalized graphene oxide and polybenzimidazole composite membranes for high temperature proton exchange membrane fuel cells*. International Journal of Hydrogen Energy, 2014. **39**(15): p. 7931-7939.
163. Sharma, S., A. Ganguly, P. Papakonstantinou, X. Miao, M. Li, J.L. Hutchison, M. Delichatsios, and S. Ukleja, *Rapid Microwave Synthesis of CO Tolerant Reduced Graphene Oxide-Supported Platinum Electrocatalysts for Oxidation of Methanol*. Journal of Physical Chemistry C, 2010. **114**: p. 19459-19466.
164. Stankovich, S., D.A. Dikin, R.D. Piner, K.A. Kohlhaas, A. Kleinhammes, Y. Jia, Y. Wu, S.T. Nguyen, and R.S. Ruoff, *Synthesis of graphene-based nanosheets via chemical reduction of exfoliated graphite oxide*. Carbon, 2007. **45**(7): p. 1558-1565.
165. Jeong, H.-K., Y.P. Lee, R.J.W.E. Lahaye, M.-H. Park, K.H. An, I.J. Kim, C.W. Yang, C.Y. Park, R.S. Ruoff, and Y.H. Lee, *Evidence of Graphitic AB Stacking Order of Graphite Oxides*. Journal of The American Chemical Society, 2008. **130**(1362-1366).
166. Ganguly, A., S. Sharma, P. Papakonstantinou, and J. Hamilton, *Probing the Thermal Deoxygenation of Graphene Oxide Using High-Resolution In Situ X-ray-Based Spectroscopies*. The Journal of Physical Chemistry C, 2011. **115**(34): p. 17009-17019.
167. Bayer, T., S.R. Bishop, M. Nishihara, K. Sasaki, and S.M. Lyth, *Characterization of a graphene oxide membrane fuel cell*. Journal of Power Sources, 2014. **272**: p. 239-247.
168. Wang, F., M. Hickner, Y.S. Kim, T.A. Zawodzinski, and J.E. McGrath, *Direct polymerization of sulfonated poly(arylene ether sulfone) random (statistical) copolymers: candidates for new proton exchange membranes*. Journal of Membrane Science, 2002. **197**(1-2): p. 231-242.
169. Chen, W., L. Yan, and P.R. Bangal, *Preparation of graphene by the rapid and mild thermal reduction of graphene oxide induced by microwaves*. Carbon, 2010. **48**(4): p. 1146-1152.
170. Paredes, J.I., S. Villar-Rodil, P. Solis-Fernandez, A. Martinez-Alonso, and J.M. Tascon, *Atomic force and scanning tunneling microscopy imaging of graphene nanosheets derived from graphite oxide*. Langmuir, 2009. **25**(10): p. 5957-68.
171. Dikin, D.A., S. Stankovich, E.J. Zimney, R.D. Piner, G.H. Dommett, G. Evmenenko, S.T. Nguyen, and R.S. Ruoff, *Preparation and characterization of graphene oxide paper*. Nature, 2007. **448**(7152): p. 457-60.
172. Chua, L.L., S. Wang, P.J. Chia, L. Chen, L.H. Zhao, W. Chen, A.T. Wee, and P.K. Ho, *Deoxidation of graphene oxide nanosheets to extended graphenites by "unzipping" elimination*. J Chem Phys, 2008. **129**(11): p. 114702.
173. Vengatesan, S., E. Cho, H.-J. Kim, and T.-H. Lim, *Effects of curing condition of solution cast Nafion® membranes on PEMFC performance*. Korean Journal of Chemical Engineering, 2009. **26**(3): p. 679-684.
174. Laporta, M., M. Pegoraro, and L. Zanderighi, *Recast Nafion-117 thin film from water solution*. Macromolecular Materials and Engineering, 2000. **282**: p. 22-29.
175. Zook, L.A. and J. Leddy, *Density and Solubility of Nafion: Recast, Annealed, and Commercial Films*. Analytical Chemistry, 1996. **68**(21): p. 3793-3796.
176. Moore, R.B., III and C.R. Martin, *Chemical and Morphological Properties of Solution-Cast Perfluorosulfonate Ionomers*. Macromolecules, 1988. **21**: p. 1334-1339.
177. Gebel, G., P. Aldebert, and M. Pineri, *Structure and Related Properties of Solution-Cast Perfluorosulfonated Ionomer Films*. Macromolecules, 1987. **20**: p. 1425-1428.
178. Jung, H.-Y., K.-Y. Cho, Y.M. Lee, J.-K. Park, J.-H. Choi, and Y.-E. Sung, *Influence of annealing of membrane electrode assembly (MEA) on performance of direct methanol fuel cell (DMFC)*. Journal of Power Sources, 2007. **163**(2): p. 952-956.
179. Liu, X., S. He, Z. Shi, L. Zhang, and J. Lin, *Effect of residual casting solvent content on the structure and properties of sulfonated poly(ether ether ketone) membranes*. Journal of Membrane Science, 2015. **492**: p. 48-57.

180. Robertson, G.P., S.D. Mikhailenko, K. Wang, P. Xing, M.D. Guiver, and S. Kaliaguine, *Casting solvent interactions with sulfonated poly(ether ether ketone) during proton exchange membrane fabrication*. *Journal of Membrane Science*, 2003. **219**(1-2): p. 113-121.
181. Cheng, Q., M. Wu, M. Li, L. Jiang, and Z. Tang, *Ultratough artificial nacre based on conjugated cross-linked graphene oxide*. *Angew Chem Int Ed Engl*, 2013. **52**(13): p. 3750-5.
182. Putz, K.W., O.C. Compton, M.J. Palmeri, S.T. Nguyen, and L.C. Brinson, *High-Nanofiller-Content Graphene Oxide-Polymer Nanocomposites via Vacuum-Assisted Self-Assembly*. *Advanced Functional Materials*, 2010. **20**(19): p. 3322-3329.
183. Xu, Y., W. Hong, H. Bai, C. Li, and G. Shi, *Strong and ductile poly(vinyl alcohol)/graphene oxide composite films with a layered structure*. *Carbon*, 2009. **47**(15): p. 3538-3543.
184. Hu, K., L.S. Tolentino, D.D. Kulkarni, C. Ye, S. Kumar, and V.V. Tsukruk, *Written-in conductive patterns on robust graphene oxide biopaper by electrochemical microstamping*. *Angew Chem Int Ed Engl*, 2013. **52**(51): p. 13784-8.
185. Niu, Z., J. Chen, H.H. Hng, J. Ma, and X. Chen, *A leavening strategy to prepare reduced graphene oxide foams*. *Adv Mater*, 2012. **24**(30): p. 4144-50.
186. Putz, K.W., O.C. Compton, C. Segar, Z. An, S.T. Nguyen, and L.C. Brinson, *Evolution of Order During Vacuum-Assisted Self-Assembly of Graphene Oxide Paper and Associated Polymer Nanocomposites*. *ACS Nano*, 2011. **5**(8): p. 6601-6609.
187. Huang, Z.-D., B. Zhang, S.-W. Oh, Q.-B. Zheng, X.-Y. Lin, N. Yousefi, and J.-K. Kim, *Self-assembled reduced graphene oxide/carbon nanotube thin films as electrodes for supercapacitors*. *Journal of Materials Chemistry*, 2012. **22**(8): p. 3591.
188. Chen, C.-M., J.-Q. Huang, Q. Zhang, W.-Z. Gong, Q.-H. Yang, M.-Z. Wang, and Y.-G. Yang, *Annealing a graphene oxide film to produce a free standing high conductive graphene film*. *Carbon*, 2012. **50**(2): p. 659-667.
189. Park, S., J. An, J.R. Potts, A. Velamakanni, S. Murali, and R.S. Ruoff, *Hydrazine-reduction of graphite- and graphene oxide*. *Carbon*, 2011. **49**(9): p. 3019-3023.
190. Han, D., L. Yan, W. Chen, W. Li, and P.R. Bangal, *Cellulose/graphite oxide composite films with improved mechanical properties over a wide range of temperature*. *Carbohydrate Polymers*, 2011. **83**(2): p. 966-972.
191. Khan, R., A. Kaushik, P.R. Solanki, A.A. Ansari, M.K. Pandey, and B.D. Malhotra, *Zinc oxide nanoparticles-chitosan composite film for cholesterol biosensor*. *Anal Chim Acta*, 2008. **616**(2): p. 207-13.
192. Bissessur, R., P.K.Y. Liu, W. White, and S.F. Scully, *Encapsulation of Polyanilines into Graphite Oxide*. *Langmuir*, 2005. **22**: p. 1729-1734.
193. Cote, L.J., R. Cruz-Silva, and J. Huang, *Flash Reduction and Patterning of Graphite Oxide and Its Polymer Composite*. *Journal of American Chemical Society*, 2009. **131**: p. 11027-11032.
194. Bissessur, R., P.K.Y. Liu, and S.F. Scully, *Intercalation of polypyrrole into graphite oxide*. *Synthetic Metals*, 2006. **156**(16-17): p. 1023-1027.
195. Jung, H.-Y. and J.W. Kim, *Role of the glass transition temperature of Nafion 117 membrane in the preparation of the membrane electrode assembly in a direct methanol fuel cell (DMFC)*. *International Journal of Hydrogen Energy*, 2012. **37**(17): p. 12580-12585.
196. Venables, J.D., *Adhesion and durability of metal-polymer bonds*. *Journal of Materials Science*, 1984. **19**: p. 2431-2453.
197. Kumpfer, J.R. and S.J. Rowan, *Directed Self-Assembly of Metallosupramolecular Polymers at the Polymer-Polymer Interface*. *ACS Macro Letters*, 2012. **1**(7): p. 882-887.
198. Awaja, F., M. Gilbert, G. Kelly, B. Fox, and P.J. Pigram, *Adhesion of polymers*. *Progress in Polymer Science*, 2009. **34**(9): p. 948-968.
199. Wang, L., J. Kang, J.D. Nam, J. Suhr, A.K. Prasad, and S.G. Advani, *Composite Membrane Based on Graphene Oxide Sheets and Nafion for Polymer Electrolyte Membrane Fuel Cells*. *ECS Electrochemistry Letters*, 2014. **4**(1): p. F1-F4.

200. Liang, Z.X., T.S. Zhao, C. Xu, and J.B. Xu, *Microscopic characterizations of membrane electrode assemblies prepared under different hot-pressing conditions*. *Electrochimica Acta*, 2007. **53**(2): p. 894-902.
201. Kim, H.-M., S. Sohn, and J.S. Ahn, *Transparent and super-hydrophobic properties of PTFE films coated on glass substrate using RF-magnetron sputtering and Cat-CVD methods*. *Surface and Coatings Technology*, 2013. **228**: p. S389-S392.
202. Carbonell, J.M., I.S. Martin, A. Santos, A. Pujol, J.D. Sanz-Moliner, and J. Nart, *High-density polytetrafluoroethylene membranes in guided bone and tissue regeneration procedures: a literature review*. *Int J Oral Maxillofac Surg*, 2014. **43**(1): p. 75-84.
203. Quéré, D., *Non-sticking drops*. *Reports on Progress in Physics*, 2005. **68**(11): p. 2495-2532.
204. Phillip, W.A., B. O'Neill, M. Rodwogin, M.A. Hillmyer, and E.L. Cussler, *Self-assembled block copolymer thin films as water filtration membranes*. *ACS Appl Mater Interfaces*, 2010. **2**(3): p. 847-53.
205. Azad, A.K., N. Sermsintham, S. Chandkrachang, and W.F. Stevens, *Chitosan membrane as a wound-healing dressing: characterization and clinical application*. *J Biomed Mater Res B Appl Biomater*, 2004. **69**(2): p. 216-22.
206. Wolfbeis, O.S., M. Schaferling, and A. Durkop, *Reversible Optical Sensor Membrane for Hydrogen Peroxide Using an Immobilized Fluorescent Probe, and its Application to a Glucose Biosensor*. *Microchimica Acta*, 2003. **143**(4): p. 221-227.
207. Banerjee, S. and D.E. Curtin, *Nafion® perfluorinated membranes in fuel cells*. *Journal of Fluorine Chemistry*, 2004. **125**(8): p. 1211-1216.
208. Budd, P.M., E.S. Elabas, B.S. Ghanem, S. Makhseed, N.B. McKeown, K.J. Msayib, C.E. Tattershall, and D. Wang, *Solution-Processed, Organophilic Membrane Derived from a Polymer of Intrinsic Microporosity*. *Advanced Materials*, 2004. **16**(5): p. 456-459.
209. Pekny, M.R., A.R. Greenberg, V. Khare, J. Zartman, W.B. Krantz, and P. Todd, *Macrovoid pore formation in dry-cast cellulose acetate membranes: buoyancy studies*. *Journal of Membrane Science*, 2002. **205**: p. 11-21.
210. Ma, W., C. Yang, X. Gong, K. Lee, and A.J. Heeger, *Thermally Stable, Efficient Polymer Solar Cells with Nanoscale Control of Interpenetrating Network Morphology*. *Advanced Functional Materials*, 2005. **15**: p. 1616-1622.
211. Chirvase, D., J. Parisi, J.C. Hummelen, and V. Dyakonov, *Influence of nanomorphology on the photovoltaic action of polymer–fullerene composites*. *Nanotechnology*, 2004. **15**(9): p. 1317-1323.
212. Bakangura, E., L. Ge, M. Muhammad, J. Pan, L. Wu, and T. Xu, *Sandwich structure SPPO/BPPO proton exchange membranes for fuel cells: Morphology–electrochemical properties relationship*. *Journal of Membrane Science*, 2015. **475**: p. 30-38.
213. Hattenberger, M., *Composite Proton Exchange Membranes for Intermediate Temperature Fuel Cells*, in *School of Chemical Engineering 2015*, University of Birmingham. p. 264.
214. Loser, N., *Desenvolvimento de Membranas mistas a Base de Poli(indeno) Sulfonado e PVA Reticulado com Objetivo de Aplicacao em Célula a Combustível Tipo PEM*, in *School of Engineering 2011*, Universidade Federal do Rio Grande do Sul. p. 70.
215. Brum, F.J.B., *Membranas Catiônicas a Base de Poli(indeno) Sulfonado/PVA para Uso como Eletrólito em Célula a Combustível tipo PEMFC*, in *School of Engineering 2013*, Universidade Federal do Rio Grande do Sul. p. 149.
216. Binsu, V.V., R.K. Nagarale, and V.K. Shahi, *Phosphonic acid functionalized aminopropyl triethoxysilane–PVA composite material: organic–inorganic hybrid proton-exchange membranes in aqueous media*. *Journal of Materials Chemistry*, 2005. **15**(45): p. 4823.
217. Chen, S.-L., A.B. Bocarsly, and J. Benziger, *Nafion-layered sulfonated polysulfone fuel cell membranes*. *Journal of Power Sources*, 2005. **152**: p. 27-33.

218. Yildiz, Y. and M.M. Sundaram, *Cryogenic machining of composites*, in *Machining Technology for Composite Materials*, H. Hocheng, Editor 2011, Elsevier. p. 488.
219. DeLongchamp, D.M. and P.T. Hammond, *Fast Ion Conduction in Layer-By-Layer Polymer Films*. *Chemistry of Materials*, 2003. **15**: p. 1165-1173.
220. Decker, B., C. Hartmann-Thompson, P.I. Carver, S.E. Keinath, and P.R. Santurri, *Multilayer Sulfonated Polyhedral Oligosilsesquioxane (S-POSS)-Sulfonated Polyphenylsulfone (S-PPSU) Composite Proton Exchange Membranes†*. *Chemistry of Materials*, 2010. **22**(3): p. 942-948.
221. De Martino, F., N. Vattistas, and V. Tricoli, *Concept to Design Membranes for PEMFC: Triple-Layer Ion-Conducting Membrane*. *Journal of The Electrochemical Society*, 2009. **156**(1): p. B59.
222. Jiang, R., H.R. Kunz, and J.M. Fenton, *Multilayer Structure Membranes with Sulfonated Hydrocarbon Methanol Barrier for Direct Methanol Fuel Cells*. *Journal of The Electrochemical Society*, 2006. **153**(8): p. A1554.
223. Pinnau, I. and B.D. Freeman, *Formation and Modification of Polymeric Membranes: Overview*. 1999. **744**: p. 1-22.
224. Kamiya, M., M. Yoshizawa-Fujita, Y. Takeoka, and M. Rikukawa, *Preparation and characterization of multilayer-type electrolyte membranes with hydrocarbon polymers*. *Electrochimica Acta*, 2010. **55**: p. 1385-1388.
225. Alberti, G., M. Casciola, L. Massinelli, and B. Bauer, *Polymeric proton conducting membranes for medium temperature fuel cells (110–160°C)*. *Journal of Membrane Science*, 2001. **185**: p. 73-81.
226. Novoselov, K.S., A.K. Geim, S.V. Morozov, D. Jiang, Y. Zhang, S.V. Dubonos, I.V. Grigorieva, and A.A. Firsov, *Electric field effect in atomically thin carbon films*. *Science*, 2004. **306**(5696): p. 666-9.
227. Yoo, B.M., H.J. Shin, H.W. Yoon, and H.B. Park, *Graphene and Graphene Oxide and Their Uses in Barrier Polymers*. *Journal of Applied Polymer Science*, 2013.
228. Zhang, L., J. Xia, Q. Zhao, L. Liu, and Z. Zhang, *Functional graphene oxide as a nanocarrier for controlled loading and targeted delivery of mixed anticancer drugs*. *Small*, 2010. **6**(4): p. 537-44.
229. Kuilla, T., S. Bhadra, D. Yao, N.H. Kim, S. Bose, and J.H. Lee, *Recent advances in graphene based polymer composites*. *Progress in Polymer Science*, 2010. **35**(11): p. 1350-1375.
230. Sun, Y. and G. Shi, *Graphene/polymer composites for energy applications*. *Journal of Polymer Science Part B: Polymer Physics*, 2013. **51**(4): p. 231-253.
231. Jiang, Z., X. Zhao, and A. Manthiram, *Sulfonated poly(ether ether ketone) membranes with sulfonated graphene oxide fillers for direct methanol fuel cells*. *International Journal of Hydrogen Energy*, 2013. **38**(14): p. 5875-5884.
232. Heo, Y., H. Im, and J. Kim, *The effect of sulfonated graphene oxide on Sulfonated Poly (Ether Ether Ketone) membrane for direct methanol fuel cells*. *Journal of Membrane Science*, 2013. **425-426**: p. 11-22.
233. Chien, H.-C., L.-D. Tsai, C.-P. Huang, C.-y. Kang, J.-N. Lin, and F.-C. Chang, *Sulfonated graphene oxide/Nafion composite membranes for high-performance direct methanol fuel cells*. *International Journal of Hydrogen Energy*, 2013. **38**(31): p. 13792-13801.
234. Zarrin, H., D. Higgins, Y. Jun, Z. Chen, and M. Fowler, *Functionalized Graphene Oxide Nanocomposite Membrane for Low Humidity and High Temperature Proton Exchange Membrane Fuel Cells*. *The Journal of Physical Chemistry C*, 2011. **115**(42): p. 20774-20781.
235. Paneri, A., Y. Heo, G. Ehlert, A. Cottrill, H. Sodano, P. Pintauro, and S. Moghaddam, *Proton selective ionic graphene-based membrane for high concentration direct methanol fuel cells*. *Journal of Membrane Science*, 2014. **467**: p. 217-225.

236. Wang, J., Y. Mo, S. Mahendra, and E.M.V. Hoek, *Effects of water chemistry on structure and performance of polyamide composite membranes*. Journal of Membrane Science, 2014. **452**: p. 415-425.
237. Fu, R.S., J.S. Preston, U. Pasaogullari, T. Shiomi, S. Miyazaki, Y. Tabuchi, D.S. Hussey, and D.L. Jacobson, *Water Transport Across a Polymer Electrolyte Membrane under Thermal Gradients*. Journal of The Electrochemical Society, 2011. **158**(3): p. B303.
238. Kim, J., L.J. Cote, F. Kim, W. Yuan, K.R. Shull, and J. Huang, *Graphene Oxide Sheets at Interfaces*. J Am Chem Soc, 2010. **132**: p. 8180-8186.
239. Zinadini, S., A.A. Zinatizadeh, M. Rahimi, V. Vatanpour, and H. Zangeneh, *Preparation of a novel antifouling mixed matrix PES membrane by embedding graphene oxide nanoplates*. Journal of Membrane Science, 2014. **453**: p. 292-301.
240. Peng, K.-J., J.-Y. Lai, and Y.-L. Liu, *Nanohybrids of graphene oxide chemically-bonded with Nafion: Preparation and application for proton exchange membrane fuel cells*. Journal of Membrane Science, 2016. **514**: p. 86-94.
241. Dai, W., Y. Shen, Z. Li, L. Yu, J. Xi, and X. Qiu, *SPEEK/Graphene oxide nanocomposite membranes with superior cyclability for highly efficient vanadium redox flow battery*. Journal of Materials Chemistry A, 2014. **2**(31): p. 12423.
242. Zhang, B., Y. Cao, S. Jiang, Z. Li, G. He, and H. Wu, *Enhanced proton conductivity of Nafion nanohybrid membrane incorporated with phosphonic acid functionalized graphene oxide at elevated temperature and low humidity*. Journal of Membrane Science, 2016. **518**: p. 243-253.
243. Vinothkannan, M., R. Kannan, A.R. Kim, G.G. Kumar, K.S. Nahm, and D.J. Yoo, *Facile enhancement in proton conductivity of sulfonated poly (ether ether ketone) using functionalized graphene oxide—synthesis, characterization, and application towards proton exchange membrane fuel cells*. Colloid and Polymer Science, 2016. **294**(7): p. 1197-1207.
244. Kausar, A., *Study on poly(imide-ethylene glycol) and graphene oxide-based hybrid proton exchange membrane*. International Journal of Polymer Analysis and Characterization, 2016. **21**(6): p. 537-547.
245. Bae, B., K. Miyatake, and M. Watanabe, *Sulfonated Poly(arylene ether sulfone ketone) Multiblock Copolymers with Highly Sulfonated Block. Synthesis and Properties*. Macromolecules, 2010. **43**(6): p. 2684-2691.
246. van de Ven, E., A. Chairuna, G. Merle, S.P. Benito, Z. Borneman, and K. Nijmeijer, *Ionic liquid doped polybenzimidazole membranes for high temperature Proton Exchange Membrane fuel cell applications*. Journal of Power Sources, 2013. **222**: p. 202-209.
247. Hatakeyama, K., M.R. Karim, C. Ogata, H. Tateishi, A. Funatsu, T. Taniguchi, M. Koinuma, S. Hayami, and Y. Matsumoto, *Proton conductivities of graphene oxide nanosheets: single, multilayer, and modified nanosheets*. Angew Chem Int Ed Engl, 2014. **53**(27): p. 6997-7000.
248. Kannan, R., M. Parthasarathy, S.U. Maraveedu, S. Kurungot, and V.K. Pillai, *Domain size manipulation of perfluorinated polymer electrolytes by sulfonic acid-functionalized MWCNTs to enhance fuel cell performance*. Langmuir, 2009. **25**(14): p. 8299-305.
249. Yin, Y., H. Wang, L. Cao, Z. Li, Z. Li, M. Gang, C. Wang, H. Wu, Z. Jiang, and P. Zhang, *Sulfonated poly(ether ether ketone)-based hybrid membranes containing graphene oxide with acid-base pairs for direct methanol fuel cells*. Electrochimica Acta, 2016. **203**: p. 178-188.
250. Tsai, L.-D., H.-C. Chien, W.-H. Huang, C.-P. Huang, C.-y. Kang, J.-N. Lin, and F.-C. Chang, *Novel Bilayer Composite Membrane for Passive Direct Methanol Fuel Cells with Pure Methanol*. International Journal of Electrochemical Society, 2013. **8**: p. 9704-9713.
251. Treekamol, Y., M. Schieda, L. Robitaille, S.M. MacKinnon, A. Mokrini, Z. Shi, S. Holdcroft, K. Schulte, and S.P. Nunes, *Nafion®/ODF-silica composite membranes for medium temperature proton exchange membrane fuel cells*. Journal of Power Sources, 2014. **246**: p. 950-959.